UNIVERSITÉ DU LUXEMBOURG

PhD-FSTM-2023-034

Faculty of Science, Technology and Medicine

DISSERTATION

Defence held on 24/03/2023 in Esch-Sur-Alzette

To obtain the degree of

DOCTEUR DE L'UNIVERSITÉ DU LUXEMBOURG EN SCIENCES DE L'INGENIEUR

By

Lorenc BOGOVIKU

Born on the 27th of December 1993 in Tirana, Albania

INVESTIGATIONS ON THE CIRCULARITY OF CONCRETE AS A CONSTRUCTION MATERIAL

Dissertation defence committee

Prof. Dr. -Ing. Danièle Waldmann, Dissertation supervisor

University of Luxembourg, Faculty of Science, Technology and Medicine

Prof. Dr. Felix Norman Teferle

University of Luxembourg, Faculty of Science, Technology and Medicine

Dr. Romain Trauchessec

University of Lorraine, Institut Jean Lamour

Dr.-Ing. Vishojit B. Thapa

Administration de l'Environment, Luxembourg

Dr. Alexandre Bertrand

Luxembourg Institute of Science and Technology

Abstract

The present thesis titled « Investigations on the circularity of concrete as a construction material » aims to address the sustainable use of construction and demolition waste (CDW) arising from mineral construction material and investigate the feasibility of using recycled concrete in industrial applications. The study is carried out in collaboration with a consortium of industrial partners (Cimalux, Recyma, Carrieres Feidt, Entrapaulus, Eneco, Cloos, Administration des Ponts et Chaussées Luxembourg and Administration de l'Environnement Luxembourg).

Depletion of natural resources is one of the main global environmental risks. Mineral reserves show a special vulnerability in this aspect, as they are not renewable in nature. The world's demand for sand and aggregates is recorded to be 40 – 50 billion tonnes per year and projected to further increase to 60 billion tonnes per year by 2030. The global generation of waste is, on the other hand, increasing. In Europe, construction and demolition waste (CDW) is assessed to be 25 – 30 % of the total waste, with the largest fraction (>90%) being concrete waste. Concrete recycling offers a viable solution for the reuse of waste, as it can offer tangible benefits in offsetting carbon emissions, as well as conserving the material reserves.

Recycled concrete is tested using locally sourced recycled aggregates in Luxembourg. The data show that a general decrease in mechanical performance is to be expected when using recycled concrete. The loss in compressive strength is tested as 74% for a full substitution. The recycled aggregates show a significantly higher water absorption than the normal aggregates and a lower density due to the crushing process. However, when utilizing high quality aggregates, the loss in mechanical properties can be limited to 25% for a full substitution and is insignificant for up to 50% substitution of aggregates.

As the main contributor to the quality of recycled concrete, the interfacial bond between the recycled aggregate and the new mortar matrix is investigated in laboratory tests comprising of slanted shear loading tests. The failure parameters show an internal interfacial friction coefficient ranging from 0.69-0.88 and cohesion values between 0.13 MPa and 4.60 MPa, depending on the substitution ratio. Generally, an increase in interfacial strength is observed for low to medium substitution ratios, due to the unhydrated cement paste in the recycled aggregates. For full substitutions, this benefit is not present anymore and the interface is further weakened due to

microcracks present in the matrix. Furthermore, a numerical model is built based on the phase-field modelling approach to simulate the fracture of recycled concrete. The model is able to accurately predict the crack initiation and propagation as well as mechanical properties of recycled concrete.

Furthermore, an investigation is done regarding the critical masses of CDW in Luxembourg to allow for a feasible economical concrete recycling. A modelling approach based on a combination of GIS and image analysis is used to define the built-in mineral construction material in Luxembourg. Based on an analysis of old topographic cartography, an estimation of the deconstruction trends is done. The total built in mineral material stock in Luxembourg is estimated to be 276.75 Mt and records a growth of up to 24.39% in the last 30 years. Based on stochastic predictions, the generated CDW weight can be up to 226.29 Mt by the year of 2100. It is estimated that the expected volumes of CDW give the opportunity and the feasibility to create a feasible economic activity in terms of concrete recycling if the production of recycled aggregates is well managed locally. This approach has significant potential to serve as a starting base for a material cadastre in the country and for a management system of not only CDW, but also the built-in environment in general.

Keywords: sustainability, concrete recycling, construction and demolition waste, interfacial transition zone, circular economy

Preface and acknowledgements

This document represents a compilation of a work spanning four years between 2018 and 2022, where I had the great pleasure to be part of the research community of the University of Luxembourg, as a doctoral student of civil engineering at the Faculty of Science Technology and Medicine.

I want to thank and express my deep gratitude to Prof. Danièle Waldmann for giving me the opportunity to make this journey, for trusting me since the very beginning and for giving me the neccessary guidance in every step of my doctoral research. I want to thank her for all the constructive and friendly exchanges, as well as all for always being ready to share all the helpful tips that allowed me to learn and grow. Without her professionality, presence and comprehension, I would not imagine to have ever taken such an endeavour.

I want to thank my CET members, prof. Teferle and Dr. Trauchessec for all the constructive discussions, suggestions and support that they gave me during these four years. Their remarks made this work better in many ways. To Prof. Teferle, I want to extend my gratitude for all his

efforts as doctoral school director that made the life as a PhD student more fulfilling and created a sense of community without which no University can thrive. I want to thank Dr. Thapa and Dr. Bertrand for kindly accepting to be part of my thesis defence committee.

Moreover, I am deeply grateful to our research partners, more specifically, Mr. Rech and Dr. Simon from Cimalux, Mr. Klöppner and Mr. Philipps from Eneco, Mr. Wertz from Carrieres Feidt, Mr. Blasen from Administration des Ponts et Chaussées, Mr. Schmit from Admninstration de l'Enironment, Mr. Schlink from Cloos, Mr. Wagner from Entrapaulus and Mr. Faber from Recyma. Without your kind support and professional feedback, this work would not have been possible.

I want to thank the team of the engineering laboratory at the University of Luxembourg, Marc Seil, Gilbert Klein, Claude Colé, Ed Weyer, Logan Freitas, Vicente Reis Adonis, Ken Adam, Cédric Bruyère, Markus Schlienz and Grace Ligbado for all their constant support, professional help and for always being available to accommodate my technical request.

My deepest gratitude goes to my colleagues. Sinan, Hooman, Tarik, Anna, Suzanne, Justin, Brice, Bhagya, Patrick, Vish, Dolgion, Gael for making everyday a bit special and for creating a work environment that was joyful, friendly and supportive. We created memories that will always remain with me.

I would like to thank my friends, who were always there for me, especially in the toughest of times and were a reason for me to go on and believed in me even when I didn't believe in myself. I will definitely get the time to hug you all one by one and to offer all my love and appreciation.

Finally, but not less importantly, I want to thank my family, for their unconditional love and support. Without them, nothing would have been possible.

Lorenc,

Vienna, 04.03.2023

Statement

The following document is a detailed report on the academic work in light of project CIRECON (Circular Economy of Recycled Concrete) which was carried out during the period 2018-2022 at the University of Luxembourg. The document is structured, in compliance with the regulations of the University of Luxembourg, as an accumulative thesis of the following peer-reviewed documents: two published scientific articles, one submitted paper (at the time of defense) and two published conference papers. The structure, content and contribution of these documents in relation to the overall topic of the thesis is described in chapter 1.

Table of contents

Table of figures

"Humanity has the ability to make development sustainable to ensure that it meets the needs of the present without compromising the ability of future generations to meet their own needs."

Report of the World Commission on Environment and Development: Our Common Future

1987

Chapter 1 | Introduction

1.1. Scope of the study and main research questions

The present study aims to address the circularity of concrete as one of the main construction materials worldwide and at the same time one of the largest industrial polluting fractions. It presents a common effort of several stakeholders in the Luxembourgish construction industry to make building activities greener and to accelerate the adaption of the circular economy nation-wide. Even though several aspects are studied with Luxembourg as the reference study, the author believes that the research results reflect a broader audience and give a contribution to the global scientific efforts in the topic of sustainability of the construction sector. Since circularity and circular economy in itself is a broad concept, it is important to outline the major research questions that this thesis addresses.

Is circularity of concrete a feasible scenario for Luxembourg and beyond?

This is the predominant issue of the project and one of the most complex topics that is treated throughout this document. The reason lies in the complexity and inter-disciplinary nature of circular economy in itself and to obtain a satisfactory result, the entire life-cycle of concrete must be considered. The main scope is to create a realistic picture, not simply in a narrow perspective but also on a global aspect on how what are the driving factors of circularity, how can it be assessed, quantified and optimized. This question is therefore addressed in different perspectives, as a global issue, as a management issue and also as a technological issue.

What is the quality of secondary raw materials in Luxembourg and what quality of concrete can be derived from them?

One very important aspect of the life cycle of concrete is the end-of-life scenario, recycling and reuse. As for the moment, no data are available for Luxembourg, it is crucial to have a full characterisation of the local secondary raw aggregates as well as understand the properties and

limits of their use in high-quality applications, such as new concrete production. This scenario would fully close the material loop on concrete and will be a significant step towards circularity.

Is it possible to improve the material properties in an economically viable way while keeping into consideration the environmental goals?

It is known from literature and several studies that recycled aggregates will exhibit lower performance compared to normal raw aggregates. An important scope towards standardization is to create certainty towards these materials and to attempt to use them in concrete, without compromising on its soundness and quality. At the same time, it is important to minimise further costs on industries that will use these materials. Therefore, enhancement of the materials in a sustainable and economic way needs to be studied.

Can the demolition processes be improved in order to maximise the reuse and recycle of building components?

As demolition represents the first phase of the end-of-life for construction materials, it is crucial to have regularized processes, which encourage the re-use and recycle of materials. The state-of-the-art of the selective demolition in the country needs to be assessed and further ways to regularize the process need to be formulated and suggested.

1.2. Project highlights and structure of the thesis

The project structure attempts to reflect the main issues facing the circularity of concrete as a building material. In terms of system thinking, the thesis is organised and worked in a way to address the links that connect the processes and the life cycle of concrete. It was the aim of the project to address every aspect of the end-of-life stage of concrete, by being as extensive and as grounded in practicality as possible. The structure of the outcomes can be seen on Figure 1-1 and it has a funnelled approach coming from the most global approach and ending with material specific studies.

Figure 1-1. Structure of the project

This thesis is structured to address the circularity of concrete in two main paths that are seen as supplementary in the study of circularity, namely, a global-management aspect, which is discussed in terms of literature in chapters 2.1 and 2.2. These chapters feed directly into the results presented in chapter 5 and 6. The other aspect, the technical-mechanical aspect is discussed on chapters 2.3 and 2.4, which serve as a literature basis for the results presented in chapter 3 and 4. The transition between the literature and the results section is done in a mirrored way in order to facilitate the reading experience. Each of the result chapters are organized as self-standing publications and include a literature review which is intended to be complementary to chapter 2 and lead the reader directly into the specific topic of each chapter.

More specifically, the document is organized as follows:

- Chapter 2 contains an extensive literature review on sustainability, circular economy and more specific aspects of the circularity and recycling of concrete. The literature is organized into two main blocks: the circular economy (2.1) and technical aspects of recycled concrete (2.2, 2.3, 2.4).
- 2.5 contains laboratory tests made on recycled aggregates and recycled concrete as well as results and comparison to the existing literature. This chapter is the main technical background relating to recycled concrete as a construction material. It aims to analyse the mechanical feasibility of using recycled concrete in the construction industry.

- Based on findings of the previous chapters, as well as the literature background, Chapter 4 addresses the interfacial transition zone (ITZ) in recycled concrete as the main influencing factor of the quality of recycled concrete. This is done through an experimental program designed to assess the strength of the ITZ and determine the failure parameters. Furthermore, it contains a numerical model built on the basis of the phase field approach to model and predict the behaviour of the recycled concrete matrix and interface during mechanical loading.
- After, the technical assessment of the material quality, the question regarding critical masses is addressed in Chapter 5, which contains the global approach through a dynamic material flow analysis done for the concrete stock in Luxembourg as well as the extension into a circular economy database by including life cycle analysis indicators.
- Chapter 6 is addressed to the first step of the end-of-life phase of concrete which is the demolition/deconstruction. This is done through a deconstruction certification approach, based on one case study.
- Chapter 7 contains the summary of the thesis.
- Annex A presents the work done in light of the Interreg project SeRaMCo on the recycled concrete produced with aggregates of known origin.

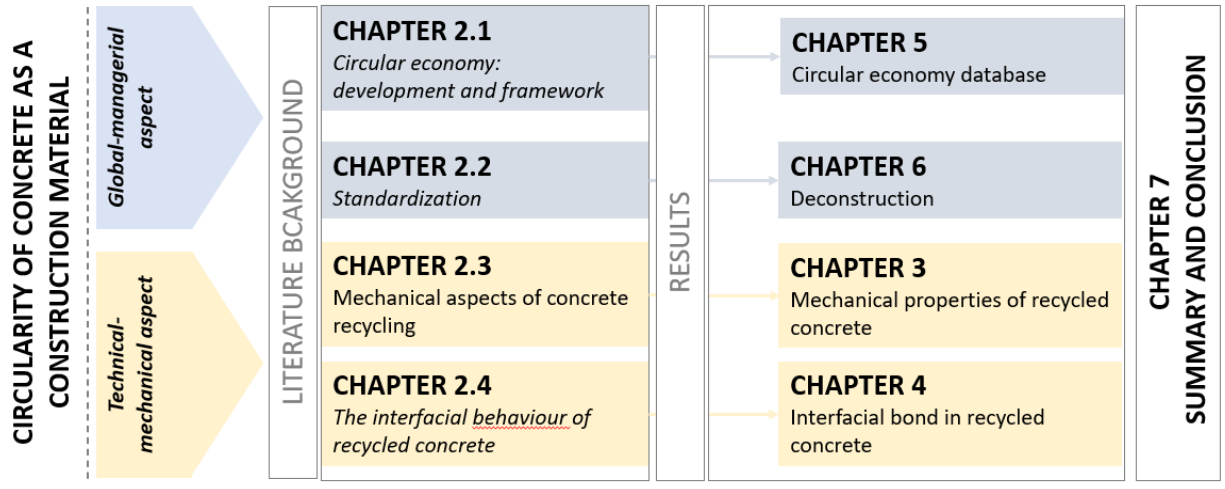

Figure 1-2. Structure of the dissertation

1.3. Scientific disseminations of the project and the coherence between the papers

The present study produced at the moment of writing two accepted journal articles, two accepted conference papers and one additional submitted manuscript. It is furthermore completed with intermittent results in order to give a complete spectrum of this complex topic and create a cohesive study structure.

The first journal paper titled «Modelling of mineral construction and demolition waste dynamics through a combination of geospatial and image analysis » (https://doi.org/10.1016/j.jenvman.2020.111879) is published in the Journal of Environmental Management and it intends to address the global aspect of circularity, mainly the material flows that are existing at the moment and whether those are enough for a feasible concrete recycling at a large scale. This is furthermore expanded with an accepted conference paper tittled « A coupled spatial - environmental approach as decision-making tool for the circular economy of the built environment » which intends to expand the proposed methodology and build the basis of a system for circular management of the built environment. The contents of these papers comprise the entirety of chapter 5 (Circular economy database).

The second journal paper titled « Experimental investigations on the bond strength of the interface of the adhered mortar paste in the recycled concrete matrix » (https://doi.org/10.1016/j.conbuildmat.2022.128509) addresses a more specific problem of the interface of recycled aggregates, in order to better characterize the material and make concrete recycling a more feasible practice in a technological aspect. The improvement of recycled concrete in terms of mechanical properties if further investigated in the third journal manuscript « Phase-field model for mixed-mode inelastic fracture in recycled aggregate concrete material » where a numerical model is built to simulate the properties of recycled concrete. These papers are part of sub-chapters 4.1 and 4.2.

An overview of the scientific disseminations can be found on Table 1-1.

Table 1-1. Overview of the scientific disseminations

Journal papers		
L. Bogoviku, D.Waldmann	Modelling of mineral construction and demolition waste dynamics through a combination of geospatial and image analysis	Journal of Environmental Management, 2021
L. Bogoviku, D.Waldmann	Experimental investigations on the bond strength of the interface of the adhered mortar paste in the recycled concrete matrix	Construction and Building Materials, 2022
J. Kinda, B. Kabore, L. Bogoviku, D.Waldmann	Phase-field model for mixed-mode inelastic fracture in recycled aggregate concrete material	submitted, under review
Conference papers		
L. Bogoviku, D.Waldmann	A coupled spatial - environmental approach as decision-making tool for the circular	Circularity in the Built Environment CiBEn_Conference at TU Delft, 2021
D.Waldmann, L.Bogoviku, G. Chewe Ngapeya	Development of new concrete mixes from	SeRaMCo Final Conference, Kaiserslautern, 2021

Chapter 2 | Literature review

2.1. Circular economy: development and framework

2.1.1. Historical overview

Circular economy is a model considering the whole lifetime of a product with the aim of maintaining the material flows in the economical loop for as long as possible. The aim of the principle is the reduction (ideally elimination) of waste from the economy by enhancing the level of sharing, reuse, repair and recycle. Circular economy is a regenerative model that gets inspiration from natural cycle of components and seeks to implement the organic cyclic principles in the anthropogenic industry. To better understand circular economy, one can refer to the traditional idea of the linear economy. The linear economy model was heavily introduced during the first industrial revolution and boosted by the development of the production line. It is sometimes referred to as the "take-make-use-dispose" method and considers the products and resources to have a definite life-cycle which ends eventually in the form of waste products. Circular economy contrasts this idea by referring to the life-cycle of materials as a closed loop and by valorising waste, improving system effectiveness and using innovation to create further value in the system.

The concept of circular economy was first introduced in the 1960s by Boulding [1]. He was the first to contemplate on our planet as a closed system and effectively critique the open-loop model of the economic model. His work is often referred to as the "closed spaceship economy" as he puts forward the comparison of our planet with a spaceship with closed input of energy and material sources. This idea was later built on by Stahel and Reday [2], [3] by the introduction of concepts such as the loop economy and the service economy as a sustainable alternative to the current product economy. It was not until the late 1990s and early 2000s until popular ideas such as cradle-to-cradle, regenerative design, life cycle management, industrial ecology and looped economy were introduced [4]. Nowadays, the most influential driver of the circular economy idea

is the Ellen MacArthur Foundation [5] who works on accelerating circularity by supporting policymakers, institutions and research worldwide.

2.1.2. Economic growth: the current economic model and circularity

Circularity is first and foremost an environmental philosophy. However, it is inevitable when speaking about circularity to address the current global economic model simply due to the fact that there are undeniable links between the economic activity and environmental impacts. Economic growth, which is the most commonly used metric for measuring the wellbeing of a society, comes with an increased production, increased material consumption, increased pollution and adverse environmental impacts. Many approaches have already suggested the idea of "uneconomic growth" and there are several proposals for the substitution of the metrics used for growth and wellbeing. The gross domestic production (GDP) is by far the most common indicator of eco-social wellbeing. However, there is extensive literature that shows the causality between the GPD and environmental impacts. As seen on Figure 2-1, in the last decades, there is a steep increase in global GDP, but also on the greenhouse gas emissions and material footprint.

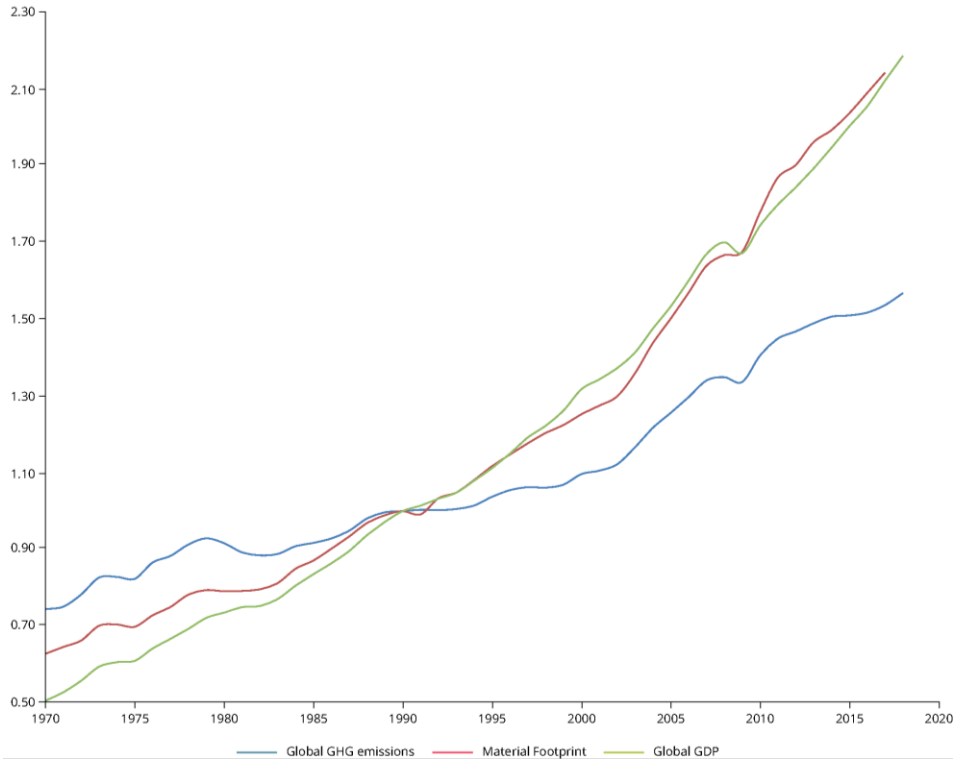

Figure 2-1. Relative change in main global economic and environmental indicators from 1970 to 2018 (https://www.eea.europa.eu/legal/copyright)

This becomes even more evident when considering the concept of the Country Overshoot day. The Overshoot day is a yearly indicator that shows how the world yearly resources would be depleted if all the world consumed like that country [6]. For the year 2022, the earliest country overshoot day was Qatar with 10th of February, shortly followed by Luxembourg with 14th of February. However, the relation between the each country's GDP and it's earth overshoot day shows a precise flaw in the current economical model when considering the environmental aspect. Figure 2-2 shows how every country's overshoot day relates to its economical performance in terms of GDP per capita. It can be seen that the richest countries, those with a higher GDP/capita, have an earlier overshoot day. This enforces the relationship between economic growth and environmental impact as displayed also on Figure 2-1. Therefore, economic growth, as perceived at the moment, seems to not be the sustainable choice and there is an urgent need in dissociating negative environmental impacts from economic growth. This has led to the proposal of several alternatives to the GDP which incorporate the environmental aspects into the metric, such as, among others, the Human Development Index (HDI) [7], the Genuine Progress Indicator (GPI) [8], the green GDP [9] and the Happy Planet Index (HPI) [10]. However, the employment of such

metrics entails several risks because that would require an adaption to the extensive network of policies, legislation and statistical infrastructure in a global scale, which is unlikely to happen in rapid terms due to sheer convenience [11].

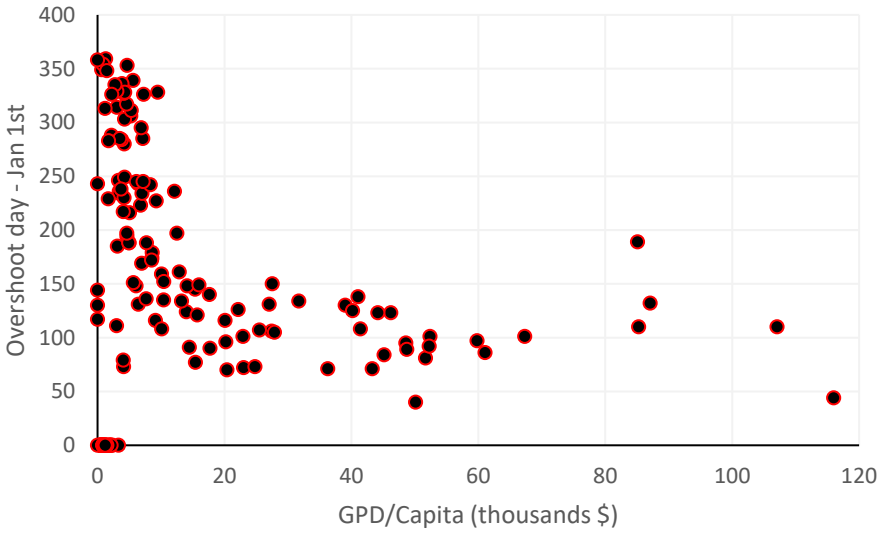

Figure 2-2. The plot shows every country and its relation between the overshoot day and its GDP/capita

The assessment metric for measuring resource use from an economy is the domestic material consumption (DMC). To judge sustainable growth, it is common practice to divide the GDP with the DMC in order to obtain a metric on the resource efficiency of an economy. In principle, if the GDP grows faster than the DMC, it indicates a more sustainable economy due to resource decoupling. However, research shows DMC not to be the best way to measure a country's material depletion, simply because a significant amount of processes in highly developed countries is outsourced to third parties, therefore simply shifting the environmental impact [12]. Thus, a more global assessment is needed. Dittrich et al [13], through a simulation based on a "business-as-usual" case, show that by 2050 the global material consumption will increase by up to 264%, which is a level of resource use that is totally unfeasible for the planetary boundaries. Wiedmann et al [14] argue that affluence is the key factor in resource depletion and pollutant emission, enforcing the need for a behavioural change and regulatory framework to address overconsumption. While there are several approaches, the EU and the Organisation for Economic Co-operation and Development (OECD) favour the green growth approach by still keeping a priority on economic growth while decoupling it from the environmental impacts. The "European Green Deal" [15], beyond the strong focus on reducing greenhouse gas emissions, aims for a shift in the European

industry and economic sector by encouraging circular economy, smart mobility, agriculture and industrial design to bridge the gap between the current economic growth rate and a green decoupled economy. However, recent studies show that absolute decoupling is unrealistic and, at best, temporary [16], because design optimization and material efficiency will have, undoubtedly, a natural limit. On the other hand, GDP growth cannot be sustained in the long term and a shift towards a green economy is imperative. The shift towards green economy comes with several challenges, as described by Söderholm [17], such as dealing with environmental risks, achieving sustainable technological change, the uncertainty of business as usual scenario, designing of appropriate policies and dealing with distributional concerns and impacts. In general, the promotion of green innovation must build upon not only instruments that push forward technological development, but also, very importantly, policies that pull such technological approaches and the construction of an adapt infrastructure to allow for such developments.

Therefore, it is crucial to tackle sustainability research in a global and multi-disciplinary way. Innovation, digitalization and optimization in strict technical terms must go hand in hand with policymaking and impact evaluation at every stage of our industrial design. Therefore, the contribution of research towards closing the material loops and encouraging circularity must not be a traditional one, simply focused on a design approach, but it is vital to keep a global perspective and a system-thinking approach.

2.1.3. Definitions and circular economy indicators

Before entering into a more technical aspect of circular economy, it is important to explain some terminology that was mentioned in the previous paragraph and to have an overview on the mechanisms that foster circularity.

loop economy (or closed loop economy)	refers to an idealized business model where no waste is generated. The traditional “waste” is valorised and re-cycled into the economy.
cradle-to-cradle	is the concept of mirroring the manufactured materials as “nutrients” in the natural world, therefore, as natural cycles,

	one must create closed cycles of process to achieve sustainability [18]
regenerative design	the concept of re-aligning human and natural systems [19] by creating a net positive impact of human activities in the ecosphere through the consideration of planetary boundaries and the natural cycles of the living world
life cycle management	is the methodology of quantitively evaluating the environmental impact of a process or product throughout its lifetime. It is further explained in section 2.1.5.
industrial ecology	is the umbrella term for the science and discipline that tackles sustainability in terms of scientific approach, industrial approach and policy making
biomimicry	is the practice of applying natural and organic mechanisms to engineering design [20]
system thinking	is the practice of a problem solving approach though the consideration of the system as a whole and connections between its parts, rather than deconstructing it in smaller aspects [21]

However, circular economy remains indeed a philosophy and the boundaries of its practicality are most probably one of the reasons of its latent use and the initial inertia that it faced in its application. This is especially true when considering that a vast majority of circular economy applications relate to industrial design and policymaking, both of which are based on objective indicators, most preferably standardized frameworks. Therefore, the question of circular economy indicators becomes relevant. In light of system thinking methodologies, several approaches focus on a macro or global scale, which sets circular economy as a management and monitoring problem. This is unsurprising when one considers the waste hierarchy steps listed in the Waste Framework Directive [22]: prevention, reuse, recycle, recovery and disposal, with reuse, recycle and recovery are all dependent on a global scale. Therefore, the three main approaches on a global scale are based on material flow analysis (MFA), energy analysis and input-output analysis [23]. All these

approaches are multi-dimensional practices that allow for implementation of several aspects such as the material flows, economic, spatial, and environmental aspects, however, MFA appears to be the most established approach in literature and policies. MFA refers to the process of defining the flows of a material or substance in space and time. According to Brunner and Rechberger [24], [25], MFA comprises in 6 steps: definition of objective and monitoring indicators, system definition, identification of relevant flows, design of material flow chart, mass balancing and illustration of results.

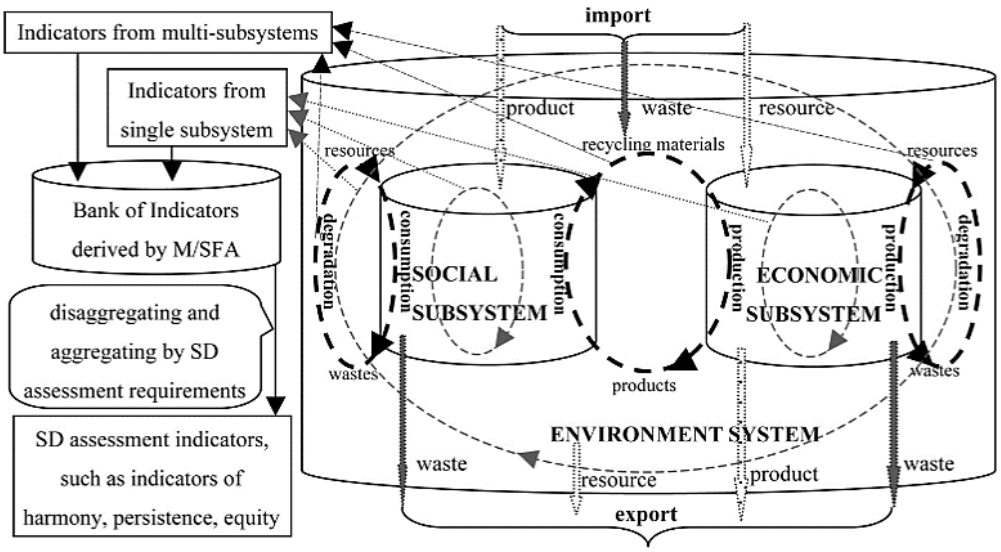

Figure 2-3. Diagram showing the link between MFA and sustainable development (SD) [25]

The MFA's main advantage is that it solves the issue of data flow and information regarding the material stock, paving the way for stock optimization. It is indeed true that there is a close relationship between the material flows and sustainable development as shown on Figure 2-3. On the right side of Figure 2-3 the material balance

MFA, in contrast with traditional methods of resource management, offers a global approach [26]. While many other design-based methods strictly focus on one specific aspect of the system, MFA allows for a global perspective which enhances the system-thinking approach, which is crucial for circularity. Not only does MFA provide a systematic database for the material quantities, but it also provides the system nodes where the flow of materials is inefficient in terms of sustainable goals. This is critical when thinking of procedures such as recycling, which relies on a constant flow of materials and an efficient logistics. Furthermore, most MFA data can be implemented in a resource bank or cadastre which promotes a better use of resources. Additionally,

since most of our economic and environmental indicators are linked to the unit product or material, MFA is adaptable and extendable, resulting in a highly important methodology. This adaptability has resulted in a significant increase in research based on MFA. Based on the database on Scopus, there is a 17.34% annual growth rate in research articles containing the keywords “material flow analysis”. Since 2008, there is a mean production of 1112 articles per year containing these keywords, which shows the current importance of the methodology in scientific research.

Goldstein et. al [27] have proposed a combined MFA-LCA approach as an essential approach to the sustainability in the built environment, but also hinting at essential improvements needed on the approach. By being a black box model, it has difficulties in linking the environmental impacts with the complex socio-economic aspects that characterize the urban environment. Therefore, more complexly layered models are necessary to fully support the decision-making criteria needed for policy making and account for a intricated system.

Müller [28] was the first one to have a dynamic approach in MFA by forecasting the need for concrete in the Dutch housing stock up to 2100, paving the way for the use of MFA as a tool for prediction and scenario-based forecasting. This aspect has a particular importance in policy making processes. Since then, an extensive number of scientific publications have been produced to assess the material quantity in the built environment in several geographical areas such as Norway [29], Ettlingen (Germany) [30], Vienna [31], Munich [32], Rotterdam [33], Shenzen (China) [34] and Esch-sur-Alzette (Luxembourg) [35]. Therefore, MFA becomes an important tool in the circular approach and further development is needed in bridging the gap between the historic database and the current digital-aided construction. Through MFA, it becomes not only possible to estimate the volumes and flows, but also to set the basis for national or regional databases for construction information flow and implement it in a cadastral approach, creating a permanent solution to data uncertainty in the generation of construction waste.

2.1.4. The global climate crisis: carbon emissions and the impact of the construction industry

The climate emergency refers to the ongoing and rapidly worsening crisis of global climate change. This crisis is caused by human activities, primarily the burning of fossil fuels such as coal,

oil, and natural gas, which releases large amounts of greenhouse gases such as carbon dioxide and methane into the atmosphere. These gases trap heat from the sun, causing the Earth's average temperature to rise. This warming trend has been well established by decades of scientific research and monitoring. The Intergovernmental Panel on Climate Change (IPCC) has reported that the Earth's average temperature has already risen by about 1°C since pre-industrial times, with the majority of this warming occurring in the past few decades (Figure 2-4). This warming has already led to significant impacts on the planet, including melting glaciers, rising sea levels, more frequent and severe heatwaves, droughts, and natural disasters, and harm to biodiversity and ecosystems. The impacts of climate change are expected to worsen in the coming decades, and will have far-reaching and profound consequences for humanity. For example, rising sea levels are projected to displace millions of people and render many coastal cities uninhabitable. The increasing frequency and severity of extreme weather events such as hurricanes, floods, and wildfires will cause widespread damage and loss of life. Changes to rainfall patterns and water availability will cause food and water shortages, which will lead to social and political instability. The loss of biodiversity and ecosystems will have negative impacts on the services they provide, such as food, medicine, and pollination. In response to the climate emergency, many countries, cities, and businesses have pledged to reduce their greenhouse gas emissions and transition to a low-carbon, sustainable future. However, much more action is needed. The IPCC has reported that to limit global warming to less than 2°C, compared to pre-industrial levels, global greenhouse gas emissions need to reach net zero by mid-century or earlier. This means that emissions must be reduced to as close to zero as possible, and any remaining emissions must be offset by removing an equal amount of carbon dioxide from the atmosphere.

Achieving this goal will require a rapid and concerted effort from all sectors of society. The energy sector must transition from fossil fuels to low-carbon sources such as wind, solar, and hydropower. The transportation sector must transition from cars and trucks powered by gasoline and diesel to electric vehicles powered by renewable energy. Buildings must be made more energy-efficient and powered by clean energy. Agriculture and forestry must be managed in ways that reduce emissions and increase carbon storage.

In addition to reducing emissions, we must also prepare for the impacts of climate change that are already unavoidable. This means investing in infrastructure that is resilient to extreme weather and sea-level rise, such as sea walls and levees. It also means supporting communities that are

already suffering the impacts of climate change, such as those affected by droughts, heatwaves, and sea-level rise.

As of the moment this document is being written, the level of global warming stands at 1.2°C

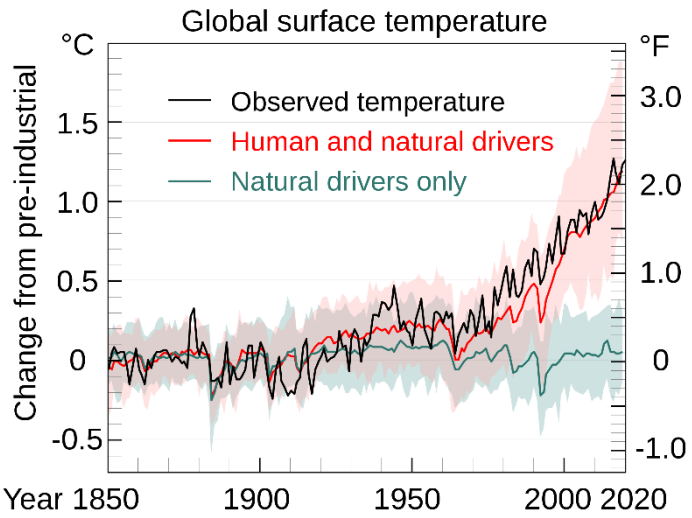

Figure 2-4. Observed global average temperature change [36]

As can be seen on Figure 2-5, the greenhouse gas emissions in Europe are at an average of 8.2 tons/capita according to 2019 data from Eurostat. Luxembourg is currently the highest emitter with 2.48 times the average mean. This is due in part to the economic model of the country, where the scale of the industrial activity does not correspond to the size of the country. Indeed, a majority of the workforce is non-resident therefore the true mean value per capita if commuters are included would be lower. Furthermore, the majority of emissions (81.7%) are represented from embodied emissions for products and services [37]. Nonetheless, this number is reflective of the urgency for climatic action in countries such as Luxembourg, that has limited natural resources and a surging economy. To reach the Paris accord targets, Luxembourg needs to remain below 1.6 tons per capita of CO_2-eq [38] which would entail a reduction by more than 90% of its carbon emissions.

With this goal, a wide campaign of national consultation was launched in 2020 involving all the major stakeholders of the industry in Luxembourg and the greater region, as well as a large number of institutes. « Luxembourg in transition » [39] includes 10 main workgroups with different approaches to sustainability and spatial planning in the greater region. While the majority of the projects rely on case-study investigations for the reduction of carbon, the neccessity of a suitable metric to define and quantify sustainability is highlighted. On the other hand, even though

the necessity and likelihood of a drastic increase in population number and density, little to no attention is given to the resource intensity that will accomplish such a change, nor to the incease in waste production that will accompany the growth.

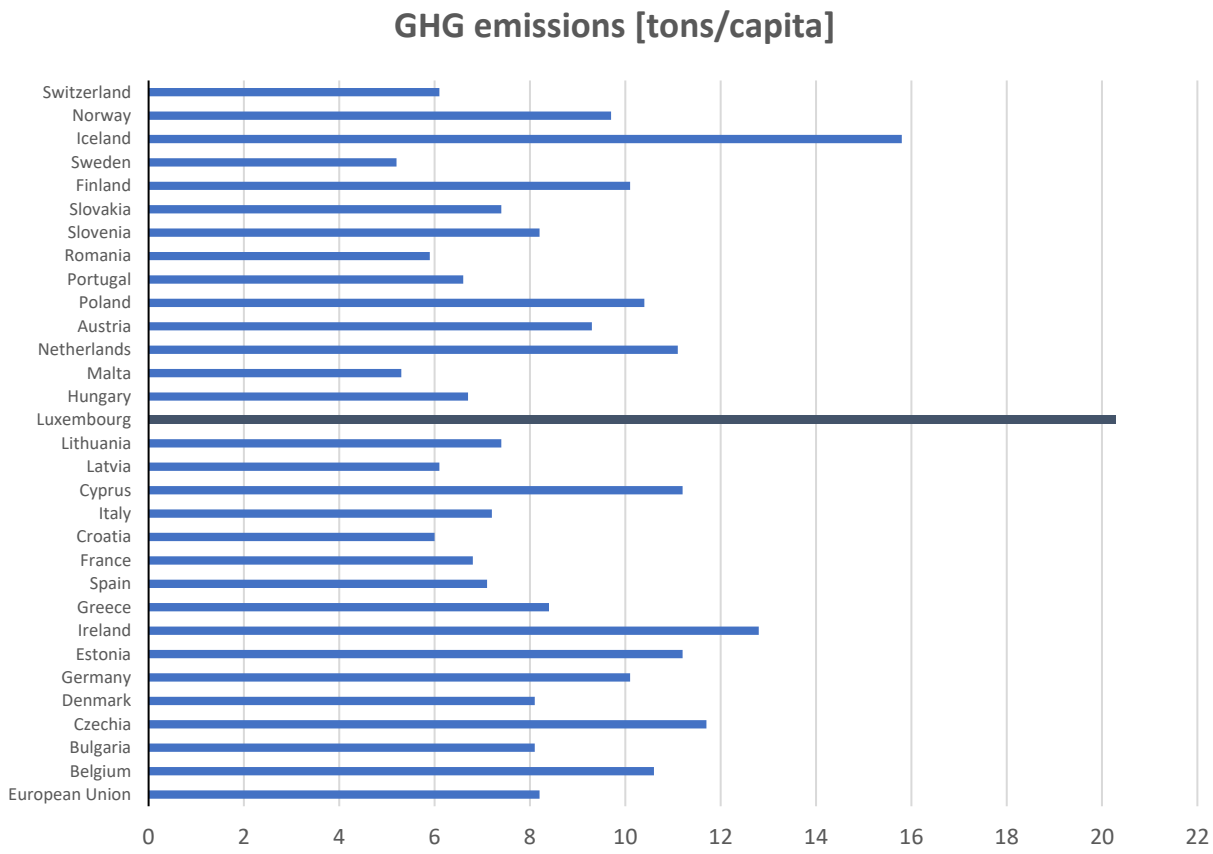

Figure 2-5. Greenhouse gas emissions in tons/capita in Europe (Source:Eurostat)

2.1.5. Beyond CO_2: Life cycle assessment (LCA), life cycle impact (LCI) and circularity

However, the carbon aspect is only one aspect in a complex, multi-phase and interlinked system. As expressed by Konietzko (Figure 2-6) through the "carbon tunnel vision" principle, it is unproductive and incorrect to equate the sustainability transition goals to simply carbon emissions. This is also reflected through the most common environmental impact quantification method, which is the life cycle assessment.

The idea of life cycle assessment (LCA) was brought forward first in the 1960s and 1970s as a reaction to studies containing emission data but little assessment on the impacts of such emissions [40]. It was not until the 1990s that the first methodologies were compiled such with a prime example being the CML 1992 method [41]. In later years, a standardization took place to regulate the procedure and the standards ISO 14040 (standard LCIA) and ISO 14042 (life cycle inventory modelling) are today the main references in LCA applications. Furthermore, countries have developed local impact assessment methods to address specific economic, technical and environmental conditions [42].

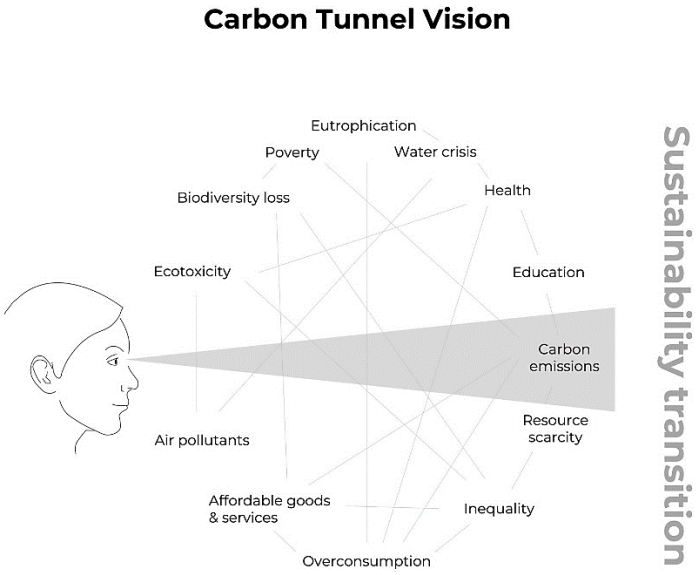

Figure 2-6. Concept of carbon tunnel vision (credit: Jan Konietzko)

The main working principle of LCA analysis according to ISO 14044 [43] relies on the following main steps [42]:

a. *selection*; choosing the impact categories, category indicators and characterisation models
b. *classification*; assignment of the elementary flows to the relevant impact categories
c. *calculation of the category indicator result*; which is the inherent choice of the weight that an impact category has on the total impact of an elementary flow. Practically is a multiplication of the value of the impact category with a characterisation factor
d. *normalisation*; which is the calculation of the value of impact in relation to a baseline information

e. *weighting*; which is the multiplication of the impacts with an importance factor which defines the comparison information between impact categories of an LCA

The importance of the above-mentioned steps is further highlighted when one considers on of the main principles of circular economy which is stock optimization. The idea of stock optimization brings the circular economy from a technical problem which is inherently CO_2-centered to a management problem. Figure 2-7, shows the structure of a circular economy as proposed by the Ellen MacArthur Foundation [44]. The first principle focuses mostly on preservation and prevention of waste by highlighting the need of "controlling" and "balancing" material stocks. The second principle refers to the optimisation of the flows. This is the principle which is mostly relevant to today's industry because it brings focus to the stakeholders and the production logistics that are already in place for the majority of industrial branches. And lastly, the third principle mainly refers to the design phase and the minimization of the negative externalities.

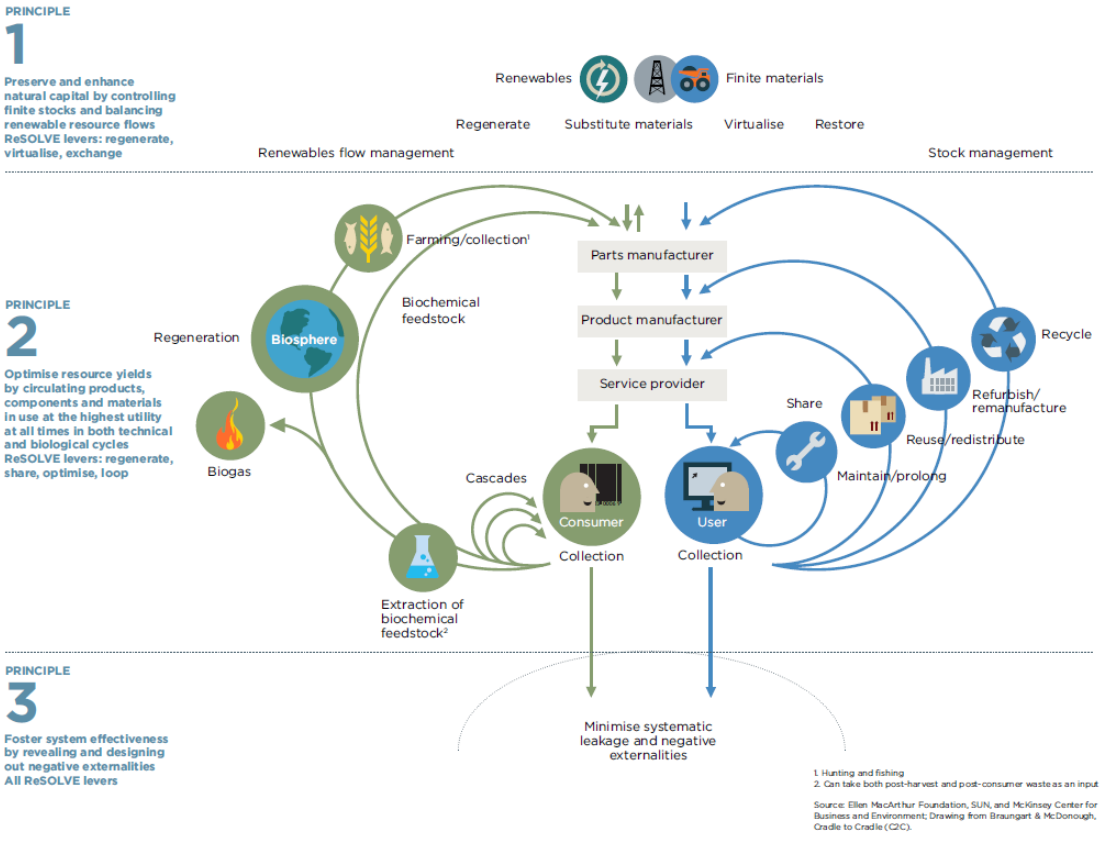

Figure 2-7. Outline of a Circular Economy [44]

The contents of this thesis will largely rely on the second principle by reflecting ways and methods to address the circularity in the built environment. Indeed, the relevant keywords at this stage are “optimization” and “management”, which undoubtedly must, by definition, refer to one or a structure of systems with the necessary information flow that allows for analytical decision-making. In this aspect, the technological advancements of the last decades become relevant tools and drivers of the entire system. Digitization of the construction industry allows for more data than ever before to be produced. Through approaches such as GIS and BIM, it is possible to create the necessary database that allows for a dynamic simulation of the performance of the entire built environment as a global system. Moreover, both these technologies are compliant with one another, with BIM offering the local approach and GIS the global approach and the industry foundation classes (IFC) being compatible with the major GIS sematic languages [45]. However, the integration of BIM and GIS presents numeral challenges, such as the difference in data structure and LOD specifications, which makes detailed models very difficult to integrate [46]. Furthermore, the data coming from the construction sector is highly fragmented, since the BIM models are not yet a tender requirement in most countries and there is no cadastral records of the 3D models, making data mining still an important research aspect in the MFA studies. And a standard analysis of the state-of-the-art and of the potential end-of-life scenarios of construction materials is still in its infancy. This becomes clear when referring to extensive literature devoted to data mining of the construction sector, such as, among others, the proposal for a “Waste Index” [47], “Component Index” [48], the stocks and flow approach [35], [49], [50] and the material and component bank [51]. Therefore, digitalization of the built environment is one of the most efficient ways of accessing the necessary data flow for building an efficient circular economy and for creating the tools to optimize the inputs and outputs of the system. In this regard, this document focuses on two main aspects: Building Information Modelling (BIM) as the local approach to single buildings (Chapter 6) and material flow quantification as the global approach (Section 5.1). These two approaches must not be regarded as alternatives but rather as complementary, therefore, information exchange between them must be allowed and facilitated. Therefore, this aspect is addressed on a proposal in Section 5.3.

2.1.6. Concrete - lifecycle and environmental impacts

When speaking about the production of concrete as material it is crucial to distinguish between each phase. As a composite material, concrete is composed of cement which acts as a binder, aggregates (both fines and coarse) that act as filler and water that makes possible the hydration of the cement. For special purpose concretes, additives are incorporated to ensure higher performance in special conditions. The lifecycle of concrete as a material can be simplified in seven major phases (Figure 2-8): resource extraction, resource treatment, design, construction, service life, demolition and end-of-life stage. In reality however, each of the constituents and each of the lifecycle stages will have its own lifecycle and its own environmental impact.

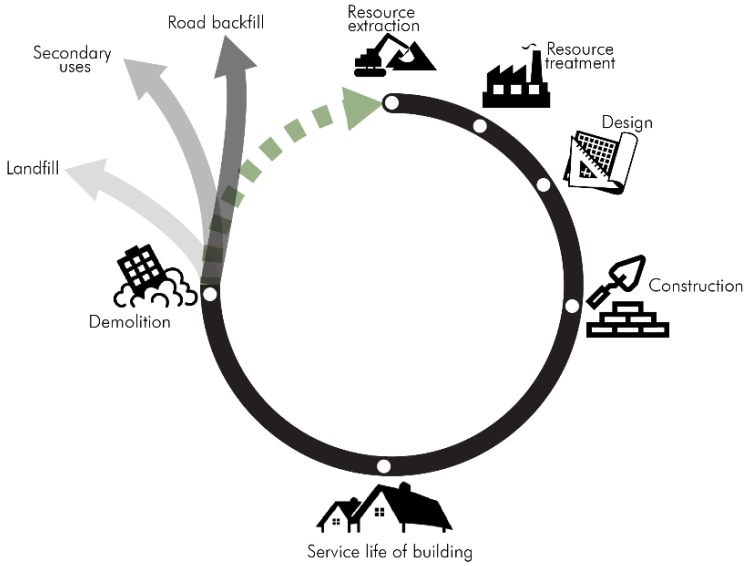

Figure 2-8. Lifecycle of concrete

The lifecycle environmental indicators are shown on Figure 2-9 for a typical concrete of C30/37 strength. It is clear that the manufacturing process is the most environmentally impactful process, taking in all indicators more than 75% of the total environmental impact of the lifecycle. This is due to the energy and carbon intensive cement production [52]. The environmental benefits from recycling the concrete, according the Ökobaudat [53] database, include a reduction by 8.71% of the GWP, 0.22% of the ODP, 18.42% of POPC, 11.73% AP, 11.30% EP, 1.20% ADPE and 16.93% ADPF. This shows that recycling of concrete is not simply a way to lower carbon emissions of the concrete production but it has numerous environmental benefits. The significant potential of concrete recycling to produce a more sustainable concrete is extensively shown in

literature. Knoeri et. al [54] show a significant environmental benefit of 30% for 12 different recycled concrete mixes studied. Ding et al. [55] confirm the benefits, but point out at the environmental impact of the cement as a constitutive element and at the need for an optimization of the mixture in order to maximize the benefits. In terms of the mixture, Colangelo et al. [56] concluded that a 25% substitution of recycled aggregates is an optimum in terms of environmental benefit. This threshold is furthermore in line with the optimum substitution for maximum mechanical performance which is discussed in Section 2.3.

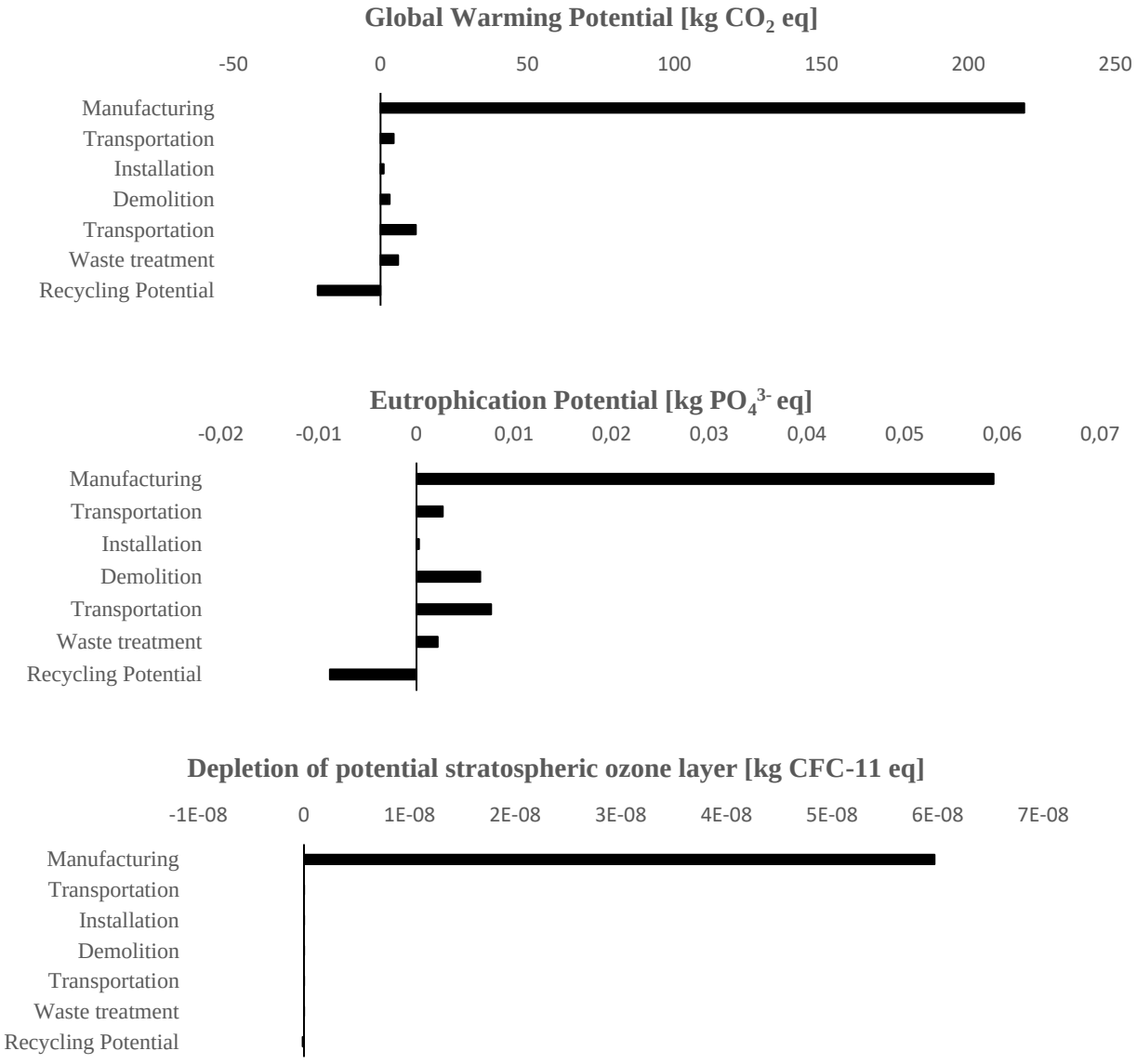

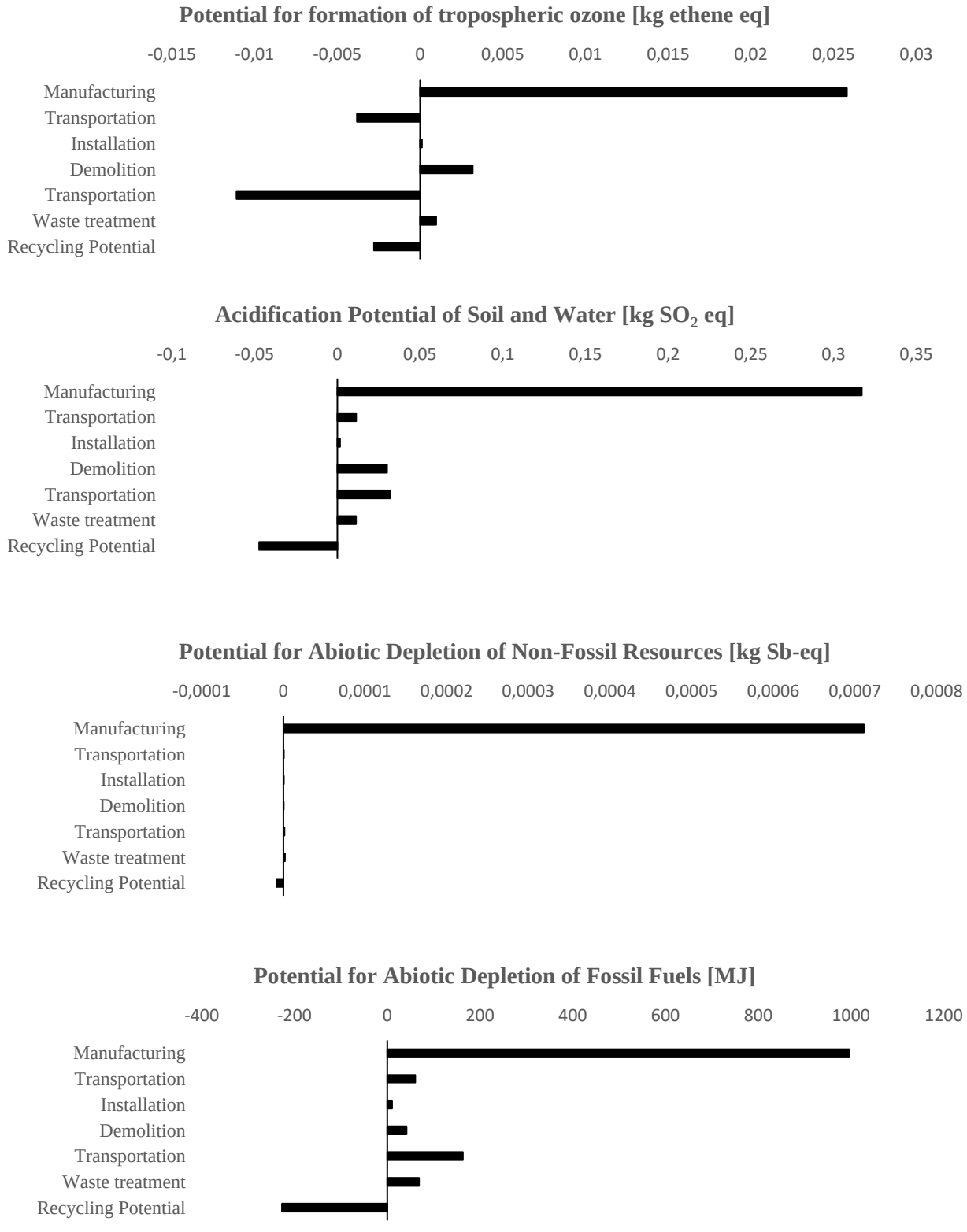

Figure 2-9. Environmental impact indicators per 1m3 of concrete class C30/37 (source:Ökobaudat)

2.1.7. Recycling of concrete

Recycling of concrete refers to the reuse of construction and demolition waste (CDW) as an inert filler on new concrete mixtures. The re-use of old structure fragments in new constructions are known since the Roman times, where remains of ceramic bricks and tiles have been shown to be reused as part of the city walls. In the Eifel Aqueduct in Cologne (ca. 80 AD), the binder included crushed brick fines [57] making it one of the first known examples of recycled binders. In the aftermath of the Second World War, many German cities lay in rubbles and there is a need for an immediate solution to clearing the rubble and simultaneously fulfilling the exorbitant need for construction materials in the reconstruction efforts. Until 1956, recycling plants in Germany produced an amount of 11.5 million m^3 of recycled aggregates which were integrated in nearly 175000 buildings [58]. After the reconstruction and the clean-up of the debris, most of these plants were shut down.

In the last decades, by a rise in environmental impact assessment and more stringent regulations in the construction industry, CDW reuse shifted from being a practical necessity to an ever more common practice. The recycling of concrete can be defined as a three-step procedure: demolition of the old structure, processing and re-use. The demolition aspect of the end-of-life stage is discussed in Chapter 6. Processing of CDW refers to the procedure of turning CDW into secondary raw aggregates that can be used in new concrete production. The recycling plants can be either stationary or mobile. The mobile crushing plants have the advantage that can be transported on site and therefore avoid transportation of waste, but they offer generally a lower output quality [59]. The output efficiency of mobile crushers ranges from 50 to 1200 tons/h [60]. The choice of the type of plant depends on the volume flow of CDW in the plant, the geographical area where the plant is located in terms of the proximity to the demolition sites, type of waste and economic aspects.

Figure 2-10. Mobile crushing plant (https://www.at-minerals.com/en/artikel/at_Combined_mobile_crushing_and_screening_plant_2029848.html)

The main components of a concrete recycling plant include a feeding area with storage capabilities, sieving, a crusher, magnetic strip to remove reinforcement and other metal parts, screening and sieving stages to obtain the required gradation, sorting devices and optional treatment steps such as washing and manual sorting of waste fragments [61]. Generally, the more steps the recycling plant has, the better the end quality of the recycled aggregates and the higher the production costs. The crusher can be of different types and has a significant impact on the quality of the aggregates. The main types of crushers include the jaw crusher (Figure 2-11) and the impact crusher (Figure 2-12).

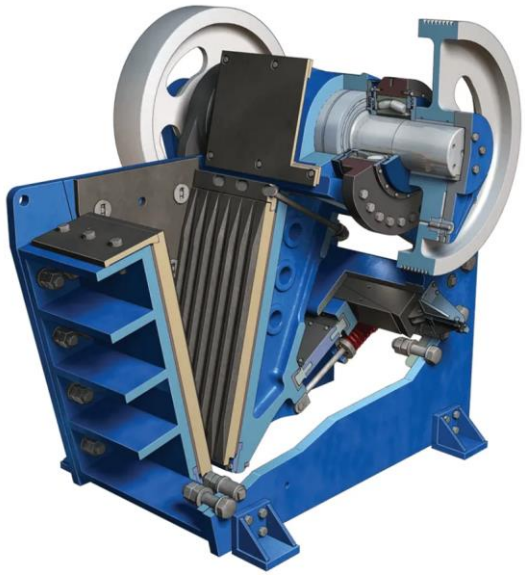

Figure 2-11. Jaw crusher (https://www.chinawearpro.com/jaw-crusher-parts/)

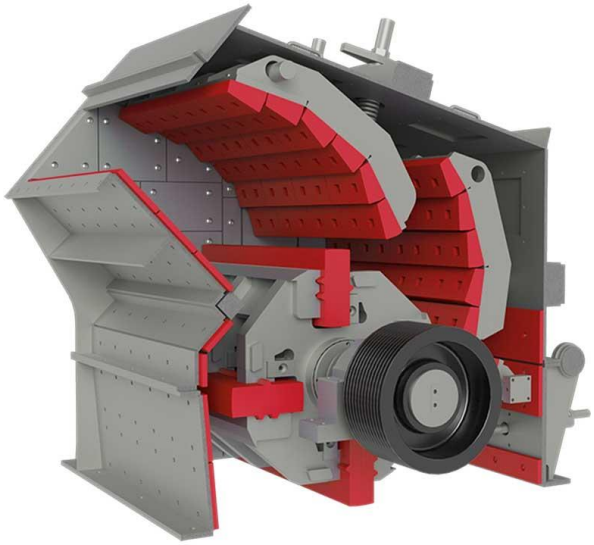

Figure 2-12. Impact crusher (https://www.zjfei.com/impact-crusher-wear-parts/)

Both of these mechanisms are constructed in steel and the inner layers are made of an abrasion resistant steel such as manganese steel or chrome steel. In the jaw crusher, one of the jaws is stationary, while the other is moveable through a hydraulic press. The CDW is crushed through the compressing effect of the jaws. On the other hand, the impact crusher utilises rotation of the waste through a central wheel and the impact of the material on inner walls of the chamber to cause fracture. The jaw crusher has an advantage of having a larger feed of materials, therefore a higher efficiency, but is limited in the minimum granulometry of product by the fixed distance between

the two jaws. The impact crusher on the other hand, produces aggregates that are rounder in shape compared to the jaw crusher.

After the demolition and treatment process, the recycled aggregates are ready to be used in new concretes or as a backfilled material. The latter is a common practice due to lower costs and very low qualitative parameters, but it offers only a temporary partial solution to the waste. The use of recycled aggregates in new concrete is discussed thoroughly in Section 2.3, 2.5 and Chapter 4.

Figure 2-13. Recycled aggregates as produced by a mobile jaw crusher

2.2. Standardization

The ultimate step of an industrial material or element is to have clear definitions of its integrity, as well as suggestions for its use. Recycled aggregates have been researched now for more than a decade, however, their inclusion in the European Norms is only partial. The goal of research is to give scientific recommendations on the use of these materials, as well as to set targets, limits and ideas for the use of different waste streams.

The standardization of concrete as a composite material, is done through several standards, which work in synergy in a hierarchical order from the constitutive raw materials to concrete as a construction element. An overview of the main technical European standards is given in Figure 2-14 (adapted from Müller, "Latest development in the standardization of concrete", Presentation) [62]

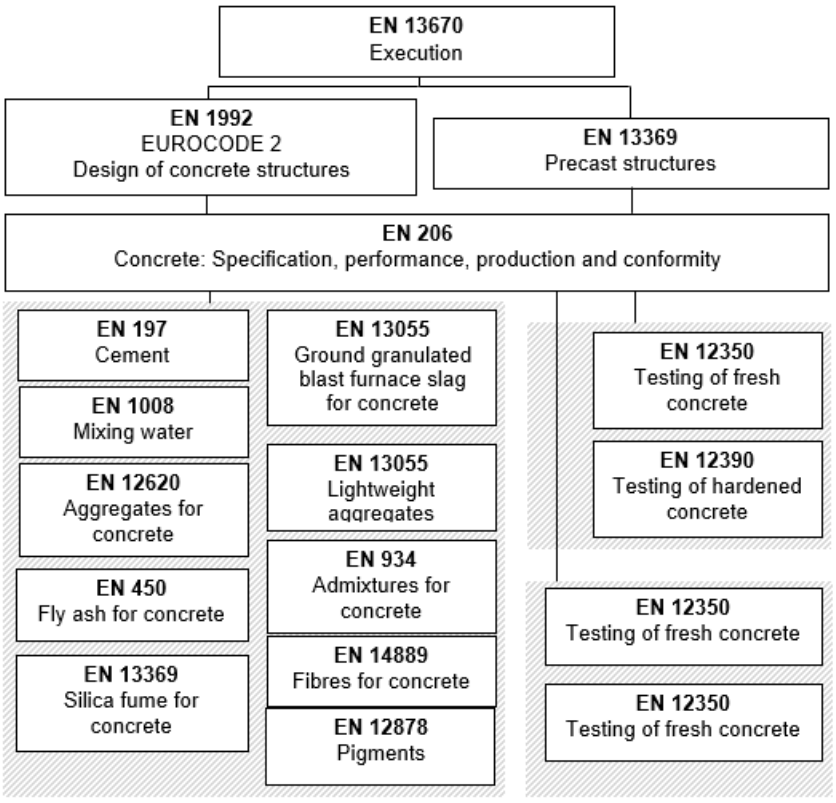

Figure 2-14 Overview of the European technical standards

2.2.1. Recycled concrete in the existing norms

During this brief review, a special focus will be given to standards EN 206-1 [63] and EN 12620 [64] as the main regulator mechanism for recycled aggregates. Furthermore, a comparison will be made between the national annexes of Luxembourg and the border countries. The following comparison is made with the state-of-the-art of the standardization at the time of the start of the research project in January 2019.

2.2.1.1. European Norms

The main European standard for concrete production is *EN 206-1: Concrete – Part 1: Specification, performance, production and conformity*. This standard defines different types of concrete: normal-weight, light-weight, heavy-weight; mixed on site, precast; compacted, self-compacting; and gives all the requirements for the constituents of concrete, such as: properties and their verification, limitations for concrete composition, specifications of concrete, delivery, production control, etc. The latest version of this standard dates back to 2013 and it was revised in 2016, when Annex A1 was added.

The main European standard for aggregates in concrete production is *EN 12620 – Aggregates for concrete*. It specifies the properties of aggregates obtained as natural, manufactured and recycled, in conformity with the abovementioned EN 206 – 1. It covers recycled aggregates with particle densities greater than 1500 kg/m3. Part of this standard are geometrical requirements such as sizes, grading, flakiness, shape, angularity, etc.; physical requirements such as resistance to fragmentation, wear, density, water absorption, bulk density, resistance to abrasion, etc; chemical requirements such as petrographic description, classification of constituents of coarse recycled aggregates, chlorides, carbonate content, etc.; durability such as freeze-thaw resistance, alkali-silica reactivity, etc.; evaluation and conformity , designation and marking and labelling. The latest version of this standard was updated in 2013. In addition, two other technical standards directly related to recycled aggregates are published:

- *EN 933-11, Tests for geometrical properties of aggregates – Part 11: Classification test for the constituents of coarse recycled aggregate*

– *EN 1744-6, Tests for chemical properties of aggregates – Part 6: Determination of the influence of recycled aggregate extract on the initial setting time of cement*

2.2.1.2. Definitions

The definitions of recycled aggregates in EN 206 and EN 12620, consider two main types of re-use: recycling and reclaiming. Reclaiming refers to the process of directly re-using the secondary raw materials by the same producer. One example is the use of washed aggregates, where, in case of surplus of fresh concrete production, the company washes the concrete in a fresh state by removing the cement and water part and recovering the coarse aggregates, which are still not bound in the matrix. The difference between the two is not very distinct in terms of definition. The standard states that when the reclaimed aggregates count for more than 5% of the total mass of aggregates used for concrete, they must be considered as recycled and be standardized according to 12620. These materials can be used for concrete production only internally from the producer. Recycled aggregates on the other hand have a clear definition as: *"aggregates resulting from processing of inorganic material previously used in construction"* [64]. This definition is consistent with all the other national versions of this standard.

2.2.1.3. Classification

The classification of recycled aggregates is given in the informative annex E. This classification is relevant only to coarse fractions with a diameter larger than 4 mm. The constituents of recycled aggregates are coded and a summary can be found in the following table.

Constituent	Description
Rc	Concrete, concrete products, mortar Concrete masonry units
Ru	Unbound aggregate, natural stone Hydraulically bound aggregate
Rb	Clay masonry units (i.e. bricks and tiles) Calcium silicate masonry units Aerated non-floating concrete
Ra	Bituminous materials
FL	Floating material in volume
X	Other: Cohesive (i.e. clay and soil) Miscellaneous: metals (ferrous and non-ferrous), non-floating wood, plastic and rubber Gypsum plaster
Rg	Glass

Figure 2-15. Different fractions of waste codes according to Annex E of EN12620:2002 [4]

The proposed classification is based on these specific waste classes and is represented in table 20 of annex E (Figure 2-15). There are in total 9 categories that depend not only on the type of waste, but also on its content and the combinations between different fractions. This is based on the standard EN 933-11 where the assessment method is described. Even though it may not be very practical, this methodology of classification is important in an industrial sense because it makes possible to trace the origin of waste and to have a common method of evaluating their use in concrete. The only aspect that may be improved is the percentage categories and their allocation. It is still to be evaluated how this change of the constituents has an effect on the material properties and what sensitivity is there.

Regarding the substitution ratios, this standard first introduces a larger division into two types: A and B, where type A includes Rc_{90}, Rcu_{95}, Rb_{10-}, Ra_{1-},FL_{2-},XRg_{1-} and type B includes Rc_{50}, Rcu_{70}, Rb_{30-}, Ra_{5-},FL_{2-},XRg_{2-}. Definitions on the terminology can be seen on Figure 2-15 and Figure 2-16, where the different types of recycled aggregates are described depending on the waste fraction they contain. The number in subscript describes the amount of the material in percentage by mass. For example, Rb_{30-} means recycled aggregates containing clay masonry units, calcium silicate masonry units or aerated non-floating concrete in less than 30% of its total mass. The remaining can be described through another waste code or can be heterogeneously mixed waste with no dominant fraction. The substitution ratio depends on the type and the exposure classes and is limited to 50%. As an indication, type A aggregates from known origins are allowed to be used

in exposure classes to which the original concrete was used, with a replacement ratio of 30%. Type B aggregates should not be used in concrete classes higher than C30/37. Tests on shrinkage, creep and modulus of elasticity are suggested before using this material. It should be noted that the use of recycled aggregates may affect the setting time. This standard does not cover recycled sands.

Table 20 — Categories for constituents of coarse recycled aggregates

Constituent	Content Percentage by mass	Category
Rc	**≥ 90**	Rc_{90}
	≥ 80	Rc_{80}
	≥ 70	Rc_{70}
	≥ 50	Rc_{50}
	< 50	$Rc_{Declared}$
	No requirement	Rc_{NR}
Ru	**≥ 90**	Ru_{90}
	≥ 70	Ru_{70}
	≥ 50	Ru_{50}
	< 50	$Ru_{Declared}$
	No requirement	Ru_{NR}
Rc + Ru	**≥ 95**	Rcu_{95}
	≥ 90	Rcu_{90}
	≥ 70	Rcu_{70}
	≥ 50	Rcu_{50}
	< 50	$Rcu_{Declared}$
	No requirement	Rcu_{NR}
Rc + Ru + Rg	≥ 90	$Rcug_{90}$
	≥ 70	$Rcug_{70}$
	≥ 50	$Rcug_{50}$
	< 50	$Rcug_{Declared}$
	No requirement	$Rcug_{NR}$
Rb	**≤ 10**	Rb_{10}
	≤ 30	Rb_{30}
	≤ 50	Rb_{50}
	> 50	$Rb_{Declared}$
	No requirement	Rb_{NR}
Ra	≥ 95	Rc_{95}
	≥ 80	Rc_{80}
	≥ 50	Rc_{50}
	≥ 40	Rc_{40}
	> 30	Rc_{30}

	≤ 30	Ra_{30}
	≤ 20	Ra_{20}
	≤ 10	**Ra_{10}**
	≤ 5	**Ra_{5}**
	≤ 1	**Ra_{1}**
	No requirement	**Ra_{NR}**
Rg	≤ 2	Rg_{2}
	≤ 5	Rg_{5}
	≤ 25	Rg_{25}
	No requirement	Rg_{NR}
X	≤ 1	X_{1}
X + *Rg*	**≤ 0,5**	**$XRg_{0,5}$**
	≤ 1	**XRg_{1}**
	≤ 2	**XRg_{2}**
	No Requirement	**XRg_{NR}**
	Content cm^3/kg	
FL	**≤ 0,2** [a]	**$FL_{0,2}$**
	≤ 2	**FL_{2}**
	≤ 5	**FL_{5}**
	≤ 10	FL_{10}
	No Requirement	**FL_{NR}**

[a] The ≤ 0,2 category is intended only for special applications requiring high quality surface finish.

where, according to EN 933-11:

Figure 2-16. Classification of waste fractions according to Annex E of EN12620:2002 [4]

Table E.2 — Maximum percentage of replacement of coarse aggregates (% by mass)

Recycled aggregate type	Exposure classes			
	X0	XC1, XC2	XC3, XC4, XF1, XA1, XD1	All other exposure classes [a]
Type A: (Rc_{90}, Rcu_{95}, Rb_{10}, Ra_{1}, FL_{2}, XRg_{1})	50 %	30 %	30 %	0 %
Type B [b]: (Rc_{50}, Rcu_{70}, Rb_{30}, Ra_{5}, FL_{2}, XRg_{2})	50 %	20 %	0 %	0 %

[a] Type A recycled aggregates from a known source may be used in exposure classes to which the original concrete was designed with a maximum percentage of replacement of 30 %.

[b] Type B recycled aggregates should not be used in concrete with compressive strength classes > C30/37.

NOTE For the risk of alkali-silica reaction with recycled aggregates, see EN 12620:2002+A1:2008, G.3.2.

Figure 2-17. Table E.2 on the maximum percentage of replacement ratios [4]

NOTE For the risk of alkali-silica reaction with recycled aggregates, see EN 12620:2002+A1:2008, G.3.2.

Table E.3 — Recommendations for coarse recycled aggregates according to EN 12620

Property [a]	Clause in EN 12620:2002+A1:2008	Type	Category according to EN 12620
Fines content	4.6	A + B	Category or value to be declared
Flakiness Index	4.4	A + B	$\leq FI_{50}$ or $\leq SI_{55}$
Resistance to fragmentation	5.2	A + B	$\leq LA_{50}$ or $\leq SZ_{32}$
Oven dried particle density ρ_{rd}	5.5	A	$\geq$ 2 100 kg/m^3
		B	$\geq$ 1 700 kg/m^3
Water absorption	5.5	A + B	Value to be declared
Constituents [b]	5.8	A	Rc_{90}, Rcu_{95}, Rb_{10}, Ra_{1}, FL_{2}, XRg_{1}
		B	Rc_{50}, Rcu_{70}, Rb_{30}, Ra_{5}, FL_{2}, XRg_{2}
Water soluble sulfate content	6.3.3	A + B	$SS_{0,2}$
Acid-soluble chloride ion content	6.2	A + B	Value to be declared
Influence on the initial setting time	6.4.1	A + B	$\leq A_{40}$

[a] Category NR (no requirements) applies for all other properties not stated in this table for which a category NR can be declared according to EN 12620.

[b] For special applications requiring high quality surface finish the constituent *FL* should be limited to category $FL_{0,2}$.

Figure 2-18. Table E.3 on the recommendations for coarse recycled aggregates [4]

2.2.1.4. Physical properties

The physical properties and their limits for recycled aggregates are treated in chapter 6 of this standard. Eight different aspects are described.

The water soluble sulphate and chlorides content can be tested in accordance to EN 1744–1. Four different classes are defined based on the assessed value. The categories are displayed on table 23 of this standard (Figure 2-19).

Table 23 — Categories for maximum values of water-soluble sulfate content of recycled aggregates

Water-soluble sulfate content Percentage by mass	Category *SS*
≤ 0,2	$SS_{0,2}$
≤ 0,7	$SS_{0,7}$
≤ 1,3	$SS_{1,3}$
No requirement	SS_{NR}

Figure 2-19. Table 23 on the content of water-soluble sulphate content on recycled aggregates [4]

In recycled aggregates, the presence of organic matter is common, especially in the sub structural elements such as foundations and deposits. The presence of elements such as humic acid and fulvo acids can alter the setting time of cement. Their effect on the hardening time of mortar should not be greater than 120 min and they should not lower the compressive strength of mortars with more than 20% at 28 days. The chemical tests on aggregates are described in EN 1744.

Table 24 — Categories for influence of water-soluble materials from recycled aggregates on the initial setting time of cement paste

Change in initial setting time, *A* min	Category *A*
≤ 10	*A*10
≤ 40	*A*40
> 40	$A_{Declared}$
No requirement	A_{NR}

Figure 2-20.Table 24 on the influence of water soluble materials on the initial setting time of cement paste [4]

With regards to volume stability, two relevant aspects are present: drying shrinkage and expansion. The later is not yet fully investigated, therefore, no standardization is present. Drying shrinkage should be limited to 0.0075% (in accordance to EN 1367-4) [65]

Chlorides are expected to be calculated through EN 1744-5 [66]. According to the document, the achieved value is likely to be an overestimation, however it should be still used as it will provide an extra margin of safety. Sulphates may also be present in recycled aggregates and could lead to expansive disruption of concrete. Additionally, it is important to assess that the original concrete does not possess reactive aggregate and that the alkali content of the recycled aggregates is limited. The standard proposes to treat the recycled aggregates as being a reactive aggregate, unless proven otherwise.

Other constituents of aggregates can adversely affect the rate of hydration of cement altering the rate of setting and hardening of concrete. Humus and sugar-type materials are two examples of substances that have such an effect. Some clay mixtures also adversely affect the rate of development of strength, the strength and the durability of concrete in which they are incorporated.

Constituents of recycled aggregates that can adversely affect the rate of setting and hardening of concrete can be inorganic, and therefore not detected by the procedures given in 15.3 of EN 1744-1:2009. The procedures given in EN 1744-6 should be used for recycled aggregates. These two basic norms are completed as described in the text by various testing standards, such as *EN 933-11- Tests for geometrical properties of aggregates. Classification test for the constituents of coarse recycled aggregate.*

2.2.1.5. Luxembourg

In Luxembourg, there is a national version of EN 206: Document Combine <Beton>, the latest version of which dates back to 2007. This norm is completed by the European EN 12620, where the quality properties of aggregates are described. As an addition, a specification on aggregates: Cahier des Charges: Granulats (CDC-GRA08), published by Ponts et Chaussees Luxembourg, acts as a complementary national standard for aggregates. The latest version of this document dates back to 2008.

In these documents, recycled aggregates are narrowly mentioned, making their standardization in the country still significantly unclear. In the EN 206:2007, page 33, it is stated that recycled aggregates need to be priorly certified for use in concrete by a certified laboratory which is compliant with the German standards.

In the CDC-GRA08, a definition for recycled aggregates is present. This definition comes directly ratified from the EN 12620 and offers no specificities related to the country. The domain of application is strictly addressed to roads, pavements and secondary infrastructural elements. It is however missing the mechanical properties, limit values and other relevant specifications that could serve as a guidance for industries. It is also unclear on the exact restrictions for using such materials in concrete, as this document does not clearly state any restrictive qualities for recycled aggregates.

It can be stated that for the moment, in Luxembourg there are no specifics for the quality of recycled material. Recycled aggregates are treated as raw aggregates and are expected to undergo the same quality assessment. Following that, there is also no suggestion on the use of this material on different purposes or suggestions on substitution rates.

2.2.1.6. Germany

In Germany, the national version of EN 206 is DIN EN 206: 2017-01. This is the latest update of the norm and offers two distinct definitions of recycled aggregates. The first is the main definition from the European version of the norm. In addition, reclaimed aggregates are also discussed, by stating that the industries can use internally recovered aggregates up to 5% of the total amount. It is unclear if this refers to weight or volume. If quantities exceed the 5% limit, it is required to be divided into fine and coarse fractions. In these cases, their uses are predicted to be according to EN 12620 as if they were normal recycled aggregates. The properties of recycled aggregates are ratified from annex E of the EN 12620 standard and they are to be considered through the same quality controls. There is also a line present related to the hardening problem of recycled aggregates mixtures, even though no technical suggestions are given.

In addition, Germany has approved the EN 12620 and EN 933-11 norms, which contain remarks on recycled aggregates as described in the previous section. Concerning national regulations, the old German norm DIN 4226 of the German Institute for Standardization, contained the German requirements for concrete and mortar. More specifically, the fourth part of this document contained suggestions on the use of recycled aggregates. This standard is currently partly annulled, and the first three parts are included in the DIN EN 12620. The part regarding recycled aggregates is DIN 4226-102:2017, which is a much more simplified version of the first norm, taking in consideration and being conform with the European standard.

2.2.1.7. France

In France, the two main European norms are adapted into national standards, with additions in the form of national annexes, further specifying the requirements using national industrial

experience. The latest version of NF EN 206-1, dates back to 2014 and defines two types of secondary aggregates: recovered crushed aggregates which are strictly coming from the crushing of hardened concrete and recycled aggregates which are defined as aggregates obtained from treatment of minerals previously used in construction.

In terms of classification, the French standard foresees a slightly different typology classification of the recycled fractions. The waste composition method is kept consistent with EN 12620 (please refer to Figure 2-15 and Figure 2-16). Three types of recycled aggregates are defined:

- Type 1 – At least 95% unbound concrete or aggregates and the characteristics are defined as CR_b
- Type 2 – At least 95% unbound concrete or aggregates and the characteristics are defined as CR_b Or CR_c
- Type 3 – At least 70% unbound concrete or aggregates and the characteristics are defined as CR_b or CR_c or CR_d

Table 2-1. Types of recycled aggregates (NF EN206-1:2014)

Code	Principal constituents according to NF EN 12620	Secondary constituents				Frequency of tests	
		Categories according to NF EN 12620				Temporary	Quantitative
CR_B	Rcu_{95}	Rb_{10-}	Ra_{1-}	$XRg_{0.5-}$	$FL_{0.2-}$	2 times/month	1 time/2000 tonnes
CR_C	Rcu_{90}	Rb_{10-}	Ra_{1-}	XRg_{1-}	FL_{2-}		
CR_D	Rcu_{70}	Rb_{30-}	Ra_{10-}	XRg_{2-}	FL_{2-}		

What can be observed in the table is that the French standard considers only waste fractions with a high amount of unbound concrete waste (more than 70%). It also sets strict requirements for other constituents, such as clay, bitumen, floating particles and other waste fractions. It also

determines the frequency of quality control, which is a special feature considering other regional standards.

Other characteristics to be verified are:

- Water soluble sulphate
- Volumetric mass
- Influence on the start time of hardening
- Flattening coefficient
- Los Angeles
- Acid soluble chlorides
- Water absorption after 24 h
- Free alkaline according to LPC no37

Substitution rates are given in the table below depending on the exposition class:

Table 2-2. Substitution rates of recycled aggregates (NF EN206-1:2014)

Type of recycled aggregate	**Exposition classes**			
	X0	**XC1, XC2**	**XC3, XC4, XF1, XD1, XS1**	**Others**
Type 1	60 %	30 %	20 %	0 %
Type 2	40 %	15 %	0 %	0 %
Type 3	30 %	5 %	0 %	0 %
Sand	30 %	0 %	0 %	0 %
Aggregates of type 2 and 3 as well as sands cannot be used for concretes of higher classes than C25/30				

The French standard allows for a higher replacement ratio than the European standard, if the recycled aggregates are qualitative and the exposition class is low. It does however set a limit on the targeted quality of concrete.

The conformity of aggregates, including the recycled aggregates is regulated through the national version of EN 12620, completed with the national annex NF P 18-545.

2.2.1.8. Belgium

Belgium currently uses the national version of the European norm NBN EN 206, dating back to 2014. It is complemented by the Belgian standard NBN B 15-001 dating in 2012. In this standard, the use of recycled aggregates is foreseen, given that they meet some quality requirements. The substitution ratio is currently limited to 20% by mass, excluding fractions smaller than 4mm.

There are two types of recycled aggregates defined:

– A+ type, consisting of only concrete debris
– B+ type, consisting of mainly concrete debris with masonry debris up to 30% of the mass

The compressive strength class is limited to C30/37 for A+ and C20/25 for B+ aggregates.

A | Overview of the field of application of A + and B + aggregates in unreinforced concrete (prNBN B 15-001: 2017).

	Unreinforced concrete						
	Environmental classes according to the new version of NBN B 15-001						
Type of aggregates	E0	EI	EE1	EE 2	EE3, EA1	ES1, ES2, ES3	EE4, ES4, EA2, EA3
Concrete aggregates type A +	50%	50%	50%	20%	20%	20%	0%
Mixed aggregates type B +	20%	20%	20%	0%	0%	0%	0%

B | Overview of the application range of A + and B + aggregates in reinforced concrete (prNBN B 15-001: 2017).

	Reinforced concrete						
	Environmental classes according to the new version of NBN B 15-001						
Type of aggregates	E0	EI	EE1	EE 2	EE3, EA1	ES1, ES2, ES3	EE4, ES4, EA2, EA3
Concrete aggregates type A +	-	30 %	30 %	20%	20%	0%	0%
Mixed aggregates type B +	-	20%	0%	0%	0%	0%	0%

Figure 2-21. Recycled aggregate types (NBN EN206)

The table above shows the foreseen replacement ratios according to the exposure classes as defined in the national standard. Further specifications on aggregate quality are described in NBN EN 12620.

2.3. Mechanical aspects of concrete recycling

2.3.1. State-of-the-art

The material properties can be divided into three aspects:

- Physical properties
- Chemical properties
- Mechanical properties

2.3.1.1. Physical properties and mechanical properties

Physical properties and chemical properties are usually tested in aggregates. In Europe, these properties are regulated through the EN standards and national annexes (please refer to chapter on standardization) This part is especially important for recycled aggregates, as it offers a qualification and makes a comparison to natural aggregates possible. Furthermore, the assessment of physical properties is crucial in the concrete mixture design phase. Following, some of the most important aspects will be discussed through existing literature and studies.

2.3.1.2. Gradation

The granulometric gradation of recycled aggregates is highly dependent on the production phase and on the initial gradation of the original concrete. The maximum size will be determined as the minimum opening of the crusher. This is the case for jaw crushers and cone crushers. Impact crushers, on the other hand, will deliver a granulometric distribution which is limited only by the maximum size of the original aggregates. A very important aspect for recycled concrete is the distinction of fractions between sand (<4 mm) and coarse aggregates (> 4 mm) as for the moment,

sandy fractions are not used for recycling in new concrete mixtures. This is due to the presence of unhydrated cement in the fine fractions [67]. Further studies have shown the negative effects of fine particles in concrete recycling [68][69]. However, the recycled sand normally contains a significant amount of reactive material, because during the crushing of CDW, the very fine fraction which is mostly cement, microsilica, blast furnace slag or other reactive particles are deposited in the sandy fraction of the waste. Therefore, this part does have an effect on increasing the compressive strength of concrete [70], but may cause problems in terms of dimensional stability of the mixtures.

2.3.1.3. Shape index and flakiness index

These parameters are used to assess the geometrical properties of coarse aggregates and characterize the elongation of the particles. For recycled coarse aggregates, the particle shape is generally coarser, and more irregular compared to natural aggregates. For jaw crushed CDW, an elongated shape is distinctive, due to the working principle of this type of crusher. The typical range of the SI is 0.07% - 0.47%.

2.3.1.4. Crushing value, Fine content and Sand equivalent index

The crushing value expresses the predisposition of bulk aggregates to crush under a compressive load. For recycled aggregates, it is dependent on the type of waste and not studied in depth in literature. Therefore, typical values cannot be assessed.

The fines content is a property that is influenced by the quality of pre-treatment of crushed CDW. The fine particles affect the workability and cohesion of fresh concrete and in literature, the typical values vary depending on whether it is an all-in gradation, or specific sand or coarse aggregate. Normally, their content does not exceed 2%.

To detect the clay content of the fines, sand equivalent tests are done. In terms of standardization, a limit value is only given on the Spanish standard (EHE-08,2008) and is required to be below 70 or 75, depending on exposure class. The clay content can increase in poorly stored fractions.

2.3.1.5. Density and water absorption

The density, considered as a bulk, is a very important property for concrete aggregates. Normally, the bulk density of normal aggregates used in concrete ranges from 1300 to 1750 kg/m^3 [71]. Water absorption is linked to the porosity of the material and the potential of water to flow into the pores. It is however distinct from porosity, as not all pores can be filled with water. Especially the internal porosity is unlikely to hold water. Therefore, in practice water absorption is the used parameter. Its value depends on the type of rock and its mineralogy. For example, porous sandstone aggregates express a water absorption of 5%, expanded shale 10% and trap rock 0.5% [71].

Recycled aggregates show a special condition in this aspect. As they are a result of a secondary crushing process, microcracks and microfaults are often observed in their matrix, which increases the natural porosity and sequentially lowers the density. Furthermore, the principle of concrete production relies on the bonding between the cement paste and the surface of the aggregate. During this phenomenon, the cement paste locks into the micro-porosity of the aggregates and hardens on the process. When recycled, this locking mechanism is partially broken, leaving the embedding space open. Some of the typical values from literature is summarized on the following table. It can be seen that the dry bulk density in recycled aggregates is 4%-18.6% lower compared to natural aggregates, while the water absorption can be up to 17.97 times higher.

Table 2-3. Bulk density and water absorption in recycled aggregates

Natural aggregates	**Recycled aggregates**	**Difference [%]**	**Authors**
Dry bulk density [kg/m3]			
1517	1234	-18.6	*Evangelista, de Brito* [69]
1560	1430	-8.3	*Cabral et al* [70]
1490	1433	-3.8	*Katz* [67]
1406	1329	-5.5	*Padmini et. al* [72]

1422	1163	-18.2	*Bogas et al.* [73]
Water absorption [%]			
0.8	13.1	+1637	*Evangelista, de Brito* [69]
0.42	7.55	+1797	*Cabral et al* [70]
3.1	8.8	+283.8	*Corinaldesi* [68]
0.5	3.3	+660	*Katz* [67]
0.3	5.0	+1666	*Padmini et. al* [72]
1.68	9.05	+538.7	*Bogas et al.* [73]
1.1	6.2	+563.6	*Salesa et. al* [74]

2.3.1.6. Resistance to abrasion

Due to the adhered mortar, the recycled aggregates generally express a higher Los Angeles value, which is dependent on the granulometric distribution. For all-in-one aggregates, it can be up to 53, while for coarse aggregates, it can be up to 40.22 [75].

2.3.1.7. Compressive strength and elastic modulus

The compressive strength is the main parameter used to define the quality of concrete. It is also used to describe the class of the concrete. Parameters that influence the compressive strength of the concrete include the class of the cement, the strength of the aggregates, the use of additives, the water to cement ratio, etc. The estimation of the influence of each parameter in the compressive strength of recycled concrete is more complicated compared to normal concrete. The reason lies in the nature and properties of this material. Recycled aggregates are very heterogeneous, and this aspect increases considerably the number of influencing parameters. Moreover, the presence of unhydrated cement paste alters the water to cement ratio and an exact assessment of this influence is not possible, as the origin of this waste is normally unknown. Furthermore, the presence of the paste does not appear in a certain trend in the material and there is currently no standardized testing

method. This makes it difficult to predict its presence in recycled aggregates. However, while considering present studies on the topic, the compressive strength of recycled concrete is not considerably worse than that of natural concrete. Through the graph in Figure 2-22, it can be seen that the effect of recycled aggregates on the compressive strength of concrete is minor. In some cases, the use of recycled granules increases the initial compressive strength of the concrete. This is due to the presence of unhydrated cement paste in the aggregates. It is however important to observe that this trend is not common in all of studies. While the reason behind this is unclear, it can be due to the heterogeneity of the material in terms of geographical location, treatment and concrete mixture used. It can be concluded that by using a full substitution of recycled aggregates, the compressive strength of concrete will be approximately 20% lower compared to normal concrete.

Regarding the modulus of elasticity, there is a decrease when recycled aggregates are used. This is due to the presence of old mortar which has a lower elasticity [76]. Quantitatively, this decrease is up to 20% when a full replacement is made. This is in line with the recommendations from RILEM (1994) [59]. Furthermore, Corinaldesi [68], concludes that the decrease of elastic modulus due to recycling is 17% and this is in agreement with the Italian standard.

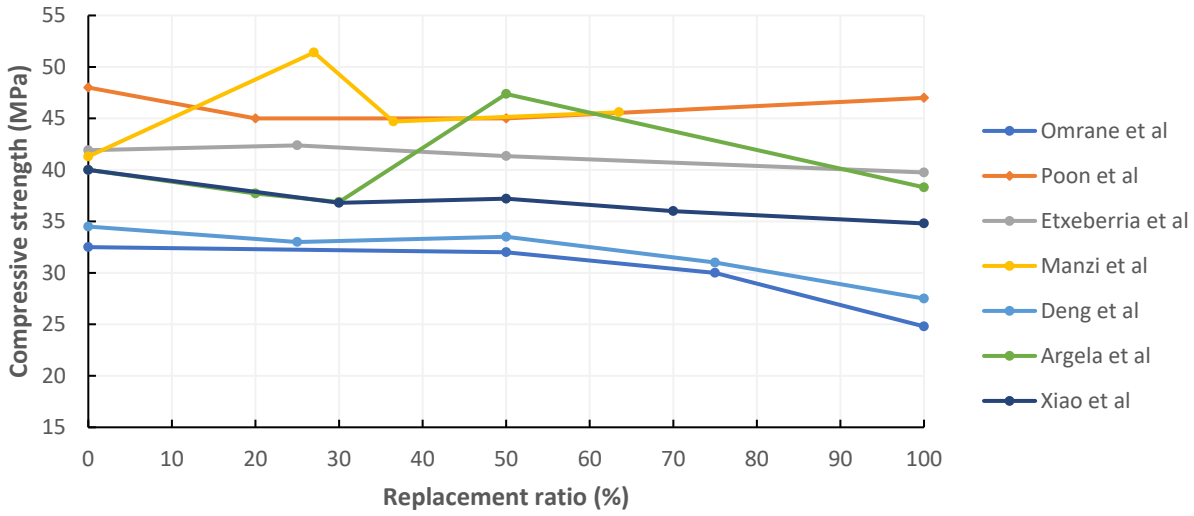

Figure 2-22. Compressive strength of recycled concrete based on the replacement ratio [59], [76]–[81]

2.3.1.8. Bending and splitting resistance

Bending and splitting tests are commonly used to describe the tensile resistance of concrete. This is important when designing the concrete for resistance to shear. It is also important in structures prone to fatigue loading, such as slabs, bridges, tanks, etc.

Similarly, to the compressive strength, there appears to be a decrease in the tensile strength of the recycled concrete. The relationship between the tensile strength of the original concrete and the recycled appears to be linear (Figure 2-23). However, the decrease is less than previously discussed. Argela et al. [59] report this difference to be 10% based on previous studies. This is due to the microstructural interfacial action of recycled concrete, where failure does not only develop on the interfacial transition zone, but also on the recycled aggregates [76].

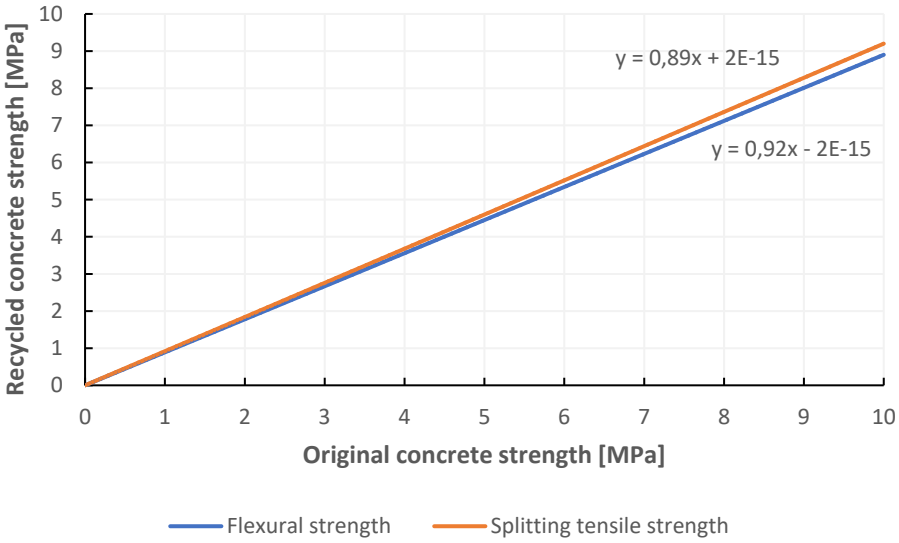

Figure 2-23. Tensile splitting strength and flexural strength on recycled aggregates (adapted from Argela et al [59]*)*

2.3.1.9. Adhered mortar content

At present moment, there is no standardized way to assess the quantity of the adhered mortar in recycled concrete aggregates. However, there are several experimental ways that it can be done, such as the sulphate solution freeze-thaw method and the quench hot method. c The sulphate solution freeze thaw method is a combination of an acidic solution methodology and freeze-thaw

separation. The proposed methodology includes the soaking of recycled aggregates in a 26% sodium sulphate solution for 24 hours and then introducing 5 freeze-thaw cycles. After washing, the difference in weight is the content of residual mortar. The quench hot method is a thermic based procedure that requires the aggregates to be heated in an oven at 800°C for two hours, then immediately placed in cold water. The thermic shock releases the bonded particles. Both of these methods however, are not economically and practically viable as they require both energy and extra workload. Abbas et al [82] introduce an alternative way through image analysis. This method consists of producing flat slabs of recycled concrete and then polishing their surface before taking high resolution images. The analysis of these images through a computer software allows for an image recognition of different particles in the matrix. There are several drawbacks of this procedure. First, concrete must be produced to assess the amount of bonded mortar. Therefore, two different mixtures need to be produced for each batch. This increases the workload and costs. Secondly, the mixtures need to be produced with white cement to achieve the necessary contrast for the image analysis. The main method of considering this mortar content in new concrete, proposed by Abbas [83], is the equivalent mortar volume. This procedure considers the mixture's cement content as comprised of the new cement and the old mortar. Thus:

$$V_{RCA}^{RCA-concrete} = \frac{V_{NA}^{NAC} \cdot (1 - R)}{(1 - RMC) \cdot \frac{SG_b^{RCA}}{SG_b^{OVA}}} \quad (2\text{-}1)$$

Where $V_{RCA}^{RCA-concrete}$ is the volume of recycled concrete, V_{NA}^{NAC} is the volume of natural aggregates, RMC is the residual mortar content, SG_b^{RCA} is the specific gravity if recycled aggregates, SG_b^{OVA} is the specific gravity if natural aggregates and R is the substitution ratio.

The study shows that the use of such method yields recycled concretes that have strength and durability parameters that are comparable to natural concretes. In the case of compressive strength, an increase was observed. The only drawback is the fact that the mortar content must be estimated using one of the methods described in the previous paragraph and will possibly be still an estimation.

In regards to the effect that the adhered mortar has on the material properties, the study by de Juan and Gutierrez [84] offers a wide panorama on this aspect. The increase of adhered mortar lowers the fraction size of the aggregates. It has a considerable effect on the bulk density and the saturated surface dry density, showing a lowering of approximately 22% when fully recycled. The water absorption is consequently higher by approximately 18%. This result is somewhat higher to other literature that suggests a change of about 10%. The study also shows that different assessment methods may yield significantly different results, highlighting the need for a standardized procedure. Considering the abrasion resistance, it is in a direct proportion with the adhered mortar. When the mortar content is high, it is this fraction that gets grinded first during the Los Angeles test, therefore the coefficient results to be higher. Additionally, the sulphate content of recycled aggregates is shown to be higher due to the sulphate content present in the mortar. On the other hand, no significant relationship was found between the quality of the original concrete and the recycled aggregates.

2.3.1.10. Shrinkage

There are many types of shrinkage, such as *thermal, plastic, chemical, drying*, etc. However, there are three main types that have the most influence on concrete elements: plastic shrinkage, autogenous shrinkage and drying shrinkage.

Plastic shrinkage happens in early stages of concrete casting. It is mainly affected by water evaporating differently in the surface and in the middle of the elements. The loss of water in the surface is naturally compensated by water flowing from the inside to the outside since cavities start to form. This causes the surface to crack. The cracks can be as large as 10000 microstrain [85] and differ from the type of concrete. The formation of cracks would also lead to a movement of the coarse aggregate particles, which would move in the direction of the cracks. Plastic shrinkage cracks are usually shallow, parallel and in the direction of the wind. It is particularly problematic for reinforced elements and can be avoided by curing methods, such as sheltering the fresh concrete from wind, sunshine or extreme temperatures.

Autogenous shrinkage, unlike plastic shrinkage, is not affected by outside conditions, but rather by the microscopic chemical activity happening in the early stages of concrete production. It was

first described by Lyman in 1934 [86] and was noted that it is prominent especially in low w/c contents. Nowadays, with the rise of high strength concrete types and the usage of admixtures, autogenous shrinkage has come to light as a practical problem. To better assess the quantity of autogenous shrinkage, Nawa and Horita [87], considered the main equation for the hydration of C_3S and transformed the elements into their proper volumes using their molecular weight:

$$C_3S + 5.2H \rightarrow C_{1.75}SH_{3.9} + 1.3CH$$

$$72.8\ cm^2 + 93.6\ cm^3 \rightarrow 95.9\ cm^3 + 42.9\ cm^3$$

$$166.4\ cm^3 \rightarrow 138.9\ cm^3$$

In the chemical equilibrium above, the hydration of cement is described. Cement phases (C_3S) come into contact with water, resulting in two hydrates, calcium silicate hydrates (CSH) and calcium hydroxide (CH), which is also referred to as Portlandite. These two resultants represent the matrix of cement after hydration. Observing the chemical equation, there is a quantitative weight reduction of about 16.5%. This is the main idea behind chemical shrinkage. Autogenous shrinkage is directly linked to it but differs in the fact that at a certain point, a solid skeleton is formed within the concrete and it restrains the concrete's ability to expand. Therefore, the value for autogenous shrinkage over time is lower than the theoretical value of chemical shrinkage. There are two main methods of measuring autogenous shrinkage. The first method measures volume change by submerging a specimen fitted in a watertight rubber balloon in water and taking values of the volume change in the water tank over time. The most popular method though, includes linear length measurements, similar to the measurement of drying shrinkage. The principle is to use a strain gauge to measure the change of length in concrete during the hardening process. However, in difference to drying shrinkage, a teflon sheet, film and steel mold make sure that the specimen is fully sealed and the water content is not altered by outer conditions.

Drying shrinkage is probably the most predominant type of shrinkage and it is especially interesting for recycled concrete mixtures. Drying shrinkage phenomena happens as result of water evaporation on the concrete specimen. Generally, when producing concrete, much more water than the volume dictated from the w/c ratio has to be inserted to assure workability (if no additives are

used). After the curing process, during the drying stage, the excess water that is not chemically bound with the cement, comes up to the surface and starts to evaporate. The reduction of length per unit length, relating to the total volume loss is called drying shrinkage. In mixtures containing recycled aggregates, shrinkage is affected differently in terms of quantity, due to the cement paste present in the crushed CDW. According to research, shrinkage is approximately linear with the water content.

There are three main mechanisms responsible for drying shrinkage. The first is attributed to the disjointing pressure occurring on the surface of C-S-H (calcium silicate hydrate). During the production and curing, the cement paste would absorb water which would form around calcium silicate molecules a layer in the shape of a film. Due to the vicinity of molecules, the presence of water would actually create pressure pushing away the particles and causing a volume increase. When water evaporates, the particles are disjointed and brought together by van der Waals forces. This is the moment shrinkage is observed.

The second mechanism is the capillary surface tension effect. This happens as a result of the increase in air volume during the hydration. As air pockets are formed, capillary pores are created. The interface (meniscus) is responsible for added tensile stress in the capillaries. The whole process would eventually create hydrostatic compression stress in the pores, resulting in the C-S-H body pulling closer, as described by Powers [88]. Mathematically, this effect can be described using the Kelvin and Laplace equations.

$$ln(RH) = -\frac{2\sigma}{r}\frac{M}{\nu RT}cos\theta \tag{2-2}$$

Where Rh is the relative humidity, σ is the surface tension of water, M is the mass of a mole of water, θ is the contact angle of water and cement body, r is the pore radius, ν is the density of water, R is the ideal gas constant and T is the temperature in Kelvin.

The Laplace equation is as follows:

$$p_c - p_v = \frac{2\sigma}{r} cos\theta \tag{2-3}$$

Combining the two equations:

$$p_c - p_v = -\frac{vRT}{M} ln(RH) = -\frac{ln(RH)}{K} \tag{2-4}$$

The equation shows that the suction pressure is inversely proportional to the relative humidity. Physically, it means that the decrease of internal humidity would increase the shrinkage.

According to different studies, the situation changes for a relative humidity below 45%. This is due to the fact that the disjointing pressure and capillarity stress no longer exist. However, shrinkage is still observed and can be explained as a change of surface energy. Since the majority of water is absorbed, surface tension is predominant in the water droplets. The pressure would be:

$$p_{ave} = \frac{2\gamma S}{3} \tag{2-5}$$

Where p_{ave} is the mean pressure, γ is the surface energy in $\frac{J}{m^2}$ and S is the specific surface area in $\frac{m^2}{g}$

Generally, for C-S-H, S is large, resulting in a large pressure, causing compression in the solid, according to Mindess et al. [89]. The stresses caused by shrinkage in the concrete can be modelled as shown on Figure 2-24.

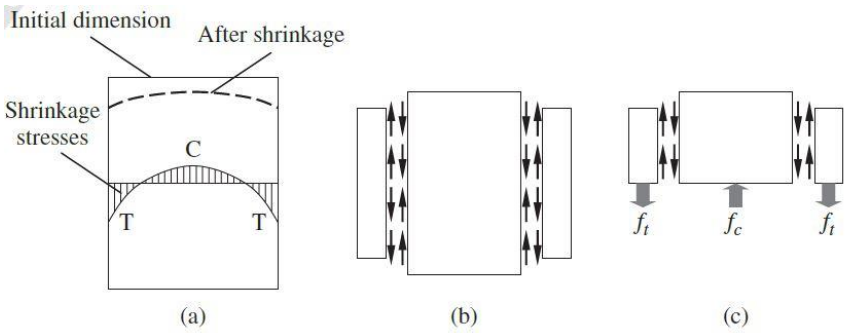

Figure 2-24. Stresses due to drying shrinkage

In a concrete cylinder for example, the water near the edges of the specimen dries faster than the internal water. This causes strains in the microstructure and as a result, a set of self-balancing internal forces are created, as shown in Figure 2-24. In this case, the difference in strains and stresses for the body, would be due to shear stresses created between the core and the shell. This shrinkage created stress would eventually have an effect on the mechanical properties of the specimen. This can be observed in large scale if members are constrained in the direction of shrinkage. An example would be column-beam joints, where the beams are constrained in the longitudinal direction by the columns and could form consequently shrinkage cracks.

The shrinkage strain is time dependent. Most of the shrinkage effects occur during the first year. These effects are proportional to outer dimensions of the elements. Large elements would shrink more as they have a larger surface and a larger evaporation of internal water. Shrinkage strain is estimated to be in the range of 0.0004-0.0007 for non-structural elements and 0.0002-0.0003 for reinforced elements.

In recycled concrete, there is a notable effect on shrinkage, therefore it has been already studied thoroughly in literature [68], [70], [72], [73], [75], [77], [78], [90], although most of the available literature considers strictly drying shrinkage on coarse aggregate replacements. In general, recycled concrete shows higher drying shrinkage strains than normal concrete. Research in literature links this increased deformation to three main factors: porosity/water absorption of recycled aggregates [91], a lower elastic modulus of recycled concrete [92] and the adhered mortar paste [93], [94]. It is nevertheless unavoidable that these three main factors are interlinked. For example, the amount of adhered mortar is directly linked to the increased porosity and water absorption of the aggregates, as well as a decrease in the elastic modulus of the recycled concrete due to a lower interfacial bond with the new cement paste.

The increase in shrinkage strains are somehow proportional to the replacement ratio. Silva et al [90] propose a correction factor of 1.20 for a 20% replacement of coarse aggregates, 1.40 for 50% replacement and 1.80 for a full replacement. Using both the fine and coarse fraction would lead to an increase of strains by 30% to 200%. There is a significant variability in these data, due to several factors, such as method of mixing, measurement type, mixture proportioning, environmental effects, etc. Figure 3.4.5 shows the results from two different reviews [59], [90] on shrinkage. Both of these graphs are mathematical fittings of results from more than 20 prior papers. Silva et. al show a completely linear relation between the substitution ratio and the effect in drying shrinkage, while Alaejos and Sanchez de Juan report a more drastic effect for higher substitution ratios.

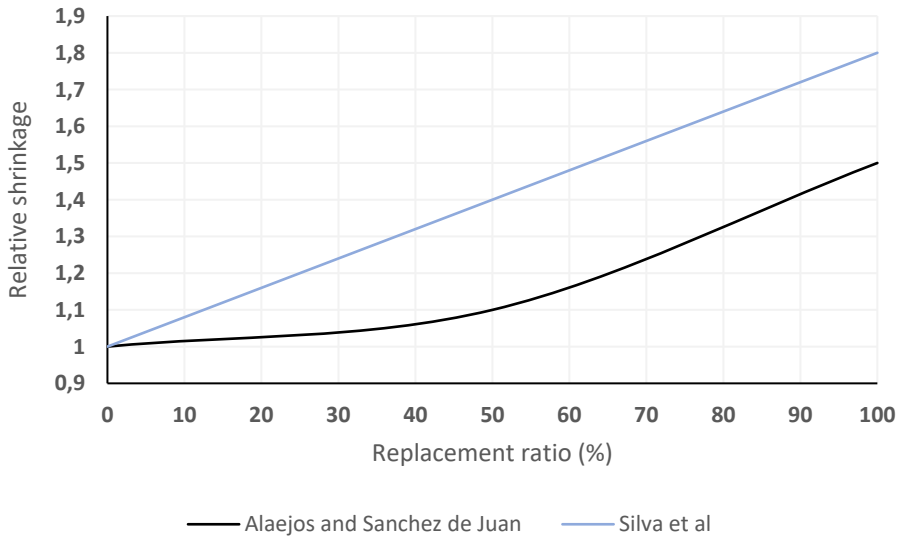

Figure 2-25. Relative shrinkage in recycled concrete

In terms of autogenous shrinkage, the behaviour is reversed. As shown on Figure 2-26, while the drying shrinkage is increased with the inclusion of recycled aggregates, a significant decrease is observed for the case of the autogenous shrinkage. According to literature [95]–[97], this is due to the internal curing effect of the recycled aggregates. Due to their higher porosity, the recycled aggregates retain an internal deposit of water which is then released during hydration to counteract the self-desiccation effect of the process. For this to happen, the aggregates must be saturated during the mixing process and the saturation degree influences the internal curing efficiency. For recycled concrete with fully saturated aggregates, the autogenous shrinkage can be compensated by up to 35% [98]. However, when compared to lightweight aggregates, the efficiency of recycled aggregates as internal curing agents is inferior due to the large number of small pores which reduce

the ability to release pore water. Indeed when compared to lightweight aggregates, most lightweight aggregates are up to 2.44 times more efficient in releasing pore water compared to recycled aggregates [99].

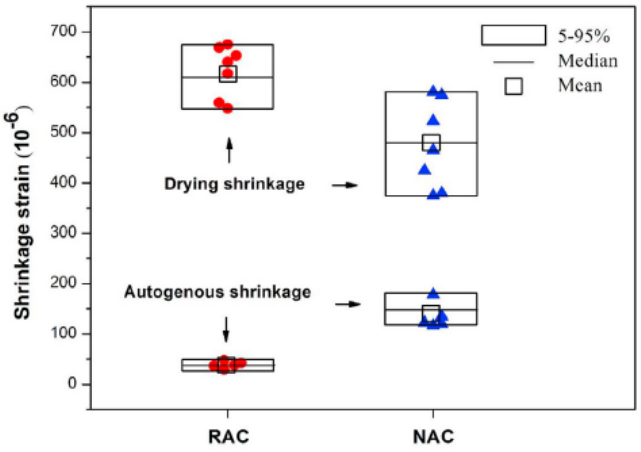

Figure 2-26. Autogenous and drying shrinkage of recycled aggregate concrete (RAC) and natural aggregate concrete (NAC) [97]

2.3.1.11. Models to predict shrinkage

Eurocode 2 model

In the EN 1992-1-1 (Eurocode 2) [100], there is a model to predict shrinkage for natural concretes. The model considers the shrinkage strain as composed by two parts: the drying shrinkage and the autogeneous shrinkage as in equation (*2-6*):

$$\varepsilon_{cs} = \varepsilon_{cd} + \varepsilon_{ca} \quad (2\text{-}6)$$

Where ε_{cs} is the total shrinkage strain, ε_{cd} is the drying shrinkage strain and ε_{ca} is the autogeneous shrinkage strain.

The drying shrinkage can be calculated through equation (*2-7*):

$$\varepsilon_{cd}(t) = \beta_{ds}(t, t_s) \cdot k_h \cdot \varepsilon_{cd,0} \tag{2-7}$$

Where k_h is a factor relating to the size of the element

$$\beta_{ds} = \frac{(t - t_s)}{(t - t_s) + 0.04\sqrt{h_0^3}} \tag{2-8}$$

Where $t\ and\ t_s$ are respectively the time and the time at the end of curing (expressed in days) and h_0 is the notional size of the section.

The basic value of the drying shrinkage strain $\varepsilon_{cd,0}$ can be calculated through the formula:

$$\varepsilon_{cd,0} = 0.85\left[(220 + 110 \cdot \alpha_{ds1}) \cdot \exp\left(-\alpha_{ds2} \cdot \frac{f_{cm}}{f_{cm0}}\right)\right] \cdot 1.55 \cdot [1 - (RH)^3] \tag{2-9}$$

Where $\alpha_{ds1} and\ \alpha_{ds2}$ are coefficients that depend on the cement type, f_{cm} is the mean compressive strength, f_{cm0} is 10 MPa and RH is the air humidity expressed in decimals.

The autogeneous shrinkage on the other hand, can be calculated through the formula:

$$\varepsilon_{ca}(t) = [1 - \exp(-0.2t^{0.5})] \cdot [2.5(f_{ck} - 10)] \tag{2-10}$$

Where f_{ck} is the characteristic concrete strength in MPa

B4 model

Wednner et. al [101] proposed the B4 model for creep and shrinkage, which is an improved version of the previous CEB-fib characterizations [102]. It allows for a separate modelling of autogeneous and drying shrinkage and it takes into account add-mixture parameters such as the cement type, water-to-cement ratio and aggregate quantity.

$$\varepsilon_{sh}(t, t_0) = -\epsilon_{sh,\infty}(t_0) \cdot k_h \cdot S(t, t_0) \tag{2-11}$$

Where ε_{sh} is the shrinkage strain, $\varepsilon_{sh,\infty}$ is the final value of the drying shrinkage over time, k_h is a factor taking into account the environmental humidity and S a function given in equation (2-12).

$$S(t, t_0) = tanh\sqrt{\frac{t - t_0}{\tau_{sh}}} \tag{2-12}$$

Where τ_{sh} is the shrinkage halftime and is calculated through the equation (2-13).

This parameter takes into account the mixture proportions, such as the aggregate content, water-to-cement ratio and the cement quantity, making this model significantly more descriptive than the Eurocode 2 model and allowing for a correlation between the mix design and the final shrinkage values.

$$\tau_{sh} = \tau_0 \left(\frac{a/c}{6}\right)^{-p_1} \left(\frac{w/c}{0.38}\right)^{-p_2} \left(\frac{6.5c}{\rho}\right)^{-p_3} (k_s D)^2 \tag{2-13}$$

Where τ_0 is the base value, k_s is a shape parameter of the cross-section, D is the effective thickness of the cross-section, a/c is the aggregate-to-cement ratio, w/c is the water-to-cement

ratio, c is the cement content, ρ is the concrete mass density, p_2 and p_3 depend on the cement type and p_1 is a constant.

The final value for the shrinkage is calculated through equation (2-14) and takes into account the aging effect through a ratio between the Young's modulus at 607 days and the Young's modulus at the end of curing.

$$\varepsilon_{sh,\infty}(t_0) = \varepsilon_{sh0}\left(\frac{a/c}{6}\right)^{-p_5}\left(\frac{w/c}{0.38}\right)^{p_6}\left(\frac{6.5c}{\rho}\right)^{p_7}\frac{E(607)}{E(t_0+\tau_{sh})} \tag{2-14}$$

Where ε_{sh0} is a base value depending on the admixture, p_6 depends on the cement type and p_5 and p_7 are constants.

The autogeneous shrinkage is also given as a function of time and it relates to the aggregate-to-cement ratio and the water-to-cement ratio as given in equation

$$\varepsilon_{au}(t) = \varepsilon_{au0}\left(\frac{a/c}{6}\right)^{-r_5}\left(\frac{w/c}{0.38}\right)^{-r_4}\left[1+\left(\frac{\tau_{au}}{t}\right)^{\alpha}\right]^{-r_2} \tag{2-15}$$

Where τ_{au} is the autogeneous shrinkage halftime, α is an exponent relating to the water-cement ratio and r_1 to r_5 are equation constants.

$$\alpha = r_7\left(\frac{w/c}{0.38}\right) \tag{2-16}$$

$$\tau_{au} = \tau_{au0}\left(\frac{w/c}{0.38}\right)^{r_1} \tag{2-17}$$

Models including recycled concrete

Several research approaches have focused on developing models to predict the shrinkage behaviour of recycled aggregate concrete. All these approaches aim at the modification of existing models, such as the aforementioned Eurocode 2 model, the B4 model or similar by introducing the particularities of recycled concrete. These include aspects such as the replacement ratio, adhered mortar content and water absorption.

Zhang et al. [103], [104], through an extensive study, developed a model based on the B4 shrinkage prediction model to predict the autogenous (2-18) and drying shrinkage of recycled concrete. Their approach considers varying substitution ratios of fine and coarse aggregates.

$$\varepsilon_{au}^{RAC} = \varepsilon_{au0}\left(\frac{(a_{NA}^{RAC} + a_{CRA}^{equ} + a_{FRA}^{equ})/c_{RAC}}{6}\right)^{-0.75}\left(\frac{(w_{RAC} + \Delta W_{CRA}^{eff} + \Delta W_{FRA}^{eff})/c_{RAC}}{0.38}\right)^{-3.5} k_{com} \quad (2\text{-}18)$$

Where $\alpha_{NA}^{RAC}, \alpha_{CRA}^{equ}, \alpha_{FRA}^{equ}$ are respectively the natural aggregate content, coarse recycled aggregate content and fine recycled aggregate content, $\Delta W_{CRA}^{eff}\ and\ \Delta W_{FRA}^{eff}$ are the effective additional water content needed for coarse recycled aggregates and fine recycled aggregates and k_{com} is a factor taking into account the compound effect of fine and coarse recycled aggregates and is calculated through equation (2-19)

$$k_{com} = 1 + \xi r_{CRA} r_{FRA} \quad (2\text{-}19)$$

Where ξ is a constant coefficient and r_{CRa} and r_{FRA} are respectively the coarse and fine recycled aggregate substitution rate.

For the drying shrinkage, they use the Eurocode model as a basis and offer a modification of equation (*2-8*) as follows on (2-20)

$$\beta_{ds}^{RAC} = \frac{(t - t_s)}{(t - t_s) + 0.04 k_{wa} \sqrt{h_0^3}} \quad (2\text{-}20)$$

Where k_{wa} is a factor considering the replacement ratio of recycled aggregates and their increased water absorption ratios as described in (2-21).

$$k_{wa} = (0.10\overline{w_{a-F}} + 2.27)(0.18\overline{w_{a-C}} + 0.52) \quad (2\text{-}21)$$

Where $\overline{w_{a-F}}$ and $\overline{w_{a-C}}$ are the average water absorption ratios for fine and coarse recycled aggregates.

The model also includes an amplification factor (k_v) which is calculated as:

$$k_v = \frac{1 - \left(V_{NA}^{RAC} + V_{CRA}^{eff} + V_{FRA}^{eff}\right)^{1/3}}{1 - (V_{NA}^{NAC})^{1/3}} \quad (2\text{-}22)$$

Where V_{NA}^{RAC}, V_{CRA}^{eff}, V_{FRA}^{eff} are the volumes of natural aggregates, coarse and fine recycled aggregates.

Thus, the final value of the drying shrinkage is a modification of equation (*2-7*):

$$\varepsilon_{cd}(t) = \beta_{ds}^{RAC}(t, t_s) \cdot k_h \cdot k_v \cdot \varepsilon_{cd,0} \quad (2\text{-}23)$$

Alternatively, Guo and Wang [105] express the drying shrinkage behaviour of recycled aggregate concrete as in (2-24) based on fitting experimental data to the shrinkage model of AASHTO2007.

$$\varepsilon_{sh}^{RAC} = 0.00048 k_s k_{hs} k_{td} k_f' \exp(0.046 v_r - 0.003) \left(1 - \exp\left(-3.38\left(1 - v_{fa}\right)^{1.18}\right)\right) \exp(-1.85 v_e - 0.026) \quad (2\text{-}24)$$

Where k_s is a size effect coefficient (), k_{hs} takes into account the environment humidity, k'_f is a coefficient which considers the concrete strength, k_{td} takes into account the time effect, v_r is the replacement ratio, v_{fa} is the amount of fly ash mixed in the concrete, v_e is the amount of the expansive agent mixed into the concrete.

$$k_s = \left[\frac{t/(26\exp(0.0142(V/S)) + t)}{t/(t+45)}\right]\left[\frac{1064 - 3.70(V/S)}{923}\right] \quad (2\text{-}25)$$

$$k_{hs} = 2 - 0.014H \quad (2\text{-}26)$$

$$k_{td} = \left(\frac{t}{61 - 0.58 f_{ci}' + t}\right) \quad (2\text{-}27)$$

Where t is the time, V is the volume, S is the cross-sectional area, H is the relative humidity.

Fathifazl et al [106] related the drying shrinkage to the shrinkage of the cement paste of the same quality through (2-28)

$$S_{RAC} = S_p(1 - V_{NA}^{RAC})^n \quad (2\text{-}28)$$

Where S_{RAC} is the shrinkage of the recycled concrete, S_p is the shrinkage of a cement paste of the same quality, measured in the same conditions, V_{NA}^{RAC} is the volume fraction of recycled aggregates and n is an empirical coefficient varying between 1.2 and 1.7.

Wang et. al [107] built upon the equation (2-28) to account for more aspects such as the residual mortar, difference in the compressive strength and the properties of the parent concrete and give more extensive formulae for S_p (in their case connotated as ε_{sh}^{TM}) and V_{NA}^{RAC} (in their case connotated as V_{TNCA}^{RAC})

$$\varepsilon_{sh}^{TM} = f(R_H)\left[\frac{V_{NM}^{RAC}}{V_{TM}^{RAC}}\exp(\alpha f_{cm}^{NAC}) + \frac{V_{RM}^{RAC}}{V_{TM}^{RAC}}\exp(b f_{cm}^{PC})\right] \quad (2\text{-}29)$$

Where V_{RM}^{RAC}, V_{NM}^{RAC}, V_{TM}^{RAC} are the volume fractions of the residual mortar, natural mortar and total mortar, $f(R_H)$ is a function relating to the relative humidity, f_{CM}^{PC} and f_{cm}^{NAC} are the compressive strengths of the parent concrete and the natural concrete, α is a coefficient that reflects the correlation between the shrinkage of the mortar and the compressive strength of concrete and b is a coefficient reflecting the relationship between the shrinkage of the residual mortar and the compressive strength of the parent concrete.

2.4. The interfacial behaviour of recycled concrete and modelling at the meso-scale

2.4.1. The interfacial transition zone (ITZ)

Concrete is a composite element, comprising of aggregates and mortar paste. Both these phases are bound during the hydration and hardening process to work as one single element. The aggregates are the stiffer part of the matrix. They have a high resistance to compression and are poor performing in tension. The mortar paste is usually less performant compared to the aggregates

and acts as a bonding agent between the different aggregates in the matrix. The interfacial transition zone (ITZ) refers to the area of contact between these different phases of concrete. The ITZ has a significant importance in the study of concrete properties because it represents the weak link of the matrix [108]–[110]. During the induction of stresses, the first microcracks form in the interface and the failure initiates in this area. This is due to the different elastic properties of the different phases of concrete. Aggregates show a very brittle behaviour, with a high elastic modulus, while the cement paste displays an elasto-plastic behaviour with a lower stiffness. The difference between these behaviours causes the contact region to be particularly influential in the composite action of the matrix.

The ITZ starts to form during the very early stages of concrete mixing. Because of the size difference between the aggregates (up to 16 mm) and the cement particles (~100 microns), water films around the aggregates as a result of surface tension, creating an area with a higher water content compared to the rest of the matrix. The size difference is as well responsible for a well effect that occurs between the cement grains and the aggregates, creating an area around the aggregates with predominantly small cement grains [71], [108]. During the hydration of cement, the dissolution of the calcium sulphates and calcium aluminates results normally in hydration products ettringite and calcium hydroxide. In the microscale, these compounds take the form of crystals; ettringite in a more elongated shape, while calcium hydroxide exhibits a more planar morphology. In the ITZ, due to a higher water concentration, these crystals are larger compared to the rest of the matrix and henceforth, the area around the aggregates displays a higher porosity than the rest of the matrix. An image of the microstructure of concrete can be seen on Figure 2-27. On the left side, the aggregate is shown and the interfacial area is marked. It is clearly visible the change in morphology of the hydration products close to the surface of the aggregate compared to the rest of the cement paste. However, it also shows that the ITZ is not a specific region that can be clearly determined in width. Even though most of the literature highlights a width of the ITZ in the range of 15-20 μm, the ITZ is not a distinct band of higher porosity but rather a smeared area around the aggregates [108].

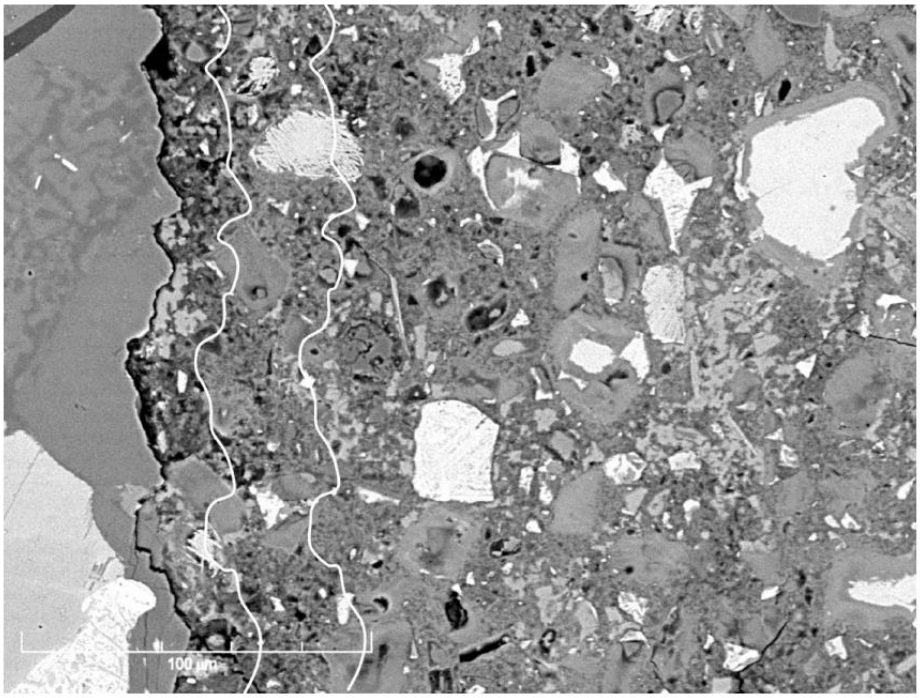

Figure 2-27. Backscattered electron image of concrete. The aggregate is shown on the left. The white lines represent a distance of 20 and 50 µm [108]

The interfacial transition zone in recycled concrete is significantly more complex. Compared to the natural concrete which has two phases (the aggregate and the mortar paste), recycled concrete has a third phase which is the attached mortar. Therefore, three different interfacial transition zones are created (Figure 2-28), the interface between the old mortar paste and the aggregate, the interface between the aggregate and the new mortar paste and the interface between the old mortar and the new mortar. The latter is the most critical one as it represents the contact region between two mortar pastes which exhibit naturally a lower mechanical performance compared to the aggregate and are furthermore, prone to microcracking induced by creep, shrinkage or environment-induced stresses. Additionally, the regions of the adhered mortar paste are irregular in relation to the morphology of the adjacent aggregate, which makes the ITZ highly irregular, discontinuous and especially prone to stress concentrations in the discontinuities. This makes the characterization of the interfacial behaviour for recycled concrete significantly more complex and highlights the importance of the investigation of the interfacial properties for each of these regions.

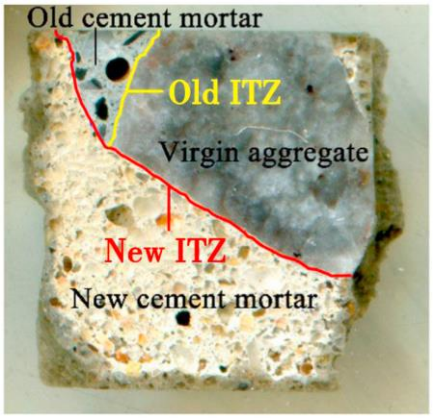

Figure 2-28. Interfacial transition zones (ITZ) in recycled concrete [111]

2.4.2. Failure mechanisms and fracture simulations of the mesoscale

There are two main mechanisms that take effect in the interfacial bond, a chemical bond and a physical bond. The chemical aspect refers to the possible reactions that happen in the contact region between the aggregate and the mortar paste. However, the majority of aggregates used in concrete production are chemically inert and, in most standards, chemically active aggregates are omitted due to the risks of alkali-silica reactions which leads to deterioration of structures. Several studies have shown that the interfacial bond is highly influenced by the physical aspect [108], [112]. Zimbelmann [113] concluded that the physical aspect is indeed the most significant in the final bond strength between aggregates and the cement paste due to epitaxial growth of hydration products such as ettringite in the perpendicular direction of the aggregate surface. This creates an interlocking effect between the hardened paste and the surface of the aggregate which constitutes the bonding mechanism. Therefore, the assessment of the interfacial bond strength becomes inherently a mechanical problem.

In brittle materials, which display a Hookean stress-strain behaviour, failure happens when the maximum principal stress in a material achieves a larger value than the uniaxial tensile stress or a lower value than the uniaxial compressive stress. Brittle materials, such as concrete are governed by an elastoplastic damage behaviour that is influenced both by hydrostatic pressure and deviatoric stresses. The most common and classical failure law for brittle materials such as rocks and concrete is the Mohr-Coulomb model. The Mohr-Coulomb model represents a correlation between the normal and shear stress applied to a material as shown in equation (2-30).

$$\tau = c - \sigma_n \tan(\varphi) \quad (2\text{-}30)$$

Where c is the cohesion, σ_n is the normal stress and φ is the angle of internal friction.

The advantages of the Mohr-Coulomb law rely on its simplicity and its ability to predict the failure of brittle materials, such as concrete, and that the facility of determining the two failure parameters through laboratory tests. Furthermore, it serves as a base for building up more complex models for numerical simulations of the meso-structure of the concrete and it is easily adaptable to other failure models such as the Drucker-Prager yield criterion (Figure 2-29).

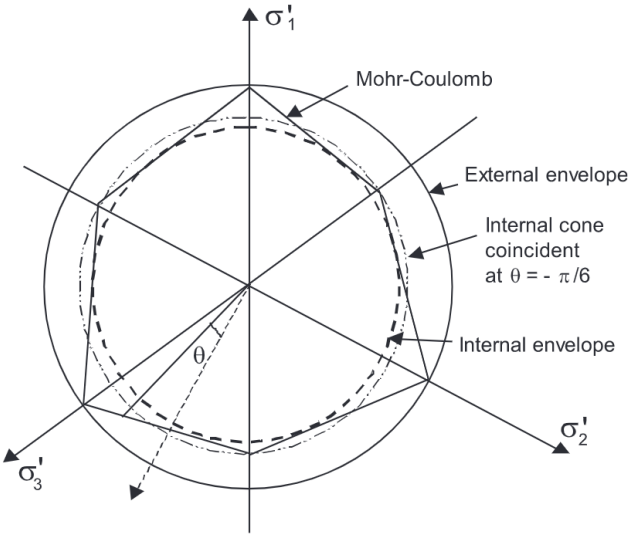

Figure 2-29. The different correlation possibilities between the Mohr-Coulomb and Drucker-Prager failure criteria [114]

Characterization of the interface can be either done through upscaled models [115]–[119], by testing the tensile strength of the contact between two phases (Figure 2-30) or by applying a combination of numerical models based on continuum mechanics and experimental data. The scale of the structure is an influencing factor on the type of criterion that must be considered. According to Bazant [120], strength criterions can be successfully used in correlation with laboratory tests, while for larger elements linear elastic fracture models are more appropriate. Testing methods to determine the interfacial strength include the direct tensile test, splitting tests, direct shear test, push-off test, slanted shear test and bending test [121] and the most popular test setups are shown

on Figure 2-30. The test setups rely on application of a shear stress on the interfacial surface between two concrete pieces. The pieces should either be cohesively glued or should be in rough contact with each other.

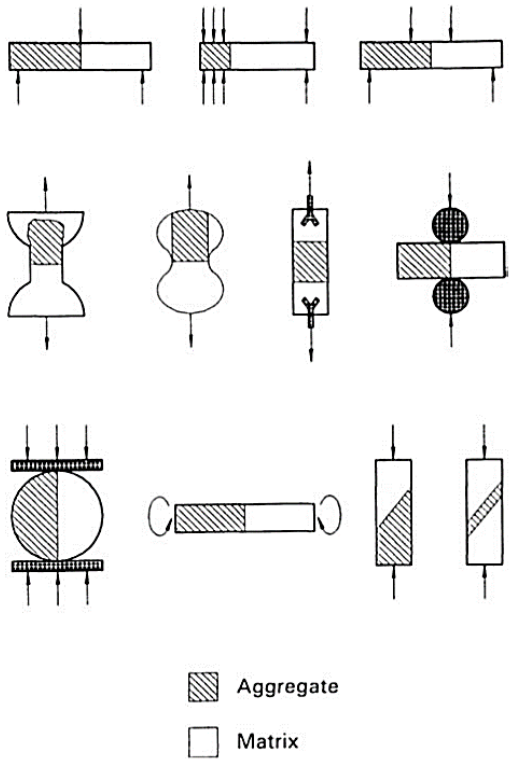

Figure 2-30. Test methods for determining the interfacial strength [122]

Jebli et al [116] showed, through direct shear tests, that the crack for concrete elements starts always at the cement-aggregate interface and determined the cohesion to be 3 MPa for the composite and 4.1 MPa for the cement paste, while the local friction angle was 47° and 54° respectively. Akcaoglu et al [119] determined that the interfacial bond is determinant for the tensile behaviour of concrete, but its contribution in the compressive strength is minimal. Caliskan and Karihaloo [117] showed that the surface roughness significantly affects the interfacial bond and that the bond behaviour is dependent on the mineralogy of the aggregates. Ceia et al [118] used slanted shear tests to conclude that the interfacial strength between a natural concrete and a recycled concrete can decrease up to 161% for a full replacement of recycled coarse aggregates and proposed the following modified correlation formulas between the strength parameters and the roughness of the surface.

$$c_a = 0.3 + \frac{R_{pm}}{15} \quad (2\text{-}31)$$

$$\mu = 0.4 + \frac{R_{pm}}{5} \quad (2\text{-}32)$$

Where c_a is the cohesion, μ is the internal friction angle and R_{pm} is the roughness of the surface

Santos and Julio [123] presented the following relationship based on an extensive testing programme of concrete-to-concrete bond:

$$C_d = \frac{1.062 R_{vm}^{0.145}}{\gamma_{coh}} \quad (2\text{-}33)$$

$$\mu_d = \frac{1.366 R_{vm}^{0.041}}{\gamma_{fr}} \quad (2\text{-}34)$$

Where: c_d is the cohesion, μ_d is the internal friction angle, R_{vm} is the mean valley peak and $\boldsymbol{\gamma}$ are safety factors

Eurocode 2 [100] presents a simpler approach for assessing the failure parameters, where the surface is first arbitrarily defined as "very smooth", "smooth", "rough" or "indented" and for each surface type a set of values for the cohesion and friction coefficient is given.

Numerical modelling of mechanical problems has now become the standard procedure when designing structures. Stemming from the finite element method (FEM), numerous research has been done to adapt mathematical correlations to material behaviour. Concrete however, as a composite, quasi-brittle material with a multi-phase structure, is particularly challenging to model. Numerical models can be done on the macro scale, meso-scale or micro-scale (Figure 2-31).

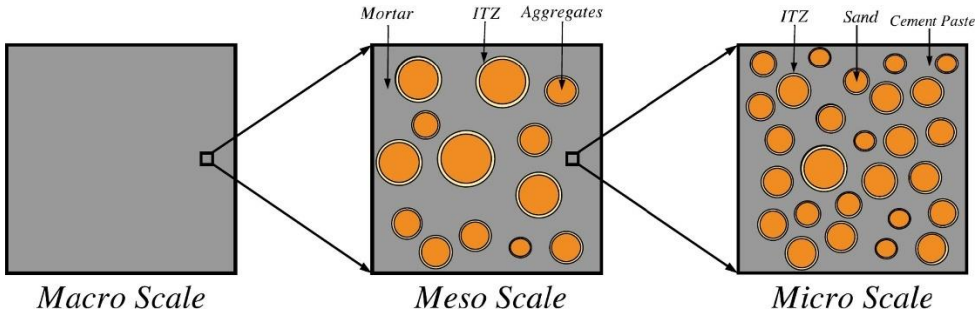

Figure 2-31. Multi-scale modelling of concrete [124]

Macro scale modelling is computationally efficient and well-used in areas such as civil engineering, but it fails at accurately predicting the non-linear behaviour of the interaction between the different phases. In the meso scale, three distinct phases are modelled: aggregates, mortar paste and the ITZ. This is the most commonly used approach in numerical studies of the concrete structure, because it allows to correlate each phase property to the performance of the concrete, therefore allowing to control and consider the effect of the mix design in the mechanical quality of the concrete. Modelling in the micro scale, on the other hand, is seldom used because of its computational complexity and inefficiency. The goal of modelling the concrete in the meso scale is to be able to understand the stress development in the concrete structure, as well as crack initiation and propagation, in order to be able to design concretes more efficiently in terms of materials used as well as production processes.

Even though the two classical models, Mohr-Coulomb and Drucker-Prager, cover significantly well the yield aspect of concretes, to fully model the internal structure of the material and to fully apply the material plasticity into the model, two additional aspects are to be considered: the flow and the hardening rule. These aspects are necessary to model the plastic behaviour of concretes after the elastic yielding point is reached. Generally, in frictional materials, damage is considered to start at the point of total loss of cohesion. Moreover, damage is dependant on the hydrostatic pressure and has an unrecoverable plasticity. Therefore, modelling the plastic behaviour of the matrix is crucial in damage modelling of concrete.

In the Mohr-Coulomb yield surface, the plastic flow (G) is given as [125]:

$$G = \sqrt{(\epsilon c_0 \tan\psi)^2 + (R_{mw} q)^2} - p \cdot tan\psi \qquad (2\text{-}35)$$

$$R_{mw}(\Theta, \mathrm{e}) = \frac{4(1-e^2)\cos^2\Theta + (2e-1)^2}{2(1-e^2)\cos\theta + (2\mathrm{e}-1)\sqrt{4(1-e^2)\cos^2\theta + 5e^2 - 4e}} R_{mc}\left(\frac{\pi}{3}, \phi\right) \tag{2-36}$$

$$R_{mc}\left(\frac{\pi}{3}, \phi\right) = \frac{3 - sin\phi}{6cos\phi} \tag{2-37}$$

Where ψ is the dilation angle which is directly correlated to the internal friction angle, c_0 is the initial cohesion stress, Θ is the deviatoric polar angle, ϵ I the meridional eccentricity, e is the deviatoric eccentricity, ϕ is the Mohr-Coulomb friction angle [126]

Among the many works devoted to the development of a damage model for concrete, one of the most prominent is the Concrete Damage Plasticity (CDP), first developed by Lubliner et. al [127], which is today embedded into the main numerical modelling software, such as Abaqus. Although CDP is not the only model, it was the first to propose major principles that allow for a continuum modelling of the concrete structure. The CDP builds onto the Mohr-Coulomb plasticity but, building on previous work, introduces a strain state decomposition between the elastic and plastic part of the strain rate as in (2-38).

$$\dot{\varepsilon} = \dot{\varepsilon_e} + \dot{\varepsilon_{pl}} \tag{2-38}$$

Where $\dot{\varepsilon}$ is the strain rate, $\dot{\varepsilon}_e$ is the elastic component of the strain rate and $\dot{\varepsilon}_{pl}$ is the plastic component of the strain rate

And the stress is then defined as:

$$\sigma = (1-d)D_0^{el} : (\varepsilon - \varepsilon_{pl}) \tag{2-39}$$

Where d is the damage and D_0^{el} is the initial undamaged elasticity of the material

The hardening effect in the concrete is described through the hardening variables in compression and in tension, which mathematically describe the cracking behaviour and crushing in the plastic stage of the concrete.

$$d\tilde{\varepsilon}_{pl} = h\left(\bar{\sigma}, \tilde{\varepsilon}_{pl}\right) \cdot \dot{\lambda} \frac{\partial G(\bar{\sigma})}{\partial \bar{\sigma}} \tag{2-40}$$

Where $\dot{\lambda}$ is called a plastic multiplier and G is the plastic flow as given by (2-35).

And finally, the yield function, as proposed by Lubliner, is the point where the cohesion of the material reaches the value of zero and is given by the equation (2-41)

$$F = \frac{1}{1-\alpha}\left(\bar{q} - 3\alpha\bar{p} + \beta\left(\tilde{\varepsilon}_{pl}\right)\langle\hat{\sigma}_{max}\rangle - \gamma\langle-\hat{\sigma}_{max}\rangle\right) - \bar{\sigma}_c\left(\tilde{\varepsilon}_c^{pl}\right) = 0 \tag{2-41}$$

Where α and γ are material constants, $\bar{p}$ is the effective hydrostatic stress, $\bar{q}$ is the effective Mises stress, $\hat{\sigma}_{max}$ is the maximum eigenvalue of the stress tensor and $\beta\left(\tilde{\varepsilon}_{pl}\right)$ is a function described by the equation (2-42)

$$\beta\left(\tilde{\varepsilon}_{pl}\right) = \frac{\bar{\sigma}_c\left(\tilde{\varepsilon}_{pl}^c\right)}{\bar{\sigma}_t\left(\tilde{\varepsilon}_{pl}^t\right)}(1-\alpha) - (1+\alpha) \tag{2-42}$$

Where $\bar{\sigma}_c\left(\tilde{\varepsilon}_{pl}^c\right)$ and $\bar{\sigma}_t\left(\tilde{\varepsilon}_{pl}^t\right)$ are the effective compression and tension cohesive stresses.

Numerous research approaches have been done on the concrete meso structure modelling based on the concrete damaged plasticity model [128]–[132]. These approaches include an elastic modelling of the aggregates and the CDP for the other two phases. The most common practices include a continuum mechanics approach based on FEM modelling, rather than a discreet modelling approach. An advantage of the continuum modelling approach rely on the parametrisation capabilities of the model and, especially, on the ability to realistically define the fracture propagation. The latter is of special interest in current research as it can create the basis for a better understanding of the fracture behaviour of different concrete mixes and pave the way for an optimized concrete. However, the applied methods range considerably in literature with no prominent methodology in effect. First approaches, such as Caballero et al [133]–[135] used cohesive models to simulate the interface. The crack propagation in these models were possible only through pre-defined paths. Zhu et al [136] used FEM to model the mesostructured of concrete and realistically detect crack propagation and networking based on the Mohr-Coulomb and the maximum tensile strain criterion. Huang et al [128] found through numerical simulations based on the CDP that at higher strains, damage forms into more complex patterns. Jayasuriya et al [137] used 2D numerical modelling to better understand the mechanical properties of recycled concrete by varying the contents of adhered mortar. They showed that increasing the amount of adhered mortar has a negative effect on both the compressive strength and the elastic modulus. Using statistical methods, they concluded that compressive strength was mainly influenced by the aggregate and matrix stiffness. Tan et al [138] showed through a discreet element method approach that the shear strength of the ITZ has a predominant influence on the strength of recycled concrete.

One of the emerging methods for solving interfacial problems is the phase field modelling approach. In this methodology, the boundary conditions at the interface are substituted by a partial differential equation, the phase field (ϕ). The phase field can take values of a certain range, usually being [0; +1], with a smooth transition between the values. In this case a value 1 of the phase field represents a cracked material and 0 represents an uncracked one. The location of a specific potential range is then possible as a collection of points with the same phase field value. The advantage of this method in fracture mechanics is the ability to achieve the location of fracture directly from an energetic approach, by relating strictly to the minimization of the elastic and fracture energies. The principle of energy minimization in the phase field approach comes from the generalization of the Griffith's theory [139], mainly based on the work of Francfort and Marigo

[140] which allows for defining the fracture path without a pre-existing crack. According to Griffith, the total energy during loading of a solid body is given as:

$$\mathcal{E} \coloneqq \psi_s + \psi_c - P \tag{2-43}$$

Where P is the external potential energy, ψ_s (2-44) is the stored strain and ψ_c (2-45) is the surface energy.

$$\psi_s(u) = \int_{\Omega \backslash \Gamma} \psi_0(\epsilon(u), \Gamma) dV \tag{2-44}$$

$$\psi_c(\Gamma) = \int_{\Gamma} G_c dA \tag{2-45}$$

Through this principle, the crack grows only when the strain-energy rate equals the rate of which it is absorbed by the crack extension. Therefore, it is inherently a balance problem between the bulk energy and the surface energy on the crack. If the phase-field approach is considered, the need for a pre-described weekended section is avoided. Moreover, the initiation of the crack is possible. Considering the case of Figure 2-32 [141] where Ω is the domain of the solid, Γ is the crack and ϕ represents the phase-field, the potential energy of the system is:

$$P(u) = \int_{\Omega} b^* \cdot u dV + \int_{\mathrm{d}\Omega_{\mathrm{t}}} t^* \cdot u dA \tag{2-46}$$

Where b^* is the body force, u are the prescribed displacements, t is the prescribed traction force, V is the volume, A is the area

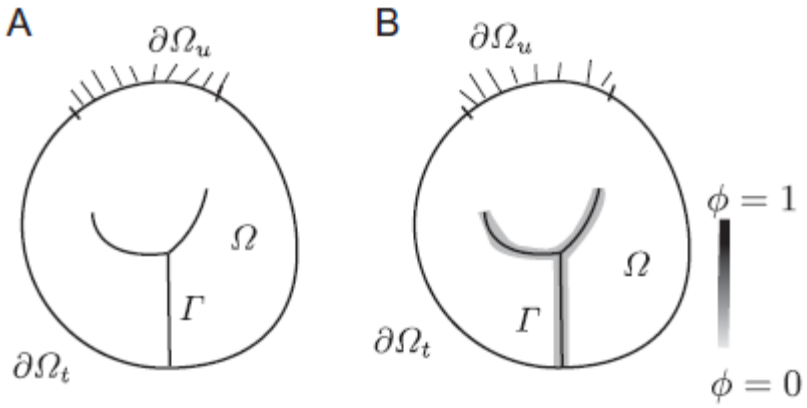

Figure 2-32. A solid body with the crack set: (A) sharp cracks and (B) diffuse crack bands [141]

If the phase-field approach is considered, the corresponding surface energy for brittle materials is given as:

$$\psi_c(\Gamma) = \int_\Gamma G_c dA = \int_\Omega G_c \gamma(\phi; \nabla\phi) dA \tag{2-47}$$

$$\gamma(\phi; \nabla\phi) = \frac{1}{2}\left[\frac{1}{l_0}\phi^2 + l_0(\nabla\phi \cdot \nabla\phi)\right] \tag{2-48}$$

Where G_c is the critical energy release rate based on the type of the material, $\gamma(\phi; \nabla\phi)$ is the crack density function which is given in equation (2-48) and is based on the work of Miehe et al. [142] and l_0 is a parameter which controls the width of the crack diffusion.

The bulk strain energy in relation to the phase-field is therefore given as:

$$\psi_s(u,\phi) = \int_\Omega g(\phi)\psi_0\big(\epsilon(u)\big)dV \tag{2-49}$$

Where the stress degradation function $g(\phi)$controls the drop of the basic energy function.

Therefore, the final energy functional can be calculated as:

$$\mathcal{E}(u,\phi) = \int_\Omega g(\phi)\psi_0\big(\epsilon(u)\big)dV + \int_\Omega G_c\frac{1}{2}\left[\frac{1}{l_0}\phi^2 + l_0(\nabla\phi\cdot\nabla\phi)\right]dV - P(u) \tag{2-50}$$

When a body is under loading, the strain increase and the elastic energy increases. At a specific threshold, the body releases part of the energy by increasing the phase field value towards 1, which increases the surface energy and eventually forming fissures and cracks in the matrix. By doing this, the model not only allows for crack initiation and propagation, but it can deal with branching cracks as well all crack networks which are heavily encountered in fracture of brittle materials. Furthermore, the phase field allows for incorporation of other aspects and multi-field approaches, making it highly adaptable for a broad range of problems. Nguyen aet al. [143] developed a multi-phase phase field model to simulate the early age hydration of cementitious materials by incorporating a thermic and hygrometrical aspect into the already existing mechanical problem. They showed that the phase field approach can be robustly applied to arbitrary boundary conditions. Hu et al. [144] successfully simulated the corrosion behaviour of reinforced concrete members with up to tens of millions of degrees of freedom showing that the ITZ properties significantly affect the cracking of the concrete cover. Huang et al. [145] used computer tomography scans as a basis for Monte Carlo simulations of the variability of the meso scale fracture process in concrete samples based on a phase field regularized cohesive zone model showing how complicated fracture behaviour can be predicted realistically by using only minimal investigation in the structure of the concrete. Pise et al. [146] used a phase field approach to analyse the pull-out behaviour of steel fibres in fibre reinforced concrete.

2.5. The research gap and the research approach

The research approach aims to answer to all the research questions listed in the introduction, while, at the same time, addressing the existing literature gap.

It is clear from the literature data that recycled aggregates show a large variation in terms of mechanical performance depending on the geographical area where they are sourced and on the treatment methods. As shown in Table 2-3, there can be a variability in the bulk density of up to 80% between values reported by different sources. This is even more prominent in the water absorption values. Therefore, due to this large spread of results, it is virtually impossible to use existing literature data without assessing a local case study. As of now and to the author's best knowledge, there are no published investigations for the mechanical properties of recycled concrete in Luxembourg. Consequently, Chapter 3 aims to do a complete investigation on the physical and mechanical properties of recycled aggregate concrete produced using a representative mix of locally sourced recycled aggregates.

However, from the existing literature (Sections 2.3.1.7, 2.3.1.8, 2.3.1.10), it is clear from the that recycled concrete is generally a weaker material compared to a corresponding natural concrete, as well as the importance of the interfacial transition zone in the mechanical performance of concrete is well-known and well-studied [108]–[110]. Nonetheless, the interfacial transition zone is still lacking deeper studies and a general characterization, especially considering the complexity of the contact regions, as discussed on Section 2.4.1. This is thoroughly addressed in Section 4.1 and subsequently in Section 4.2, where the experimental data are used to build a numerical model which allows for a parametric study of the influencing factors, such as the adhered mortar paste, the stiffness of different phases and modelling approaches. This is conceived as a basis for a more complex system which could allow for a much better understanding and prediction of the recycled concrete behavior, leading to the production of more qualitative materials and more optimized mixtures.

In terms of the global-managerial aspect, it is at the moment unclear whether recycling of concrete is economically feasible in a small geographic region such as Luxembourg. This is

because an efficient recycling plant needs a continuous feed of material which would depend on the construction and demolition waste that arises in the country. As data regarding the yearly construction and demolition waste is not available, Chapter 5 aims to extract such data from open-source databases, such as Geoportail.lu. Even though local MFA studies exist for small areas of Luxembourg [35], the proposed approach considers the entire country, since it is difficult to define a decisive geographical area in Luxembourg which can serve as a base point for the extrapolation of data. This approach is furthermore seen as a possible basis for a material cadaster and is further expandable to include further data, as shown in Section 5.2.

Chapter 3 | Mechanical properties of recycled concrete

3.1. Physical and mechanical tests on recycled aggregates and recycled concrete

Abstract

As a construction material, the mechanical performance is the basic quality parameter of concrete. For recycled concrete to be a viable product, its performance needs to be comparable to that of natural concrete. In this section, the physical properties of recycled aggregates are described through the main standardized tests and the performance is compared to commercially available virgin aggregates. The mechanical strength in compression and tension, as well as the modulus of elasticity have been measured for high-strength concrete mixtures.

The water absorption of recycled aggregates is up to 1346% higher than the natural aggregates, while the loose bulk density exhibits a 10% loss. The Los Angeles abrasion tests show values within the suggested limits for both infrastructure works and concrete production. The compressive strength decreases with the substitution ratio. For a full substitution of recycled material, there was 73.6% loss of compressive strength and 61% loss in tensile strength. Likewise, the modulus of elasticity was negatively influenced by the implementation of recycled material.

3.1.1. Materials and methods

For this, crushed CDW was obtained from the company Carrieres Feidt. The origin of the waste is unknown, although it comes from within the Grand Duchy of Luxembourg. It was part of a three-year deposit; therefore, it is expected to have a good representation on what the general quality of recycled aggregates is in the country. It was crushed using a mobile jaw crusher from Kleemann (https://www.kleemann.info/en/) and the gradation is 0/50 mm. No further processing has been done on the material. In terms of composition, through visual inspection, the waste is mainly composed of concrete fractions, with some tiles. No bricks, timber or steel is present in the bulk. The company runs a visual inspection on each waste delivery to ensure the purity of the material. Generally, waste containing soil or organic materials is not accepted on the site. Steel rebars are removed during crushing via magnetic belts. The natural aggregates are supplied by Bati-C and consists of a mixed 0/16 mm commercial bulk. In addition, recycled aggregates of known origin was used as a comparison. This material is supplied by Contern and it originates from crushing of prefabricated structures using a mobile jaw crusher.

The cement used is a CEM 42.5 S containing 10% of recycled material. A lime filler was used in combination. Microsilica was used as a microfiller and BASF MasterGlenium ACE 456 Superplasticizer as a water reduction agent.

Four different mixtures were produced by variation of the recycled material percentage, namely 100%, 50%, 20% and a reference mixture made only with virgin aggregates. The water-to-binder ratio was kept within the range 0.31-0.44 and it varies based on the different water absorption of the used aggregates. To ensure repeatability, a minimum of 3 sets of tests for each parameter were performed. A full overview of the used mixtures is shown on Table 3-1.

Table 3-1. Concrete mixtures

Consistuents \ Mix	RC100	RC50	RC20	NC
Water	271	245	210	193
Cement	432	432	432	432
Filler	185	185	185	185

Microsilica	12	12	12	12
Superplasticizer	19	19	19	19
Aggregates	1752	1752	1750	1752
W/B	0.44	0.40	0.34	0.31
Eff. W/C	0.62	0.56	0.49	0.45

Testing was done according to the European Norms (EN Standards). For the mechanical testing, cylinders of dimensions 100x200 mm were used. Curing time between production and testing was 28 days in water bath at constant temperature. The top and bottom surfaces were polished before the tests to ensure an even surface.

Table 3-2. List of tests performed and the reference norm

Test	**Norm**
Particle size distribution	EN 933-1:2002
Bulk density	EN 1097-3:1998
Water absorption	EN 1097-6:2013
Los Angeles abrasion test	EN 1097-2:2010
Slump test	EN 12350-2
Compression test	EN 1239-3:2009
Tensile splitting test	EN 1239-6:2009
Modulus of elasticity	EN 1239-12:2013

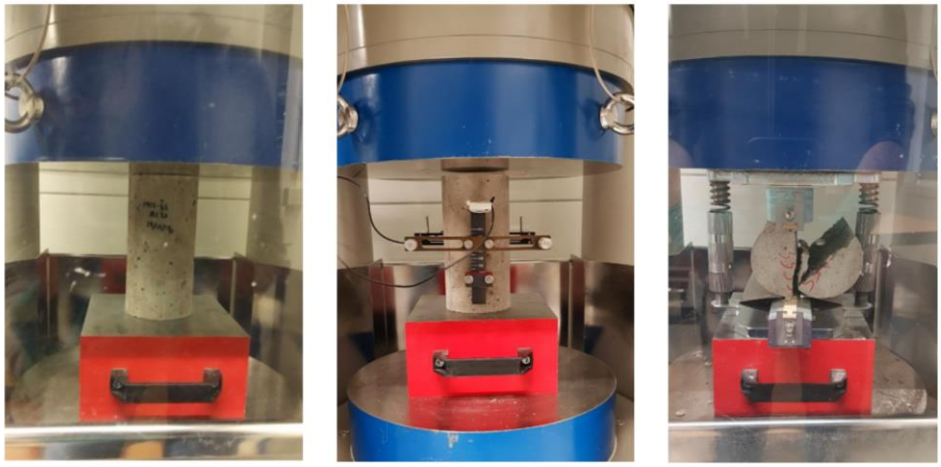

Figure 3-1. Mechanical testing on cylinders

The shrinkage testing was done in a two-step process: for the initial 24-hour shrinkage and the hardened concrete shrinkage after 24 hours. The final curve is a resulting addition of the two achieved curves. Statistical relevance of the tests was assured by analysing each mixture at least three times for each test. Three different mixture proportions were tested: natural concrete, 20% recycled aggregate substitution and 100% recycled aggregate substitution.

The 24-hour shrinkage is tested using the Schleibinger cone [147] as seen on Figure 3-2. The fresh concrete is poured into a steel cone where a plastic film is priorly set to assure moveability of the entire mixture. The measurement laser above is calibrated for each mixture and the data is recorded continuously by a logger at a resolution of 2 mikron. Simultaneously, the temperature and humidity in the room are recorded.

Figure 3-2. Schleibinger shrinkage cone [147]

The hardened concrete mixtures are measured in terms of shrinkage using a mechanism as showed on Figure 3-3. The concrete is poured on standard 160x40x40 mm modified moulds with an embedded steel stud and after 24 hours, the hardened specimen is placed on steel frames with a sensor connected on one end, while the other end is fixed. The deformations of the mixtures are continuously recorded by the sensors and the temperature and humidity in the room are also recorded through a dedicated channel. During the testing campaign both the fresh and the hardened mixtures are taken from the same concrete batch and represent the same material mixture and conditions. Furthermore, both mechanisms are placed on a dedicated room where the temperature and humidity are at a near-constant level.

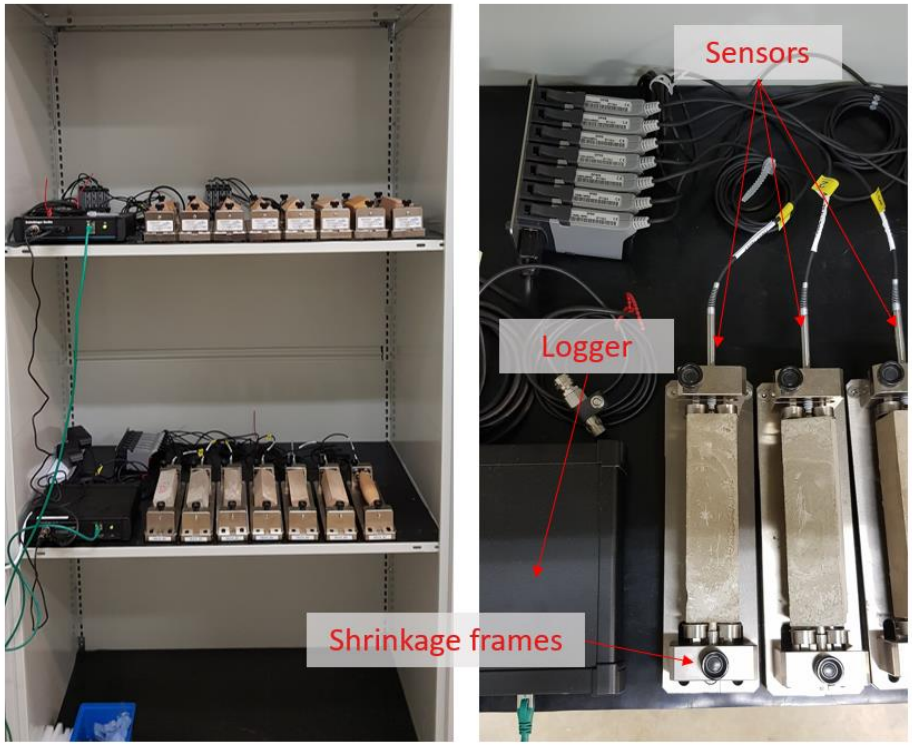

Figure 3-3. Shrinkage frames for hardened concrete

3.1.2. Results

3.1.2.1. Physical properties

The particle distribution results (Figure 3-4, Figure 3-5) show a relatively good gradation of the material. In a comparison with the ideal Fuller curve, there is a lower amount of fines (<1 mm) and a higher amount of particles above the 1 mm. For practical reasons, the gradation of the mixes was restricted to a 0/8 mm. This was mainly done to ensure good packing density, considering the size of the test cylinders chosen. The distribution of the particles during the mixing process has not been altered and the gradation resulting from the sieves has been used to simulate an industrial concrete production process.

Figure 3-4. Granulometry tests

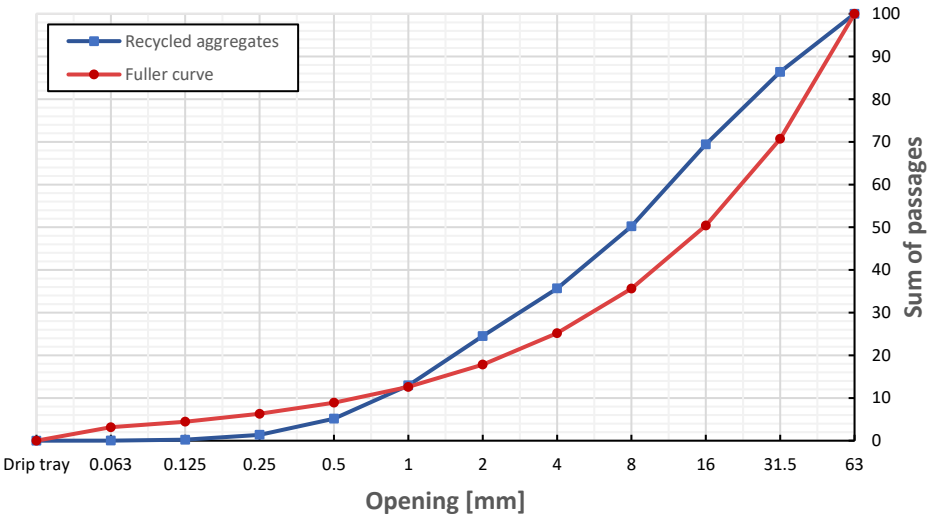

Figure 3-5. Granulometry test results

The bulk density was tested both as loose and compacted (Figure 3-6). The resulting value of the loose bulk density is within the typical values reported in the literature for similar material. In comparison to the typical value for the natural aggregate it shows a reduction of 10%, most probably due to the increased porosity and microstructural cracking caused by the crushing process. Furthermore, since the recycled aggregates are heterogeneous, they include different aggregate mineralogy as well as particles of cement and other porous materials.

The water absorption (Figure 3-7) of the tested recycled aggregates shows a drastic influence. The reported value from the pycnometer test shows a 15.21% water absorption rate, which is higher than the reported values for this type of material. The reason behind this is the lack of post-crushing treatment on the aggregates, as treatment plants for recycled aggregates are currently not available in Luxembourg. Compared to the virgin aggregates, this is an increase of 1346%, which may not adaptable for concrete production due to the negative effects it has on the durability aspect of concrete elements.

The Los Angeles abrasion values (Figure 3-8) appear to be within the range of the values from literature, but also within the practical limits. Indeed, the measured LA value of 33.41 is lower than the suggested values for concrete production (50%) and infrastructure use (40%), which shows a good performance against abrasion of the recycled aggregates.

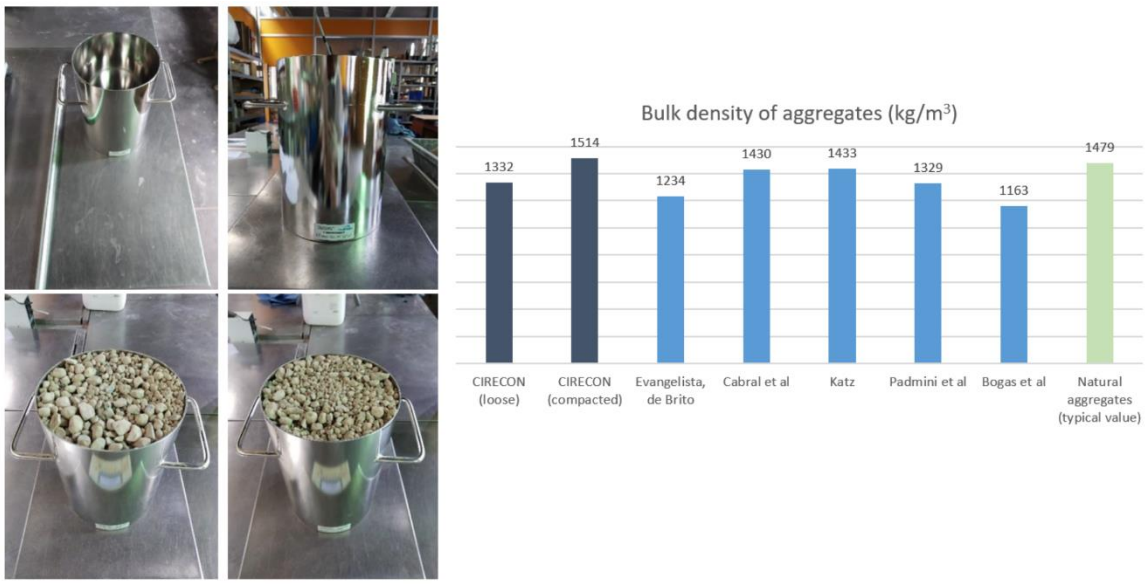

Figure 3-6. Bulk density of aggregates

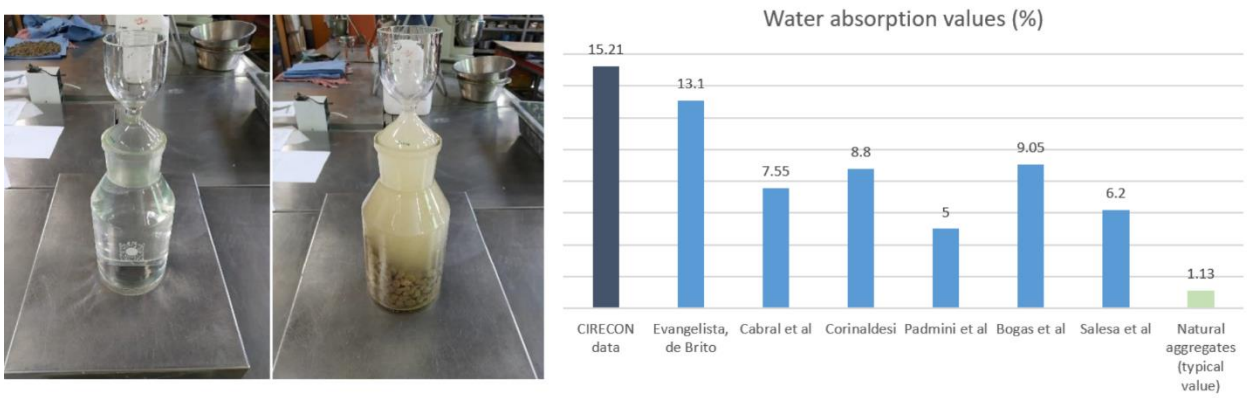

Figure 3-7. Water absorption of recycled aggregates

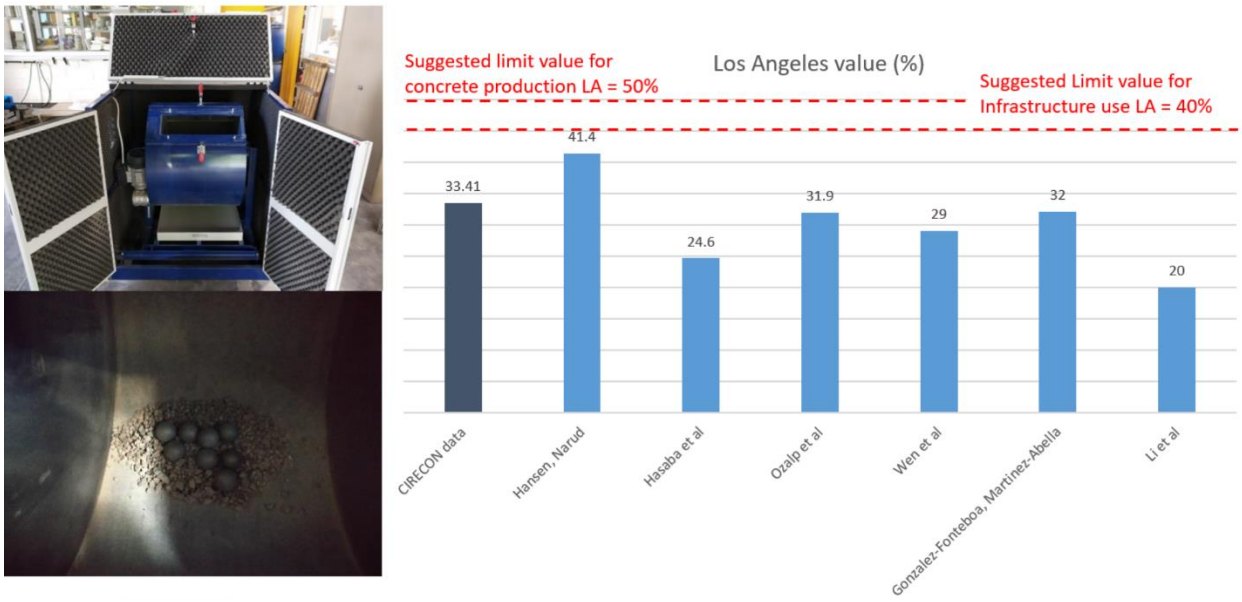

Figure 3-8. Los Angeles test of recycled aggregates

Figure 3-9. Recycled aggregates before (left) and after (right) the thermal shock

The amount of adhered mortar was assessed through the quench hot method as described on [148]. A mass coarse recycled aggregates was collected from the bulk and sieved between 2 mm and 16 mm. No modification on the gradation curve was done. Three specimens were collected, each of them having a nominal weight of 150 grams. The bulks were placed inside a laboratory scale kiln and heated at 800°C for two hours. Immediately after, they were quenched in cold water and sieved using a 2mm standard sieve. After drying in normal lab conditions for 24 hours, the masses were recorded and the mean lost mass represented 27.7% of the total, with a standard deviation of 1.3 %.

Slump tests were carried out for each produced batch of concrete. The achieved values for all the mixes are classified S3 or higher (Figure 3-10), which represents a wet mix with good workability. The fresh mixtures had slump values over 90 mm for the standard Abram's cone and can be used for high-end applications where a high flow and good compaction is needed. The highest the substitution ratio, the higher was the slump value, due to higher amount of water incorporated. The good workability is also due to the use of superplasticizer, which gives the concrete mix self-compacting abilities.

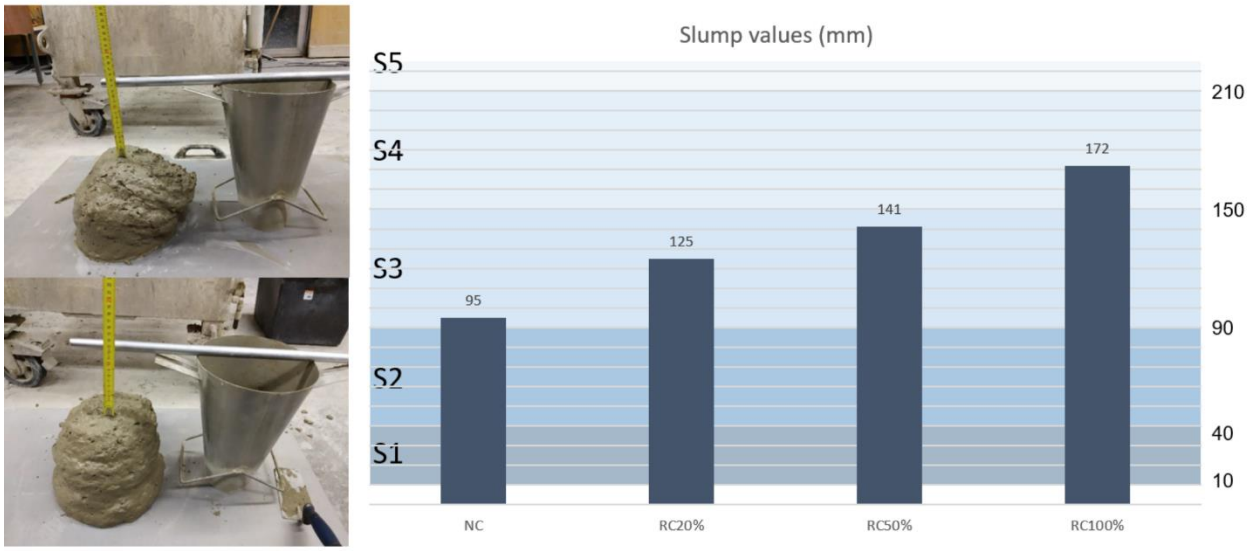

Figure 3-10. Slump values for recycled concrete mixtures

3.1.2.2. Mechanical properties

Results of the compression tests are shown on Figure 3-11. The reference concrete showed a compressive strength of 75.4 MPa and can be classified as a high strength concrete. The general accepted definition limit for the compressive strength of high-strength concrete is 55 MPa. The recycled concrete mixtures all performed lower with the strength getting lower with the increase of the recycled aggregate incorporation. For 20% substitution, there was 30% loss in strength, for 50% substitution, there was 48% of loss in strength and for a complete substitution, the mean compressive strength was only 19.87 MPa, therefore a reduction of 74% compared to the reference. These values were also compared to the mixtures from the SeRaMCo project, which were made with 100% recycled aggregates coming from known sources. In this case, the strength reduction was of only 25% and the mix can still perform as high-strength concrete in terms of mechanical resistance. This shows a noticeable difference between recycled aggregates of known origin and unknown origin and the influence the aggregate quality has on the mechanical performance of the mix.

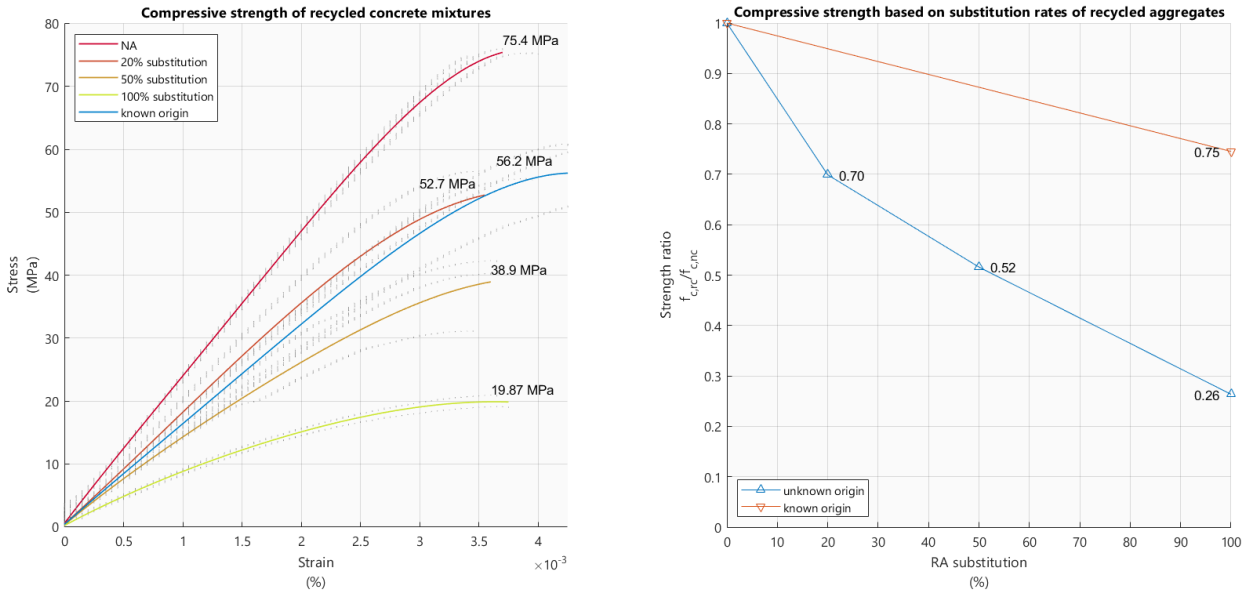

Figure 3-11. Compressive strength results

Similarly, the tensile splitting strength (Figure 3-12) showed a reduction when recycled material is incorporated. However, the behaviour is less regular compared to the compression strength when considering the slight difference between the tensile strengths achieved for substitution ratios of

20% and 50%. For a full substitution, the tensile strength was 2.02 MPa, showing a reduction of 61% compared to the reference. In contrast, the mixture made of aggregates of known origin showed only 10% of strength reduction.

Lastly, the elastic modulus (Figure 3-13) recorded for the natural concrete was 35443 MPa, which is within the typical range of concrete. The implementation of recycled material lowered significantly the elastic modulus, with the full substitution showing only 36.73% of the value of the reference. For substitution ratios of over 20%, the elastic performance of the concrete is not ideal. Similarly, to other parameters, the mixture of known origins shows a better performance and only 17.93% lower value.

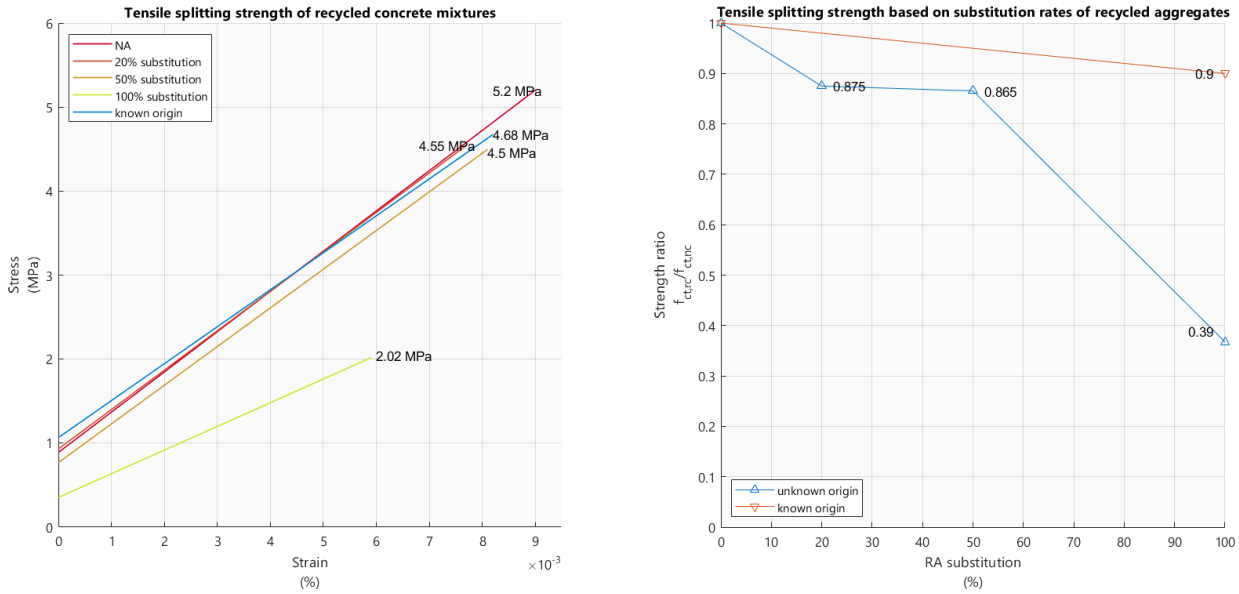

Figure 3-12. Tensile test results

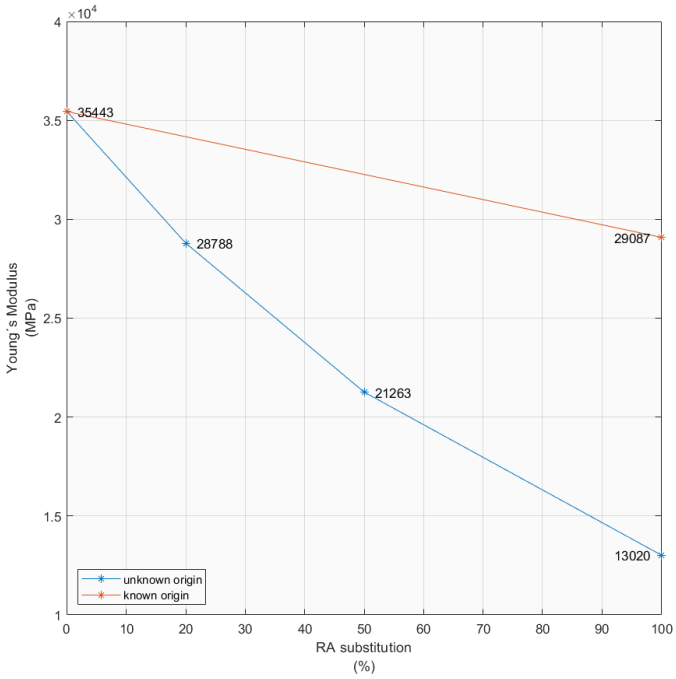

Figure 3-13. Modulus of elasticity

3.1.2.3. Shrinkage

The shrinkage results of the tested recycled concrete mixtures are shown on Figure 3-14. The three mixtures are all tested in a timeframe of 56 days after which a stabilization in the deformation values can be seen. The natural concrete mixture (NA) showed a deformation of 541 μm/m at a mean humidity of 40.94% (±6.8%) and mean room temperature of 16.5°C (±1.0°C). This value is in line with the Eurocode 2 model [100], equation 3.8, which yields a shrinkage strain value of 530 μm/m for a characteristic compressive strength of 40 MPa. The recycled concrete with a low substitution ratio (20% in volume of aggregates) shows trivial difference to NA with a shrinkage strain value of 532 μm/m after 56 days. Although this mixture shows a lower shrinkage compared to NA, due to the slight difference of only 2%, it can be concluded that for low recycled aggregate substitution of up to 20%, the effect on shrinkage is unnoticeable. For the full substitution of recycled aggregates, a significant increase in the shrinkage strain is observed. The full recycled concrete shows a strain of 633 μm/m after 56 days. This increase by 17% is in line with the existing literature [149][150] [104]. However, the reported studies shows a large variation of drying

shrinkage increase ranging 15%-80%, hinting at a significant effect of the quality of the recycled aggregates used.

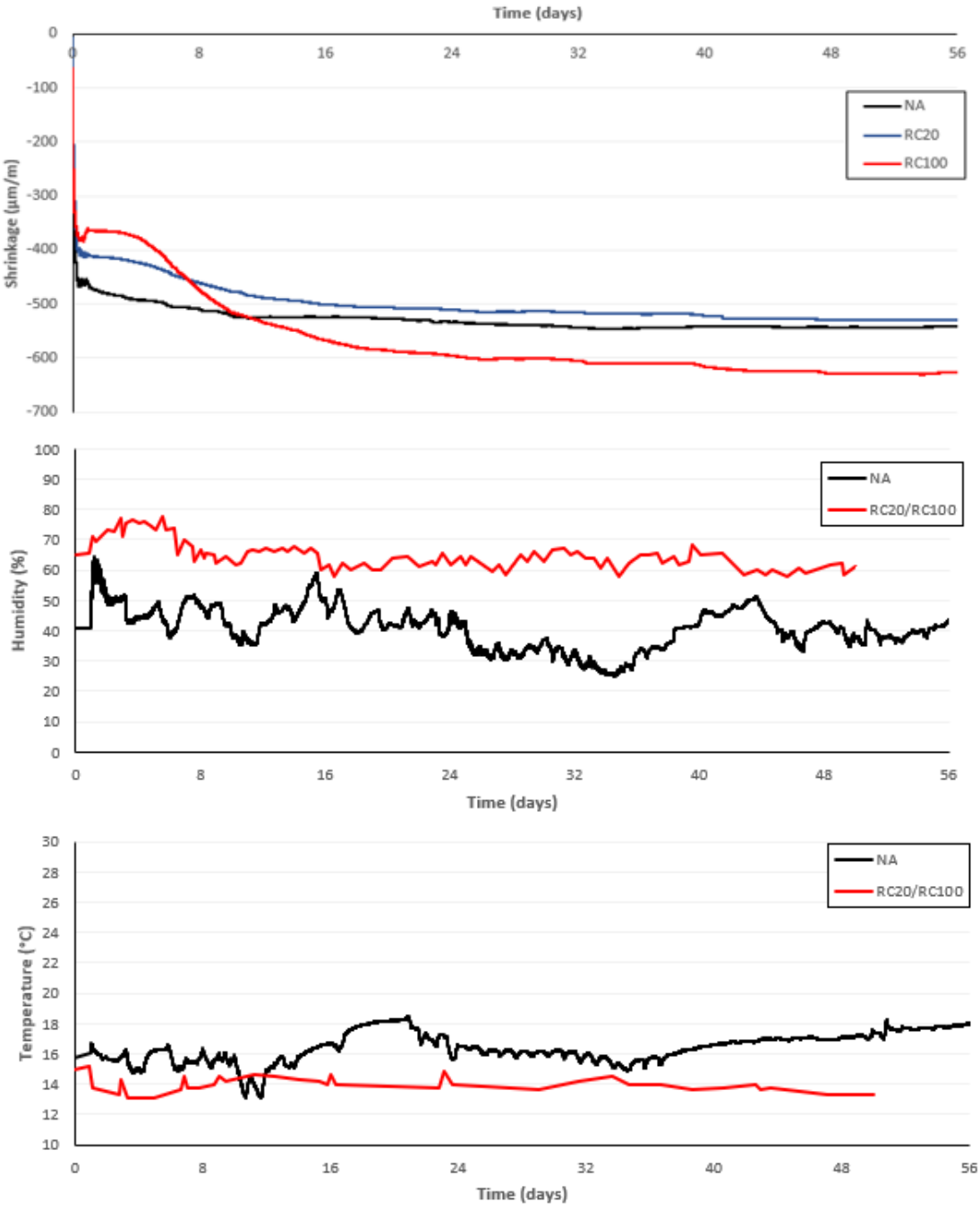

Figure 3-14. Shrinkage of the tested specimen

Moreover, it can be noted that the development of shrinkage is uniform in all mixtures, with the major strain happening in the first 24 hours and the deformation following a hyperbolic development with regards to the age of concrete. This shows that the difference between the

shrinkage strains of a normal and a recycled concrete can be assessed as an order of magnitude and the inclusion of secondary raw materials does not have an intrinsic effect on the hydration mechanism of the concrete for water/binder ratios ranging from 0.31 to 0.44, which include the most common ratio used in the industry. Through the considered tests and the existing influencing factors in the shrinkage strains, it can be concluded that the increased strains of the recylced concrete mixtures is most likely due to the reduction of strength that can be attributed to the secondary aggregates.

More insight can be seen on the early-age shrinkage of the mixtures which is shown on Figure 3-15. In this case, the NA mixture has a larger strain compared to the recycled mixtures. Indeed, with a 20% substitution and 100% substitution, the strains are reduced correspondingly by 11.6% and 21.5% in comparison to NA. This is due to the internal curing effect of the recycled aggregates as reported by [97], which states that the internal curing can reduce the autogenous shrinkage of the mixture by up to 83%. This is more evident on Figure 3-16 where a comparison is shown between mortars and concretes made with normal and fully recycled aggregates/sand. Since the shrinkage of the concrete matrix depends on the shrinkage of the different phases and the mortars are expected to shrink more due to the lack of restraining effect of the coarse aggregates, the fine mixture is showing a higher shrinkage value in the early age compared to the coarse mixture for the NA case. However, when referring to the recycled mixtures, the strains after 24 hours are showing insignificant difference. This result is of high interest as it shows that the early age shrinkage of recycled concrete mixtures is not simply affected by the internal curing effect, but the fine particles in the recycled aggregates are also a determining factor.

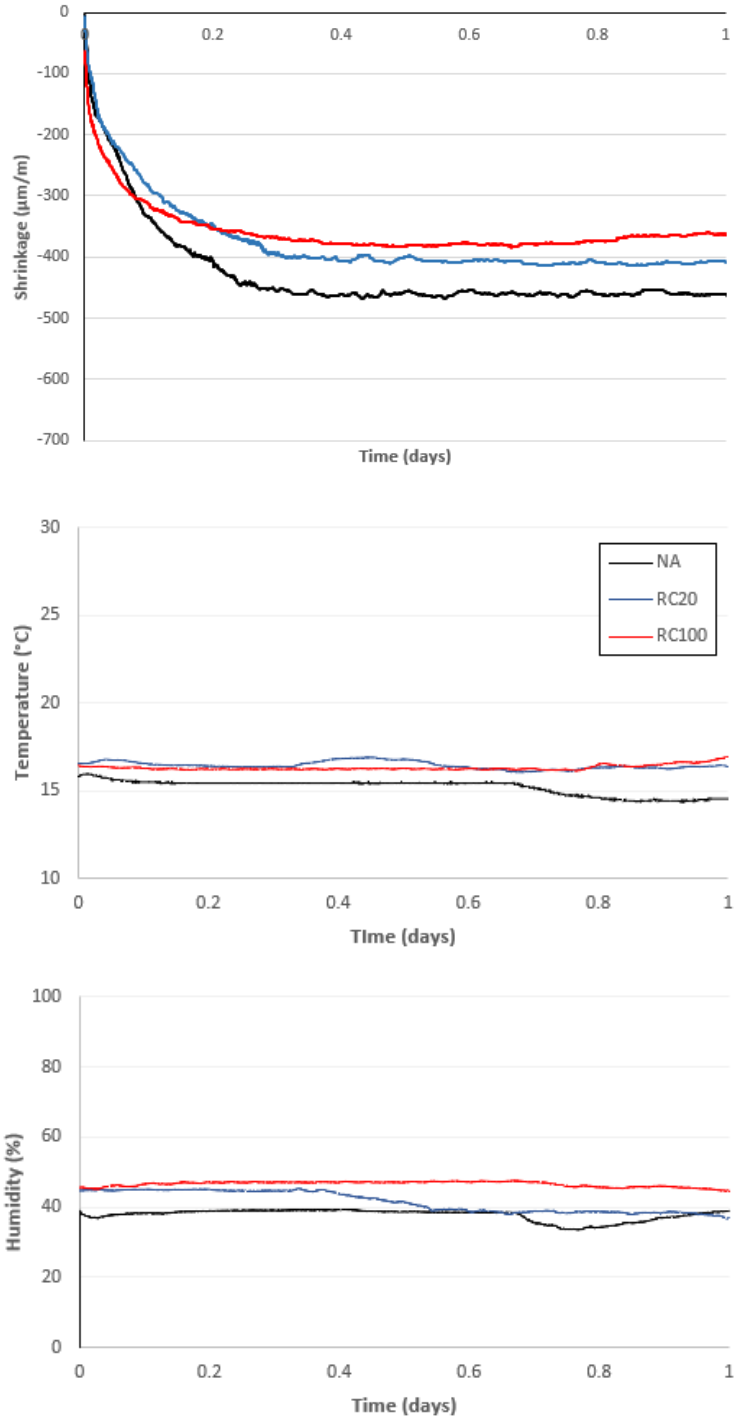

Figure 3-15. First 24-hour shrinkage of the tested concrete specimen

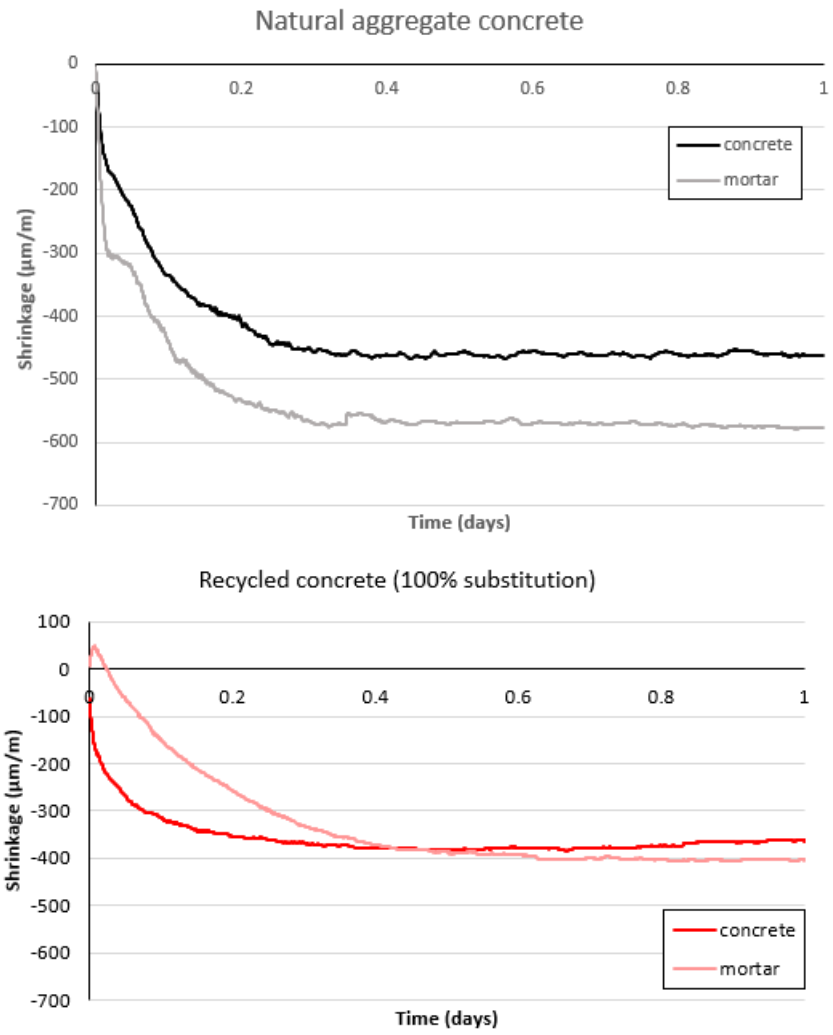

Figure 3-16. Early age shrinkage for the tested concretes and mortars

3.1.3. Conclusions and discussion

The main physical properties of the recycled aggregates were tested according to the European Norms, as well as the mechanical properties of recycled concrete mixtures containing different substitution ratios. The bulk density of recycled aggregates was 1332 kg/m^3. This value is within the range of the literature and only 10% lower than the density of natural aggregates. The Los Angeles abrasion value was 33.41% which is within the limits set for both concrete and infrastructural use. The water absorption is significantly high at 15.21% in comparison to 1.13% recorded for natural aggregates. This excessive water absorption can cause issues in the long-term behaviour of recycled concrete structures.

Four medium to high-strength concrete mixtures were developed by varying the substitution percentage of recycled aggregates at 0%, 20%, 50% and 100%. All mixtures showed good workability with slump values over 90 mm. All mixtures exhibited significant losses in compressive and tensile strength, as well as modulus of elasticity. For full substitution, the observed compressive strength was 74% lower compared to the reference, while the tensile strength showed a loss of 61%. The reported modulus of elasticity was 13020 MPa compared to 35443 MPa of the reference mixture. Recycled concrete specimen made with aggregates of known origin performed significantly better in all the mechanical tests.

The test results highlight the current issues that need to be tackled regarding recycled aggregates, as well as the impressive influence of the origin of waste in the properties of recycled concrete. Indeed, for the same crushing method used and no post-crushing treatment, recycled concrete of 100% substitution ratio produced with aggregates of known origin performed better than any recycled concrete mixture of unknown origin. This means that post-crushing treatment such as washing and sorting is more crucial for aggregates of unknown origin.

The high water absorption is currently the most significant aspect that needs to be improved, as the observed values are exceptionally high. This is furthermore demonstrated by the high values of the adhered mortar percentage coming from the quench hot method. However, it is important to point out that this method is indeterministic in distinguishing between the adhered mortar and dust or clay attached to the aggregates during crushing and storage. It is to be suggested that the method must be specifically defined for treated and untreated aggregates. The first will, undoubtedly, show lower values from the thermal shock while the later will have higher percentages. It is also important to set a threshold and correlate the quench hot value to the water absorption by testing different aggregates coming from different sources, origins and treatment.

Low substitution ratios have little to no effect in the shrinkage behaviour of recycled concrete, while for a full substitution ratio, an increase of the strains by 17% can be observed. In the early age, two different mechanisms are present: the internal curing effect of the recycled aggregates and the shrinkage-reducing effect of the fines. Therefore, the early-age shrinkage of recycled aggregate concrete can be reduced by up to 21.5% compared to natural concrete. Both of these mechanisms show a noteworthy potential for future research.

Chapter 4 | Interfacial bond in recycled concrete

4.1. Publication III: Experimental investigations on the bond strength of the interface of the adhered mortar paste in the recycled concrete matrix (Bogoviku, Waldmann)

Abstract

The present study describes an experimental approach to the assessment of the bond strength in the interface between adhered mortar paste and new mortar paste in recycled concrete based on slanted shear tests. The mortar mixtures were made of recycled sand with 0%, 20%, 50% and 100% of substitution ratio and three different roughness of the interface were considered.

The roughness affects the bond strength significantly, especially for substitution ratios of 20% and 50% which showed a higher strength compared to the control mixture. This increase can be linked to the presence of unhydrated cement and clay particles in the recycled sand. This effect is not visible for full substitution, where SEM analysis show a significant network of microstructural cracks.

The friction coefficient ranged between 0.69 and 0.88 and the cohesion between 0.13MPa to 4.60MPa. The present material models only partially fit with the experimental data.

4.1.1. Introduction

Concrete recycling has been gaining popularity in research in the last decades [68], [73], [74], [77], [151]–[155] and is included in the European Standard EN 12620 [156], where substitution is

currently allowed at the ratio 20% - 30% of recycled aggregates, depending on the national annex of each member state. However, at the moment, only the coarse fraction (> 2mm) is allowed for use in concrete. The exclusion of the recycled sands not only reduces the available recyclable material, but also increases cost of the treatment of the waste, influencing the economic and environmental feasibility of recycled concrete as a material. Furthermore, the sands, fine fractions and crushed old mortar fractions are still embedded in the coarse aggregates or present as larger fractions (Figure 4-1), therefore the influence of the finer or sandy recycled particles cannot be avoided. This is more visible in the interfacial contact region between the coarse aggregates and the concrete matrix. In natural concrete, the coarse aggregates are bound to the paste through a single interfacial region between two explicit phases: the aggregate and the paste. This is generally the weaker region of the matrix and the crack formation is initiated in this zone [108], [157]. The properties of the contact region depend on the chemical and mechanical nature of the bond. However, as chemically reactive aggregates are not used for concrete production, the strength of the bond is mainly influenced by the morphology of the recycled aggregates [158]. In recycled concrete, a more complicated contact region can be observed due to the residual mortar paste that is embedded in the recycled aggregates (Figure 4-1). Therefore, three distinct contact regions can be detected in the matrix: the old aggregate to old matrix, the old aggregate to the new matrix and the old matrix to the new matrix.

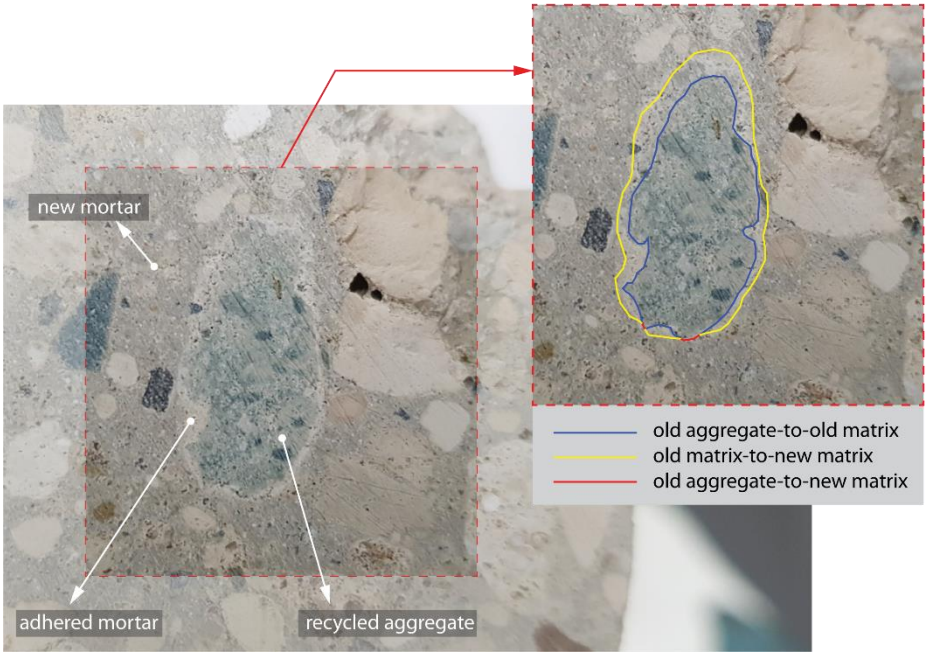

Figure 4-1. Interfacial contact setup in recycled concrete

The interface between the old aggregate and the new matrix, as well as the original interface between the old aggregate and old matrix, in principle, do not differ from the normal interfacial contact within a natural concrete. The third sub-region however can be defined as a contact between an old mortar and a new mortar, and is, currently little pondered in literature.

When considering the failure mode of a composite material, the interface can be modelled as a separate phase with a thickness between 20 μm and 50 μm [71] and lower mechanical parameters than the constituting materials. The first approach to standardize the concept of the interfacial transition zone (ITZ) is considered to be the work of the RILEM Technical Committee 159-ETC [115]. The lower mechanical properties of the ITZ are attributed to the wall effect and segregation that occurs during the hydration of the cement in the region around the aggregates, which leaves a zone where the products of cement hydration have lower density than the paste [158]. The elasticity modulus of the concrete decreases with the increase of the volume of aggregate-mortar interface, especially in high water/cement ratios and the mechanical properties of concrete depends on the composite action of its constituents [116]. This change in properties generates a non-linearity in the stress-strain behaviour and creates tensile micro-stress peaks [159], which contributes in the initiation of the first cracks and ultimately to the deterioration of the concrete matrix.

Brittle materials, such as concrete are governed by an elastoplastic damage behaviour that is influenced both by hydrostatic pressure and deviatoric stresses. Therefore, the two most popular failure models are the Mohr-Coulomb failure criterion and the Drucker-Prager failure criterion. The Mohr-Coulomb failure criterion, can be written as:

$$\tau = c - \sigma_n \tan(\varphi) \quad (1)$$

Where: $\boldsymbol{\tau}$ is the shear stress, $\boldsymbol{\sigma_n}$ is the normal hydrostatic stress, **c** is the cohesion and $\boldsymbol{\varphi}$ is the angle of internal friction

On the other hand, the Drucker-Prager criterion is expressed by:

$$\alpha I + \sqrt{J_2} + k = 0 \quad (2)$$

Where: $\boldsymbol{\alpha}$ and **k** are material constants and **I** and $\mathbf{J_2}$ are the first and second invariant of the deviatoric stress.

The correlation between these two failure laws can be done in function of the angle of internal friction and cohesion after first choosing the correlation criteria as shown in Figure 4-2.

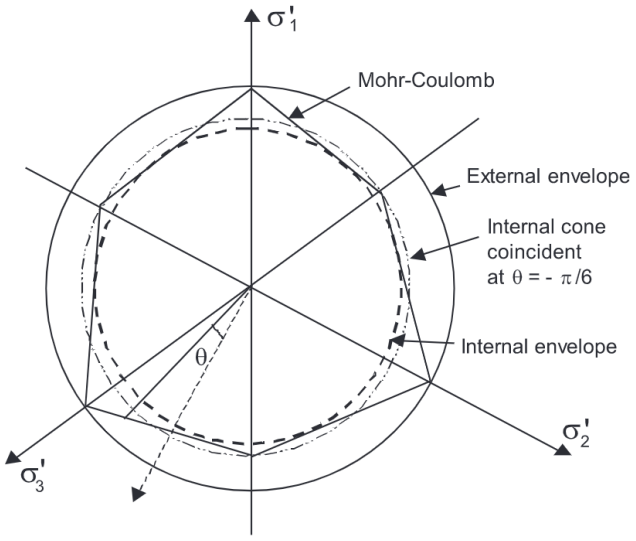

Figure 4-2. The different correlation possibilities between the Mohr-Coulomb and Drucker-Prager failure criteria [114]

Characterization of the interface can be either done through upscaled models [115]–[119], by testing the tensile strength of the contact between two phases or by applying a combination of numerical models based on continuum mechanics and experimental data. The scale of the structure is an influencing factor on the type of criterion that must be considered. According to Bazant [120],

strength criterions can be successfully used in correlation with laboratory tests, while for larger elements linear elastic fracture models are more appropriate. Testing methods to determine the interfacial strength include the direct tensile test, splitting tests, direct shear test, push-off test, slanted shear test and bending test [121].

Jebli et al [116] showed, through direct shear tests, that the crack for concrete elements starts always at the cement-aggregate interface and determined the cohesion to be 3 MPa for the composite and 4.1 MPa for the cement paste, while the local friction angle was 47° and 54° respectively. Akcaoglu et al [119] determined that the interfacial bond is determinant for the tensile behaviour of concrete, but its contribution in the compressive strength is minimal. Caliskan and Karihaloo [117] showed that the surface roughness significantly affects the interfacial bond and that the bond behaviour is dependent on the mineralogy of the aggregates. Ceia et al [118] used slanted shear tests to conclude that the interfacial strength between a natural concrete and a recycled concrete can decrease up to 161% for a full replacement of recycled coarse aggregates and proposed the following modified correlation formulas between the strength parameters and the roughness of the surface.

$$c_a = 0.3 + \frac{R_{pm}}{15}$$

$$\mu = 0.4 + \frac{R_{pm}}{5}$$

Where: $\mathbf{c_a}$ is the cohesion, $\boldsymbol{\mu}$ is the internal friction angle and $\mathbf{R_{pm}}$ is the roughness of the surface

Santos and Julio [123] presented the following relationship based on an extensive testing programme of concrete-to-concrete bond:

$$C_d = \frac{1.062 R_{vm}^{0.145}}{\gamma_{coh}}$$

$$\mu_d = \frac{1.366 R_{vm}^{0.0.041}}{\gamma_{fr}}$$

Where: $\mathbf{c_d}$ is the cohesion, $\boldsymbol{\mu_d}$ is the internal friction angle, $\mathbf{R_{vm}}$ is the mean valley peak and $\boldsymbol{\gamma}$ are safety factors

Eurocode 2 [100] presents a simpler approach for assessing the failure parameters, where the surface is first arbitrarily defined as “very smooth”, “smooth”, “rough” or “indented” and for each surface type a set of values for the cohesion and friction coefficient is given.

However, the contact behaviour between the adhered mortar paste and the new concrete matrix is still to be fully described in terms of its failure mechanism and failure parameters. The evaluation of such aspects can make feasible a complete numerical study of the recycled concrete matrix and will significantly aid the design and improvement of recycled concrete elements. The aim of the present study is to offer a clear mechanical characterization of the interfacial bond between the old mortar and the new recycled sand mortar through experimental investigations. The Mohr-Coulomb parameters of friction and cohesion are assessed and the effects of recycled sand content and surface roughness are correlated.

4.1.2. Methods and materials

4.1.2.1. Experimental setup

The experimental methodology is based on slanted shear tests. This type of test was selected for its easy application and for the possibility of controlling the failure surface angle. The later aspect is not possible through other testing methods, such as direct shear tests. According to EN 12615 [160], the slanted shear tests may be done at a 30° angle. However, in this work, four different failure angles are considered (26.6°, 29.7°, 33.7° and 38.7°) with the aim of locating the true internal friction angle by regression analysis through four sets of experiments. Another modification to the standard was regarding its size. To specifically address mortar paste, a reduction of the specimen was done by using the standard EN 196 [160] prismatic specimen of 160x40x40 mm. Slanted shear components were produced in the four desired angles in order to produce the prismatic elements composed of two separate mortars (Figure 4-3).

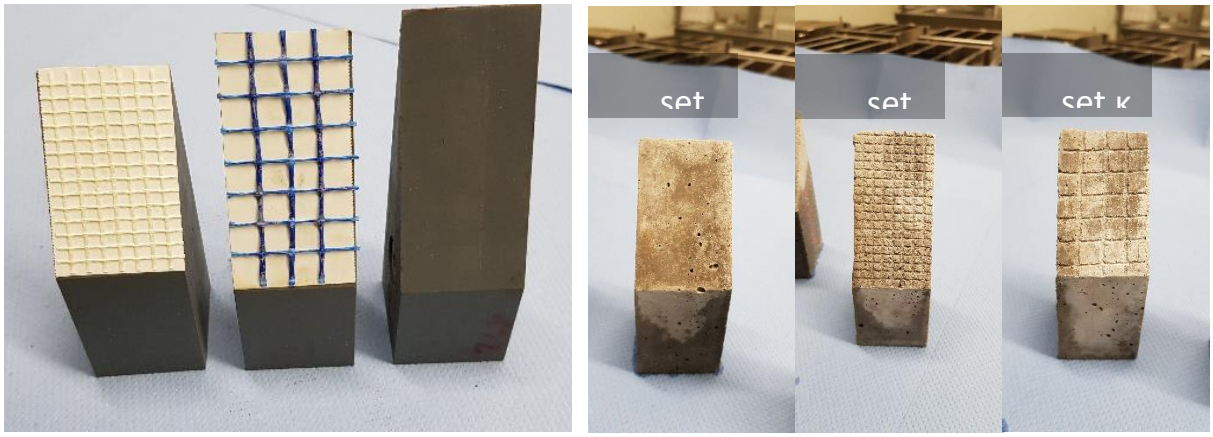

Figure 4-4. Roughness imprint meshes and hardened specimen after removal from the mould.

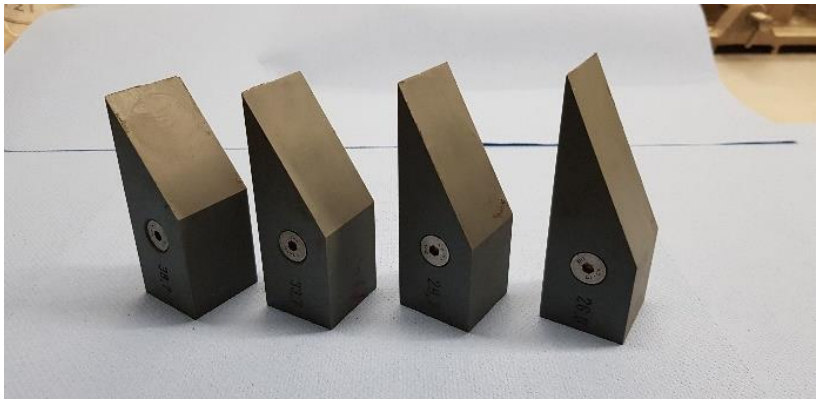

Figure 4-3. Slanted shear components

The contact surface was also modified to have a total of three variation of surface roughness. This was achieved by adhesion of plastic meshes into the surface of the slanted components. Therefore, the roughness variations are nominated α for the totally smooth surface (the mortar is cast against the slanted component), β for a rough surface achieved through a square mesh of 0.5 mm distance and κ for a rough surface achieved through a square mesh of 1 mm distance (Figure 4-4).

The testing program consisted of casting one part of the slanted prism in natural mortar while the other one was varied between natural mortar and recycled mortars with 20% (RM20), 50% (RM50) and 100% (RM100) replacement ratios of recycled sand.

The used mortar mixture was a standard recipe as described in EN 196-1 with ratios of cement:sand:water of 2:6:1 according to weight. CEN Norm Sand (0-2 mm) and a commercial 42.5N cement was utilized. These simplifications allowed to reduce the influence of other factors

such as the mix design, constituents or additives, thus increasing the control over the considered influencing factors (surface roughness and recycled sand content). The recycled sand is originating from a local inert landfill and is adjusted to the same granulometry as the Norm Sand to avoid grain size effects. The recycled sand was beforehand tested for bulk density and water absorption and the compensation method was used to modify the mortar recipe to account for the increased water absorption.

The mixing procedure was done in three steps, first dry mixing of sand and cement for 30 seconds, then the incorporation of half of the water content and mixing for 60 seconds and finally the addition of the rest of the water and mixing for 90 seconds. The moulds were vibrated to ensure compact filling. After the first slanted pieces were cast, they were left to cure in water for 28 days. Following this curing period, the second part was cast in contact with the first hardened piece to form prisms. The prisms were then left to cure in water for 28 more days. No adhesive agent was used between the two slanted pieces. After the curing period, the compression was done using a 250 kN hydraulic press with a loading rate of 0.7 kN/s (Figure 4-5)

Figure 4-5. Compression setup

For each variation, four repetitions were completed to achieve a good statistical distribution of the results. In total 192 specimen were tested. The entire experimental setup is summarized on Figure 4-6.

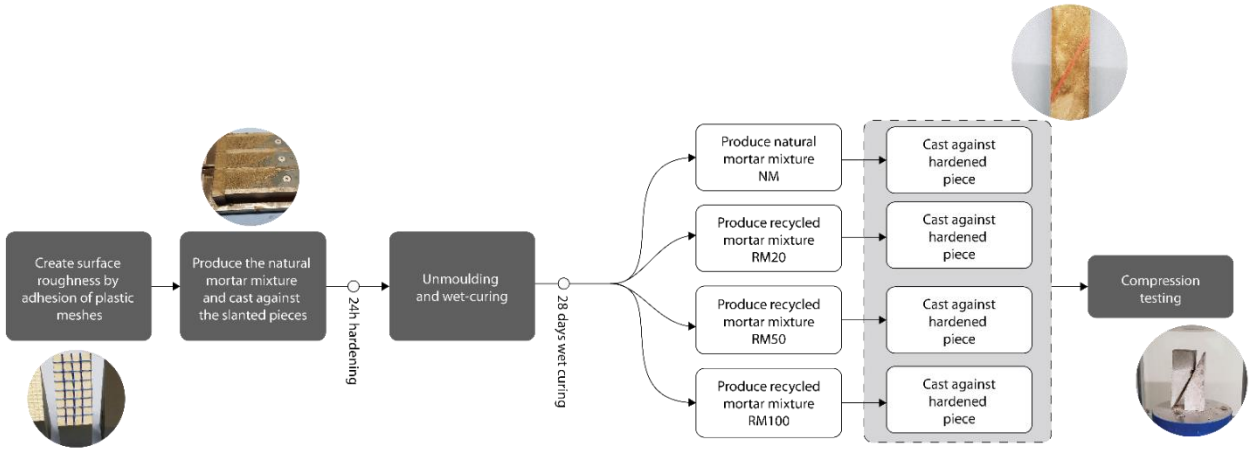

Figure 4-6. Overview of the experimental procedure

4.1.2.2. Assessment of the surface roughness parameters

The roughness of a surface parameters can be assessed through several methods, such as, among others, the sand patch test, mechanical stylus, 3D Laser Scanning, ultrasonic or microscopy [161]. In this paper, a photogrammetric method is utilized, by analyzing a set of photos into the commercial software Recap Pro. Through its built-in cloud computing, it was possible to obtain a 3D mesh of the surface (Figure 4-7), which was later analyzed for deducing the roughness parameters with Matlab. The images were taken using a Canon 2000D DSLR camera with a 24.5 MP resolution. The affinity of the reconstructed models is ±1 pixel. The standard deviation between measurements was kept lower than 0.025 mm.

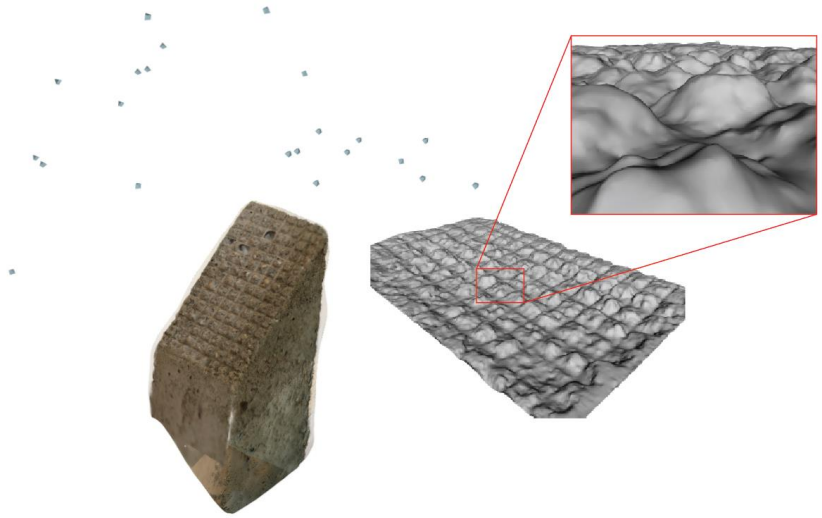

Figure 4-7. 3D model of the slanted element created through photogrammetry

The surfaces parameters were calculated for each of the produced surfaces (α, β, κ) by taking the mean value of three different point clouds to achieve a statistically sound sample. An overview of the considered roughness parameters as well as their calculation formulas can be seen in Table 4-1.

Table 4-1. Roughness parameter definition

Arithmetic average height	$R_a = \frac{1}{l}\int_0^l \lvert y(x)\rvert dx$
Root mean square roughness	$R_q = \sqrt{\frac{1}{l}\int_0^l \{y(x)\}^2 dx}$
Ten-point height (according to the ISO norms)	$R_{z(ISO)} = \frac{1}{n}\left(\sum_{i=1}^{n} p_i - \sum_{i=1}^{n} v_i\right)$
Ten-point height (according to the DIN norms)	$R_{z(DIN)} = \frac{1}{2n}\left(\sum_{i=1}^{n} p_i + \sum_{i=1}^{n} v_i\right)$
Maximum height of peaks	$R_p = \max(p_i)$
Maximum valley depth	$R_v = \max(v_i)$
Mean height of peaks	$R_{pm} = \frac{1}{n}\left(\sum_{i=1}^{n} p_i\right)$

Mean depth of valleys	$R_{vm} = \frac{1}{n}\left(\sum_{i=1}^{n} v_i\right)$
Maximum height of profile	$R_t = \max(p_i) + \max(v_i)$
Mean of maximum peak to valley height	$R_{tm} = \frac{1}{n}\sum_{i=1}^{n} R_{ti}$
Third point height	$R_{3y} = \max(p_i) + \min(v_3)$
Mean of third point height	$R_{3z} = \frac{1}{5}\left(\sum_{i=1}^{n} R_{3yi}\right)$

Where: l is the profile length, y the perpendicular (height) dimension of the surface, x the longitudinal coordinate of the point, p points above the mean line (peaks), v points below the mean line (valleys), n number of samples or points and v_3 the three lowest valleys.

For more information regarding the calculation of roughness parameters, the reader can refer to Gadelmawla et. al [162].

4.1.3. Results

4.1.3.1. Analysis of the roughness parameters

The calculated roughness parameter can be seen on Table 4-2 and the analysed surfaces are displayed on Figure 4-8 for sets of alpha, beta and kappa, where a significant amount of detail is visible, such as surface irregularities and porosity. It is noticeable that the values of roughness parameters are highly dependent on its calculation method, therefore a clear trend cannot be determined. However, as expected, the smooth set (alpha) had the lowest values. Set beta shows roughness values ranging from 66% to 766% compared to the initial values of alpha, while kappa showed values ranging from 25% to 3849% of alpha set. The comparison between the three surface topologies is shown on Figure 4-9 with respect to the smooth surface. On Figure 4-9, the quality of the roughness parameters can be assessed. In the majority of cases, the smoothest set is alpha, while the roughest surface appears to be kappa. However, this trend is reversed for the parameter

R_z (ISO). This is mainly due to the fact that this parameter considers 10 equidistant segments from which the Z-values are considered. Therefore, the measurement values are taken in an arbitrary way, without considering the full surface. This method appears to be significantly affected by surface irregularities and thus cannot be used as a roughness parameter for the targeted purpose of this work.

Table 4-2. Roughness parameters for the three surface variations

Roughness parameter	**Roughness variations considered (units in mm)**		
	α	**β**	**κ**
R_a	0.020	0.151	0.760
R_q	0.022	0.034	0.092
$R_{z(ISO)}$	0.366	0.240	0.092
$R_{z(DIN)}$	0.447	0.766	1.261
R_p	0.020	0.151	0.764
R_v	0.643	0.890	1.344
R_{pm}	0.201	0.573	0.789
R_{vm}	0.459	0.737	1.246
R_t	0.908	1.537	2.565
R_{3y}	0.660	1.309	2.035

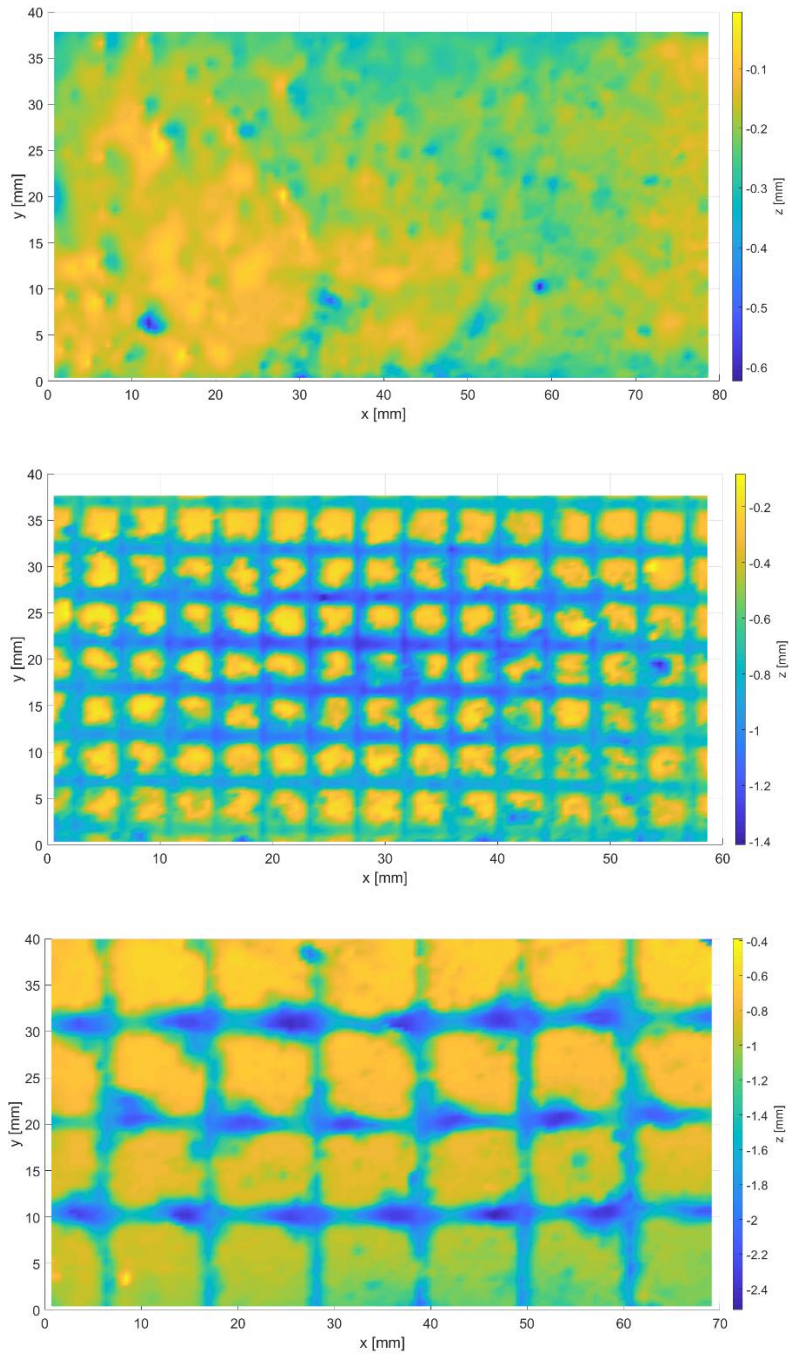

Figure 4-8. Surface topology: alpha, beta, kappa

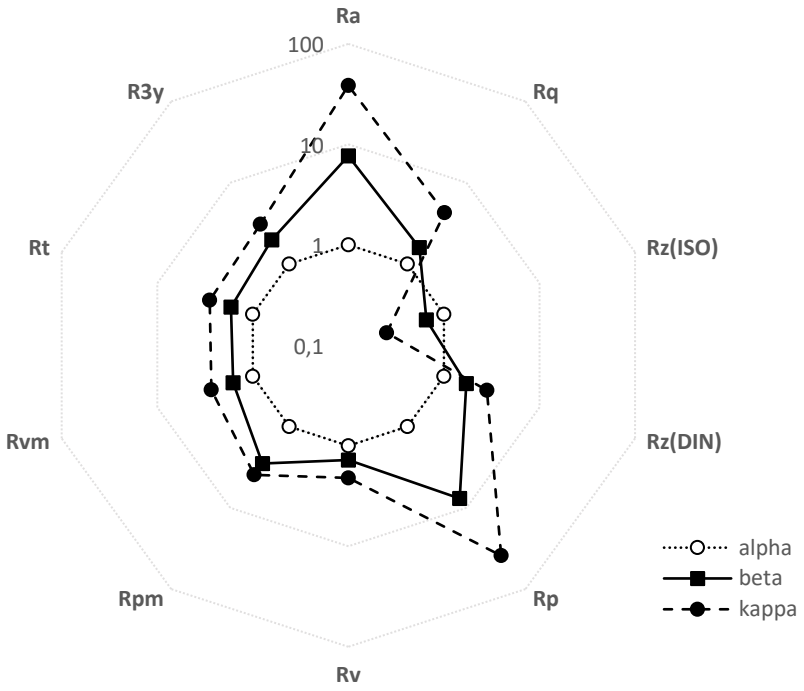

Figure 4-9. Relative roughness parameters in reference to the smooth surface alpha (logarithmic scale)

4.1.3.2. Influence of the recycled sand in the internal friction angle and cohesion

The produced mortars were first tested in strength in tension and compression to test their quality and understand the impact of recycled sand in the material itself. In terms of compression, the use of recycled sand lowered the strength proportionally to the substitution ratio. The loss of strength compared to the natural mortar was 22.8%, 49% and 75.5% respectively for a substitution rate of 20%, 50% and 100%. The tensile strength showed a slightly different trend. As it can be seen on Figure 4-10, the tensile strength drop was marginally higher for the 20% substitution ratio compared to the 50% substitution ratio with tensile strengths of 2.19 MPa and 2.25 MPa.

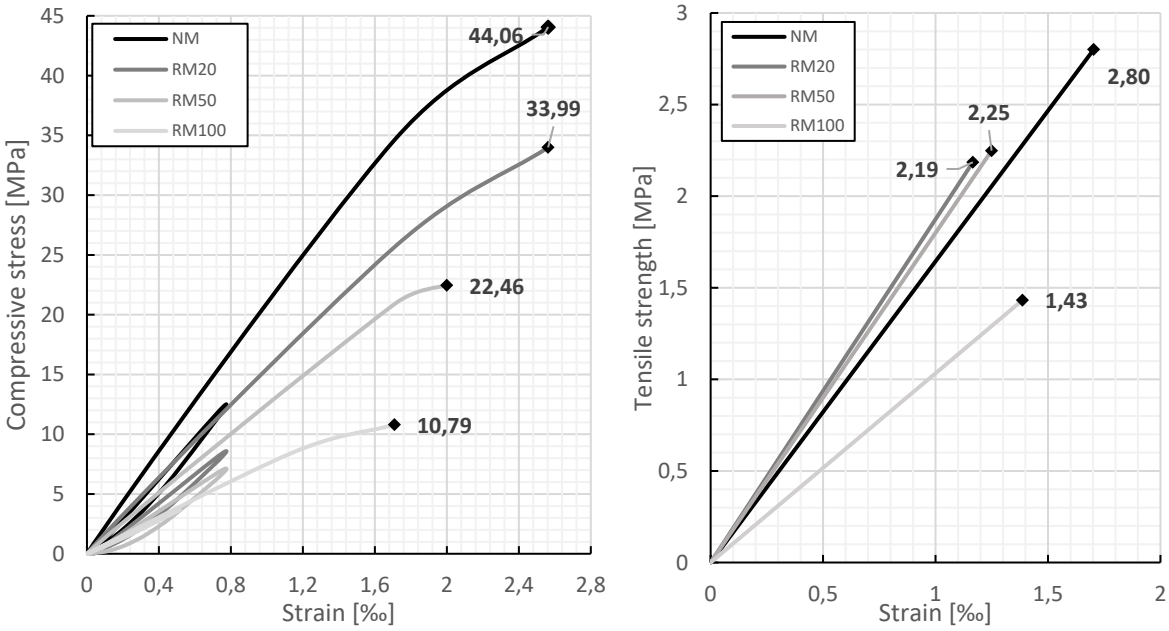

Figure 4-10. Compressive and tensile strength of the produced mortar pastes

The constructed Mohr-Coulomb plane yield stress surface can be seen on Figure 4-11. The reduction of the yield surface is progressive as the amount of recycled sand increases and has a reduction of 40.3%, 73% and 93.5%respectively for substitution rates of 20%,50% and 100%

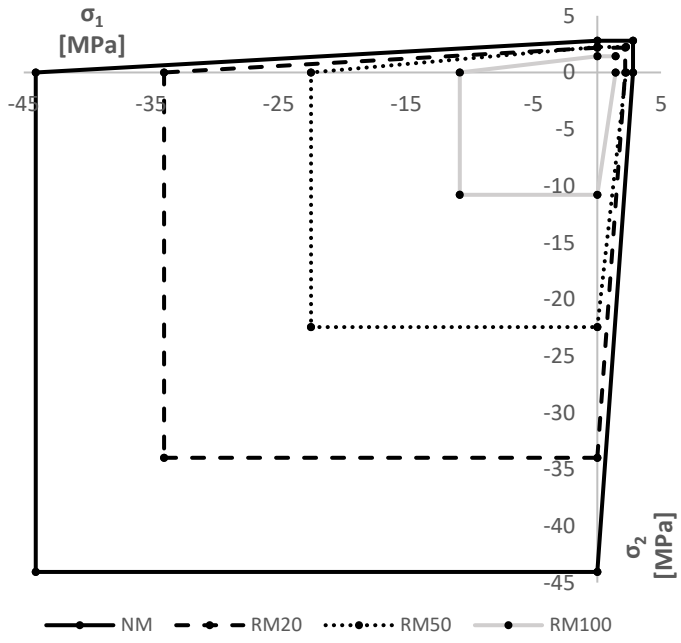

Figure 4-11. Mohr-Coulomb plane yield stress surface for the produced mortars

The Mohr-Coulomb law for the interface in the different substitution ratios, depending on the surface roughness is shown in Figure 4-12. For the natural sand (12a), there is no significant change in the failure envelope when comparing the different surface roughness. The friction coefficient varies between 0.79 and 0.88, while the measured cohesion is between 1.52 MPa and 2.21 MPa. For the 20% substitution ratio (12b), a different trend is observed. In this case, the interfaces containing recycled sand showed higher strengths in the rough surfaces (beta and kappa) compared to the smooth set. This difference is mainly due to the cohesion which is higher by up to 3462%. The increase in cohesion is to be expected, as the interlocking effect is facilitated by a rougher surface. For this set, the friction coefficient was between 0.62 and 1.49, while the cohesion was between 0.13 MPa and 4.60 MPa. A similar effect can be seen for the 50% substitution ratio as well (12c). However, in this case, the smooth set showed a significantly higher friction coefficient with an 46% increase compared to the rough sets. The friction coefficient for the 50% substitution ratio varied between 0.58 and 0.85 and the cohesion between 1.25 MPa and 3.68 MPa. In the full substitution of recycled sand, a similar trend to the natural sand is seen with no substantial difference in the interfacial strength between the surface treatments. The friction coefficient was between 0.69 and 0.87 and the cohesion between 0.73 and 1.72 MPa.

As expected, in a full substitution, the interfacial strength is significantly lower compared to the natural sand with the cohesion having a reduction of 30.5%. On the other hand, the friction coefficient was lowered by only 6%, which shows that the loss of strength in recycled mortars and concretes is mostly due to a change in the cohesion. This can be due to the impurities present in recycled sand which prevent a good bonding with the cement. Additionally, the recycled sand granules are generally more porous compared to the natural sand and have in them microcracks and shells of embedded cement and other particles. However, for a limited substitution ratio, as seen for the sets with 20% and 50%, an increase in the interfacial strength was noticed when compared to the natural mortar. This can be explained with the presence of unhydrated cement in the recycled sand, but the positive effects of this additional pozzolanic activity seem to be limited and, for full substitutions, are not observable anymore.

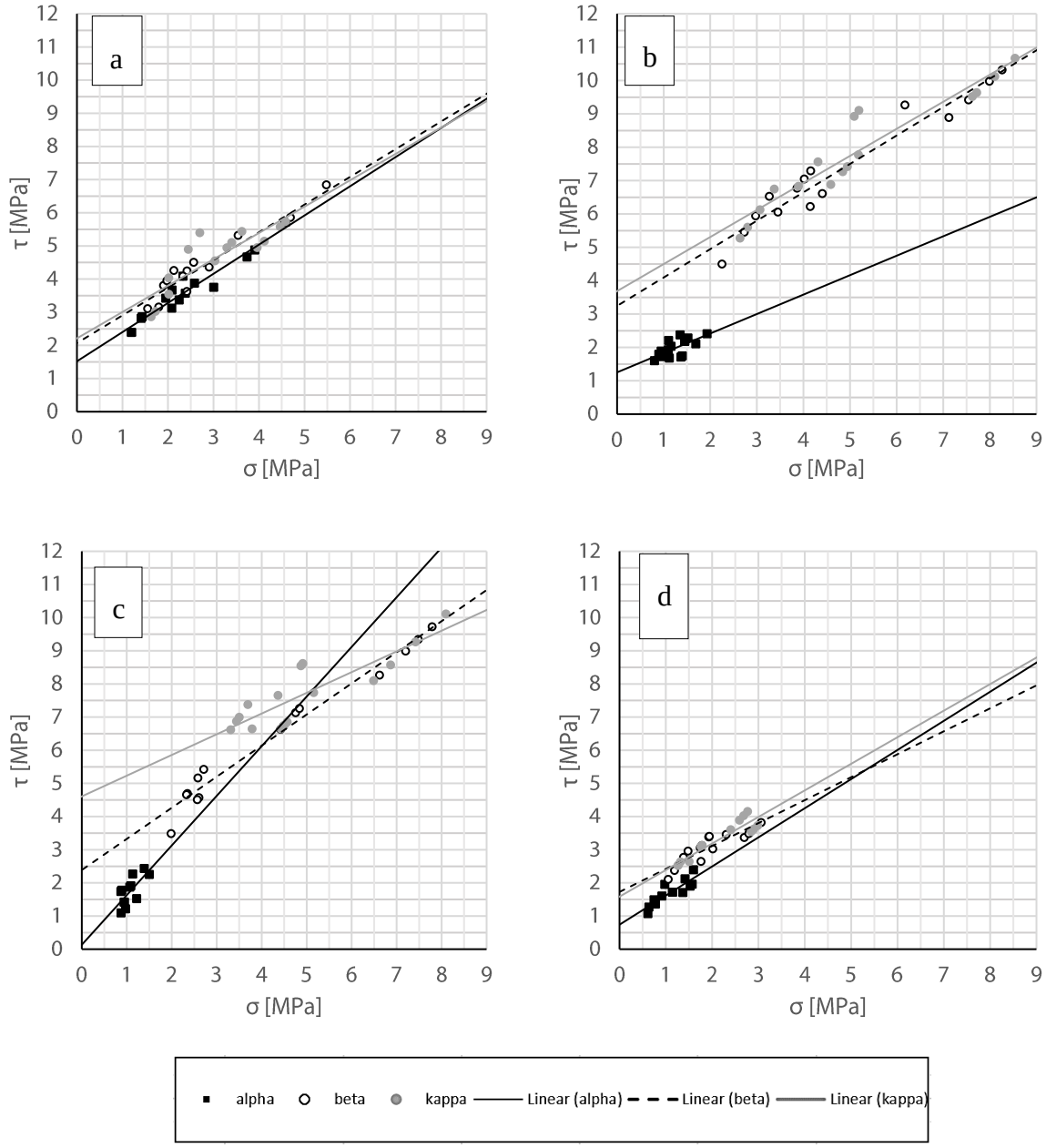

Figure 4-12. The Mohr-Coulomb law for the interface: a) natural sand; b) 20% recycled sand; c) 50% recycled sand; d) 100% recycled sand

On Figure 4-13, the relation between the interfacial shear strength and the substitution ratio of recycled sand is shown. It is noticeable that the smooth set (alpha) exhibits a different trend compared to the two rough sets. Indeed, on set alpha, there is no increase of strength for the 20% and 50% substitution ratio. This is a further indication on how the roughness of the surface facilitates cohesion between the recycled mortar and the natural mortar. However, in reality, the adhered mortar paste or the mortar covered aggregates generally show a rounded shape due to the

fact that the shape is determined by the impact during the crushing process and the roughness in itself is influenced by the size of the granules of fines and cement as seen on Figure 4-14. Therefore, it can be postulated that set alpha shows the real behaviour of the interfacial behaviour at this scale. However, further study is needed to quantify the typical range of roughness levels that appear in practice.

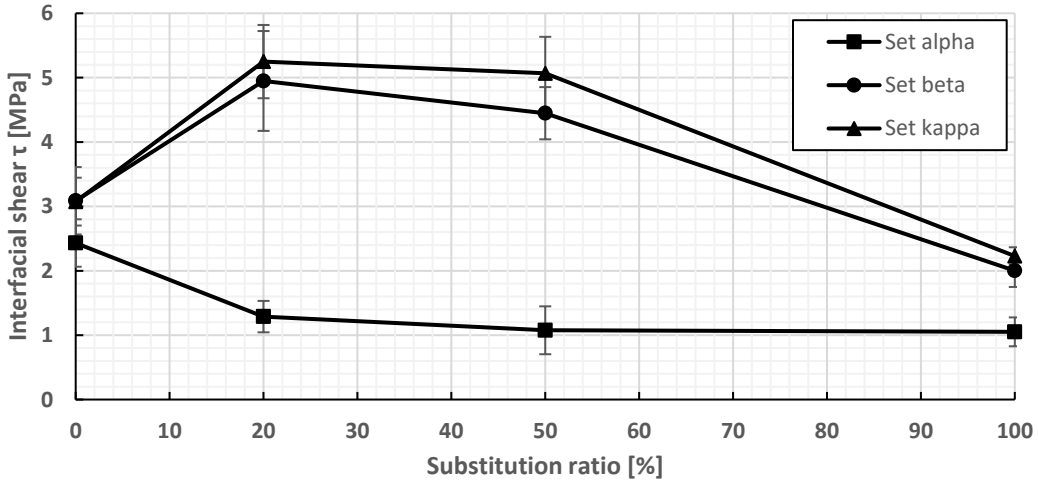

Figure 4-13. Variation of the interfacial shear strength in relation to the substitution ratio

Figure 4-14. Typical mortar-covered recycled aggregate

4.1.3.3. Influence of the surface roughness on the interfacial bond strength

The Mohr-Coulomb failure law of the tested specimen depending on the surface roughness sets can be seen on Figure 4-15. The smooth set (alpha) showed, in general, lower failure stresses and displays the weaker interface. Within set alpha, the natural mortar displayed a higher failure strength. For the two rough sets (Figure 15), the increase of interfacial strength for the low to mid substitution ratios is visible, as the 20% and 50% substitution ratios show a stronger interface in both cases.

The influence of the roughness variations in the interfacial strength can be seen on Figure 4-16 for the different substitution ratios used. For all cases, a higher roughness parameter leads to a higher interfacial strength due to the increased interlocking effect which affects the friction between the two parts. For the natural mortar (NM) and the full substitution of recycled sand (RM100) the effect of the roughness is lower compared to the other set. Specifically, a 30.5% increase in interfacial strength was noticed between roughness α and β for NM and 75.7% for RM100. For the other two substitution ratios, this increase is more significant, at respectively 378% for RM20 and 341% for RM50. This increase of strength in recycled cementitious materials has been reported for concrete mixtures by several studies ([59], [79], [80]) and it is believed to be caused by the amount of unhydrated cement paste remaining in the recycled aggregates. Furthermore, the presence of other fractions, such as clays, can further increase the cohesive adhesion, especially in rough surfaces. Clays in particular can be transmitted to the recycled sands during deposition time in landfills and are comprised of finer particles with mineral phases that differ in shape from the sand particles. Due to this, the fine particles of unhydrated cement and clays are prone to stratification and adhere better, especially when the surface roughness is high. However, the studies of this effect on mortar mixtures are scarce and further investigations are necessary in the future to understand the underlying mechanism that cause this increase in strength.

The increase in strength appears to occur when there is a significant surface roughness in the contact. It is noticeable, that for a low roughness parameter, the interfacial strength of all recycled mortar mixtures is very similar at an average of 1.88 MPa with a 6% variation between them, while the strength of the normal mortar is approximately twice as high. The behaviour of the interface

for low surface roughness follows a similar trend as the general material strength (Figure 4-10), although with a lower variation. It can be expected that for recycled aggregates showing a complete shell of adhered mortar paste and are produced either from old smooth gravel (such as riverbed gravels) or crushed through an impact crusher, that the influence of increased interfacial strength for low to medium substitution rates to be less evident.

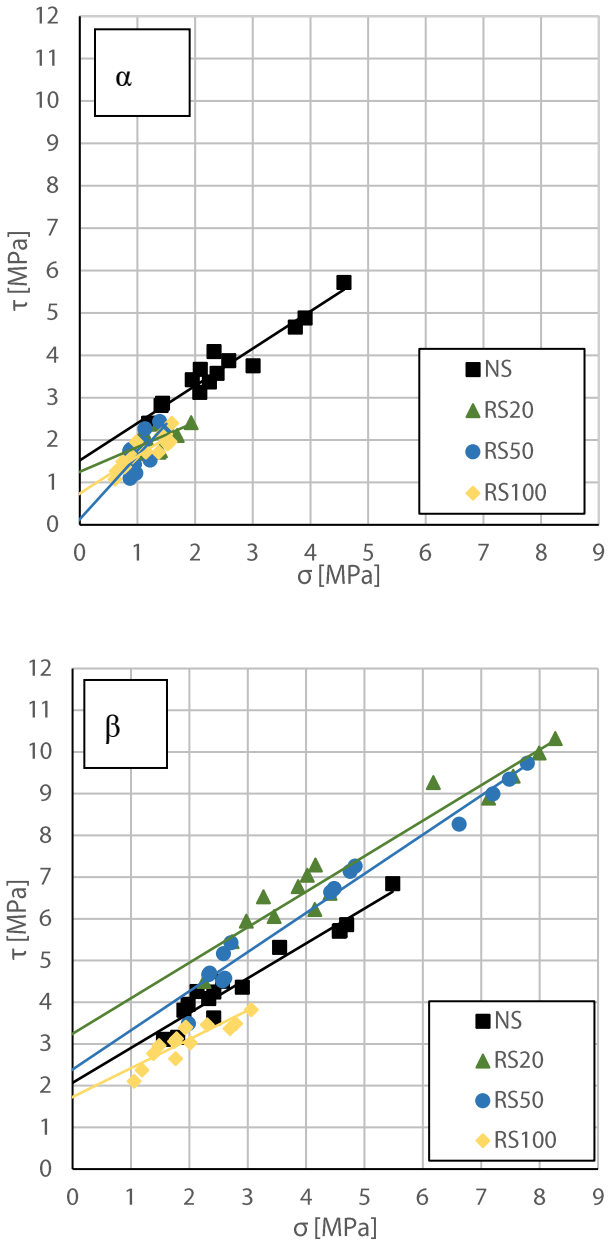

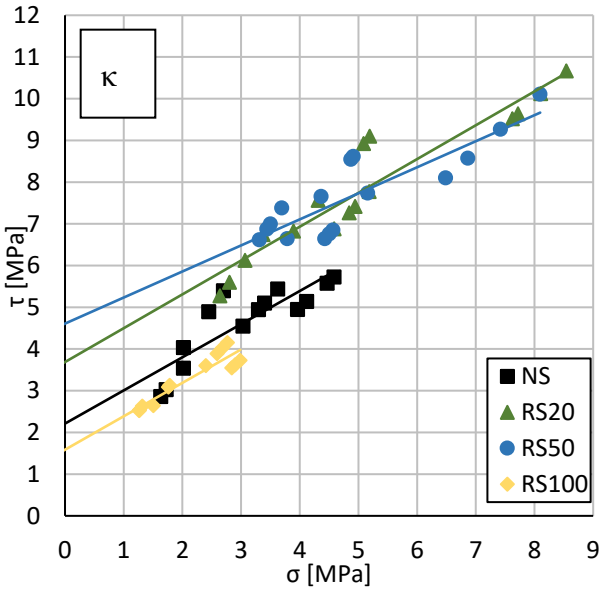

Figure 4-15. Mohr-Coulomb failure criterion for the tested substitution ratios

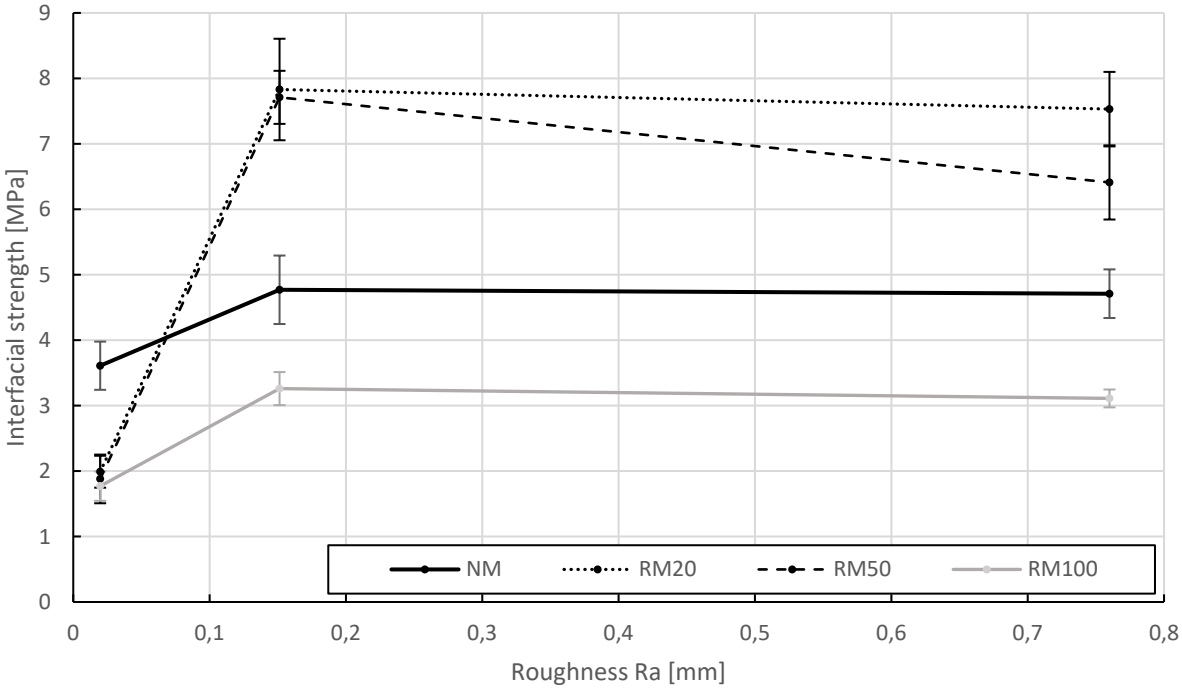

Figure 4-16. The interfacial strength in relation to the roughness for the prepared mixes

4.1.3.4. Influencing factors and comparison with the existing models

As general overview, the experimental investigation results are displayed on Figure 4-17 where the interfacial shear strength is plotted in relation to the roughness and the substitution ratio. It is visible that there exists an area between 20% and 50% substitution ratio and above 0.151 mm roughness where the interfacial strength is higher. This was also reflected in the failure lines shown on Figure 4-12 and Figure 4-15. It can be seen that for no substitution ratio, a higher interfacial strength can be achieved even at low roughness, while with the inclusion of recycled sands, a higher roughness is needed to achieve higher strengths.

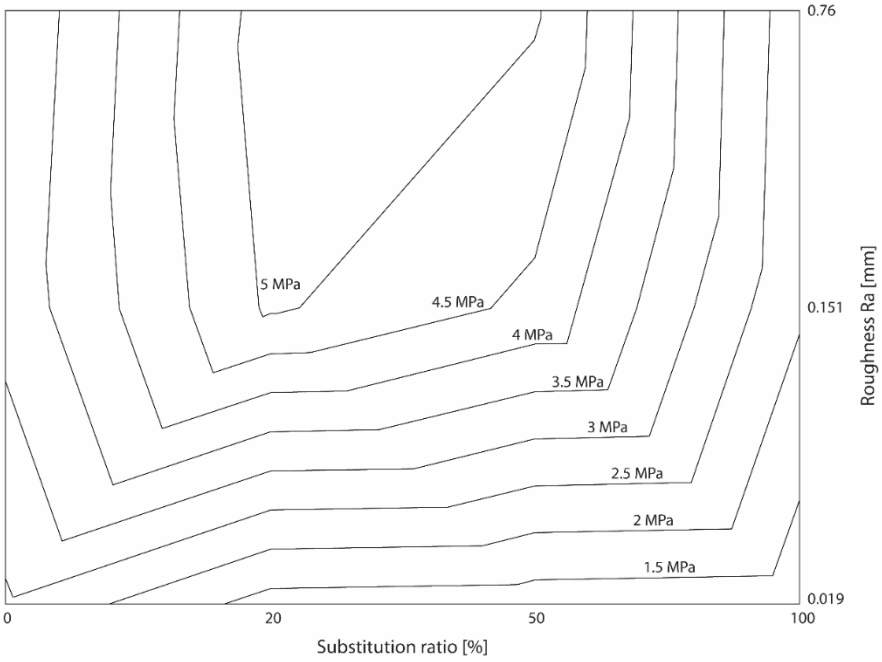

Figure 4-17. The influence of the substitution ratio and the roughness on the interfacial shear strength

The Mohr-Coulomb parameters assessed from the experimental data are also compared to the models existing in literature.

Figure 4-18 and Figure 4-19 show the friction coefficient and the cohesion in comparison to three existing models, from Eurocode 2 [100], Ceia et. al [118] and Santos [123]. In terms of the friction coefficient, the values given by the Eurocode seem to be overestimating the friction coefficient, especially for the “rough” and “indented” denominations. The other two appear within the range of the experimental data. On the other hand, for the cohesion, the Eurocode gives very conservative values. As it can be seen from Figure 4-19, virtually all experimental data show a

higher cohesion compared to the model. Since cohesion appears to be the determining factor in the interfacial bond, it can be said that the Eurocode model may be used conservatively for the characterization of the interfacial bond parameters. However, the roughness of the surface should not be considered "rough" in order for the friction coefficient not to be overestimated. As outlook, it is necessary for the Eurocode to be amended by adding numerical values for the roughness in the interfacial model for cementitious materials.

A similar trend is shown for the cohesion in the other two models considered. Even though these models include a clear relation between the roughness and interfacial parameters, both of them undervalue the cohesion in the majority of test data points. For the friction coefficient, on the other hand, the model from Santos appears to give an upper limit, while the model from Ceia shows a better affinity to the experimental data.

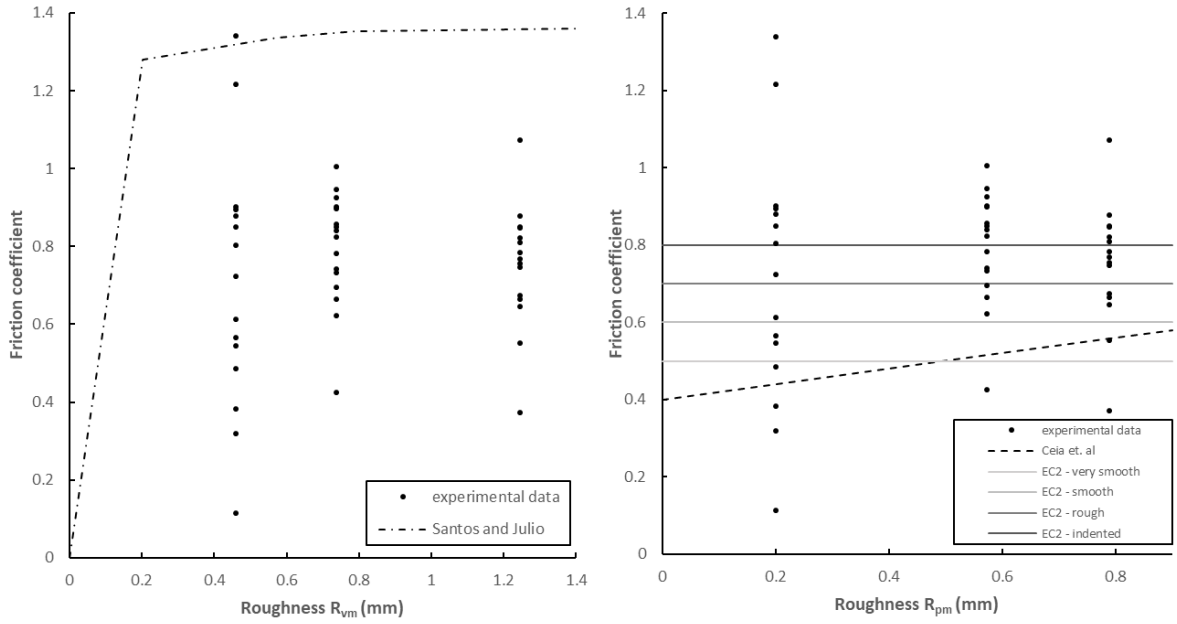

Figure 4-18. Friction coefficient: Comparison between the test results and some existing models

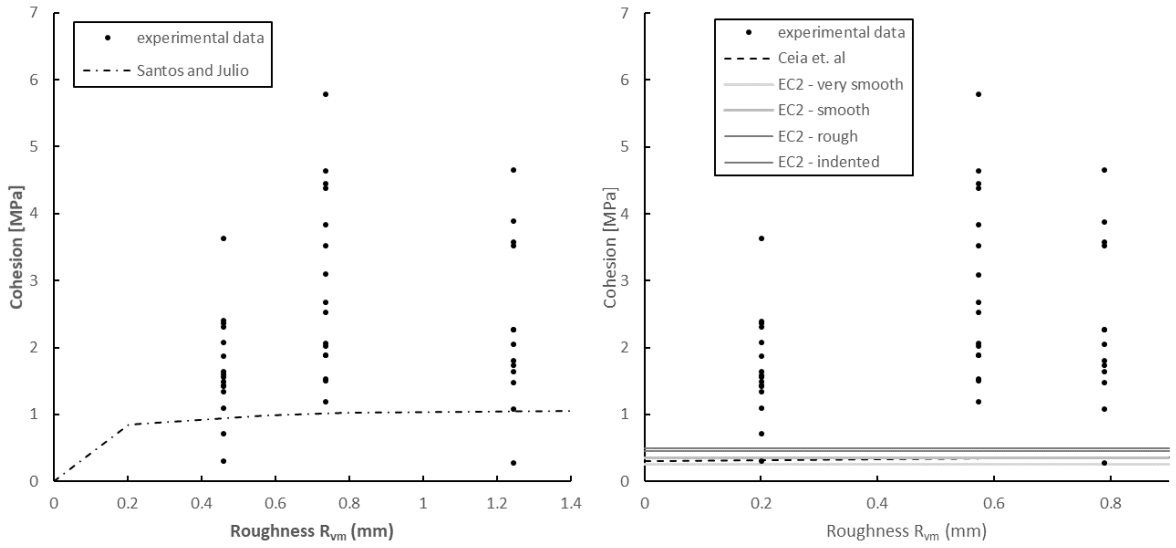

Figure 4-19. Cohesion: Comparison between the test results and some existing models

4.1.3.5. Scanning electron microscopy (SEM) of the interfacial transition zone

To have additional insight in the interface between the adhered mortar and the new mortar, additional tests were performed on a scanning electron microscope. Samples were prepared consisting of a single recycled aggregate, covered in mortar with 0%, 20%, 50% and 100% substitution of recycled sand, while keeping the same mix proportions as used for the slanted shear tests. A special consideration was given to the interface between the two mortar phases to understand the difference in strength between the low to medium substitutions (20% and 50%) and the full substitution.

As it can be seen on Figure 4-20, the interface between the old adhered mortar and the new recycled mortar paste with 50% recycled sand, exhibits significant cracking and porosity in the contact region between the old mortar and the new one. The layer of adhered mortar paste in the recycled aggregate showed a width of up to 1159 µm. As expected, the interface appeared to be a purely mechanical contact and the difference between the phases is clearly visible. The recycled mortar with a 50% recycling ratio displayed some microcracks in its matrix. However, if a comparison is made with the specimen with full substitution (Figure 4-21), there is a substantial

difference in the amount of porosity and cracking. This expectingly lowers the mechanical properties of the material and subsequently, the interfacial contact is further weakened. It is possible that this microcracking is the main reason for a lowered mechanical behaviour in the mixtures with a full substitution of recycled sand and that there is a limit where the added strength due to the pozzolanicity of the recycled sand is offset by excessive micro-cracking of the mortar matrix. The excessive cracking on the matrix of the fully recycled mortar appears to be due to drying shrinkage since the specimen were under no external load at any time before the SEM imaging. However, a deeper understanding of this phenomenon is still needed to be studied.

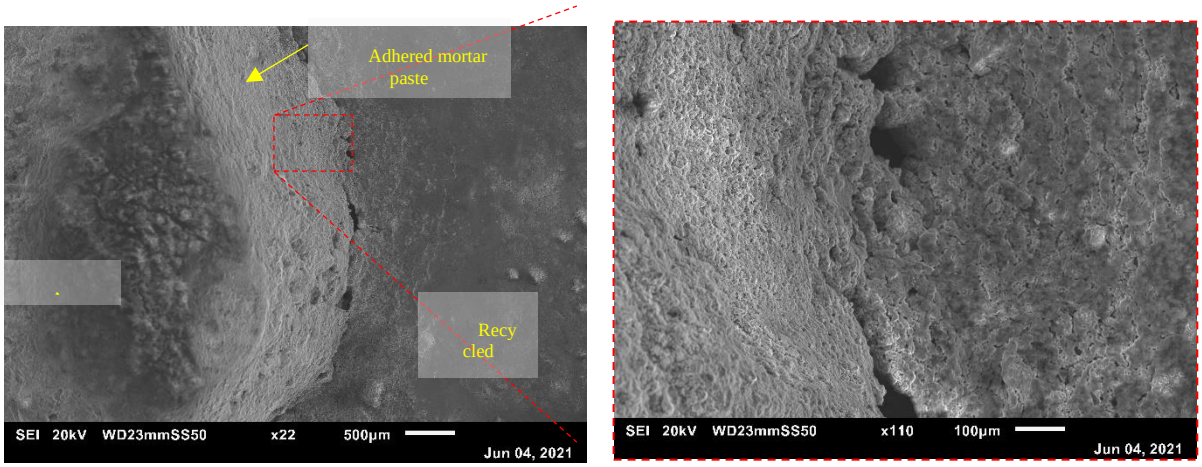

Figure 4-20. SEM images in the interface for the 50% recycled mortar

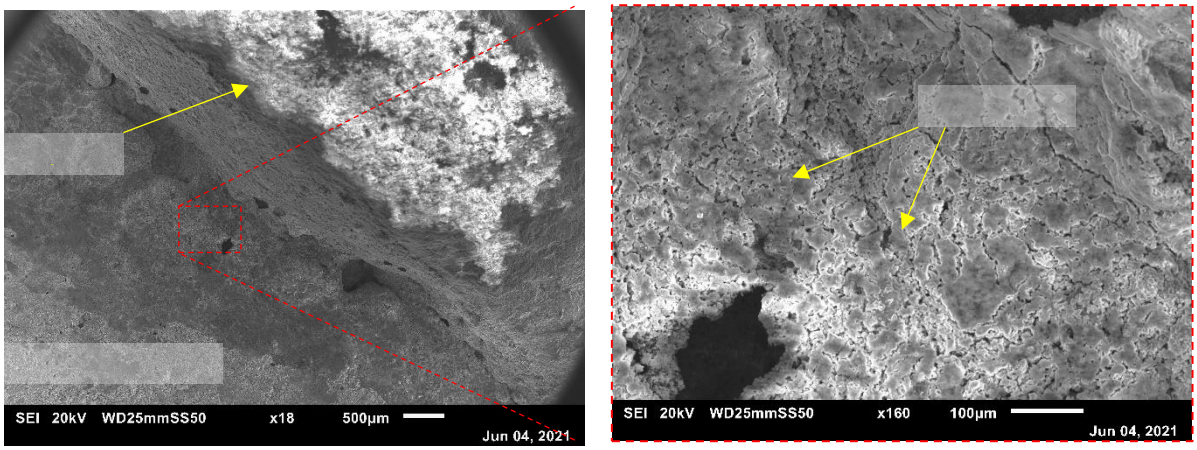

Figure 4-21. SEM images of the recycled mortar structure with the cracking pattern visible

4.1.4. Discussion

The presented experimental test results indicated the effect of the adhered mortar paste in the recycled concrete matrix. The increased bond strength in the low to medium substitution ratios shows promising potential for the use of recycled sand and its inclusion on the current standards, as its influence on the interfacial bond strength does not represent specific drawbacks in terms of the mechanical properties. However, there are still a few aspects that need to be considered in future investigations.

The present study only considers untreated recycled sand fractions. This choice was done as an investigation on the worst-case scenario, but also to explore the possibility of using recycled aggregates with minimal costs. Therefore, a study on different treatment methods and how they influence the interfacial bond could lead to a technical and economic break-even point with optimized cost-benefit.

Further investigation is also needed on the limit of the peak strength for low to high substitutions and describing on a qualitative and quantitative aspect the underlying mechanism. Since the current study only considers the compression and shear behaviour, it is important to see how the interface behaves for other aspects such as durability and dimensional stability. In addition, the high variability of recycled aggregates needs to be considered. The present study only considers one type of recycled sand which is originating from bulk construction and demolition waste in Luxembourg. However, the quality and composition of recycled aggregates is never uniform and can change from one geographical region to another. To give definite answers and build models to finely describe the behaviour of such materials, a more extensive study needs to be done with materials coming from different areas, different demolition processes, different storage and treatments.

Finally, the effect of the roughness needs to be deepened, especially in bringing it into context of what a realistic roughness value is for a recycled aggregate. This would be important in defining a clear set of parameters, lowering the number of variables and defining a clear standardized procedure for the testing of the mechanical strength in concretes and mortars. In this context, the challenges are numerous as the true roughness of the surface depends on the shape of the aggregate, the typology of the rock, the treatment procedure and the amount of adhered paste. Furthermore,

the characterization of a surface roughness in a three-dimensional spheroid and its potential effect on the stress distribution needs further investigations.

4.1.5. Conclusions

The present paper presents a series of experiments made to characterize the interfacial bond strength between normal mortars and recycled mortars in terms of mechanical performance. The aim of the experiments was to investigate the interfacial strength between the adhered mortar and new mortar in the recycled concrete matrix.

The conclusions of the paper can be summarized as in the following:

- Recycled sandy fractions (0-2 mm) can reduce the compressive strength of the mix by up to 75.5% for a full substitution. The tensile strength on the other hand is less affected and shows a reduction of up to 51%.
- The roughness of the surface affects the bond strength significantly. For smooth contact surfaces, there is a progressive loss of bond strength by 181%, 192% and 204% respectively for substitution ratios of 20%, 50% and 100% when compared to the control mixture. For rough surfaces, mixtures with 20% and 50% recycled sand show a higher bond strength compared to the control mixture. The further increase of the surface roughness R_a beyond 0.082 mm did not further increase the bond strength.
- The Mohr-Coulomb strength parameters range between 0.69-0.88for the friction coefficient and 0.13MPa-4.60MPa for the cohesion. From all the experiments, the cohesion appears to be the most variable and influencing parameter.

- For no substitution and for the full substitution of recycled sand, there is no significant influence of the roughness in the interfacial strength parameters.
- The interfacial strength is significantly lowered for a full substitution, while for partial substitution, an increased strength was observed due to the presence of impurities and unhydrated cement. The limit and turning point for this strength increase still need to be assessed.
- Existing models can only partially characterize the failure parameters of recycled mortars. The Eurocode model and the model proposed by Santos overestimate the friction coefficient, while the model from Ceia shows a better affinity. All models are very conservative in the cohesion definition when compared to experimental data.
- Scanning electron microscopy (SEM) images show a visible difference between the matrix of the mortar with partial sand replacement and full sand replacement, with the latter displaying a definite network of microcracks. Such a network was not visible for mortars made with 20% and 50% recycled sand, justifying the strength increase exhibited in the interface of partially recycled mortars.

Finally, it can be said that research in the interfacial behaviour of recycled concrete still needs further development to be able to construct a material law that describes its mechanical behaviour, especially while considering the vast variability of the material itself.

4.2. Publication V: Phase-field model for mixed-mode inelastic fracture in recycled aggregate concrete material (Kinda, Kabore, Bogoviku, Waldmann)

Abstract

In this paper, a finite element-based concrete model is developed within a phase-field fracture modelling framework and includes treatment of interfaces allowing to predict evolution crack under external loading. The approach introduces zero-thickness interface elements equipped with fracture energy. The asymmetric behaviour between tension and compression is also taken into account by splitting the total deformation energy. We employ this model to investigate the load-bearing capacity and the crack developing at the interface in recycled aggregate concrete (RAC). After the calibration and validation of the experimental results, a parametric study has been undertaken to analyse the effects of ITZs and the new mortar matrix on the stress-strain relationship. It is revealed that the mechanical properties of the new mortar matrix and comparable mechanical properties between ITZs and mortar matrices play a significant role in the overall stress-strain relationship and failure patterns of RAC under uniaxial compression loadings. The model allows predicting fracture behaviour of complex structure heterogeneity due to recycled aggregate.

Keywords: Phase-field fracture, Plasticity, Recycled aggregates concrete (RAC), Compressive failure, Parametric study

4.2.1. Introduction

The demand in aggregates continues to drastically increase due to globally expanding construction markets [163]. As a result, construction industry actors have sought more sustainable and clean resources amid environmental concerns and the rapid depletion of natural resources. Furthermore, there is an increase in material waste from demolition driven by urbanization, disasters, and renewal to meet new energy efficiency and safety standards; it opened the opportunity for a large stock of readily available material that can be used as a constituent of new concrete mixtures. Thus, concrete waste can be crushed and processed to extract the coarse aggregates to be used in full or partial replacement of natural aggregates [164]. Moreover, materials for structures must meet standards and building code requirements for mixed composition and mechanical properties for safety and sustainability issues. But concretes made with recycled aggregates exhibit different behaviour than concretes with normal aggregates. Studies in the literature show that the replacement of natural aggregates by recycled aggregates leads to a decrease in mechanical performance [165], resistance to freezing and thawing [166] while increasing the drying shrinkage [167].

Therefore, recycled aggregate concrete (RAC) has attracted ever-growing interest in the construction industry and among researchers seeking to improve its performances, mainly the load-bearing capacity, durability for the hardened concrete, and workability for the fresh concrete. However, two main facts, namely the strength reduction and increase in drying shrinkage, constitute significant barriers to the massive use of recycled construction materials.

Recycled aggregates have specific distinctions compared to natural aggregates, as they are fundamentally heterogeneous, depending on the origin of waste and the type of deconstruction [168]. Numerous experimental studies revealed that, in general, the strength is reduced when natural aggregates are replaced with recycled aggregates [169]. This has been attributed to different factors such as the crushing process [170], [171], the geometry of the RA [172], [173], the strength of the concrete where the recycled aggregate originates from [174], the amount of residual adhered cement mortar at the aggregate originates surface [174], [175],[176]. Research has shown that recovered cement mortar has a massive influence on the performance of RAC [169], [177].

Although many studies have been performed in the literature to understand better the behaviour of the RAC at the macroscopic level, the fracture behaviour is still not well understood at the mesoscopic level. According to [178], the matrix-aggregate bond strength in RAC is superior or at least equal to that developed with natural aggregates; this has been proved by [179] in their earlier experiments. On the opposite, [180] pointed out that RAC had lower quality due to the much higher water absorption, increased porosity and weaker ITZ; [181] conducted a study of the mechanical properties of high-strength concrete made from recycled aggregates and found that the properties of the original concrete have a significant influence on the mechanical properties of the RAC. So, the driving factor of the mechanical performance of recycled aggregates is still poorly understood; It is also widely accepted that the local mechanism at the microscale (crack initiation and propagation) are known to govern the macroscopic behaviour [182].

The modelling of the fracture process of recycled concrete aggregates at the mesoscopic level by considering the effective properties of the old attached mortar ITZ is a promising way to close this gap. This paper proposes a 3D mesoscale fracture modelling of concrete based on the phase-field approach. From a numerical perspective, modelling the mechanical response of RAC is challenging. Due to the complex interface between the new mortar matrix and the RA, increased likelihood of weak and strong discontinuities from the initial loading stage. Indeed, microvoids and preexisting cracks present in the old attached mortar add more difficulty in modelling RAC behaviour.

In section 2, we begin with a literature review and challenges in RAC research. Section 3 presents assumptions, thermodynamics formalism and a detailed description of the adopted constitutive model. Section 4 presents the results of the experiments and the identification of the parameters of the model. Section 5 presents the results of the parametric study.

4.2.2. Mechanical properties of RAC: Literature review and challenges

As recycled aggregates result from a crushing process, microcracks and micro faults are observed in their matrix, leading to an increase in porosity and consequently a reduction in density. Recycled aggregates are shown to have a bulk density which is from 3.8 % [67] to up to 18.6 % [183] compared to natural aggregates and an increased water absorption from 538.7 [73] to 1797

percent [184]. Since various factors are likely to impact the mechanical behaviour, the experimental studies sometimes lead to different conclusions. For instance, according to [185]–[187] , the mechanical properties of RAC are inferior to those of concrete made with normal aggregates: the quality of recycled aggregates and ITZ (Figure 4-22) impact the mechanical properties of RAC. While studies in [179], [185] found that the global failure behaviour of RAC specimens under compression, tension, or flexion is similar to that of conventional concrete specimens. Besides the global mechanical performance, the fracture process at the microscopic level plays a key role. The initiation and propagation of microcracks are different between RAC and normal concrete.

Cracks in RAC appear around the ITZs (both old and new) and then propagate into the mortar matrix. The initiation and propagation of microcracks are different between RAC and normal concrete [188], [189]. As concerning recycled aggregates, the adhered mortar paste, which is old mortar bound to each aggregate, either fully or partially encasing the particle. This paste has a higher porosity than the aggregate itself and influences most of the mechanical properties of recycled concrete. The compressive strength varies depending on the substitution ratios of recycled aggregates and can reduce up to 27.07 % for complete substitution of recycled coarse aggregates [190], while [191] reports a decrease of 17 % in the modulus of elasticity [191]. In terms of tensile failure, Argela et al. [59] report a loss of 10 % in tensile strength. Consequently, the cracking behaviour is more complex than conventional concrete due to the presence of the old mortar, which creates an additional weaker interfacial transition zone (ITZ) [185], [189]. A quantitative analysis of the fracture process of RAC and a deep understanding of its impact on the load-carrying capacity are highly needed. Most of the mesoscale models for the fracture of cement composites are in 2D and cannot predict non-planar 3D fracture surfaces in reality. One of the main difficulties in developing a mesoscale model for concrete is defining each phase of the composite and its corresponding mechanical properties. But recent developments in X-Ray computer tomography open new opportunities for the investigation of materials' behaviour at mesoscale [192], [193]. This motivates the development of mesoscale models since the material properties can be retrieved from these tests.

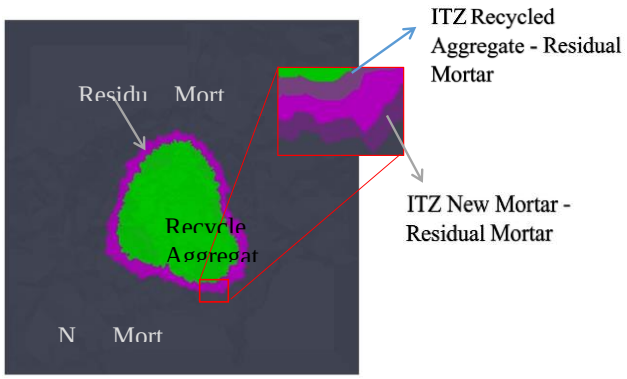

Figure 4-22. Illustration of phases in the RAC

4.2.3. Model

4.2.3.1. Kinematics

The context of this study is considerable strain and significant rotation of the element. We consider the standard multiplicative decomposition of the total deformation gradient into an elastic part Fe and a viscoplastic part Fvp as follows:

$$F = F^e F^{vp} \tag{1}$$

The spatial velocity gradient L representing the total deformation rate is defined as:

$$L = \dot{F}F^{-1} = L^e + F^e L^{vp} F^{e-1}, L^e = \dot{F}^e F^{e-1}, L^{vp} = \dot{F}^{vp} F^{vp-1} \tag{2}$$

where L_e and L_{vp} represent the elastic and viscoplastic deformation rate.

The viscoplastic part of the velocity gradient is then decomposed into stretching, and spin tensors are defined as:

$$L^{vp} = D^{vp} + W^{vp}, W^{vp} = \frac{1}{2}(L^{vp} - L^{vpT}), D^{vp} = \frac{1}{2}(L^{vp} + L^{vpT}) \tag{3}$$

D_{vp} and W_{vp} are the symmetric part and skew symmetric part of L_{vp} respectively.

The left Cauchy-Green strain tensor are given:

$$\mathbf{b} = FF^T; \mathbf{b}^{\mathrm{e}} = F^e F^{eT}; \mathbf{b}^{\mathrm{vp}} = F^{vp} F^{vpT} \tag{4}$$

Furthermore, each part of the deformation gradient can be decomposed into volumetric and isochoric/deviatoric stress:

$$F = F_{dev} F_{vol}; \mid \mathbf{b}_{\mathrm{dev}} = (J)^{-\frac{2}{3}} FF^T; \mathbf{b}_{\mathrm{vol}} = (J)^{\frac{2}{3}} I \tag{5}$$

where J = detF and I the identity matrix.

The following invariant are employed:

$$I_{b1}^e = \lambda_1^{e2} + \lambda_1^{e2} + \lambda_1^{e2} = b_1^e + b_1^e + b_3^e \tag{6}$$

λ_{ei}=1,2,3 are the principal stretches and b_i=1,2,3 the principal components of b_e.

The first principal invariant I1 and the invariant of the deviator J_2 of a tensor T:

$$I_1(T) = t_1 + t_2 + t_3, J_2(T) = \frac{1}{2} \mathrm{dev}\,(T) \colon \mathrm{dev}\,(T) \tag{7}$$

t_i =1,2,3 are the eigenvalues of T obtained by spectral decomposition:

$$T = \sum_{i=1}^{3} t_i e_i \otimes e_i, t_i = 2\rho \frac{\partial \Psi}{b_i} b_i = \rho \frac{\partial \Psi}{\lambda_i} \lambda_i \tag{8}$$

where e_i are the eigenvectors of b.dev(T) = T $-\frac{1}{3}$ tr(T)I is the deviator operator.

The following formulation is purely mechanical without consideration of thermal effects. The temperature only has an indirect effect through the material parameters.

4.2.3.2. Thermodynamic formalism

We consider a rigid body $\Omega \subset R^3$ with a mass density ρ, bounded by the surface $\partial\Omega$ and a surface traction t over $S \subset \partial\Omega$. The reference configuration is denoted Ω_0. The balance between internal and external work reads:

$$\int_{\Omega} \rho\dot{\Psi} dV = \int_{\Omega} b \cdot L dV + \int_{\partial\Omega} t \cdot L dS + \int_{\Omega} \rho \cdot \dot{L} L dV \tag{9}$$

where $\dot{\Psi}$ is the rate of change of the Helmholtz free energy Ψ, b represents a body force.

The present study aims at modelling the mechanical response of a material undergoing physical processes, including large elastic energy storage, rate and pressure-dependent dissipation mechanism, micro-cracks and failure. The following formulation is purely mechanical and does not directly consider temperature gradient or heat transfer effects. The thermal influence in the material is indirectly included through temperature-dependent material parameters

We assume that the body forms a decoupled system which allows additive decomposition of the free energy density function into an elastic, viscoplastic parts:

$$\Psi = \Psi_e + \Psi_{vp} \tag{10}$$

where Ψ_e the elastic free energy, Ψ_{vp} is the stored viscoplastic free energy describing the rate dependent hardening of the material.

Following the first law of thermodynamics, the rate of work per unit volume $\dot{W}$, is the sum of the Helmholtz free energy density $\dot{\Psi}$ and the rate of dissipation D:

$$\dot{W} = \rho\dot{\Psi} + \mathbf{D} = T : \dot{D} \tag{11}$$

The term T:D denotes the stress power per unit volume in the material configuration.

The rate of work is decomposed into elastic and viscoplastic parts as follows:

$$\dot{\boldsymbol{W}} = \dot{\boldsymbol{W}}_e + \dot{\boldsymbol{W}}_{vp} \tag{11}$$

The elastic work is the sum of the elastic free energy and the energy used for creating new surfaces through crack:

$$\dot{\boldsymbol{W}}_e = \rho\dot{\Psi}_e + \mathbf{D}_d = T : D^e \tag{12}$$

Likewise, the viscoplastic work is the sum of the viscoplastic free energy and the viscoplastic energy dissipated through heat D_{vp}:

$$\dot{\boldsymbol{W}}_{vp} = \rho\dot{\Psi}_{vp} + \mathbf{D}_{vp} = T : D^{vp} \tag{13}$$

As required by the second law of thermodynamics, the entropy production rates is non-negative. For an isothermal process, the Clausius-Duhem inequality reduced to the Clausius-Planck relation is given by:

$$\mathbf{D} = \mathbf{D}_{vp} + \mathbf{D}_d \equiv T : D - \rho\dot{\Psi}\Psi \geq 0 \tag{14}$$

According to thermodynamics, the state of a material undergoing any process at any given time can be described by a set of observable state variables and internal variables. Therefore, the following internal variables are introduced to describe the viscoplastic behavior:

$$Q^k = \frac{\partial\Psi_{vp}}{\partial D^{vp}}, Q^i = \frac{\partial\Psi_{vp}}{\partial p} \tag{15}$$

where Q^i is the hardening stress, associated with isotropic hardening and is conjugate to p. Q^k is the backstress, associated with kinematic hardening and is conjugate to internal variable D^{vp}.

4.2.3.3. Elastic constitutive model

We employ the compressible neo-Hookean material model for the elastic behavior. For an undamaged material, the strain energy density function is defined as addition of the dilational and distortional terms as follows:

$$\Psi_{eo} = \frac{1}{2}\mu\left(J^{e-\frac{2}{3}}\mathrm{tr}\,(\mathbf{b^e}) - 3\right) + \frac{1}{2}K(\log(J^e))^2 \tag{17}$$

where μ is the shear modulus and K the bulk modulus. The strain energy can be conveniently writen in term of principal stretches as:

$$\Psi_{eo} = \frac{1}{2}\mu\left(\lambda_1^{e2} + \lambda_2^{e2} + \lambda_3^{e2} - 3 - 2\log\left(J^e\right)\right) + \frac{1}{2}K(\log(J^e))^2 \quad (18)$$

The Kirchoff stress tensor can be derived from equation 20 as follows:

$$T_0 = \mu\left(\mathbf{b}^{\mathrm{e}}_{dev} - \frac{1}{2}J^{e-\frac{2}{3}}I^e_{b1}\mathbf{I}\right) + K(\log J^e)I \quad (19)$$

In this paper, the phase field method is applied to hyperelastic fracture in the context of anisotropic damage. Therefore the neo-hookean energy density function is employed for elastic behavior:

$$\Psi_{eo} = \frac{1}{2}\mu\left(J^{e-\frac{2}{3}}\mathrm{tr}\left(\mathbf{b}^{\mathbf{e}}\right) - 3\right) + \frac{1}{2}K(\log(J^e))^2 \quad (20)$$

4.2.3.4. Viscoplastic constitutive model

For materials presenting discontinuities, the plastic-free energy can be regarded as the energy expended for particles rearrangement, while the plastic dissipation energy is related to energy lost through frictional sliding and heat [194]. The origin of plastic-free energy is specific to the type of material. For example, in granular materials, it is attributed to irreversible rearrangement of the granules rather than their permanent deformation [195]. Consequently, the plastic flow is particularly complex and is influenced by hydrostatic pressure, unlike in metals.

We consider a non-associated Perzyna-type viscoplastic flow model to describe the rate dependent irrecoverable deformation:

$$\dot{D}^{vp} = \dot{\gamma}^{vp}\frac{\partial \mathcal{P}}{\partial T} \quad (21)$$

where $\dot{\gamma}^{vp}$ denotes the viscoplastic multiplier and P the viscoplastic dissipation potential.

In this study, we adopt the following viscoplastic dissipation function potential based on the non-associated Prager model:

$$\mathcal{P} = \sqrt{J_2(R)} - \beta I_1(R) \tag{22}$$

where $R = \text{dev}\,(T) - Q^k$ defines the relative stress, β is the dilation angle which is linked to the rise of internal friction.

The viscoplastic multiplier also known as the consistency parameter is expressed as follows:

$$\dot{\gamma}^{vp} = \frac{1}{\eta\eta}\left(\frac{f}{\tau_0}\right)^N \tag{23}$$

where η is the viscosity parameter, the term $\frac{f}{\tau_0}$represents an overstress function, *N* is a parameter determining the rate sensitivity of the viscoplastic flow and τ_0 the initial yield stress.

Furthermore, we allow the flow rule to account for temperature through the dependency of η and *N* on the temperature. For instance, the Arrhenius law can be employed:

$$\eta = \eta_0 e^{(-E_a/R\Theta)} \tag{24}$$

where E_a, *R* and Θ are the activation energy, the gas constant and the temperature respectively.

We assume that the viscoplastic flow occurs after the material has reached a yielding point. The existence of yield surfaces for viscoplastic heterogeneous materials is debated because many geomaterials exhibit irreversible flow early during the loading. Several yield criteria have been developed to address cohesion, friction and pressure-dependency in materials. This includes the well-known Mohr-Coulomb and Drucker-Prager yield functions. However, the M-C model does not account for the difference between tension and compression, and the yield surface does not meet the smoothness requirement. The Drucker-Prager criterion, a circle on the octahedral plane, satisfies the smoothness requirement but does not include tension-compression asymmetry. Therefore, we employed a modified version of the Drucker-Prager yield function presented in [54] as follows:

$$f = \sqrt{J_2(R)}\rho(r,\phi) - \alpha I_1(R) - \kappa \leq 0 \tag{25}$$

q_{kin} stress-like internal variable for the kinematic hardening, q_{iso} scalar stress-like internal variable for the isotropic hardening α scalar internal variable

I_1 is the first invariant Kirchoff stress and J_2, the second invariant of the deviatoric part of the Kirchoff stress tensor. α and κ are material parameters related to the cohesion and angle of internal friction. They are usually determined by making the Drucker-Prager yield surface coincide with the Mohr-Coulomb edges. When matched with the internal edges of the Mohr-Couloumb surface, the D-P corresponds to M-C in uniaxial tension and biaxial compression:

$$\alpha = \frac{6\sin\ \phi}{\sqrt{3}(3 + \sin\ \phi)}, \kappa = c\frac{6\cos\ \phi}{\sqrt{3}(3 + \cos\ \phi)} \tag{26}$$

For the external edges the D-P corresponds to M-C in uniaxial compression and biaxial tension:

$$\alpha = \frac{6\sin\ \phi}{\sqrt{3}(3 - \sin\ \phi)}, \kappa = c\frac{6\cos\ \phi}{\sqrt{3}(3 - \cos\ \phi)} \tag{27}$$

Alternatively, κ can be defined as a function of the plastic strain as hardening function. The function ρ(*r*,θ) was introduced to modify the yield surface shape according to the loading type, creating a distinction between tension and compression. The parameters are the ratio between the yield strength in tension and compression *r* and the *lode angle* θ. We use the function defined by [54] which ensure convexity of the yield function:

$$\rho(r,\theta) = r_1\cos\left[\frac{1}{3}\cos^{-1}\left(r_2\cos\ 3\theta\right)\right] \tag{28}$$

where

$$r_1 = \frac{2\sqrt{1-r+r^2}}{\sqrt{3}r} \qquad r_2 = -\frac{3\sqrt{3}}{2}\frac{(1-r)r}{(1-r+r^2)^3}$$

The Drucker-Prager yield function in equation 25 can be formulated in such a way that the kinematic and isotropic hardening are taken into account.

$$f = \sqrt{J_2(R)}\rho(r,\phi) - \alpha I_1(R) - \kappa = f_t\left(T, Q^k(D^{vp})\right) - Q^i(p) - \tau_y \leq 0 \qquad (29)$$

Q^k is a stress-like internal variable for the kinematic hardening, Q^i scalar stress-like internal variable for the isotropic hardening, p a scalar internal variable and τ_y the yield stress.

The evolution of the the backstress Q^k is given by the Prager's linear kinematic hardening:

$$\dot{\boldsymbol{Q}}^k = \frac{2}{3}H_k D^{vp} \qquad (30)$$

where H_k is the kinematic hardening modulus.

From the thermodynamic perspective, both Q^k and Q^i are derived from the following viscoplastic free energy:

$$\rho\dot{\Psi}^{vp} = \frac{H_k}{2}D^{vp}{:}D^{vp} + \frac{\kappa}{2}\dot{p}{:}\dot{p} \qquad (31)$$

4.2.3.5. Phase-field description of fracture

A phase-field model is a powerful tool for describing fracture and is therefore employed in this study. The concept (Figure 4-23) is to describe the crack discontinuity by a damage phase represented by a scalar field $d \in [0,1]$, 6.

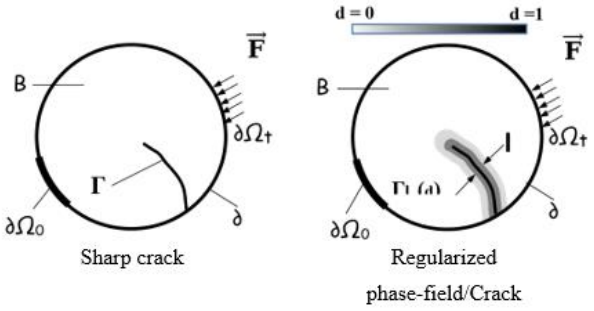

Figure 4-23. The phase field approach

The sharp crack surface is regularized into a smeared topology easing the strong discontinuity of the displacement field around the crack, and thus allowing efficient numerical implementation. The Griffith's representation of fracture energy is therefore regularized as follows [196]:

$$\int_{\Gamma} G_c \Gamma dV = \int_{\Omega} G_c \frac{1}{2\ell}(d^2 + l^2|\nabla d|^2)dV \tag{32}$$

where G_c is the critical fracture energy, Γ is the sharp crack surface, the term $\frac{1}{2\ell}(d^2 + l^2|\nabla d|^2)$ is the crack surface density and ℓ is a length scale parameter.

The introduction of damage alters the free energy of the system and modifies the total energy balance in equation 9 as follow [196], [197]:

$$\int_{\Omega} \bar{\Psi} dV + \int_{\Omega} G_c \frac{1}{2\ell}(d^2 + l^2|\nabla d|^2)dV = \int_{\Omega} \boldsymbol{b} \cdot \boldsymbol{u} d\Gamma + \int_{\partial\Omega} \boldsymbol{t} \cdot \boldsymbol{u} dS \tag{33}$$

$$\bar{\Psi} = [g(d) + k]\Psi \tag{34}$$

where k is a positive infinitesimal used for numerical stability, $g(d)$ represent degradation function.

We employ the degradation function as in [196]:

$$\mathrm{g(d, p)} = (1 - \mathrm{d})^2 \tag{35}$$

In ductile fracture, the degradation may be modified so that the viscoplastic displacement is taken into account. For further details about the contribution of the plastic strains to the damage growth, the reader is advised to refer to [198]. For the sake of simplicity we use the degradation function defined in equation 35.

The above fracture model has proven to predict fracture in tension accurately. However, several studies have shown that the unrealistic crack arises and fracture surfaces interpenetrate in compression. To cope with these limitations, several authors proposed an additive split of the stored elastic energy [196], [199], [200] into two parts, one of which is used as a driving force for the fracture phase. Methods for such energy split can be regrouped in three categories: the volumetric-deviatoric [199], the spectral split [196] and the directional split [201], [202].

The widely used volumetric-deviatoric split proposed by [199] is based on the assumption that the damage growth is driven by volumetric expansion and deviatoric deformation:

$$\Psi(\epsilon^e)^+ := 0.5\, K_n \langle \epsilon_1 + \epsilon_2 + \epsilon_3 \rangle_+^2 + \mu\left(\epsilon^{dev} : \epsilon^{dev}\right) \Psi(\epsilon^e)^- := 0.5\, K_n \langle \epsilon_1 + \epsilon_2 + \epsilon_3 \rangle_-^2 \qquad (36)$$

with $K_n = \lambda + \frac{2\mu}{n}$, n being a constant, ϵ^e is the elastic part of the infinitesimal strain.

Miehe et al [196] proposed that the evolution of the damage field is driven by tensile loading and volumetric expansion. The split is based on spectral decomposition of the strain as follows:

$$\Psi(\epsilon^e)^{\pm} := 0.5\lambda \langle \epsilon_1 + \epsilon_2 + \epsilon_3 \rangle_{\pm}^2 + \mu\left(\langle \epsilon_1 \rangle_{\pm}^2 + \langle \epsilon_2 \rangle_{\pm}^2 + \langle \epsilon_3 \rangle_{\pm}^2\right) \qquad (37)$$

with $\Psi(\epsilon^e)^+$ being the driving force for the phase-field.

To apprehend the fracture behaviour, it is crucial to model the closing and opening of cracking. A combination of the spectral decomposition and deviatoric-volumetric split has been proposed by [29]. We adopt the volumetric stretching split of the Neo-Hookean energy density:

$$\Psi_e^+ = 0.5 \cdot \sum_{n=1}^{3} \left(C_n - 1 - \log\left(C_n\right)\right)\Big|_{J>1} + 0.5 * \lambda (\log J)^2|_{J>1} \qquad (38)$$

$$\Psi_e^- = 0.5 \cdot \sum^{3}\left(C_n - 1 - \log\left(C_n\right)\right)\Big|_{J<1} + 0.5 * \lambda(\log J)^2|_{J<1} \tag{39}$$

Shear-tension decomposition Mode I and II fracture:

$$\Psi(\epsilon^e)_I^{\pm} := 0.5\lambda\langle\epsilon_1 + \epsilon_2 + \epsilon_3\rangle_{\pm}^2 \tag{40}$$

$$\Psi(\epsilon^e)_{II}^{\pm} := \mu\left(\langle\epsilon_1\rangle_{\pm}^2 + \langle\epsilon_2\rangle_{\pm}^2 + \langle\epsilon_3\rangle_{\pm}^2\right) \tag{41}$$

is adopted. Accounting for different fracture toughness G_{cI} , G_{cII} in each fracture modes as follows:

$$(1-d)\left(\frac{\Psi(\epsilon^e)_I^{\pm}}{G_{cI}} + \frac{\Psi(\epsilon^e)_{II}^{\pm}}{G_{cII}}\right) - \frac{1}{2l_0}d = 0 \tag{42}$$

4.2.3.6. Summary of the model

The Helmholtz free energy density of the system is now expressed as function of the state variables:

$$\Psi = \Psi(D^e, D^{vp}, p, d) \tag{43}$$

Using equation (16) into (9) gives the following balance equation:

$$\begin{aligned}&\int_\Omega \left(\frac{\partial\bar{\Psi}_e}{\partial D^e} : D^e + \mathrm{Q}^k : D^{vp} + \mathrm{Q}^i : \dot{p} + \frac{\partial\bar{\Psi}}{\partial d} : \dot{d}\right) dV + \int_\Omega G_c \frac{1}{2\ell}(d^2 + l^2|\nabla d|^2) dV = \\ &\int_\Omega \boldsymbol{b}\cdot\boldsymbol{L} dV + \int_{\partial\Omega} \boldsymbol{t}\cdot\boldsymbol{L} dS + \int_\Omega \boldsymbol{\rho}\cdot\dot{\boldsymbol{L}}\boldsymbol{L} dV\end{aligned} \tag{44}$$

For the present case, we restraint the analysis in the framework of rate-independent plasticity, which represents a limit case of viscoplastic flow.

4.2.4. Experimental investigation

Laboratory experiments were prepared as validation of the results. The samples consist of a single recycled coarse aggregate embedded in mortar paste. The samples were cubes of dimensions 40x40x40 mm. The recycled aggregates were chosen randomly in a mix of construction and demolition waste (CDW) of unknown age or origin. The size of the aggregates was chosen from the standard EN 933-2 sieve 8. Each aggregate was washed to remove dust and clay from the surface with the aim of improving the adherence and interfacial strength. However, all aggregates showed signs of adhered old mortar paste on their surface. The new mortar paste was chosen to be a standard mortar based on standard EN 196-1 with the ratios of cement:sand:water as 2:6:1 in weight. The utilized sand is a CEN Norm Sand of gradation 0-2 mm according to EN 196-1 and the cement is a 42.5N class commercial cement. These chosen standardized specifications allow for a reduction of uncertainties in the mix by avoiding other influencing factors, such as admixtures and focusing strictly on the influence of the recycled aggregate.

Figure 4-24. Compression of the cubic specimen

The specimen were prepared in a controlled environment and tested after 28 days of wet curing. For the compression tests a 250 kN hydraulic press was utilized keeping the speed of loading constant at 0.7 kN/s. In total 5 cubic specimen were compressed showing a mean strength of 33.55 MPa (Figure 4-24). The prepared mortar paste was also tested separately in compression and 3-

point bending at 28 days according to EN 12390, showing a mean compressive strength of 49.30 MPa and a mean tensile strength of 7.44 MPa. The results can be seen on figure 2.

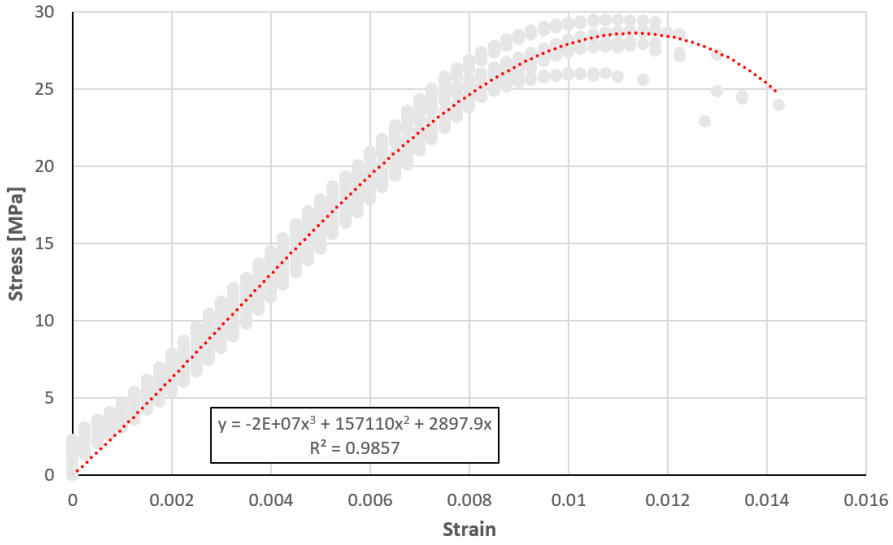

Figure 4-25. Stress-strain curve of the tested cubic specimen

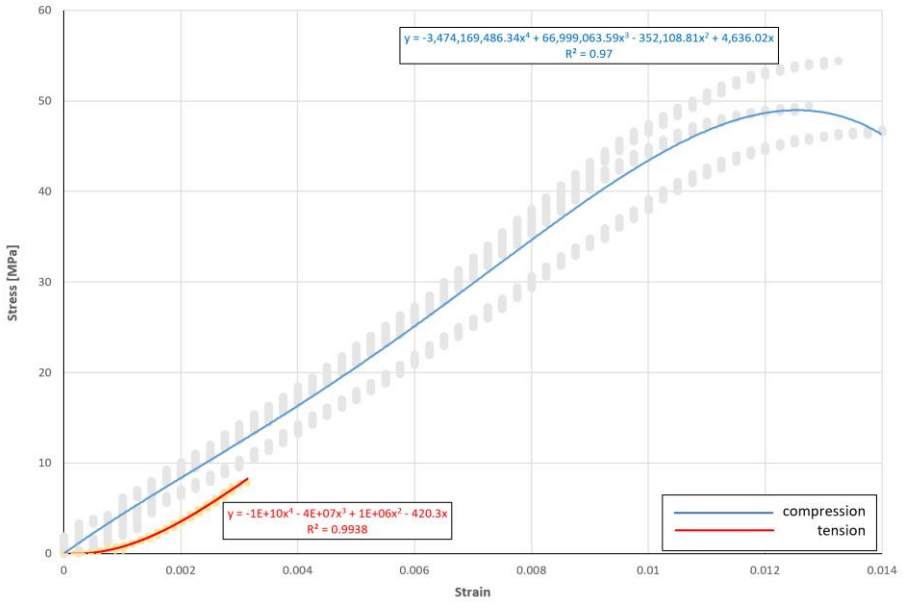

Figure 4-26. Compressive and tensile behaviour of the mortar paste

4.2.5. Model validation

4.2.5.1. Mesh generation

In this study, the microstructure of the recycled aggregate is described explicitly such that each phase occupies a specific sub-domain. This study's first part considers a cubic volume containing a single aggregate as a representative volume. Irregular tetrahedral mesh has been employed to capture complex topology ensure versatility. Python codes have been used to capture individual regions and the interfaces and allocate numerical markers as mesh functions that will be used during the calculation for a material assignation. An initial tetrahedral mesh is generated, a first loop consists of detecting elements near the inter-facial zone using a collision detection algorithm [203] and refining them by subdividing the respective cells. This selective refinement allows reducing the mesh's size while capturing the interfaces with high precision. Using collision detection from an initial mesh cell contained within the aggregate mesh are identified and marked according to the phases present in the matrix, i.e., aggregate, new mortar, and old mortar. Linear elements are used. This process is iterated until the mean cell volume represents the micro-structural size. The total number of cells inside an element is 4n, n being the number of iterations.

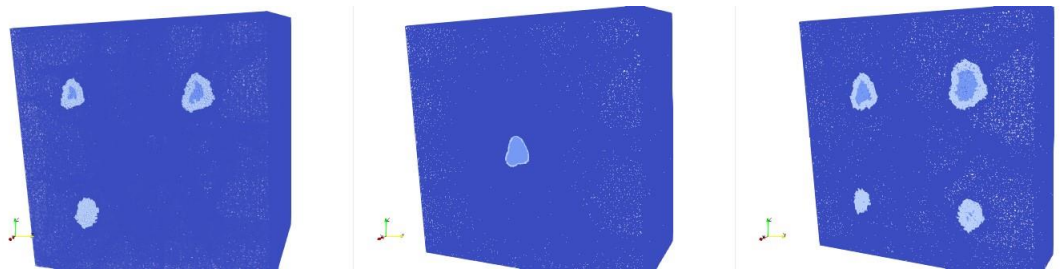

Figure 4-27. Multiple aggregate sample

4.2.5.2. Model parameters

The parameters of the model are adjusted (tab.1) to fit the experimental tests. The Elastic stiffness, compressive strength, and plasticity hardening, softening regimes are captured. A qualitative comparison of the 3D fracture pattern obtained by the numerical simulation (fig.6) is

also compared to the cracking pattern by experiments, which is satisfactory. The model built at mesoscale can inform the macroscopic behaviour taking into account the heterogeneous properties of the RAC while capturing the 3D complex crack pattern (Figure 4-30).

Table 3. Material properties of the model for comparison between experimental campaign results and simulations

Material	K (MPa)	ν	α(rad)	c	G_c	H	l_o
Aggregate	32000	0.3	0.48	3200	2.6		
New mortar	31	0.21	0.42	3.1	0.006		
Residual mortar	32	0.21	0.42	3.1	0.007		

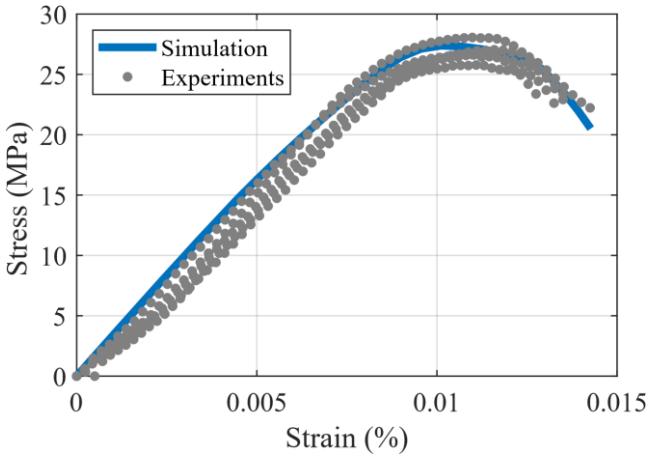

Figure 4-28. Validation of the stress-strain simulation vs experiments

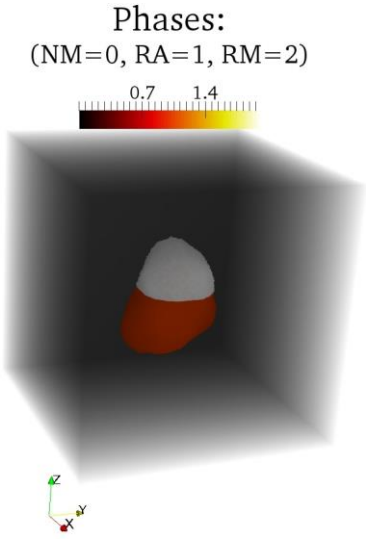

Figure 4-29. Considered phases

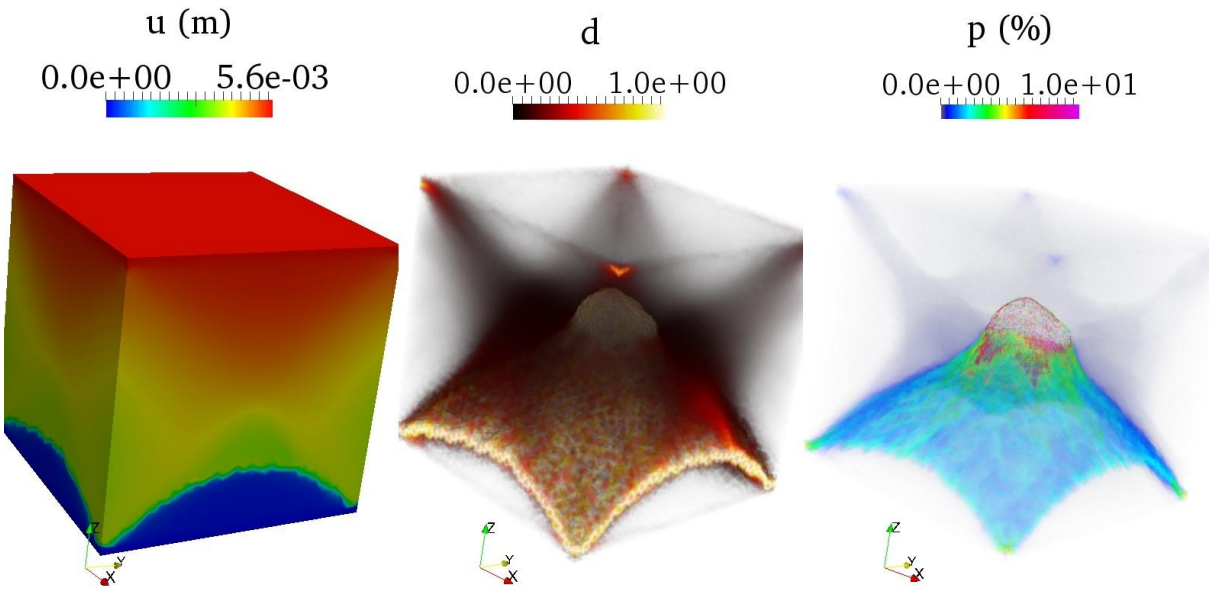

Figure 4-30. Displacement u, damage variable d, equivalent plastic strain

4.2.6. Parametric study

The reference parameters match the experimental results, and the corresponding plot is labelled "reference".

4.2.6.1. Elastic properties

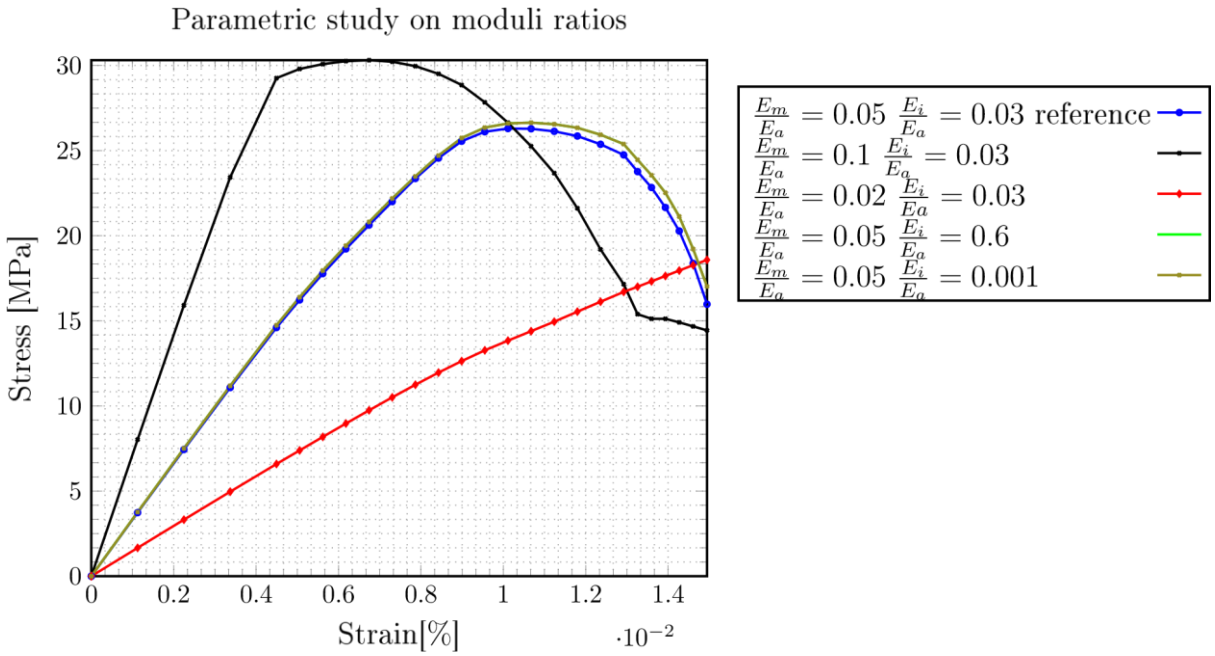

Figure 4-31. Effect of the regularization interface, matrix and aggregates moduli ratio on the stress-strain response

According to [178], the matrix-aggregate bond strength in RAC is superior or at least equal to that developed with natural aggregates; this has been proven by [179] in their earlier experiments. On the opposite, [180] pointed out that RAC had low quality due to the much higher water absorption, increased porosity and weaker ITZ; [181] conducted a study of the mechanical properties of high-strength concrete made from recycled aggregates and found that the properties of the original concrete have a significant influence on the mechanical properties of the RAC. So, the driving factor of the mechanical performance of recycled aggregates is still poorly understood; In this study, we take the opportunity to investigate numerically, the effect of elastic properties of aggregates, matrix and ITZ at mesoscale.

For that purpose, we carry out a parametric study on the elastic modulus of different components. We studied the influence of the elastic properties of the phases (aggregates, matrix, interface) on the compressive strength, stiffness and crack evolution.

First, we investigate the impact of $\frac{E_m}{E_a}$, the ratio of elastic modulus between matrix over that of aggregates. It is representative of the quality of the matrix for a fixed value. In the following, the

elastic modulus of aggregates is E_a = 500 GPa. A higher ratio $\frac{E_m}{E_a}$ is representative of a high-performance matrix, while the low ratio is representative of the low-quality matrix. On the one hand, when we increase the ratio $\frac{E_m}{E_a}$ by two times, we obtain a significant increase of both the stiffness and the compressive strength, but the material becomes more brittle. On the other hand, decreasing the ratio $\frac{E_m}{E_a}$ by half reduces the stiffness and the compressive strength drastically while improving the ductile behaviour of the material. In another manner, the ratio $\frac{E_m}{E_a}$ has a significant effect on the elastic energy storage capacity of the material, and therefore dictate the transition form from brittle to ductile behaviour.

Second, we investigate the effect of $\frac{E_i}{E_a}$, ITZ/aggregates modulus ratio at mesoscale. Figure 4-31 shows that increasing two times or decreasing by half this factor does not affect the mechanical response. The response of the model is not sensitive to $\frac{E_i}{E_a}$ ratio. It can be concluded from this parametric study on elastic properties that the compressive strength and the stiffness are very sensitive the $\frac{E_m}{E_a}$ ratio, and not that much to $\frac{E_i}{E_a}$. Also, the stiffness is more sensitive than the compressive strength to $\frac{E_m}{E_a}$ which agree well with the literature.

As confirmed by previous studies experimental studies on the effect of RA on the mechanical properties of concrete, the loss of stiffness (i.e., elastic modulus) is greater than the loss of strength [26]. However, it is generally argued that the RA reduces the concrete compressive strength due to the weak residual mortar layer and sometimes the poor quality of the aggregate itself. In [40], it was observed that concrete made with recycled aggregates derived from high-performance concrete has better compressive strength than concrete made with recycled aggregates derived from standard concrete; the former matched the strength level of concrete made with natural crushed granite aggregates after 90 days of cure. The authors attributed these differences to the disparities between the strength of the coarse aggregate and the micro-structural properties of the ITZ. The study we carried out here show that the new mortar quality has significant effect. Thus, the driving force of the mechanical performance is intimately related to the relative matrix-aggregate stiffness.

4.2.6.2. Fracture properties

In the following, the the fracture energy G_c has unit of $N.mm/mm^2$ and the regularization length l_0 is expressed in *mm*. The impact of the phase-field regularization length l_0 and the fracture energy G_c on the material response are investigated. From references values where a perfect match was obtained with experimental data, G_c and l_0 are varied, respectively, while keeping other parameters fixed.

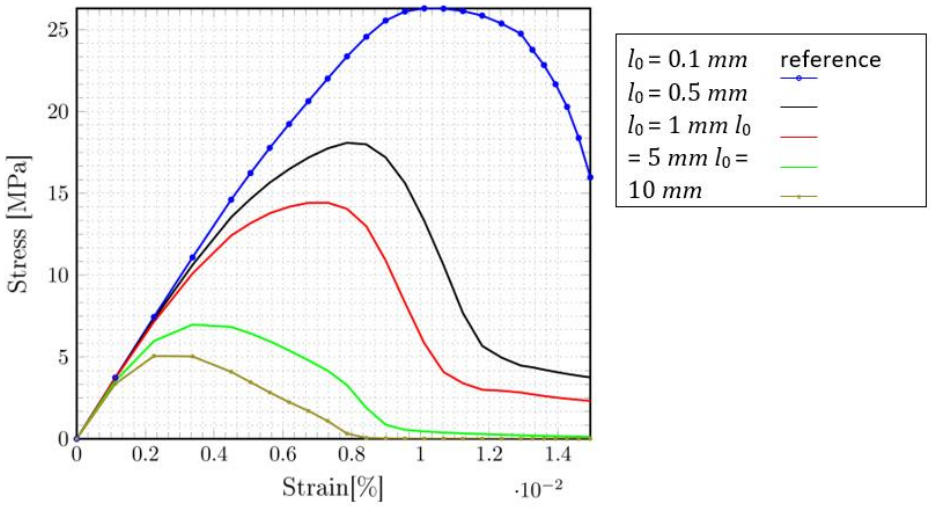

Figure 4-32. Effect of the regularization length on the stress-strain response

The regularization length is an important parameter for the phase-field model. Initially, it was introduced as a geometric parameter for sharp approximation of the cracks to remove the singularity at the crack tip. It has been proven that the regularized formulation converges [204] to the original variational formulation when $l_0 \rightarrow 0$ [205]. Hence, this length should be set as small as possible since it has a physical meaning from a numerical point of view. Subsequently, l_0 will be referred as the length parameter.

Figure 4-32 shows the dependence of the critical stress upon the length parameter l_0, the critical stress is a function of l_0. In fine, quantitative prediction of stress-strain response with phase-field modelling relies on determining the regularization parameter l_0.

In fine, quantitative prediction of stress-strain response with phase-field modelling relies on the determination of both the critical energy (Figure 4-34) and the length scale (Figure 4-32).

In Figure 4-33 the variation of the predicted compressive strength with demonstrate that there is a threshold value $l_0 = 0.2\ mm$

below which the phase-field model response is independent of the regularization parameter.

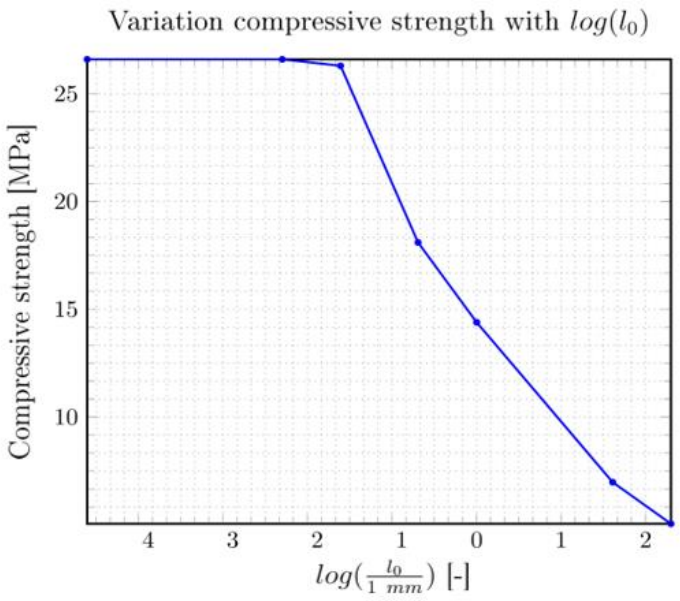

Figure 4-33. Variation of the maximum compressive strength regarding the logarithm of the internal length

Above this threshold value, the evolution of the compressive strength is quite linear with $log(l_0)$. The phase-field simulations are valid when the internal length scale is sufficiently small compared to the specimen size. To evaluate the sensitivity of the stress-strain response to the fracture energy, simulations are carried out with different energy release rate values: reference that corresponds to the identified values on the experimental test, 10× of references values. The results are presented in Figure 4-34. When increasing the fracture energy per unit area of aggregates (G_{ca}) or of the matrix (G_{cm}) or G_{ci} by a factor of 10× from the reference value, only the latter improves the compressive strength significantly. The two formers', G_{ca} and G_{cm} have no significant change in the material response (Figure 4-34).

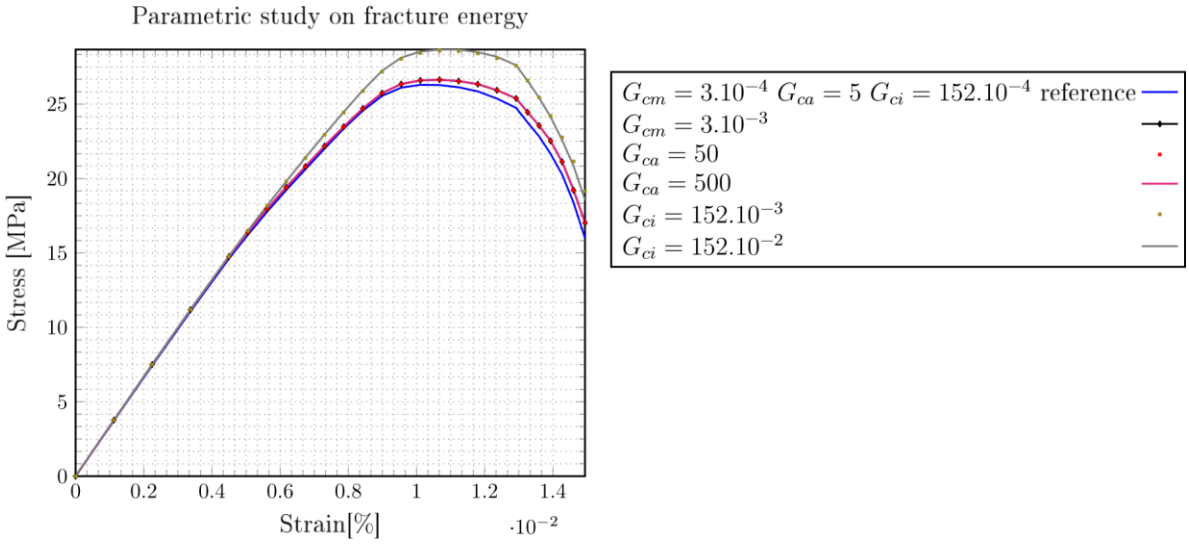

Figure 4-34. Effect of the fracture energy values on the stress-strain response

Further increasing by factor 100× the critical energy release rate G_{ci} does not improve the compressive strength compared to increasing it by 10×. This makes sense because it is the phase with the lowest energy release rate, compared to the aggregates and the matrix; it is the one that dictates the failure initiation, and therefore the compressive strength of the material at the mesoscopic scale. Hence, the knowledge of the critical energy of the ITZ, which can be done by mesoscale modelling is important for prediction of RAC. However, determining the critical energy release at the macro-scale is challenging. For instance, the fracture energy values determined from a series of three-point bending tests may differ significantly [39], especially for composite materials [206].

4.2.6.3. Plasticity

The impact of the two parameters of Drucker-Prager plasticity model (cohesion and friction angle) on the stress strain response is investigated in this section. The reference values of cohesion, friction angles of the three phases are those obtained by identification on the experiment. The cohesion and the friction angle of the matrix is varied leading to different $\frac{c_m}{c_a}$ and $\frac{\kappa_m}{\kappa_a}$ (c: cohesion, κ: friction angle m: matrix, a: aggregate.). Figure 4-35 shows the sensitivity of the stiffness and maximum stress to the cohesion and friction parameters of the matrix. Doubling the cohesion of the matrix causes a decrease of material stiffness and maximum peak stress while increasing the

maximum strain at peak stress. Inversely, decreasing by half c_m causes a gain in material strength of about 26 to 30 MPa but does not change the stiffness. Similarly, increasing the friction coefficient by a factor of two improves the stress slightly at the peak state, while the elastic response remains unchanged.

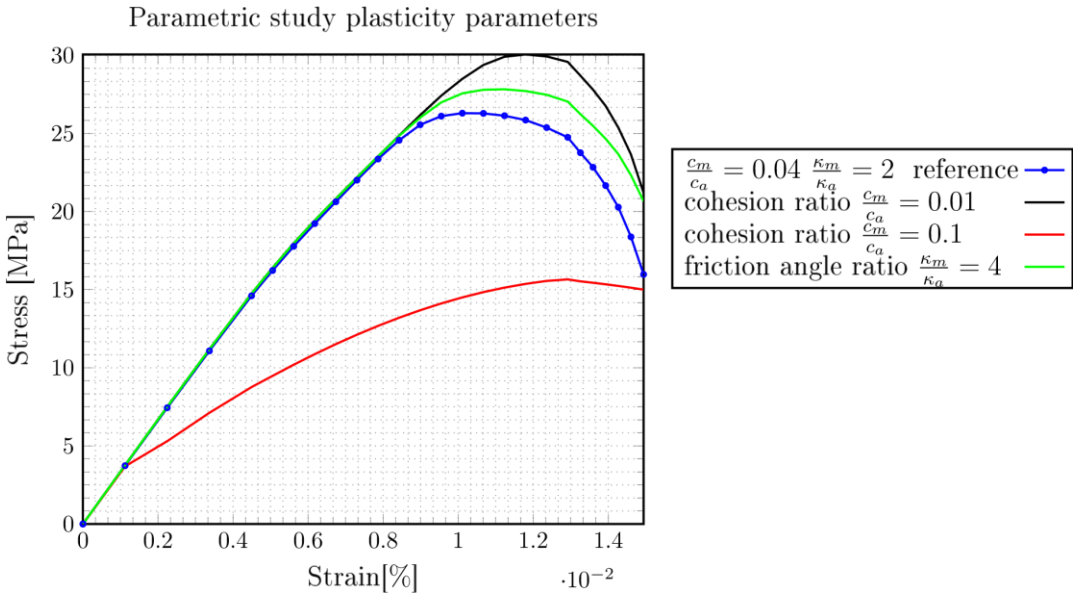

Figure 4-35. Effect of the cohesion and friction angle values on the stress-strain response

4.2.6.4. Parametric study of aggregates

This section compares the results of simulations carried out with one aggregate and multi-aggregates specimens. Indeed, the numerous studies in literature reveal that the critical characteristic properties at macro-scale such as compressive strength, tensile strength, elastic modulus, and fracture energy decrease with the increase of recycled aggregate content [58]. Figure 4-36 presents the stress-strain evolution for RAC with one aggregate and nine aggregates samples together with the experimental measurement. The model predicts high compressive strength in the case of multi-aggregate (Figure 4-36). Let's note that this increase of compressive strength at the meso-scale does not comply with the experimental observations at the macro-scale. Indeed, a study in [207] reports that replacement levels up to about 30% of coarse recycled concrete aggregates (RAC) or 20% of fine RAC have marginal effects on the strength development of concrete. And increasing the RA content above these limits decrease the compressive strength. For 100% RCA replacement level, a decrease in compressive strength compared to the original concrete is found

to be in the range of 15%–25%. Regarding the elastic modulus, the relative feeble effect of the RA content on the elastic modulus agrees well with literature findings for low replacement content (less than 30%). However, a significant loss of elastic modulus may occur for higher replacement content. In, [203] 476 concrete mixtures, made with RA of different sizes, types and origins, have been compiled from 35 publications; the results indicate that the modulus of elasticity varies with the replacement rate of recycled aggregates; and the authors conclude that there is a probability of 95% that RAC with 100% coarse RA content exhibit moduli of elasticity between 0.97 and 0.52 times that of the control NAC.

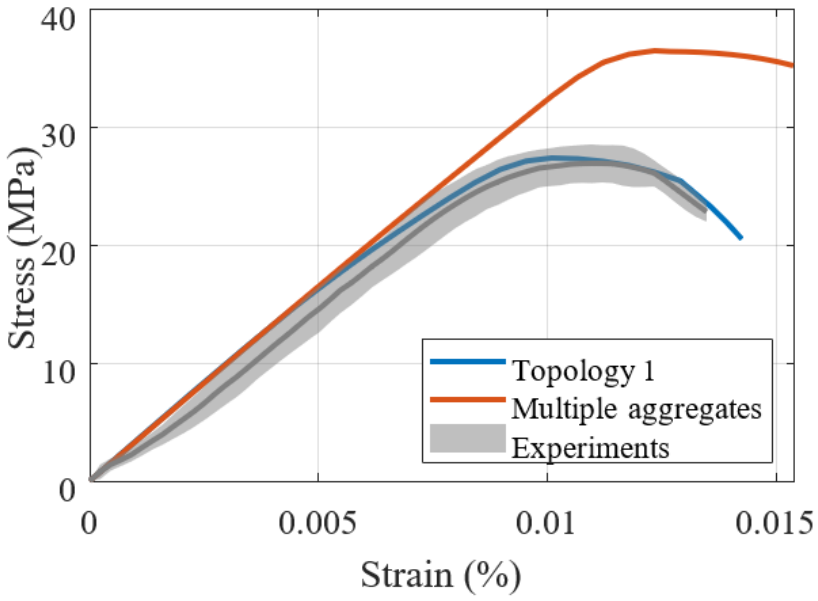

Figure 4-36. Comparisson of the stress-strain response between nine aggregates and one aggregate content

4.2.6.5. Parametric study on the residual mortar

To study the impact of residual mortar on the fracture mechanism, five topologies of aggregates are tested: Topology 1 corresponds to virgin aggregate (no residual mortar), topology 2 is RAC fully recovered old mortar, and finally, topology 3,4,5 correspond to partially recovered old mortar. Figure 4-37 presents the stress-strain simulation result for these topologies. The influence of the residual mortar on the mechanical response regarding the peak load and crack pattern is not significant. Other authors in literature [41] agree with that conclusion only for normal concrete, which is the case for the concrete studied in this paper. Other research in literature has shown that

old cement mortar has a huge influence on the performance of RAC [169], [177]. However, we do not observe such mechanical behaviour. For further analysis, the local damage at initial and final simulations stages for different residual mortar topologies are analyzed hereafter. The recycled aggregate inclusion is presented in Figure 4-38.

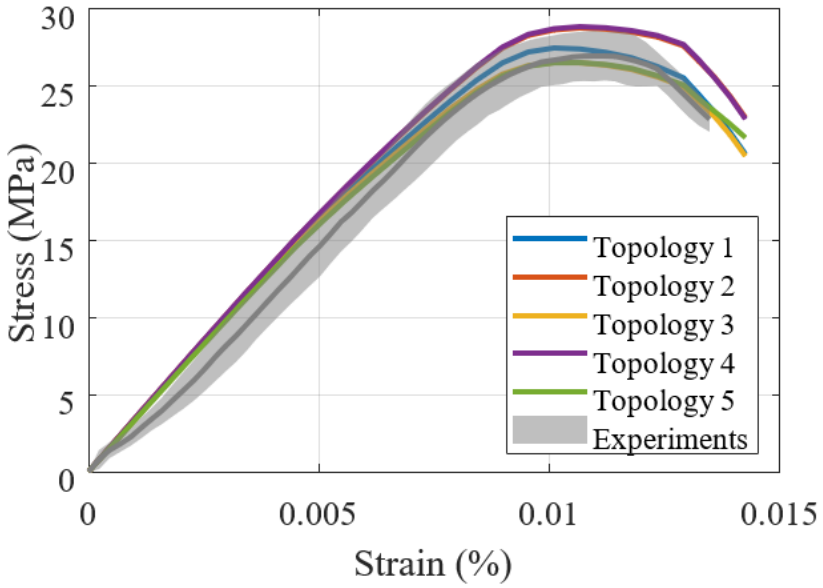

Figure 4-37. Stress-strain for different typology of recycled aggregates

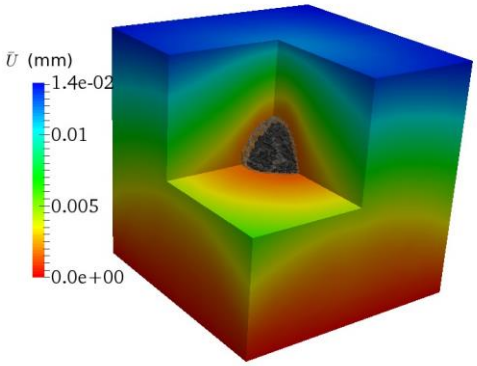

Figure 4-38. Illustration of inclusion of single-aggregate in the mortar matrix

The cracking maps in the case of recycled aggregate concrete without residual is shown in Figure 4-39. The fracture starts at the level of the sharp edges of the aggregate (Figure 4-39-a) then spreads around the aggregate to continue in the matrix (Figure 4-39-c). Indeed, the sharp corners are the concentration points of stresses and, therefore, potentially points of cracking initiation. Consequently, the aggregate shape plays an essential role in the fracture mechanism of concrete.

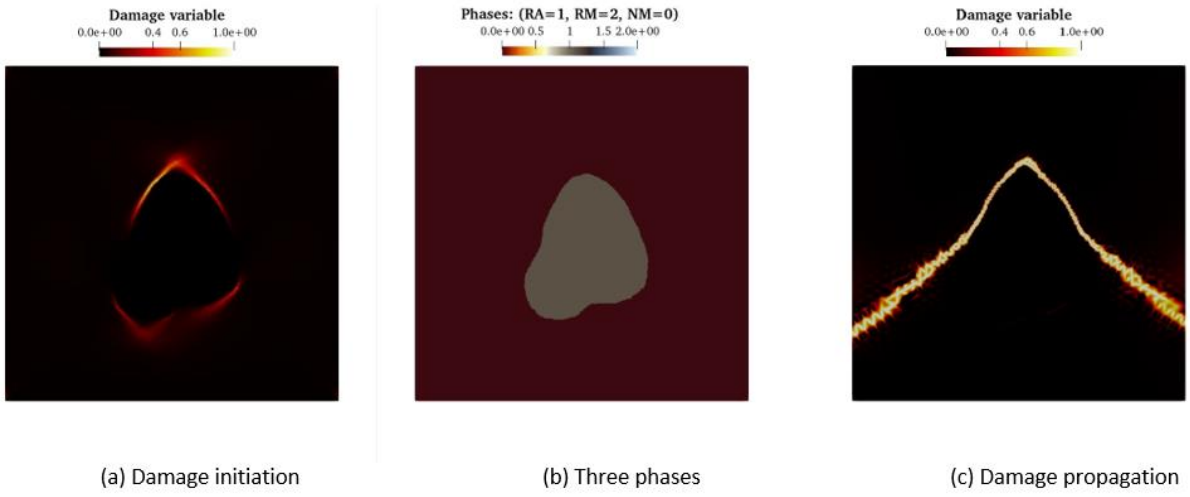

Figure 4-39. Damage at initial and final stages of simulation, with phase-field model, recycled aggregate with no old attached mortar

The cracking maps in the case of recycled aggregate concrete partially covered with old mortar is shown in Figure 4-40. In the case of a recycled aggregate concrete partially covered with residual mortar, the cracking initiates both at the level of sharp corners and residual mortar, Figure 4-40-

(a). It is then observed that cracks originating at the level of the residual mortar take over, propagating faster in the matrix, Figure 4-40-(c). The residual mortar at the matrix-aggregate interface is the weakest point as it has already been pointed out in the literature: it is prone to the formation of micro-cracks under load levels lower than those required to produce significant fracture damage

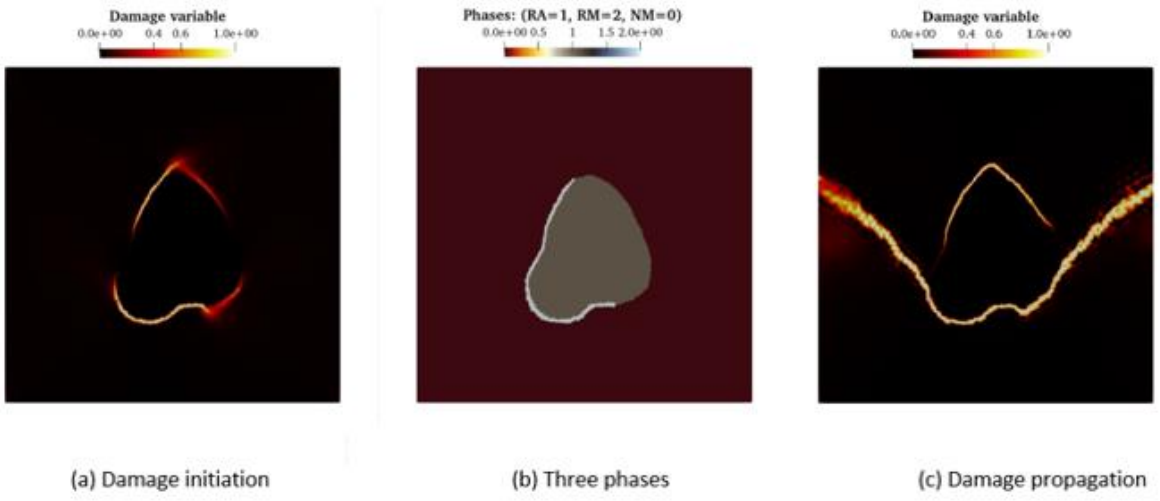

Figure 4-40. Damage at initial and final stages of simulation, with phase-field model, case of recycled aggregate partially covered by old mortar

Completely covered with residual mortar The cracking maps in the case of recycled aggregate concrete completely covered with old mortar is shown in Figure 4-41. In this case, all points of the aggregate contour are favourable for crack initiation. The cracks starting from different initiation points coalesce and then diffuse in the matrix Figure 4-41-c.

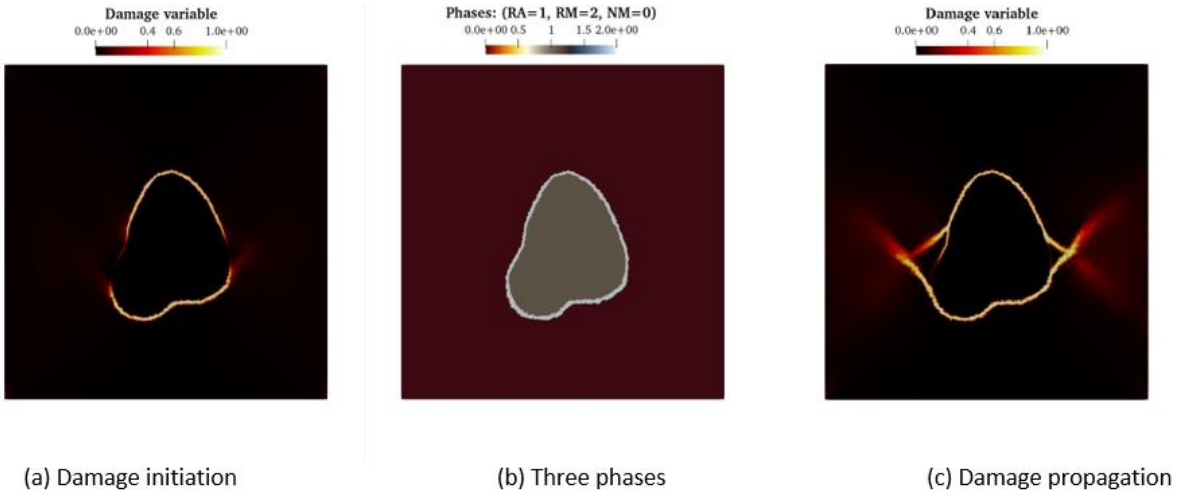

Figure 4-41. Damage at initial and final stages of simulation, with phase-field model, recycled aggregate fully recovered with old mortar

The analysis of the cracking maps for the different topologies (Figure 4-39, Figure 4-40, Figure 4-41) reveals that the cracking process always starts in the ITZ zone and eventually at the aggregate tip: it is so because the residual mortar has a higher porosity and cracks and, therefore, a lower stiffness. It makes the interface between the recycled aggregate and the new mortar a zone favoring crack initiation. Because of this, we recommend that the ITZ characteristics be taken into account when modelling the failure behavior in recycled concrete.

4.2.7. Conclusions

In this paper, a phase-field fracture model has been proposed and used to investigate the fracture properties of multi-phase composite materials with complex interfaces. This approach is convenient since it implicitly allows crack initiation and propagation through the evolution of the damage phase without the need for fine meshes in the vicinity of tightly packed inclusions. Moreover, an adapting mesh is not required to effectively apply the random damage field of the different generated microstructure realizations. The model allows predicting fracture behavior of complex structure heterogeneity due to recycled aggregate. We employ the model to investigate the effects of phase field internal length, young's modulus and fracture energy, aggregate content, residual mortar, cohesion, and friction angles on overall stiffness, compressive strength, micro-crack initiation and propagation in recycled concrete. The conclusions of the 3D mesoscale

simulations of the compressive behavior of concrete as a three-phase composite can be summarized as follows:

- Compressive strength and stiffness are very sensitive to the ratio of modulus of elasticity to the ratio of $\frac{E_m}{E_a}$, and not so much to the ratio of $\frac{E_i}{E_a}$. Furthermore, stiffness is more sensitive to $\frac{E_m}{E_a}$ than compressive strength.
- The model predicts higher compressive strength as the aggregate content increases.
- The critical energy release rate G_{ci} of the interface has the most significant stress-strain response.

It is concluded that the presented micromechanical simulations offer valuable information to relate the structure property relationship in recycled aggregate concrete to guide the use of recycled aggregates with better strengths, toughness and resistance in construction. This methodology can be applied to a coarse-scale problem using effective properties. Initial verification shows that the proposed methodology has great potential for dealing with complex microstructure. The application of the present constitutive model and computational framework to perform more realistic 3D concrete microstructure mesoscale simulations based on 3D X-ray computed tomography images will focus on future studies.

Chapter 5 | Circular economy database

5.1. Publication I: Modelling of mineral construction and demolition waste dynamics through a combination of geospatial and image analysis (Bogoviku, Waldmann)

Abstract

As the construction sector is shifting towards circular economy models, the role of mineral construction materials as main waste fraction in terms of volumes is crucial. A characterization of this mineral stock, as well as the waste derived from it is decisive in ensuring the application of the best practices of circular economy. This paper describes a methodology for assessing the mineral building stock through a combination of geospatial and image analysis. By analysing old topographic maps, buildings are grouped according to their building age into different typologies and based on these maps the construction and demolition activity is evaluated. The mineral stock is assessed and estimations of the mineral construction and demolition waste (CDW) is generated for different stochastic scenarios. This methodology is applied exemplarily on the country of Luxembourg. It was found that the total mineral construction stock for Luxembourg is 277 Mt and has been growing at a rate of 20.81% to 24.39% in the last 30 years. Furthermore, the study identified a mean age of the urban building stock of about 60 years and a typical maximum building lifetime of 122 years. Based on the stochastic projections the mineral CDW generated from the existing building stock is expected to be up to 227 Mt by 2100, while if future building scenarios are considered, it can be as high as 885 Mt. The annual CDW production is expected to be sufficient for a viable concrete recycling activity if regulations on the waste volume flows are made available.

Keywords: Concrete recycling; Material stock quantification; Geospatial analysis; Circular economy; Construction and demolition waste (CDW)

5.1.1. Introduction

Depletion of natural resources is one of the main global environmental risks. Mineral reserves show a special vulnerability in this aspect, as they are not renewable in nature. According to a recent report by the United Nations Environment [208], the world's demand for sand and aggregates is recorded to be 40 – 50 billion tonnes per year and projected to further increase to 60 billion tonnes per year by 2030. Over the last decades, the demand for sand and aggregates has triplicated. This increasing need has led to a worldwide shortage of inert construction materials and significant environmental effects. Riverbed corrosions, flooding, destruction of natural beaches and water pollution are only a few aspects. In Germany, an annual amount of 4.6 tonnes of sand per capita is being used [209]. Even though the mineral deposits are abundant, nowadays the majority of the natural reserves lies underneath forests, roads, railways and cities. This condition has led the German industry to seek sand extraction from the seabed, which could come with unexpected global effects on beaches and coastal cities. The effects are much more perceptible in countries with limited resource deposits and high economic growth.

On the other hand, the global generation of waste is increasing. In Europe, construction and demolition waste (CDW) is assessed to be 25 – 30 % of the total waste, while the level of recycling is still highly variable between the member states [210]. Typically, countries with a larger GDP and population density have a higher volume of demolished structures [211]. In terms of characterization of waste, the largest fraction of the generated waste is comprised of mineral fraction, where, considering the EU, approximately 90% of the waste volume is concrete waste [212], while in the US, it represents 51% of the total mass [213].

This fraction, while generally treated as waste, has a significant potential in re-use and recycling [73], [77], [151]–[155], [214] and can serve as an additional deposit of mineral resources. At the moment, the European technical standards for concrete production delineate a substitution ratio of 20% of recycled aggregates as a practical limit [64]. To incorporate secondary raw materials in concrete production, a continuous flow of material is needed due to the industrial needs of a concrete recycling plant [215][60]. Furthermore, knowing the spatial distribution of the concrete stock is a significant advantage in the decision-making process of the location of such sites. Limiting the transportation distances not only reduces the carbon footprint of the recycling process,

but also results in lower operational costs. On the other hand, for concrete based on recycled aggregates, the concrete production plants need to be specially regulated for each slightly different mixture, the question that arises from the industries is whether a sufficient and continuous material flow can be guaranteed to justify the investment costs of altering the production line. Although the guidelines described in the standards ensure the technical feasibility of recycled concrete, by avoiding, through a limited allowed substitution ratio, any negative influences from the recycled aggregates in the new concrete matrix, it is yet to be adopted in countries with small geographic areas. The construction industry considers it an unreachable goal given the uncertain volumes of CDW generated, which are generally perceived as too low to ensure a constant flow of materials needed for a continuous industrial production. The lack of studies and data on CDW generation and on demolition activities further increases the uncertainty of the process and the high-workload required for a full investigative record of the material stock is regarded less attractive due to the high cost/benefit ratio. Therefore, there is a dire need for a regional approach in CDW analysis for small countries to identify the scale of waste generation and to understand whether the recommended substitution ratios make sense from an economic point of view.

5.1.1.1. Literature review

The generation of CDW is strictly related to the service lifetime of each structure. The life expectancy of the building depends on several factors. According to EN 1990 [216], the target lifetime ranges from 10 to 100 years depending on the type and importance of the structure. However, very rarely these conditions are determinant to the effective duration of the structure's use. In ISO 15686 [217] a factor method is used to estimate the lifetime of a building in comparison to the ideal design life. Nevertheless, the design lifetime expectancy of the building is rarely deterministic to its real survival and a more complex regional analysis must be done to take into account the economic lifetime of a structure, which can be described as the period of time where benefits of the building use surpass the costs. O'Connor [218] reports that the majority of demolished steel and concrete buildings in North America are less than 50 years old. Liu et. al [219] determines 34 years to be the average lifetime of buildings in Chongqing, China and, according to Bradley and Kohler [220] the average lifetime of structures ranges from 120 to 300 years for Germany. The lack of consistency in the data demonstrates the need of a case-study

approach in the determination of the service lifetime of buildings. Sartori et. al [29] used a normal cumulative distribution function to model the dynamic lifetime profile of building types in Norway divided into three main groups of 75, 100 and 125 years. By comparing different scenarios, the study highlighted the likelihood of the large building stock remaining from the post second world war reconstruction to cause an additional increase in CDW in the second half of the century, due to the aging building stock, emphasizing the importance of the lifetime analysis of the building stock with regards to its construction period. Bradley and Kohler [220] followed a different methodology by adopting the Kaplan-Meier procedure to model the survival rate of residential and non-residential buildings in the town of Ettlingen, Germany. The study shows that residential buildings tend to have a longer lifespan compared to non-residential structures.

Material stock analysis has been studied in several case studies [29], [32], [220]–[227]. Kleemann et. al [31] and Heinrich et. al [32] characterized the material stock for Vienna and Munich with the aim of introducing the basis for a material database that can aid the shift towards a circular economy model for buildings. Gruen et. al [228] introduced a methodology for creating 3D models of city areas through a semi-automated procedure, emphasizing the necessity for deeper research in the building stock. Mastrucci et. al [223] combined a GIS environment with statistical datasets to aid the regulation of energy-saving retrofitting methods for the city of Rotterdam. The application of GIS as a medium for waste management has been first used by Jensen and Christensen in 1986 [229] to determine potential storage sites for industrial waste. Since then, the popularity of GIS as a medium for environmental studies has soared. Gallardo et. al [230] used GIS to obtain city maps for municipal solid waste generation areas. Blengini [231] and Mastrucci [232] combined GIS-based material stock characterization with LCA as an aid to construction and demolition waste (CDW) management in an urban scale. CDW management through a GIS platform with the aim of facilitating recycling of the mineral fraction of the waste was also studied by Wu et. [233] al for the city of Shenzhen in China.

The described approaches rely heavily on building data collections as a base for analysis of the material quantification and subsequently for the assessment of waste flows. While collecting building data, such as typologies, material composition and demolition data throughout a large timeframe yields results of high precision, it is not always a feasible approach. The data on building composition are strictly protected by privacy safeguard regulations and historic records on building demolitions are not always documented. Manual extraction of this information requires not only a

high amount of workload, but also a substantial amount of time, since the typical lifetime for buildings is between 10 to 100 years [216] without considering human, economic and environmental factors which can furthermore influence the lifetime [217]. Moreover, such approaches do not fully address the issue of availability of secondary raw materials as products of an industrial recycling process in areas with limited urbanization. This perspective leaves a significant gap on the evaluation of the feasibility of recycling as a viable option for the reuse of mineral CDW. In this paper, an alternative approach is presented, relying strictly on local open-source data and statistical records to estimate the expected flows of mineral CDW. The use of official open-source information makes this approach significantly faster, compared to a case-study technique, and openly accessible, since the source data is not bound to control mechanisms such as copyright or patents. Furthermore, the identification of the building age, as well as of the demolition behaviour are neither based on a generalized mathematical model (i.e. building lifetime models as used in [29]) nor on survival analysis based on sample building population (as used in [220]) and also neither on manual extraction of data. In the present paper, an alternative method based on an automatic extraction of the building construction age is used. This method offers a global approach based on the specific studied geographic area, therefore, offering a personalized approach that can specifically consider the local aspects of each region.

The aim of the study is to propose an analysis tool for strategic decision-making in CDW management. The availability of such a methodology is crucial in asserting critical data regarding the waste volume generation and thus enabling CDW recycling as a viable economic activity. Moreover, the implementation of geo-spatial methods, offers an additional analysis dimension that can be used for executive decisions on the location of treatment facilities and minimization of transportation distances. This method can be particularly useful in countries or cities with limited geographical areas where CDW recycling is judged inefficient due to the relatively low population, as well as in areas where the financial means for excessive manual surveying are lacking. The proposed procedure is tested on a case study for the country of Luxembourg.

5.1.2. Methods

The conceptual overview of the process is shown on Figure 5-1. The procedure includes five distinct steps:

1. Spatial analysis
2. Age analysis
3. Material analysis
4. Mineral CDW flows
5. Future projections of mineral CDW

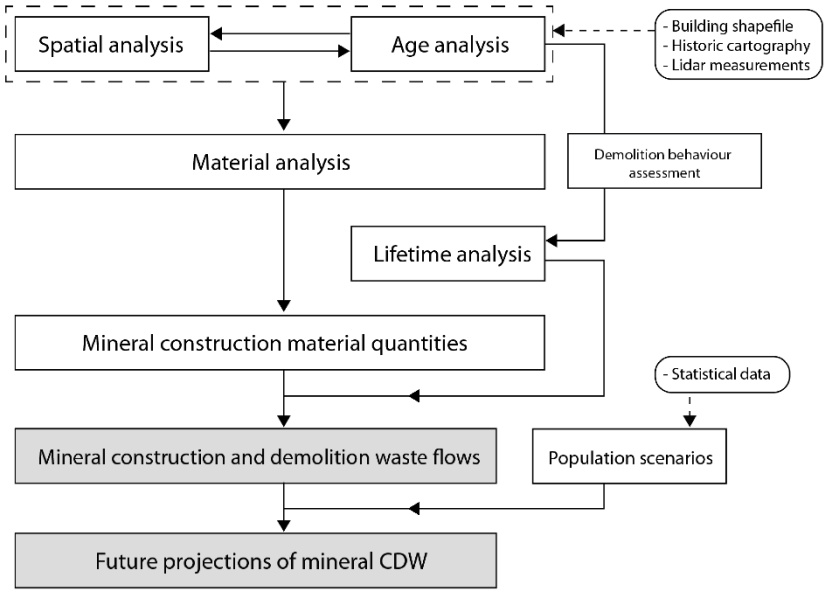

Figure 5-1 General procedure

5.1.2.1. Spatial analysis

The spatial analysis is fully completed in a GIS environment. In the present study, the software QGIS [234] is utilized. The initial basic input at this stage consists of georeferenced shapefiles consisting of a polygonal representation of the buildings and height measurements of the built environment. One of the most popular height measurement techniques is Lidar (Laser Imaging Detection and Ranging) which yields two sets of outcome cloud points: a digital terrain model (DTM) which models the height information of the terrain only and a digital surface model (DSM) which models the height information of the elevated features, such as buildings and vegetation. An example of the DTM, DSM and shapefiles are shown on Figure 5-2. Through a mathematical subtraction between the cloud points of the DSM and DTM, the height values of the buildings can be extracted and incorporated into the building shapefiles. In cases where Lidar measurements are

not available, the height information can be assigned to each building through other surveying methods such as leveling, GPS measurements or terrestrial laser scanning. These methods, however, are more time-consuming and require individual measurements for each building.

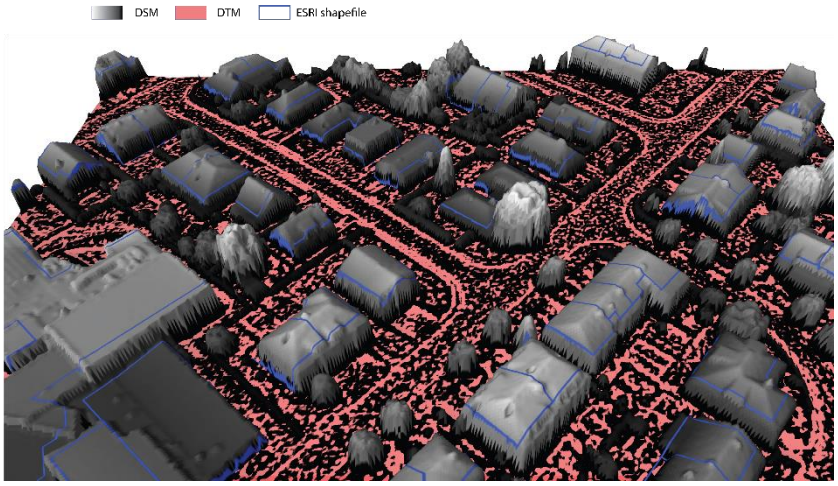

Figure 5-2 Example showing the 3D representation of the DSM, DTM and building shapefiles

5.1.2.2. Age analysis

Determining the construction age of the building stock is a challenging task, but it is central in determining the potential CDW flow of a region, considering the fact that the older the building, the higher the demolition potential. The material utilization is closely linked to the construction period of the building therefore, the age of the building is a strong influencing factor on its material composition. Furthermore, by relating the construction period of each building to its geographic location it is possible to generate maps of potential waste generation and offer a significant aid to waste management and treatment. However, recordings and cadastral inventories, rarely contain accessible information on the construction period.

In this paper, an alternative methodology based on historic maps is used (Figure 5-3).

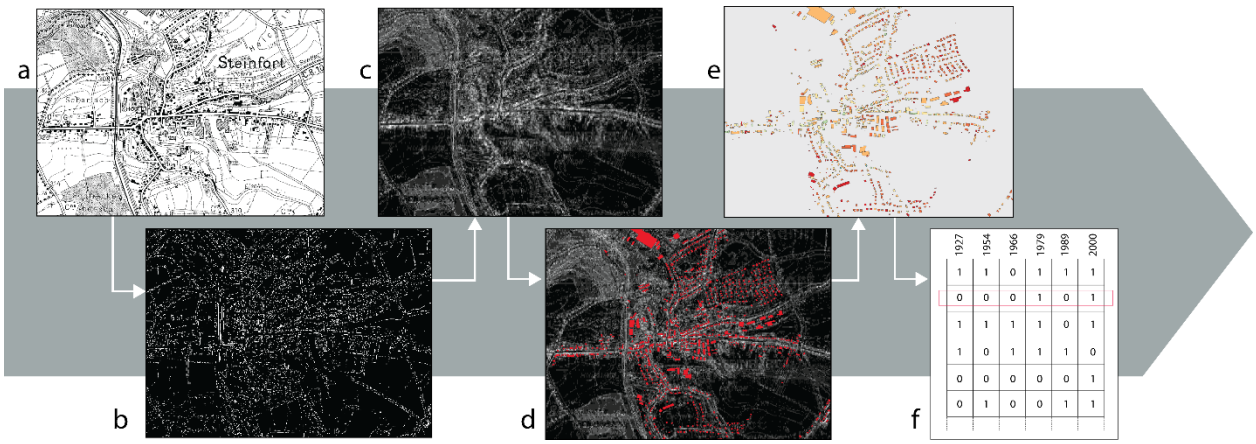

Figure 5-3 Age analysis of the building stock, example of the town Steinfort, Luxembourg analysed in QGIS

The process is based on an image analysis of the rasters derived from historic topographic maps. First, a set of maps covering the entire analysed period is to be chosen from the local cadastre administration (Figure 5-3a). The maps must be of high quality and small-scale maps must be avoided, as they do not offer enough detail in building representation. Each map is analysed individually, and the range of the RGB (red, green and blue) band values is manually registered for the pixels representing buildings (Figure 5-3b). For old maps, the buildings are generally represented in a single colour, therefore the range of the RGB bands is quite narrow. The colour scheme might vary from map to map; therefore, no generic range can be postulated. Therefore, a case-study approach depending on the given cartography is necessary at this step. For the selected RGB band values, a conditional is placed to assign values of "1" (white) for the pixels where the selected values are present and "0" (black) where it is missing (Figure 5-3c). At this stage, however, it cannot be concluded that each pixel corresponds to the presence of a building. Depending on the colour scheme of the topographic map, the pixel values can also represent other objects, such as streets, trees or even map annotations. To overcome this, a combination between the black-and-white raster images and the shapefile polygons must be done to assess whether in any given polygon a building was present at each given time (Figure 5-3d and e). This results in a logical [N x d] matrix, where N is the total number of buildings present as polygons and d is the number of analysed maps (Figure 5-3f). Using this matrix, significant information on each building's lifetime can be extracted. An example of this principle is shown on Figure 5-4. If the difference between two adjacent matrix entries is negative (0-1=-1), it represents the demolition of a structure during the period that the last index represents. If the difference is positive (1-0=1),

it represents a new construction. The construction time period of the structure is defined by using the latest string of "0" differences.

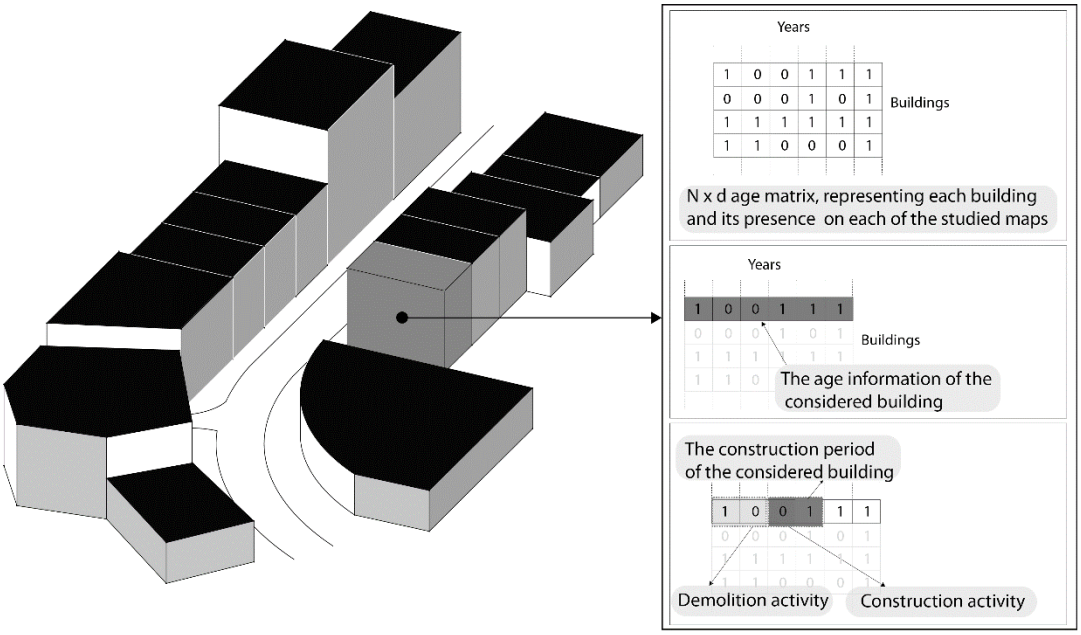

Figure 5-4 Example of the age matrix of a building

Furthermore, by combining the demolition trend of the total building stock over the entire period, a typical lifetime curve can be obtained. This curve can be used to show when buildings are typically demolished in the studied area and to describe a mathematical relation between the building age and its demolition likelihood.

5.1.2.3. Material analysis and mineral CDW flow

The mineral construction material is generally composed of four parts: the slabs, outer walls, inner walls and basements (equation 1.1). In the present study, the construction material volumes used for infrastructure works, such as roads, sewage and various public furniture are not considered.

The material weight of the slabs can be calculated through equation 1.2. The formula considers a floor height (h_{level}) and considers the potential presence of pitched roofs, which reduces the presence of mineral material due to the slabs, since pitched roofs are typically constructed with lighter materials, such as timber.

The outer walls (equation 1.3) are considered through the perimeter of the building, their height, and the wall thickness. The opening coefficient considers a reduction of materials due to windows and doors. It is used in combination to the age coefficient, which reflects the fact that the openings are influenced by the construction period. For example, the development of improved glazing systems allows for much wider openings without significant energy losses.

The inner walls are distinguished between structural (s) and non-structural (ns) ones (equation 1.4). The non-structural inner walls are thinner and have more openings. Their area has been distinguished through the useful area coefficient, which is a general real estate terminology to assess the net surface of a building excluding the walls. By using this coefficient in multiplication to the total area and reducing the known area of the outer walls, it is possible to extract the area of the inner walls (Equation 1.4a). On the other hand, the weight of the inner bearing walls considers the structural ability of the bearing system to include an economically viable maximum span between each bearing element through the number of the inner structural walls (equation 1.4b). This is done by assigning a typical mean span between the bearing elements (l_a) and running the simple logical condition to determine the number of inner bearing elements (n_{ibw}):

$$if\ \sqrt{A} > l_a; \qquad n^i_{ibw} \approx: \frac{\sqrt{A}}{l_a}$$

$$else; \qquad n^i_{ibw} = 0$$

The value for l_a is kept constant throughout the analysis, but can vary slightly depending on the considered geographical area.

Finally, the basement is only considered through the perimeter of the building and a typical basement height, which is taken in relation to the total height of the building.

$$W_{concrete} = \sum W_{slabs} + \sum W_{outerwalls} + \sum W_{innerwalls} + \sum W_{basements} \qquad (5\text{-}1)$$

$$\sum W_{slabs} = \sum_{i=1}^{N} \left[A \cdot d_s \cdot \left\lfloor \frac{h_m}{h_{level}} \right\rfloor \cdot \rho \cdot c_r \right] \tag{5-2}$$

$$\sum W_{outerwalls} = \sum_{i=1}^{N} \left[p \cdot t \cdot h_m \cdot c_{op} \cdot \rho \cdot c_a \right] \tag{5-3}$$

$$\sum W_{innerwalls} = W_{innerwalls}^{ns} + W_{innerwalls}^{s} \tag{5-4}$$

$$W_{innerwalls}^{ns} = \sum_{i=1}^{N} \left[[A - (c_u \cdot A) - A_{outerwalls}] \cdot h_m \cdot c_{opi} \cdot \rho \right] \tag{5-5}$$

$$W_{innerwalls}^{s} = \sum_{i=1}^{N} \left[n_{ibw} \cdot \sqrt{A} \cdot h_m \cdot c_a \cdot t \cdot \rho \right] \tag{5-6}$$

$$\sum W_{basements} = \sum_{i=1}^{N} [p \cdot t \cdot h_b \cdot \rho] \tag{5-7}$$

Where W – the weight of the element; A – area of the construction plot; d_s – depth of the slab; h_m – mean building height; h_{level} – mean floor height; ρ – density; c_r – roof coefficient; p – perimeter of the construction plot; t – thickness of walls; c_{op} – opening coefficient; c_a – age coefficient; c_u – useful area coefficient; c_{opi} – inner opening coefficient; n_{ibw} – number of inner bearing walls; h_b – height of the basement

The calculated material weights are fed into the GIS software, relating each material quantity to the polygonal representation of the buildings, resulting in a spatial distribution of the material quantities.

The mineral CDW can be defined to be equal to the demolished mineral construction. Therefore, the flow of CDW can be extracted by combining the lifetime curve and the material stock calculated for each structure through the equation 1.1.

5.1.2.4. Future projection of mineral CDW flows

Finally, to estimate future amounts of mineral CDW, a statistical outlook must be done. The number of buildings to be constructed in the future will be proportional to the population and the required living area per capita is unlikely to be change significantly in the near future. Therefore, at this stage, two steps are foreseen:

1. Determination of the future construction volumes
2. Estimation of the waste arising

To estimate the future construction volumes, a relation between the weight of construction material to the population can be extracted from the population records and the material stock quantification discussed in the previous section. Using this ratio and the expected population growth, a future projection of the potentially used construction material can be made. Furthermore, by using the previously obtained lifetime curves of buildings, it is possible to extract the expected CDW arising from the considered stochastic scenario.

5.1.3. Case study

This section presents the application of the described procedure for the country of Luxembourg, as an example of a small country with a combination of few highly urbanised areas and a majority of rural regions. The application of the material stock analysis in the context of geographically small areas will yield important feedback on the volumes of the mineral construction waste arising in similar regions and will be of significant help in steering the management of CDW in quantitative terms. Moreover, it will be crucial in answering the question on whether concrete recycling is a feasible option for the limited mineral CDW in such areas.

Luxembourg currently records a population of 626108 inhabitants, with an average density of 242 habitants per km^2 [235]. The local construction industry has generated a 33.9% investment increase in the period after the 2008 crisis [236] and in the period from 2013-2017, there is a 39% increase in the built volume in the country [237]. The generation of mineral waste accounts for over 95% of the total national generated waste. In 2014, the amount of mineral waste was 0.57 Mt, resulting in 1.04 tonnes of construction and demolition waste (CDW) per capita [238]. Even though the majority of the CDW is re-used, nearly all its volume is backfilled [239]. Moreover, recordings of waste streams in the country are not applied, which makes it difficult to trace the origin of the waste and to have a reliable recorded amount of CDW. Private companies operating in the demolition sites are responsible for the disposal of the waste and the majority of it never reaches the treatment plants. Despite its industrial potential, CDW is often crushed using mobile plants and backfilled on site. This situation not only results in a loss of resources, but also, due to lack of data, makes it difficult to organize and design a recycling process for concrete based on the principles of circular economy.

5.1.3.1. Geographical data collection and height analysis

The geographic data on buildings is collected from the official open database of Luxembourg's Administration of Cadastre and Topography [240]. The building's representation comes as Esri shapefiles categorized by communal codes, which allocates buildings in 105 communes. The height information is processed through the official Lidar data of 2019 [241] (Figure 5-5) which

has a point cloud with a density of 15 points per m^2 and a pixel value of 50x50cm. The subtraction between the Digital Surface Model (DSM) and Digital Terrain model (DTM) was done in Grass QGIS, obtaining a third layer, which contains the z-dimension of manufactured objects and vegetation. Furthermore, using the zonal statistics [242] in QGIS, it is possible to add the previously obtained heights to the shapefiles as a separate attribute. Since the achieved point cloud from the Lidar detects a high number of points per single building, due to the irregularities of the surface and the shape of each structure in the z-dimension (i.e. pitched roofs, chimneys, mansard roofs), the mean value of the heights has been considered in this study.

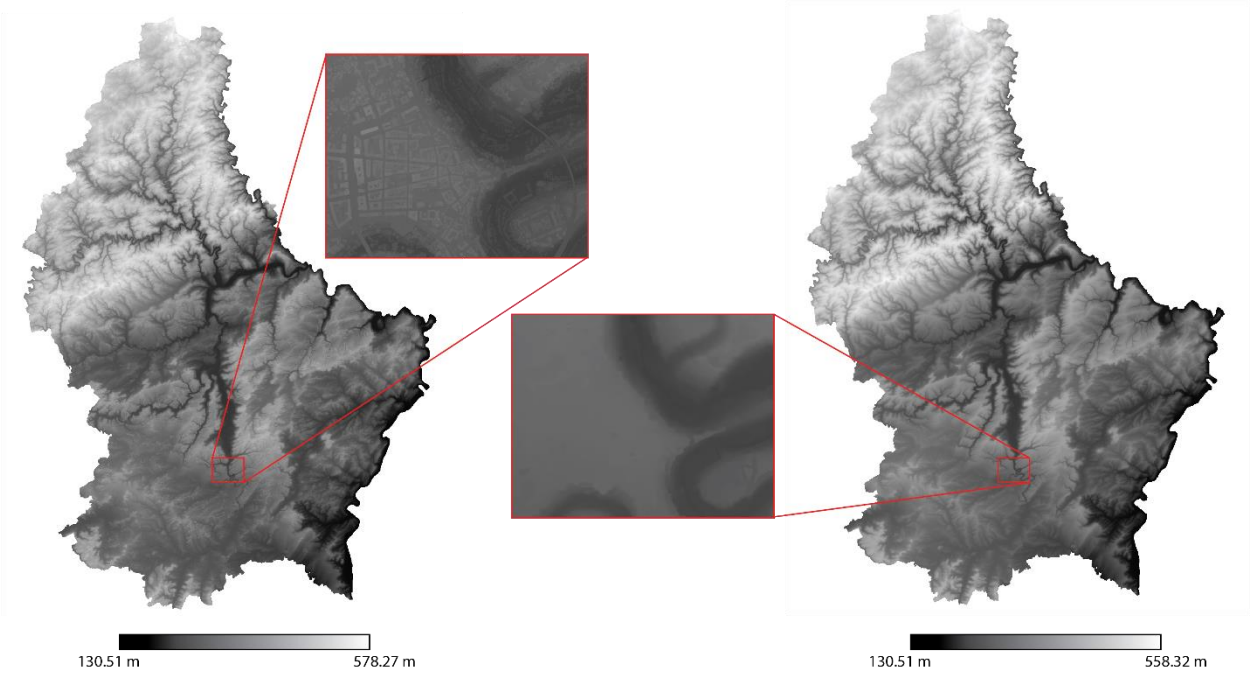

Figure 5-5 Height analysis of Luxembourg using Lidar data from DSM (left) and DTM (right)

5.1.3.2. Age analysis

The detection of the building age is done by analysing historical topographic maps. More specifically, cartography from the years 1927, 1954, 1966, 1979, 1989 and 2000 were chosen from the collection of the Administration of Cadastre of Luxembourg. The choice of the maps was done with the aim of having clear and high definition rasters distributed over the last century as uniformly as possible. Special attention was given in assurance that the representation of the

building units is clear in all maps and no colour damage exists between the different panels. The scale of the original maps was 1:20000 and 1:50000. All maps were georeferenced with the reference frame for Luxembourg: EPSG:2169, Luxembourg 1930/Gauss, which was kept constant throughout the work of this paper.

In the next step, the raster was analysed in terms of pixel count for the colour value range in which the buildings were represented. This was different for each raster, as the colour scheme of the maps was not consistent throughout the years. The pixel value range for each of the three bands of the six layers was registered manually. An operation on raster calculation, yields single band rasters with a binary code, where "1" represents pixels that fulfil the given condition of the pre-defined RGB bands and "0" represents the "empty" pixels. The analysis of the age matrix was done using a conditional loop to assess the more recent construction of the building. For every row of the matrix, a substraction between the matrix index and its precursor was done until the difference remained 0. The point where the index difference showed a negative value is considered to be the earlier record of the specific building in the considered map set and that is considered to be the age of the building. The structures that remained unclassified were recent buildings, which do not appear in topographic maps from 1927 – 2000, therefore they were classified into an additional category of structures erected between 2000 and 2019. Finally, an age-group targeted analysis was done in order to observe the demolition dynamics of each age-group. This was again realised by analysing the age matrix to assess the total number of buildings that were demolished in every considered time period. Thus, a relation between the construction age of the structures and their survival potential is compiled.

5.1.3.3. Building typology

The building typology is depending on the age group and where the building is allocated. Luxembourg has a typical North-West Europe building stock, similar mostly to the western part of Germany and the north-eastern region of France. In the buildings of the beginning of the 20th century and earlier, a massive use of stone in the walls as a bearing element is evident. The slabs of these structures are either made of timber or concrete plates, while roofs are mostly timber frames. As in all Europe, in Luxembourg, an acceleration in built volumes is noticeable as result of the post war reconstruction, especially after 1945. In the second half of the 20th century, the use

of concrete blocks and reinforced concrete has been the main technical element, particularly with the increase of building volumes. Steel structures are also present in the country, although in a number which is limited and clustered around the industrial areas of the steel industry. In the present study, the building typology has been assessed through the Tabula database [243] by relating to the German annex of the Tabula database. The steel structures are manually identified and excluded from the calculations.

5.1.3.4. Assessment of the concrete volumes

The depth of the concrete slab has been considered to be 18 cm uniformly in all considered age categories. This is a simplification based on the technology of reinforced concrete, which throughout the years has not significantly affected the depth of the slabs. The opening for stairs is not considered as reduction into volume, as the concrete volume resulting from the staircase is comparable to the volume of the opening. The roof coefficient considers the presence of a timber roof. In the case of the building stock of 1927, all structures are considered of having a timber roof which leads to the definition of the roof coefficient to be equal to 0.66, while on all other cases, it is 1.

In terms of bearing walls, there are two types: masonry walls (buildings 1927 and before) and concrete or concrete masonry walls (1954 and after). The thickness of the outer walls is considered to be 25 cm. However, older buildings tend to have thicker walls on the perimeter. To take this fact into consideration, the age coefficient (c_a) is used to double the thickness for buildings built before 1927 (c_a=2) and to increase by 50% the outer wall thickness for buildings constructed between 1927 and 1954 (c_a=1.5). For the other construction periods, this coefficient is taken equal to 1. The coefficient for the openings on the outer walls (c_{op}) are taken as 0.95 for the construction period 1927-1954; 0.85 for the construction period 1966-1979; 0.75 for the buildings constructed in 1989 and 0.7 for the buildings constructed after 2000. More modern buildings tend to have larger openings on the façade; therefore, the coefficient takes lower values for more recent buildings.

The volume of inner walls is considered through the useful coefficient c_u, which is taken as 0.75 [244]. The inner opening coefficient (c_{opi}) considers all the internal openings for doors and is taken

as 0.90. The internal bearing walls are considered through the number of inner bearing walls (n_{ibw}) which takes into consideration the structural need for bearing elements at a given horizontal distance. In the present study, the maximum distance without bearing elements (l_a) is considered to be 4 meters. The depth of the basement is considered as 1/3 of the mean height of the building, which is an assumption based on the static height of the structure. An overview of the used parameters is shown on Table 5-1.

Table 5-1Parameters used for defining the weight of mineral building materials in the studied building stock

Construction year	Slabs		Outer walls			Inner walls	
	t [cm]	c_r	t [cm]	c_{op}	c_a	c_u	c_{opi}
1927	18	0.66	25	0.95	2	0.75	0.9
1954	18	1	25	0.95	1.5	0.75	0.9
1966 - 1979	18	1	25	0.85	1	0.75	0.9
1989	18	1	25	0.75	1	0.75	0.9
>2000	18	1	25	0.7	1	0.75	0.9

7.2.2. Results

5.1.3.5. Geographical data collection and height analysis

The height profile (Figure 5-6) shows that the country is characterized by relatively small buildings in terms of area and height. The mean height is 6.66 meters, while the mean building area is 175.25 m^2. In addition, it is of interest to analyse the spatial distribution of the buildings' characteristics on a country-scale (Figure 5-7). The spatial distribution in terms of mean building height is heterogeneous within the 105 communes of the country, although there is a visible peak in the central and south-western areas. In the City of Luxembourg, the peak is due to the large urbanization scale, which includes several high-rise buildings. For the commune of Esch-sur-

Alzette (south-west), there is a high presence of industrial buildings. In terms of the building area (figure 7b), the country shows a different trend which is more heterogeneous. The northern region is characterized of buildings with larger areas, which is mostly due to agricultural structures. The percentage of built area ranges from 0.09% to 12% with the south-western area resulting the most utilized area in the country in regard to construction.

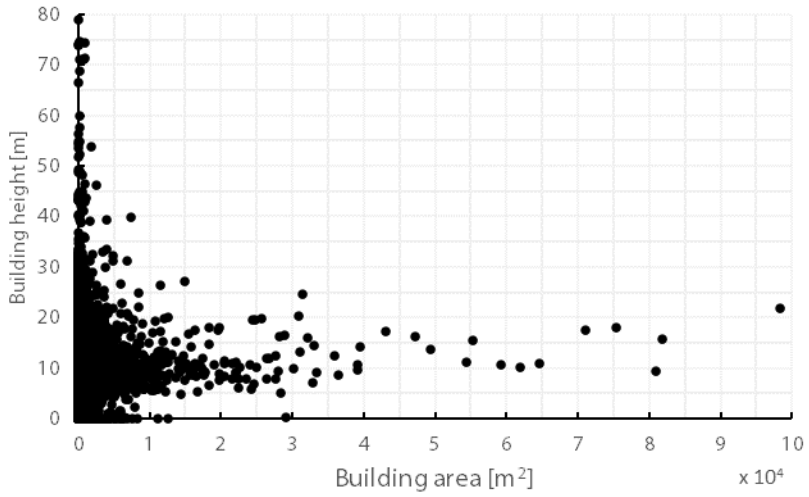

Figure 5-6. Height profile of the country showing the relation of each building area to its height

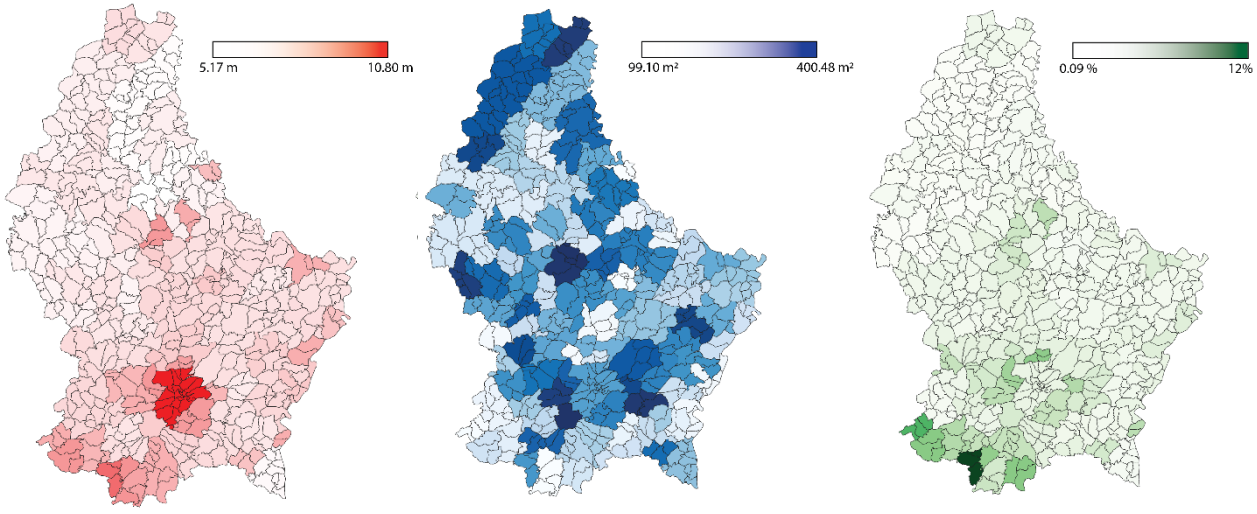

Figure 5-7. Spatial analysis of the built environment in Luxembourg: a. Mean building heights; b. Mean building areas; c. Rate of built area

5.1.3.6. Age analysis

The age matrix for the country of Luxembourg is shown on Figure 5-8. The grey colour represents the recognition of a building's presence on the considered map, while the white colour shows the absence. The subsequent change of colours from grey to white is defined as demolition.

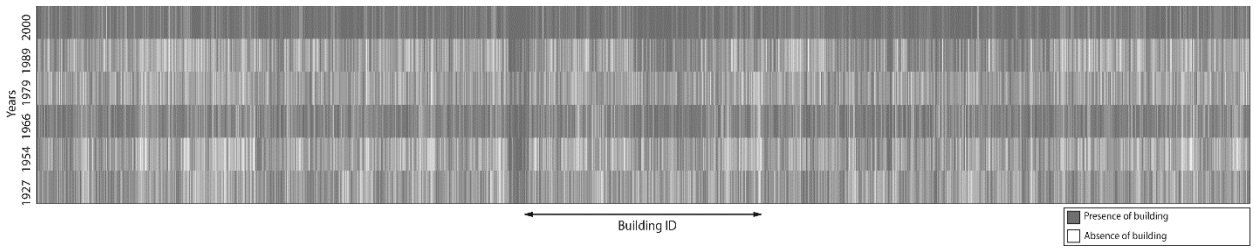

Figure 5-8 Heatmap representing the age matrix for the entire building stock of Luxembourg

From the age analysis, a characterization of the building stock based on the construction age can be made (Figure 5-9). The building stock in Luxembourg can be considered mixed in terms of age. A significant amount of structures was constructed before 1927 (31.30%). This includes the historic centres of the cities, but also the major industrial structures which were erected prior to 1927. At the beginning of the 20th century, Luxembourg was one of the largest steel producers in Europe due to the iron mineral deposits in the south of the country. At this time, there was a surge in construction of industrial structures and habitation for the growing population of workers. This is mostly noticeable in the south-western cities (e.g. Esch-sur-Alzette, Differdange, Dudelange). After the second World War, the reconstruction process caused an increasing trend leading to the construction of mainly residential structures. Following a normalization period between 1966-1979, the numbers are currently on a constant rise.

In terms of building use (Figure 5-9b), the total gross volume is comprised majorly of residential buildings. The construction of new industrial and public buildings has experienced a surge in the last 30 years. In the period 1989-2000 there is a 507% increase in gross volume of industrial buildings compared to the previous time period. This is accompanied by a further 21.9% increase of the industrial gross volume built in the last 20 years.

The mean building age per commune (Figure 5-10) gives an outlook on the potentiality of waste production. The oldest building stock is located in the south-central area, where Luxembourg city

is located and in the south western area, where the cities of Esch-sur-Alzette, Differdange and Dudelange are located. These cities constitute 32% of the total population of the country and have a population density which is 2.99 to 9.91 times higher than the national average density. Therefore, not only these areas are older in terms of their built environment, but they are also expected to have a larger concrete stock, resulting in a higher potentiality for CDW production.

According to official data from the Luxembourg Portal of Statistics (STATEC) [244], for the period 1979 -2017, there was a mean increase of 1.04 in the number of buildings constructed every year, while for the calculated model, this factor is 1.16. This difference is due to the nature of the data, which for the calculated model is accumulative in a clustered way of 10 to 20 years rather than recorded on a yearly basis, while for the statistical data, it comes from annual recordings. Additionally, the shapefiles that are used for calculating the building volumes in QGIS do not always perfectly correspond to the definition of built structure in statistical records.

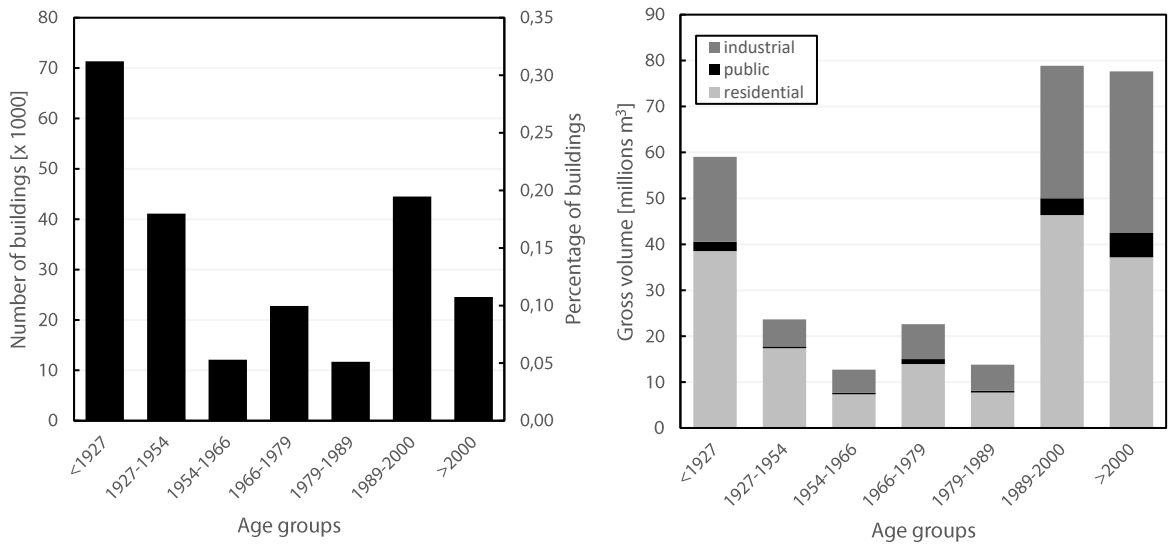

Figure 5-9. Age characterization of the building stock in Luxembourg: a. Based on number of buildings; b. Based on gross volume

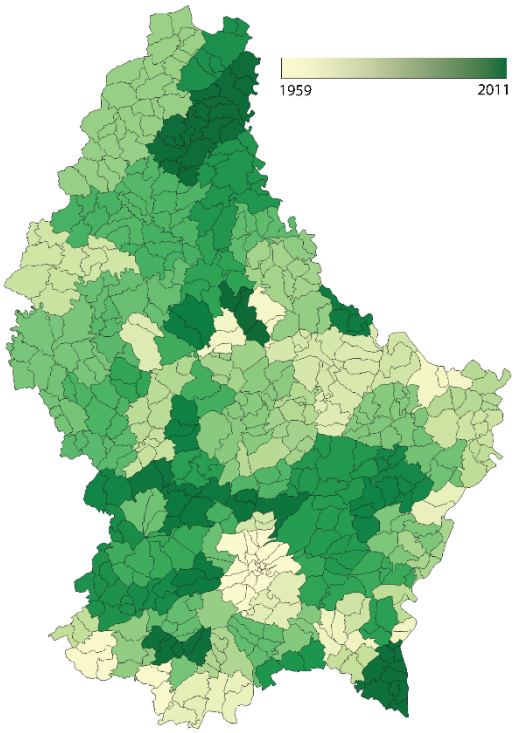

Figure 5-10. Mean age for each communal division in Luxembourg

5.1.3.7. Assessment of the concrete volumes

According to the analysed model (figure 9), the current concrete stock in Luxembourg is 276.75 Mt. It accounts for 450.817 tons/capita considering the country's population of 613894 inhabitants. The ammount of concrete stock has been growing at a rate which ranges from 20.81% to 24.39% in the last 30 years. It can be noticed that the concrete stock produced after 1979 accounts for more than half (52.84%) of the total, while the concrete stock remaining from before 1979 is mainly part of buildings which existed before 1927. This hints at a significant lack of remaining constructions from the building stock of the years 1954-1979. It can be due to several aspects. First, the World War 2 has greatly influenced the construction industry in Europe. The rapid reconstruction of the post-war era resulted in structures with a lower quality which had a major potential of depreciation. Moreover, the common use of asbesthos in structures constructed during the 20th century may be a strong reason for their low degree of survival [245].

In terms of usage of materials, the residential structures consitute the majority of the share in almost all age groups (Figure 5-11). A distinction can be made in buildings from the last 20 years,

where industrial structures have peaked. This fact is quite reasonable considering Luxembourg's soaring economy of the last years [246][247][248].

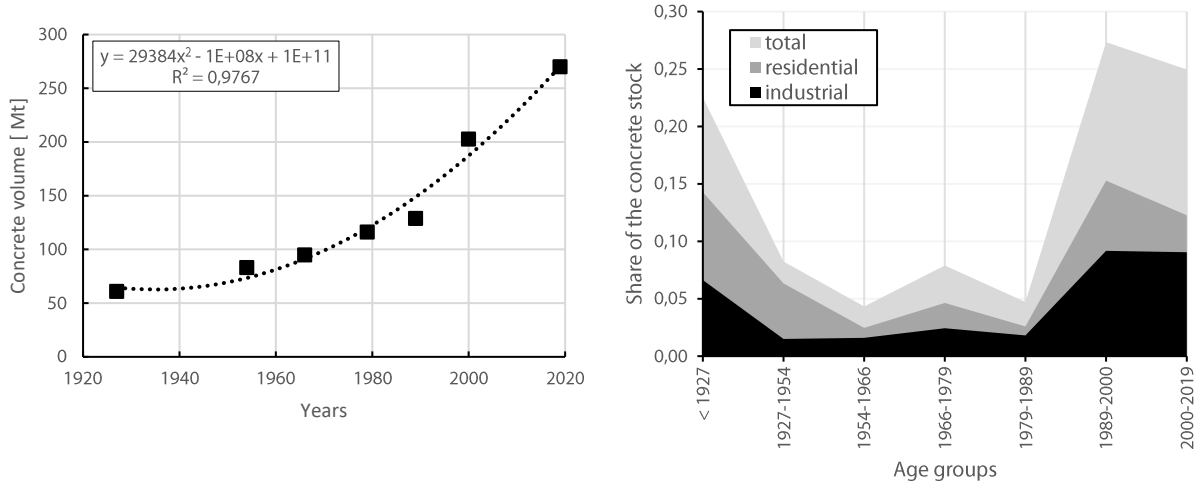

Figure 5-11. Characterization of the mineral construction material stock in Luxembourg: left: Evolution through the years, right: Material allocation depending on the use of building

5.1.3.8. Demolition behaviour and assessment of future volumes of concrete

The global survival of each building stock in relation to its construction age is shown on Figure 5-12. It shows that the survival of each building is not directly linked to its age. For example, the building stock constructed before 1927 shows a higher survival ratio compared to the buildings stock constructed between 1927 and 1954, even though the former is comprised of older structures. The buildings constructed after 1989 display a higher rigidity in terms of their demolition compared to earlier structures with less than 10% of them being demolished.

In order to analyse future mineral CDW trends, a global analysis on the survival of structures needs to be made. With this aim, a regression analysis curve (R^2 = 0.84) is extracted from the available data, as a cumulative distribution function for the survival of the building stock (Figure 5-12). By forecasting the equation to the point where the survival rate becomes 0 it is possible to assess the maximum typical lifespan of the buildings in Luxembourg from a global point of view. The typical lifespan of the building results to be 122 years. In the analysed map set, structures

constructed before 1927 are not categorized into smaller construction age groups. This lifespan is consistent with the predicted service design lifetime of structures [216] and falls within the range of other studies [29].

The cumulative distribution function for the survival of the building stock (Figure 5-12) shows a significant slow-down on the demolition of structures older than 50 years. This is most likely related to their historical value of old buildings. Thus, it is very implausible for a building stock representing a specific age group to be completely demolished. Even though a meticulous limitation on the extrapolation of survival function remains difficult, in this study a 10% of the existing building stock is considered within this category, while for future stock, it was increased to 30%. The reason behind this lies in the quality of construction materials used nowadays, which are expected to have longer lifespans and receive lower levels of devaluation. Furthermore, considering the national plan for Luxembourg regarding the energetic performance of buildings [249], it is projected that new structures will have better conditions in terms of inhabitant well-being as well as economic performance. Additionally, the use of cladding and thermic insulations will result in a lower environmental impact for the core structural materials in the long-term. From this model, a general trend for mineral CDW generation of the country can be assessed. Two additional scenarios representing a lifetime profile of 100 years and 150 years are considered as stochastic models by changing the maximum lifetime, but preserving the general mathematical shape of the function (Figure 5-12), thus creating a larger extent of consideration.

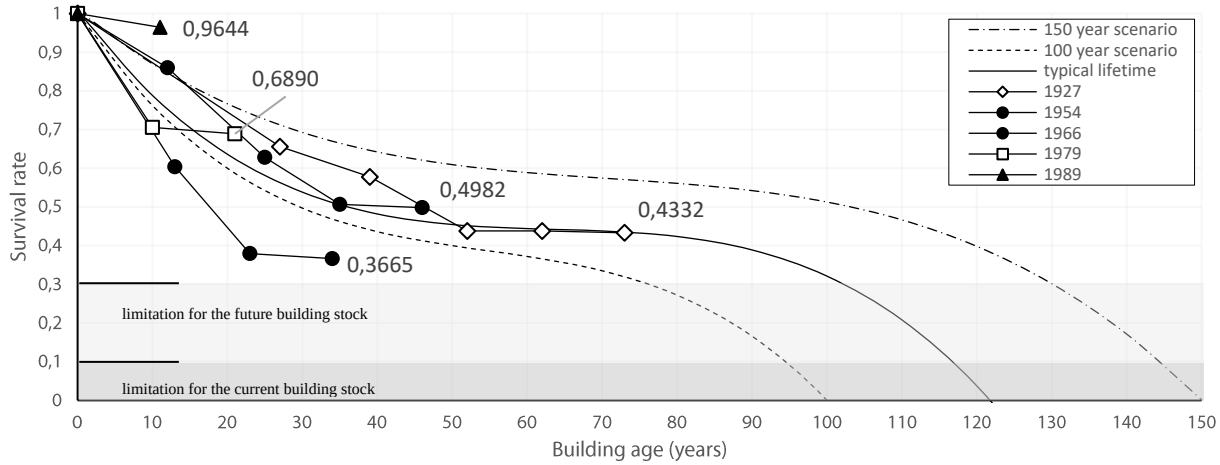

Figure 5-12. Survival analysis and typical lifetime curve for buildings in Luxembourg, as well as the two additionally considered scenario

Furthermore, it is of interest to look into the demolition dynamics of each considered age-group (Figure 5-13). The demolition rate is highly dependent on the historical situation in terms of economic and political situations and the demolition behaviour results to be different for each building stock depending on its construction age-group. Generally, there is a high-peak of demolished buildings approximately 30 years after their construction. This is consistent with the age-groups 1954, 1966 and 1979. For the building stock constructed before 1927 a complex demolition profile can be observed (Figure 5-13a). In total, 56.68% of this building stock has been demolished (Figure 5-12) until 2019 and there are two demolition peaks visible. The first one corresponds to the second World War while the second one corresponds to the shut-down of the traditional steel industry where it has been switched to a more modern process based on electric furnaces and recycled steel. Indeed, in 1994 this decision on the transition was taken, paving the way for the urbanisation of these areas [250]. This change has caused most probably a second peak in the demolition of old industrial structures, which dated back to the beginning of the 20th century. The demolition behaviour of building stocks from 1954, 1966 and 1979 (Figure 5-13b, c, d) show a similar trend represented by a bell-shaped parabola. The peak of their demolition profiles shows maximum values between 1980 and 1990, which is compatible with the second demolition peak of the building stock of 1927, reinforcing the high influence of the economic conditions on the building dynamics. In contrast, the buildings from 1989 show a lower demolition profile (figure 10e).

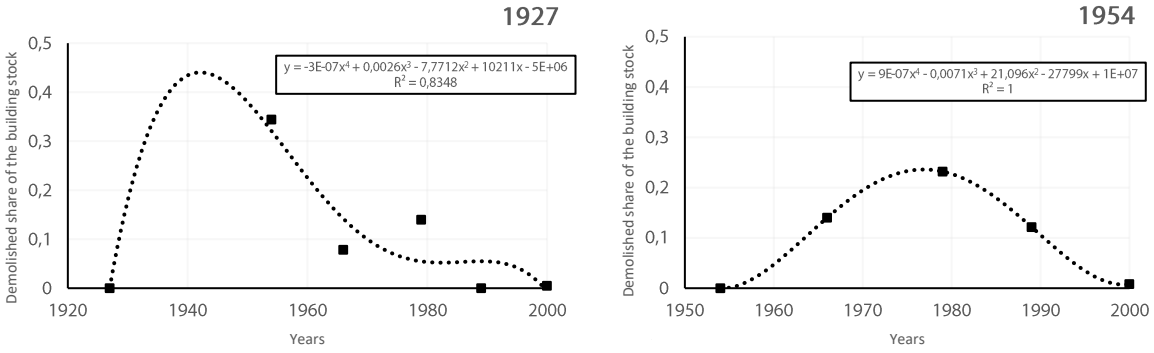

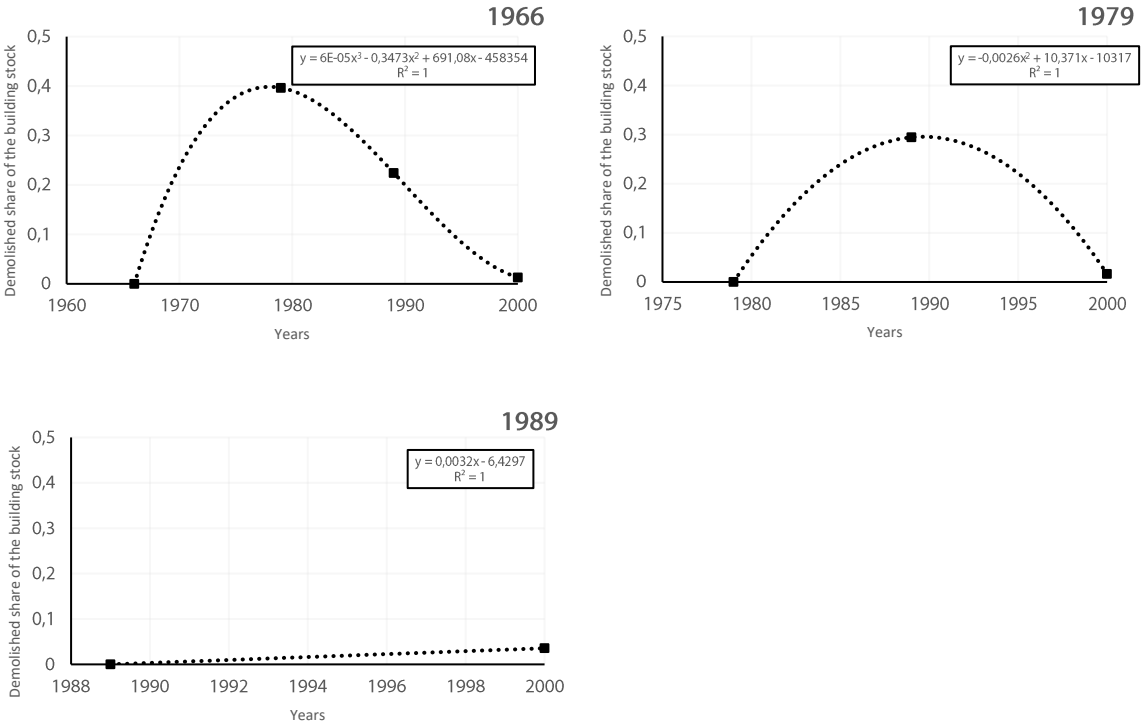

Figure 5-13. Demolition profiles of different age groups

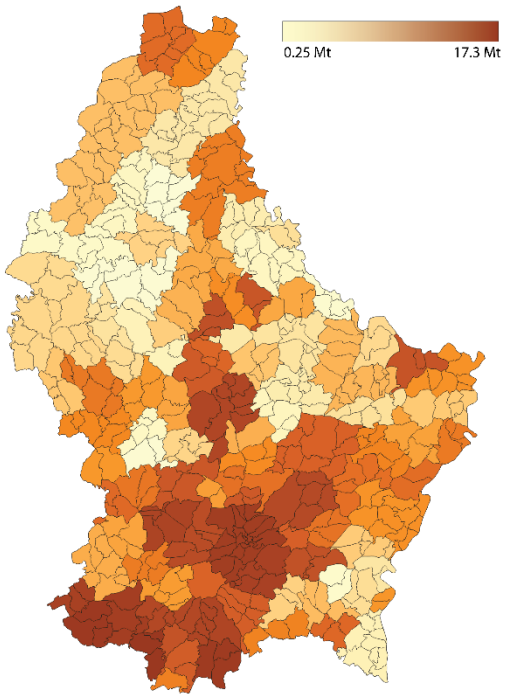

Figure 5-14. Spatial distribution of the present concrete stock in Luxembourg

The geographic distribution of concrete stock (Figure 5-14) shows a concentration of the material in the central and southern part of the country. As previously discussed, these areas resulted to be not only the highest populated regions of the country, but also the communes with the oldest building stock. The high concentration of materials confirms the highest potential of these areas for future origination of mineral CDW.

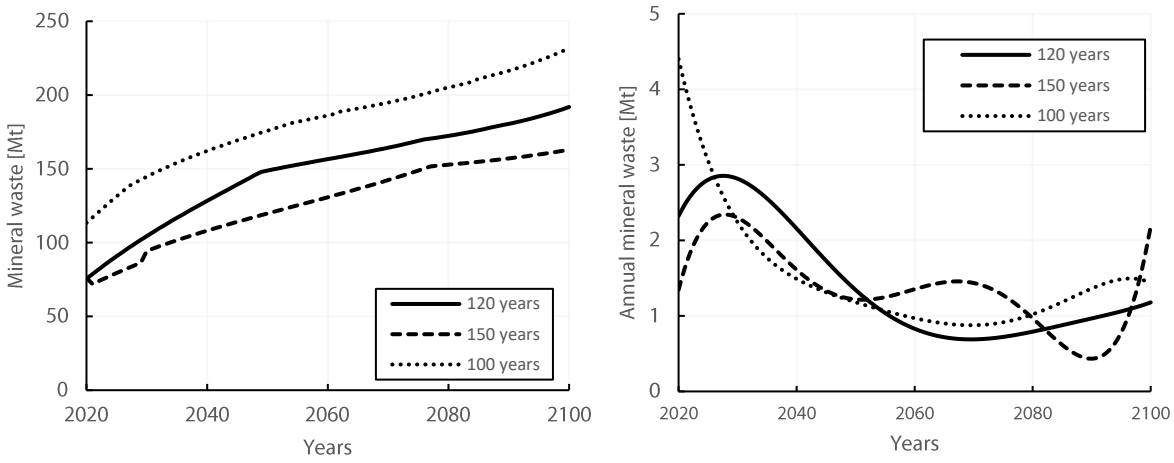

Figure 5-15. Mineral CDW generation in Luxembourg from the currently existing building stock; left: Accumulative CDW generation; right: Annual CDW generation

The accumulative amount of mineral CDW for the present building stocks, composed of buildings of different construction ages (Figure 5-15), is divided into three scenarios depending on the maximum life expectancy of the building stocks, which are based on the previously defined lifetime scenarios (Figure 5-12). Each building stock is considered though its previously assigned age, therefore, depending on the lifetime curve, each age-group has a specific survival rate throughout the considered time period, resulting in a dysphasic starting point for the three different scenarios. In general, there is a higher rate of CDW generation from 2020 to 2050 and a lower intensity from 2080 to 2100, with the 150 years scenario showing a different trend in the last part of the century. From the cumulative production curve, annual production curves are extracted in figure 13b through derivation of the regression lines from the graphs of figure 13a, making it possible to have an estimation on the annual production rate of CDW related to the current building stock. Indeed, there is a peak in the annual production related to the worst-case scenario in the period between 2020 and 2030, after that the annual production for the three scenarios fluctuates in a decreasing trend, due to the depletion of the current building stock. It can be noticed that, even without considering new construction, the annual production shows a mean of ranging from 1.38

to 1.49 Mt/year. Except for the first and last considered decades (2020 – 2030 and 2090 - 2100), there is no significant difference in the three considered scenarios.

The future projection of the population is divided into three scenarios namely with a 1.13%, 0.52% and 0.17% average yearly increase rate (Figure 5-16) during 80 years. The first increase rate is based on the current population growth of Luxembourg, while the others are considered to be lower. A higher scenario is not considered, due to the logistical issues that an increasing population density would cause in the country, thus making such scenarios unlikely. It is logical to think the construction as being proportional to the population, since an increase of population will lead to more demand for housing. Comparing the data from 1970-2020, a concrete demand per capita of 463.2 tons/capita can be extracted. This value is implausible to have a high sensitivity, since the spacing needs per person are improbable to change. Therefore, the new construction generation can be directly assessed from the population scenarios and by using the lifetime curves (Figure 5-12), the generation of mineral CDW can be evaluated both accumulatively and annually (Figure 17).

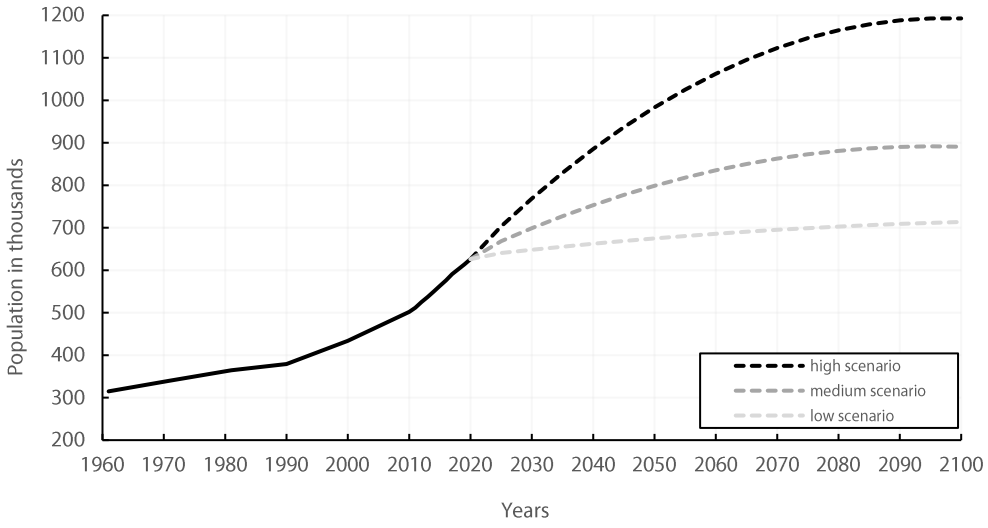

Figure 5-16. Population evolution in Luxembourg and the considered future scenarios

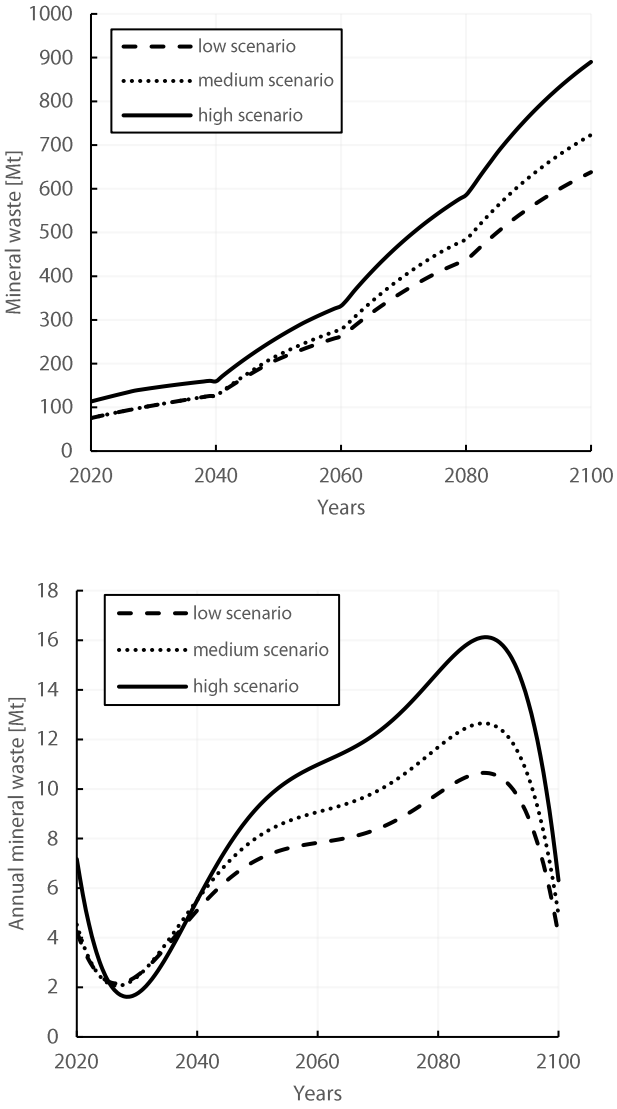

Figure 5-17. Mineral CDW generation in Luxembourg from the future building stock; left: Accumulative CDW generation; right: Annual CDW generation

The accumulative projection (Figure 5-17a) shows that in the next 80 years between 890 and 638 Mt of inert waste is expected to be generated in the country. In comparison to the data generated only from the analysis of the current building stock, the future construction will have a significantly larger influence on the country's waste stream representing 73.96% of the total inert CDW by 2100. However, the sensitivity of the data is lower than the previously considered scenario, with a maximum difference of 48% between the high and low scenarios. The annual mineral waste production graph (Figure 5-17b) is constructed through a derivation of the accumulative trend lines of mineral CDW generation (Figure 5-17a) and shows an increasing trend

independently on the scenario and a drop within the last decade of the century. Considering the predetermined projection scenarios, the largest CDW flow in the country is expected between 2060 and 2090 with a significant peak in the last 20 years of the considered time period. This surge is due to the larger volumes that are expected to be built with the increase of population, for example apartment blocks or larger housing units in this time period. By the end of the century, an average drop of 61.9% in the annual production is noticed in all three scenarios, due to the higher resilience of the newly built structures and the consideration that a large part of the future stock will result to be more rigid in terms of their demolition behaviour. Additionally, the fluctuations in the yearly generation of CDW are greatly influenced by the considered lifetime profiles (Figure 5-12). Indeed, the drop observed after 2090 can be due to the slowdown of the lifetime curves than can be observed for buildings aged between 40 and 80 years (Figure 5-12). This is a clear indication on the importance of the age analysis and the choice of suitable lifetime curves for the area in consideration.

5.1.3.9. Feasibility of concrete recycling in areas with limited urbanization scale

One of the largest uncertainties regarding recycling of mineral CDW in small geographical areas, such as Luxembourg, is related to the availability of the waste material flow. However, results show that the foreseen annual generation of CDW is comparable to that of other larger countries [251]. In terms of the availability of the secondary raw materials, a ratio can be made between the expected mineral CDW arising from all considered scenarios and the expected concrete production in the next 80 years. This ratio will yield the theoretical possible substitution ratio strictly in terms of material quantity.

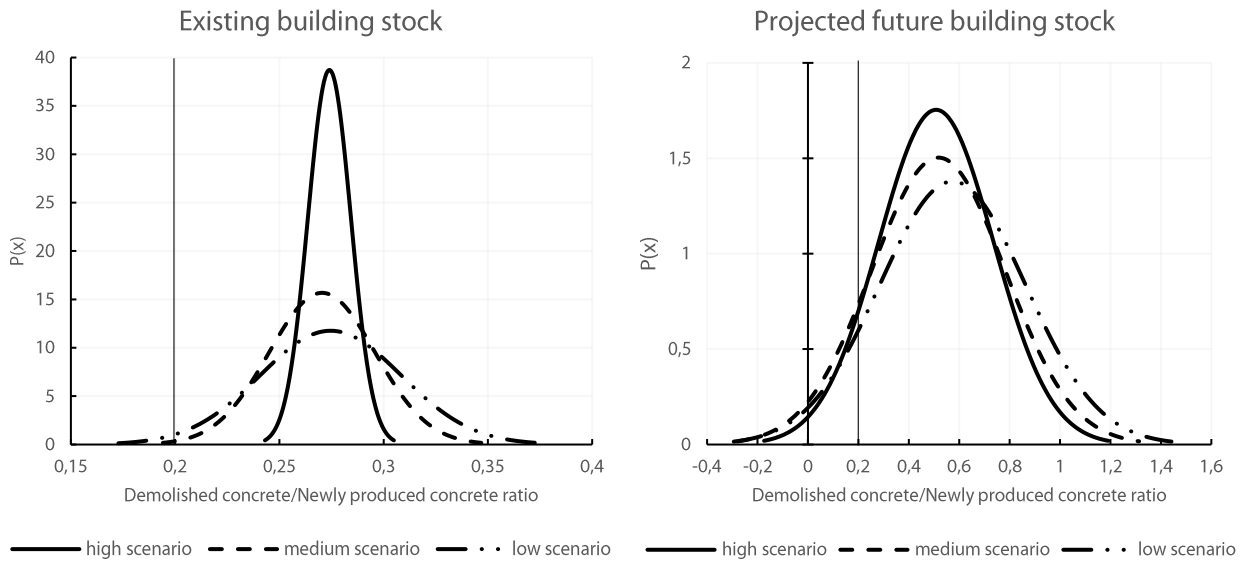

Figure 5-18. Normal distribution of the (mineral CDW/new construction) rate for the considered scenarios

A normal distribution of the ratio between the generated mineral CDW and new concrete production allows to give an overview of the considered time period (Figure 5-18). As it can be seen on Figure 5-18a, for the majority of the studied period, the ratio is larger than 0.2, which is currently the technical limit for use of recycled aggregates according to EN 12620 [64]. If the demolition of future structures is considered Figure 5-18b, the ratio remains higher than 0.2, for the majority of the studied period. However, there is a larger probability of having shortage of recycled aggregates compared to the pervious case. As it can be noticed, the normal distribution of the existing building stock yields a more statistically rigid result, while the projected results demonstrate a higher variability. This is considered evident in this case based on the assumptions that were previously made in the data calculation, such as the population evolution, construction evolution, lifetime profiles, etc. On the other hand, it should be noted that other factors are to be considered in the CDW flow, such as different stakeholder engagement in the management of waste.

In terms of economic viability, the considered models also hint at concrete recycling as a cost-effective production for Luxembourg. The feasibility study of a concrete treatment plant with a capacity of 350 t/hour [252] shows a break-even point in less than 3 years. If the lowest-case scenario is considered, namely considering only the current stock with a lifetime profile of 150 years, the flow of mineral CDW is calculated to be above 350 t/hour for the majority of the considered timeframe (Figure 5-19). However, further conditions will affect the viability of a

concrete recycling plant. For example, it may be unrealistic to consider the entire generated CDW to be treated at the same plan. Even though this is a feasible scenario for small areas as Luxembourg in logistical terms, stakeholder engagement and market conditions are expected to further influence the management of CDW.

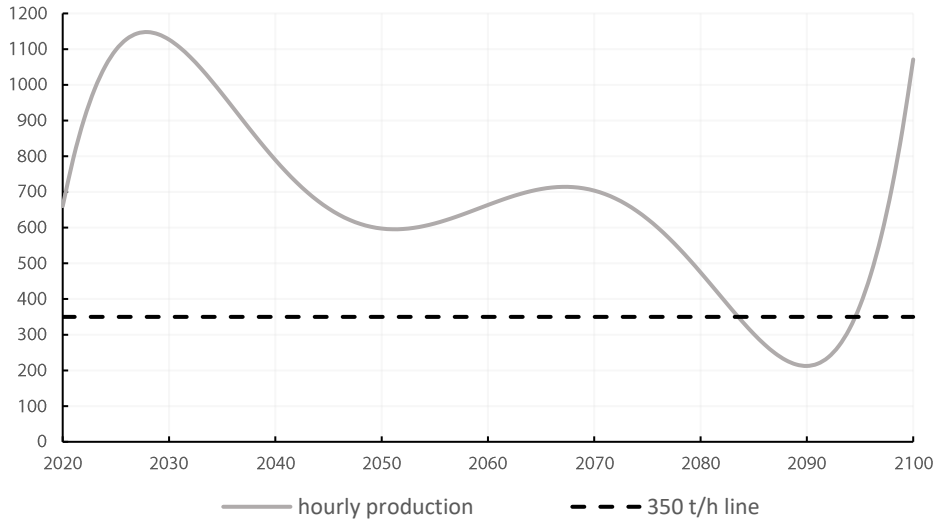

Figure 5-19 Hourly mineral CDW generation for the lowest considered scenario

7.2.3. Discussion

The presented methodology shows the remarkable potential that a combination of geospatial evaluation, image analysis and material stock quantification can have on evaluating the dynamics of mineral CDW over the next 80 years. The findings indicated promising results not only in terms of evaluation of the building stock, but also as an outlook to promote concrete recycling and the circular economy of the construction sector, indicating that the potential generation of mineral CDW is suitable for an industrially and economically viable concrete production.

There is a limitation however in considering the entire demolished mineral construction to be recyclable material. The use of CDW as road backfilling will certainly continue to occur and, if this volume were to be recorded, the considered annual generations of mineral CDW will decrease. Furthermore, on-site use of demolished fraction will further reduce the availability of recyclable CDW. Also, these applications considerably influence the recorded volumes of waste, resulting in

unreliable statistics. As shown in the results, there is a significant increase in mineral CDW if future constructions are considered, hinting at the importance of effective planning strategies that rely not simply on statistical recordings of accumulated waste, but rather on the realistic state of the art of the local CDW generation.

The evaluation of the building stock through image analysis offers a novice way of assessing the lifetime dynamics of the built environment. The importance of a geographical approach is key in this sense as the demolition behaviour is strictly tied to the socio-economic conditions of the area. Nevertheless, a few shortcomings were observed. The proposed methodology can be, at the moment, only considered globally for the intended purpose. The alternative local approach of considering all structures individually and assessing their characteristics is however unfeasible, since it is difficult to assess the realistic lifetime of a single building or a building type. The lifetime expectancy of individual structures includes significant ambiguities related to the socio-economic aspect of the region and it is not easily assessable without relying on assumptions that will increase the level of uncertainty. Therefore a normalization of the datapoints through a global regression is considered adequate for this purpose. Additional optimization can nevertheless be done through a case-study approach if the aim is to have a higher resolution (i.e., implementing the construction age into the local cadastre) and the proposed age-groups dynamics (Figure 5-13) can be utilized if an age-specific analysis is required. The considerations of mathematical functions for the lifetime curves and the limitations set during the analysis can offer significant constraints as the analysed building stock does not exceed the maximum lifetime of the buildings. Error-free assumptions can only be made once a building stock is completely demolished, which, in this study, it is not the case. Therefore, it remains difficult to make evaluations on the accuracy of the data, especially when considering a large future timeframe. Furthermore, the lack of data records on the generation of CDW and the unregulated re-use of CDW on the demolition sites implies a further difficulty in assessing the affinity of the model.

Assessing the mineral material stock in each building through the presented model must be geographically adapted if such analysis is to be done in other areas. The proposed model is constructed for a North-Western built environment mainly based on concrete as structural material. Likewise, the considered coefficients are to be chosen based on the considered area. It must be stressed however that the considered model must be regarded as approximative and an exact

analysis of the embedded materials can be done only through a case-study approach of the entire building stock.

7.2.4. Conclusions

A methodology to assess the amount of mineral CDW through material stock quantification and geospatial approaches was presented. This methodology was applied for the entire national building stock of Luxembourg to understand the typical volumes in small geographical areas and analyse the feasibility of concrete recycling based on the available volumes.

The proposed method allows for rapid analysis of large areas by relying solely on open-source data, thus avoiding extra costs and workload. By using image analysis of old cartography, a historic lifetime profile was extracted showing the demolition behaviour of buildings during the last 93 years, which rendered possible to extract the potential mineral CDW arising from the building stock through a consideration of stochastic scenarios for the next 80 years.

Results show that the 31.30% of the structures in Luxembourg are built before 1927, while the largest built gross volume is built after 1989. The total mineral materials embedded in construction in the country is 277 Mt, accounting for 451 tons/capita. Typical lifetime profiles extraced through image analysis show a mean service life of 122 years, although the survival behaviour depends on the period of construction and is not unfiform for all the considered age groups. Based on the stochastic projections the mineral CDW generated from the existing building stock is expected to be up to 227 Mt by 2100, while if future building scenarios are considered, it can be as high as 885 Mt. The annual CDW production is expected to be sufficient for a viable concrete recycling activity if regulations on the waste volume flows are made available.

The described methodology offers a viable, flexible and rapid tool for management of the built environment, especially for planning of the best practices for treatment and re-use of waste arising from the construction sector.

5.2. Publication II: A coupled spatial - environmental approach as decision-making tool for the circular economy of the built environment (Bogoviku, Waldmann)

Abstract

The building sector is linked to 38% of the global carbon emissions. Only concrete production emits 300.526 kg of CO_2-eq and use 1488.75 MJ of energy per m^3. However, through carbonation, part of the carbon emissions is offset.

A coupled spatial-environmental approach is proposed to assess the global environmental impact of the mineral construction material (MCM) stock and to serve as foundation for a database allowing a strategic decision-making at the end-of-life stage. The methodology is tested for the country of Luxembourg where the stock has been growing at a fast pace in the last two decades and is currently 277 Mt. The assessed embedded carbon emissions are 34.38 Mt CO_2-eq and 5% in average has been captured by carbonation. This translates to 13.6 kg CO_2-eq per m^3 of MCM. The data has been incorporated into a database, which can also be further enriched with other relevant environmental impact indicators.

5.2.1. Introduction

The construction industry is one of the largest industries in the planet and as such is one of the main producers of industrial waste. In Europe, construction and demolition waste represents up to 30% of the total waste generation [253] and exploits 3 billion tonnes of virgin aggregates per year [254]. In a global aspect, the building sector is connected to 38% of total global carbon emissions and the investment on energy-efficient buildings only increased by 3% between 2018 and 2019 [255].

Mineral construction materials (MCM) are one of the main contributors to the building industry. In an environmental aspect, they affect the global climate crisis. Production of concrete for example, consumes about 1.3 kg of aggregates and about 0.3 liters of water per m^3. A m^3 of concrete can cause 300.526 kg of CO_2-eq mainly due to the production of cement and use 1488.75 MJ of energy [256]. Built-in concrete can, however, absorb CO_2 during its lifetime through the carbonation process.

Carbonation in concrete is a physio-chemical process where atmospheric CO_2 reacts with products of cement hydration, resulting in calcium carbonate. During the production of cement, limestone is heated at a temperature of 1450°C, resulting in calcium oxide and carbon dioxide (equation 1). The calcium oxide is hydrated during concrete mixing, forming portlandite (equation 2). During the lifetime of the concrete, the portlandite reacts with atmospheric carbon dioxide forming limestone and water as by-product.

$$CaCO_3 + heat \rightarrow CaO + CO_2 \quad (1)$$

$$CaO + H_2O \rightarrow Ca(OH)_2 \quad (2)$$

$$Ca(OH)_2 + CO_2 \rightarrow CaCO_3 + H_2O \quad (3)$$

This process lowers the alkalinity of the concrete to a pH near 8[257]. For the pure concrete, carbonation does not imply any structural damage. In recycled aggregates, carbonation has been shown to be beneficial in improving all mechanical and physical parameters of the recycled concrete [258]. In theory, concrete can offset the entire CO_2 footprint through carbonation during

its lifetime. However, in practice a maximum of 75% of the available CaO would react [259].According to Yang et. al [260], the carbon uptake depending on the time (t) can be assessed through the following formula:

$$U_{CO_2}(t) = [\alpha_h(t) \cdot M_{ct}(t) \cdot M_{CO_2} \cdot 10^{-6}] \cdot A_{sf} \cdot x_c(t)(g) \quad (4)$$

Where $\alpha_h(t)$ is the degree of hydration of the cement paste at t, M_{ct} is the molar concentration of the carbonate constituents of the paste per unit volume of concrete, M_{CO_2} is the molecular weight of CO_2, A_{sf} is the surface area in cm^2 of the concrete exposed to carbonation and $x_c(t)$ is the carbonation depth at age t.

The carbonation depth is assessed through the model proposed by Possan et al [261]

$$y(t) = k_c \left(\frac{20}{f_c}\right)^{k_{fc}} \cdot \left(\frac{t}{20}\right)^{0.5} \cdot \exp\left[\left(\frac{k_{ad} \cdot ad^{\frac{3}{2}}}{40 + f_c}\right) + \left(\frac{k_{CO_2} \cdot CO_2^{0.5}}{60 + f_c}\right) - \left(\frac{k_{rh} \cdot (RH - 0.58)^2}{100 + f_c}\right)\right] \cdot k_{ce} \quad (5)$$

Where y(t) is the average of carbonation depth (mm); f_c is the characteristic of compressive strength in concrete (in MPa); k_c is the factor according to the kind of cement; k_{fc} is the factor relating to compressive strength of concrete, depending on which cement is used; t is the concrete age (year); ad is the percentage of pozzolanic in concrete (relative to cement mass); k_{ad} is the factor to pozzolanic additions of concrete–silica fume, metakaolin and rice husk ash, according to the used cement; RH is the average of relative humidity (in % * 0.01) k_{rh} is the factor related to relative humidity, according to cement used; CO_2 is the atmospheric CO_2 concentration, (in %); k_{CO2} is the factor related to the environment CO_2 content, according to the cement used; and k_{ce} is related to exposure to rain factor, according to exposure conditions of the structure.

Studies on carbon sequestration in concrete have been significantly emerging in the last years. This is due to the trending life-cycle analysis (LCA) studies and the need to account for carbon sequestration in the cradle-to-cradle model. Souto-Martinez et. al [262] reported that up to 19% of the initial CO_2 can be reclaimed for concrete structures of 25 years. Jacobsen and Jahren [263] reported for Norway that 16% of the produced carbon has been absorbed during its lifetime, while Andersson et. al [256] reported a similar value (17%) for the Swedish stock. A similar result was

described by Yang et. al for South Korea [260]. Furthermore, this study showed no difference in the carbonation rate between a residential and a commercial building.

5.2.2. Introduction

The present paper focuses on the proposal of a methodology to monitor and assess the global environmental performance of the built environment by combining a material flow analysis with environmental impact analysis. A case study for the carbon balance of MCM is presented based on the country of Luxembourg. The proposed procedure is shown on Figure 5-20.

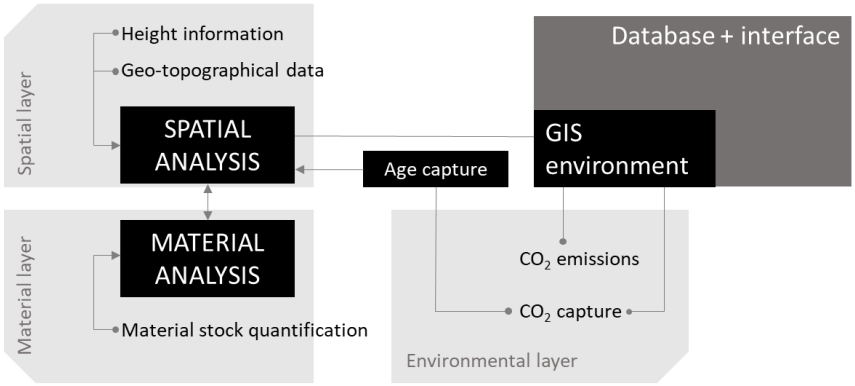

Figure 5-20. Overview of the procedure

First, a combined spatial and material analysis is done. The spatial analysis consists of the acquirement of GIS data on the built environment and attaching any missing information, such as for example, the height of the buildings. The material stock quantification is based on the structural and architectural needs for the use of MCM. The effect of age on the material stock is assessed through the age capture based on a pixel analysis of topographic imagery from the period 1927-2019, as described in [264].

The carbonation procedure was also tested on two practical projects, where cores were drilled from demolitions project dating in 1970s and 1980s. As it can be seen on Figure 5-21and Figure 5-22, there is a slight difference between the carbonation front between slabs and walls or columns. In walls and columns, the carbonation front appeared at approximately 5 cm with respect to the face, while for the slabs it was at 3 cm. This difference could be due to the different exposure

conditions between walls and slabs, a change in the relative humidity between the inside and outside or the use of a higher strength concrete for the slabs.

Figure 5-21. Carbonation samples of slab cores

Figure 5-22. Carbonation samples of slab cores

For the calculation of the carbonation depth, the model shown on equations 4 and 5 is used, based on the work of Possan et al [261] and the chosen input is shown on Table 5-2.

Table 5-2. Considered values for the carbonation depth calculation

k_c	k_{fc}	k_{ad}	f_c	k_{co2}	co_2	k_{rh}	RH	k_{ce}	ad
33.27	1.7	0.32	20	15.5	0.04	1000	0.8	0.65/1.30*	0
*0.65 is considered for the outer elements, 1.30 for the inner elements									

The carbon emissions values are obtained from the database Ökobaudat [53]. For the current study, the walls are considered to be hollow concrete bricks, while the slabs are considered to be cast-in-place concrete.

The entire MCM in the country is 277 Mt with a growth of up to 24.39% in the last three decades [264]. Considering this, the carbon emissions from the construction of the entire stock in the country is 34.38 Mt.

As it can be seen from Figure 5-23, the carbon emissions have significantly accelerated in the last 20 years with more than half of the total emissions linked to the construction activity after the year 2000. This is due to the increased construction activity in the country. However, the LCA input values do not consider the age factor. The energy efficiency of the production lines has improved over the years; therefore, the utilized values can be seen as a "best-case scenario". The modification of these values to reflect the construction period still needs to be studied in depth.

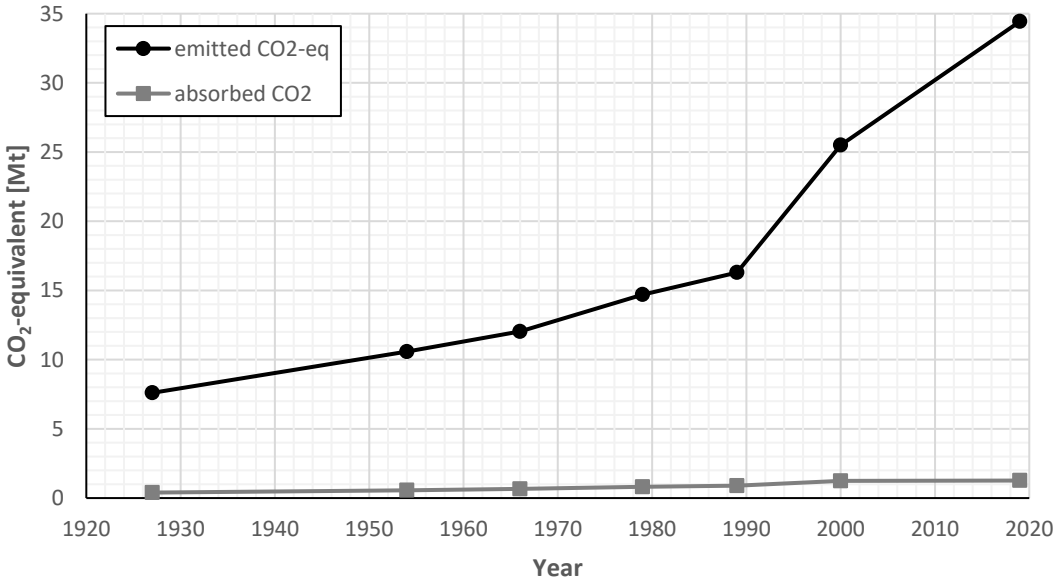

Figure 5-23. Carbonation emissions between 1927 and 2019 in Luxembourg

In terms of carbonation, the front was calculated to be between 5.95 mm and 125 mm for the outer walls and 4.58 mm and 75 mm for the inner walls. In both cases, the carbonation front was limited as half of the element's width. All elements were assumed to be exposed to carbonation on both sides. While this is a simplification, it can be assumed that all elements are in constant contact with the air, even though covering or cladding could hinder the carbonation rate. However, in this

global approach, further assumptions were judged to be unnecessary due to the lack of any base data. The sequestered carbon dioxide represents up to 11% of the initial emitted carbon during the construction of the structures. In average, 5% has been sequestered which translates to 13.6 $kgCO_2$ per m^2 of MCM. The total embedded carbon emissions are calculated to be approximately 34.3 Mt, which, in comparison to the sequestered carbon, it is more than 2700% of difference (Figure 5-23). Therefore, carbonation can potentially capture only a small fraction of the current emissions. However, there are ways to encourage carbon capture by concrete, such as for example to design walls or structures that have a higher surface in contact with the atmosphere. When planning the deconstruction of old structures, the consideration of this embedded impact in parallel to the design of new environmentally friendly buildings is crucial in offsetting the environmental load of our buildings.

5.2.3. Discussion and conclusions

The advantage of using a coupled GIS-LCA methodology are that a geographical collocation of the effects can be assessed as seen on Figure 5-24. Moreover, a database is constructed which shows for each building the assessed data, such as material quantities, age of the structure, produced carbon emissions, sequestered carbon. This database can be further extended with other environmental impact indicators, such as the abiotic depletion potential for non-fossil resources (ADPE), ozone depletion potential (ODP), acidification potential (AP), etc. This data can be accessed when designing the end-of-life stage of a building to assess the best practices to follow for minimizing and offsetting the environmental impact of the structure, but also for larger scale planning, such as design of waste processing facilities, carbon-capturing technologies and biosphere preservation planning.

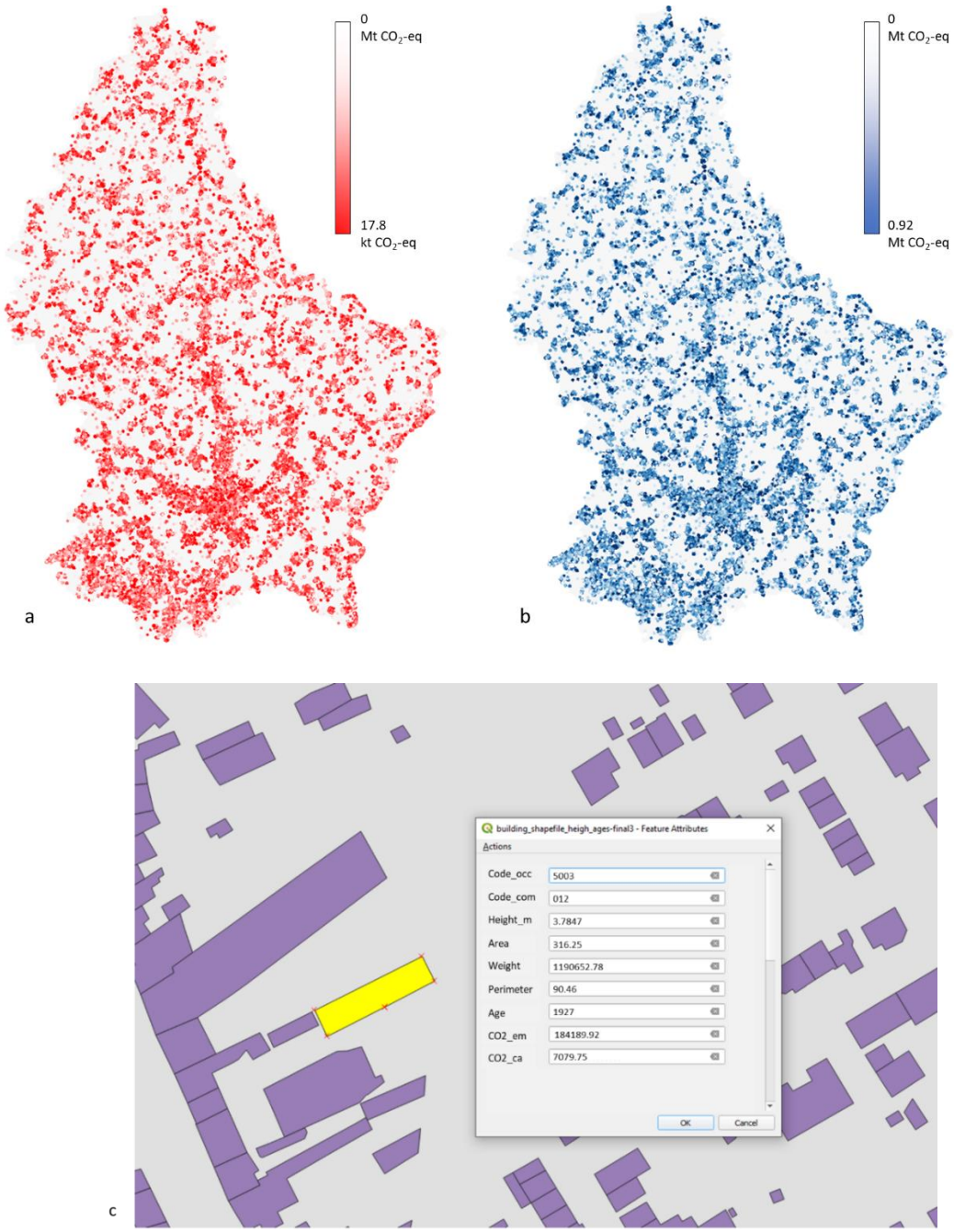

Figure 5-24.

a) Geographical distribution of the embedded carbon emissions in Luxembourg;

b) Geographical distribution of the carbon sequestration in Luxembourg;

c) Example of the proposed GIS database

5.3. Outlook

5.3.1. Quantifying the circular economy potential of mineral construction materials

The previously presented approaches in 5.1 and 5.2 show a significant potential of the proposed methodology which can be extended and further optimized in a database in the form of a digital material cadastre. The principle for this database can be the quantification of the built environment in terms of the built in volumes of construction materials and can be further enriched with further information in a layer-based system (Figure 5-25) which can contain relevant information, such as environmental impacts, cost aspects, energy demands, etc and can serve as a management system for the entire built environment. Such system can be useful to drive the circularity of the built environment, not only in waste treatment and recycling, but also during the service life of the buildings. For example, it can serve as a decision-making approach for policies and refurbishment investments in the built environment and can ultimately turn circular economy from a concept into a tangible and quantifiable process, leading to a global improvement of the environmental impacts of the construction industry. A proposal for a further study regarding the material cadastre is shown in section 5.3.2.

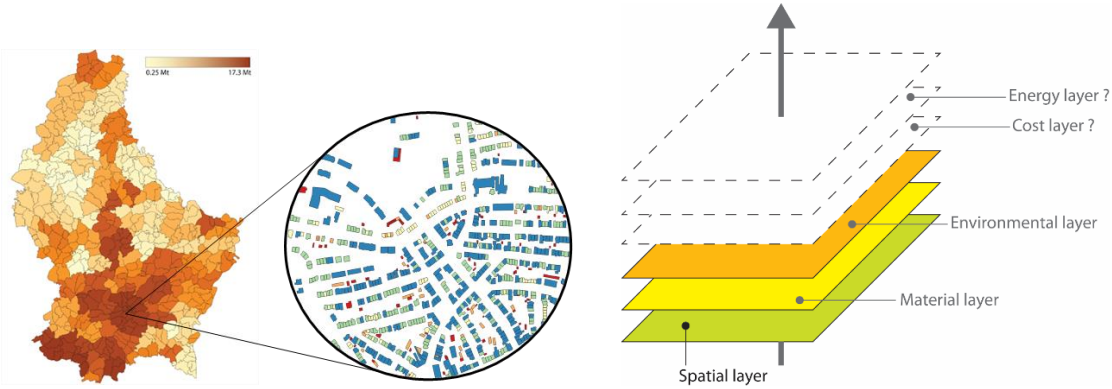

Figure 5-25. Circular economy database

5.3.2. Optimising of construction stock management in a context of circular economy by a multi-layered material cadastre approach

5.3.2.1. Introduction

The construction and demolition (C&D) waste represents the largest waste stream in Europe, accounting for 35% of the overall waste generation. C&D waste includes a wide range of materials such as gravel, sand, concrete, bricks, gypsum, glass, steel, wood, plastic, etc. The common practice of C&D waste disposal in landfills poses a significant impact on the environment such as destruction of valuable land, emits various pollutants, water contamination and consumes raw materials and energy. As a result, applying sustainability principles to the building industry to adopt environmentally friendly construction and waste management methods are a big challenge for years to come. In order to aid in the shift towards sustainable construction, there is need to develop reliable environmental impact assessment framework, which can provide quantified information on the long-term performance of buildings.

5.3.2.2. Objective

This study aims to propose a management tool for the embedded construction stock based on a multi-layered material cadastre approach.

5.3.2.3. Significance

One crucial aspect of the shift towards Circular Economy is the material inventory and database. The proposed tool can be used to accurately estimate type and amount of materials that is built in on a selected geographical area. Having such an accurate data about the material quantities is important not only for the optimal management of C&D waste, but also for strategic planning on the use of construction materials, such as sourcing, transportation and environmental impact. As a

result, this will improve the environmental and economic indicators, which would then lead to accurate, smarter decisions for our society.

In addition, with the developed and integrated database, several achievements can be obtained.

Analysis of the current raw material needs and inventory of the main material streams (concrete, bricks, steel, timber, gypsum, etc), as well as analysing historical trends and having the possibility to make future extrapolations.

By analysing the real-time condition data using GIS, the real condition can be accurately mapped to building and ground in time, then the condition can be visualized in a 3D manner;

The overall coast and environmental performance of buildings can be generated automatically and all the impacts (social, economic, technical, environmental) can be simultaneously analysed;

Strategic waste planning can be realized by conducting an analysis, prediction, and decision with the proposed integrated BIM-GIS web system.

As a layer-based system, the database can be at any time enriched with further relevant information

5.3.2.4. Approach

The proposed approach will integrate Building Information Modelling (BIM) with other approaches such as Geographic Information System (GIS), reality capture and monitoring and artificial intelligence to provide data on two main directions:

- New buildings where Building information modelling (BIM) is available. BIM technology can be used to provide detailed geometric information (e.g., dimensions and positions of building components) and semantic information (e.g., materials and historical maintenance data of building elements) of buildings. Using the information, issues related to information sharing, interoperability, and efficient collaboration throughout the lifecycle of a building (i.e., from feasibility and conceptual design through to demolition and re-cycling stages) can be addressed.
- Existing buildings where a BIM model is not available. In this category, which includes the majority of the structures, extraction models will be used to capture the material quantities. A

combination between image analysis, GIS and machine learning can be used to assign a material profile to a structure and then extract the typical quantities. Afterwards, case studies can be used to test the material profiles in real-life buildings and optimize the models.

The procedures of the proposed system are described as follows:

Stream 1 (New buildings): A building BIM model that is represented in Industry Foundation Classes (IFC) file, which is the standard file format among BIM applications, is built first. The collected data is stored in an external MYSQL database that uses Structural Query Language (SQL). A web-based user interface is developed using PHP scripts to access the database from the web server.

Stream 2 (Existing buildings): For the existing stock, a building inventory is done first by using open-source cadastral data. Building typologies are identified through remote sensing techniques (such as machine learning). Building ages are assigned to the existing stock, either from cadastral data or from extraction methodologies such as image analysis. A material intensity profile is added to each building typology depending on its geometry and age. Case studies are used to optimize the data model. The information is stored in a GIS environment and fed through the common MYSQL database to the common web server.

The process is illustrated as Figure 5-26.

5.3.2.5. Application

The proposed C&D waste estimation method is demonstrated on a pilot project of the country of Luxembourg or the Greater Region. Simulations and estimations can be made to assess the environmental impact of the built environment and each material flow. This tool can be a databank for decision-making in terms of the circularity of construction materials. It can offer data for environmental, economic, feasibility and technical studies on waste management, but also for the sustainable use of raw construction materials in the future.

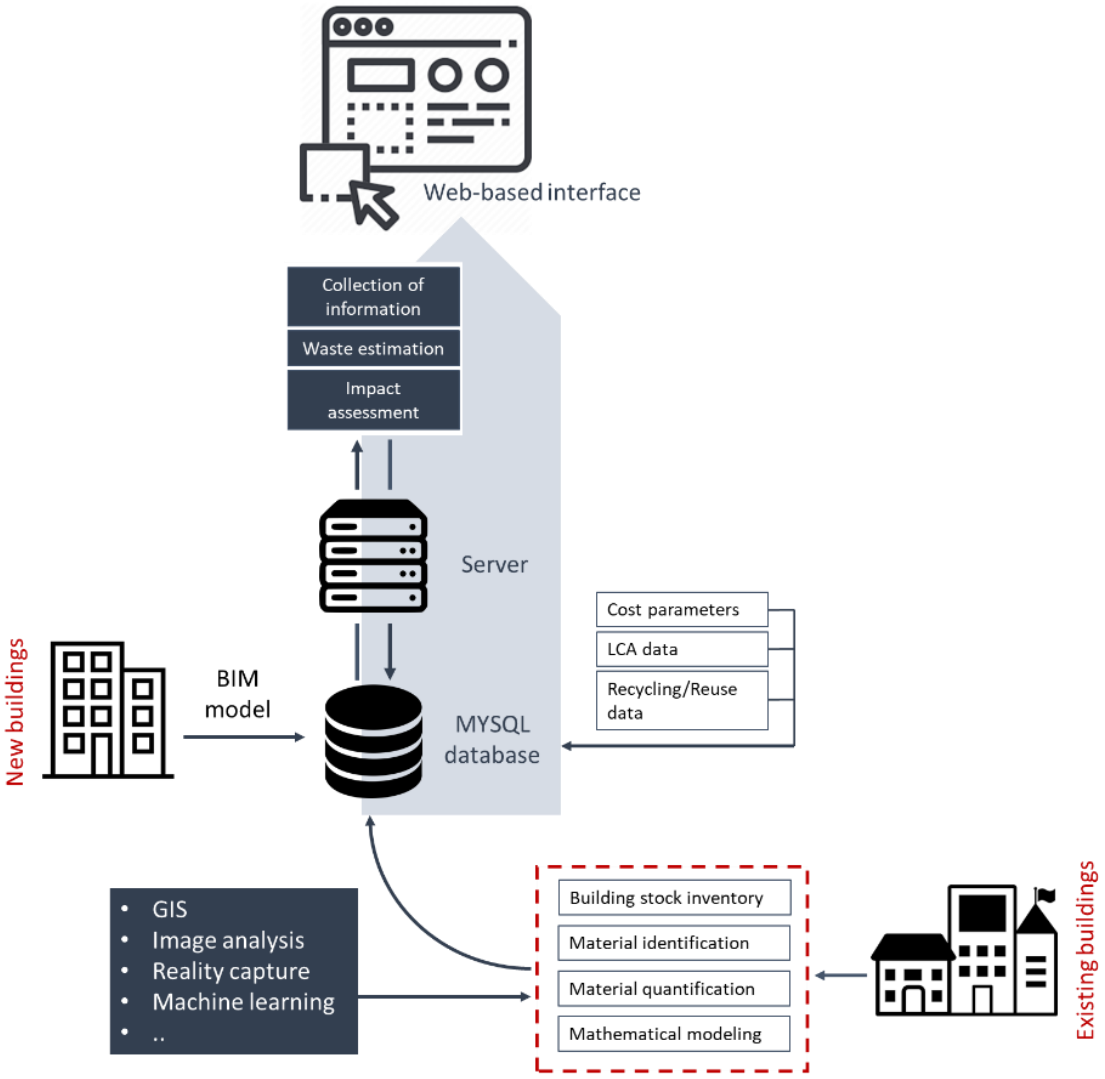

Figure 5-26. Development of BIM-GIS web system for waste estimation and environmental impact evaluation

Chapter 6 | Deconstruction

6.1. Certification process as an aid to selective demolition

6.1.1. Introduction and methodology

Selective demolition is a process that ensures material stock separation and prepares the waste for appropriate re-use of each material stream. However, this process requires also additional work and resources, both in human and technological aspects. Generally, a selective demolition is more expensive and takes more time than a traditional one. According to Coelho and de Brito [265] on a case study based in Portugal, the costs of selective demolition are estimated to be 5818 euros per 100 m^2, while traditional demolition would cost 13% less. The costs of selective demolition are significantly more levelled, as they depend on many factors, such as equipment, transportation, labour costs, etc, while traditional demolition has a high sensitivity related to transportation costs, as other aspects are less predominant. The study also concludes that, for the case of Lisbon, landfill fees need to have an increase of 150% for selective demolition to be economically effective. This is expected to have a considerable influence based on the geographical location. For example, in Luxembourg the processing sites charge different prices for separated and non-separated waste. Recyma S.A., charges 3.90 euros/ton for the acceptance of non-sorted inert waste and 1.24 euros/ton for sorted waste. [266] This considerable difference incentivizes demolition companies to deliver separated waste. Nevertheless, there are no regulations on the re-use of materials on construction sites. A demolition company can choose to re-use the waste fractions on site, which is a common case for Luxembourg. These practices have a considerable environmental impact, as in the case of recycled aggregates, they are mostly used as backfilling layers, resulting in downcycling of secondary materials.

A further way to aid selective demolition with the scope of maximising re-use and recycle of waste fraction is to include a certification process. Environmental certificates are currently a common practice for new constructions. The two major certifications are BREEAM and LEED, with the latter mostly active in the US and Asia. These certificates have a similar working principle based on credits. Through certified experts, different aspects of the building, such as energy, health and wellbeing, innovation, land use, materials, pollution, etc are assessed through a rating system. A weighted combination of all these aspects, gives the building a final evaluation from one to five stars. In these certificates, the demolition process is not included. While material recovery is considered for CDW, a definitive description on the principles of re-use is still missing. A further local certification would allow several benefits to the construction sector and general public. First, a certification can be a mean of standardization to a certain extent. If industrial projects are encouraged to follow such procedures, the needed targets can be implemented in the certification. For instance, if the goal is to standardize the material quantification methods in Luxembourg, the preferred methodology is employed in the certificate. In this way, the projects that have gained the necessary credits from the certificate are certain to have followed the correct procedure. Through public administrations, it can be directly or indirectly enforced. By having a certification process that includes a material recovery inventory, a material stock quantification can be easily obtained and suitable planning on processing plants can be done. Furthermore, it would allow a better control of the waste streams in terms of re-use potential, but also in mitigating risk for hazardous substances. Finally, it can be used to substantially close the economical gap between selective and traditional demolition.

Such procedures can be found in literature and in this case, the procedure proposed by Guy and Williams [267] is discussed. This approach is chosen for its high adaptability and wide coverage of all issues relating to the demolition. Furthermore, it is clear and practical to use. For the specific case of Luxembourg, modifications and adaptions need to be made in order for this method to be fully functional in the country. In this first presentation, general assumptions are made, which will be further optimized through case studies.

This certification method is credit-based and has three fundamental categories: building, planning and environmental, health and safety. Each of these categories is divided into further fractions which describe the specific processes. In total, there are 50 credits to be awarded and each project needs at least half of the score to be certified. This feature is interesting and differs

from the environmental certifications described above, as it does not award levels or grades, making this certification non-commercial. Ideally, the minimal requirements of the certification are aligned with the environmental goals of the country and through its enforcement in the market, a desired target can be achieved. For example, if a recycling target is set for construction materials, the minimum score of the certificate can be adapted to it and this would create the desired actions in the private industrial sector.

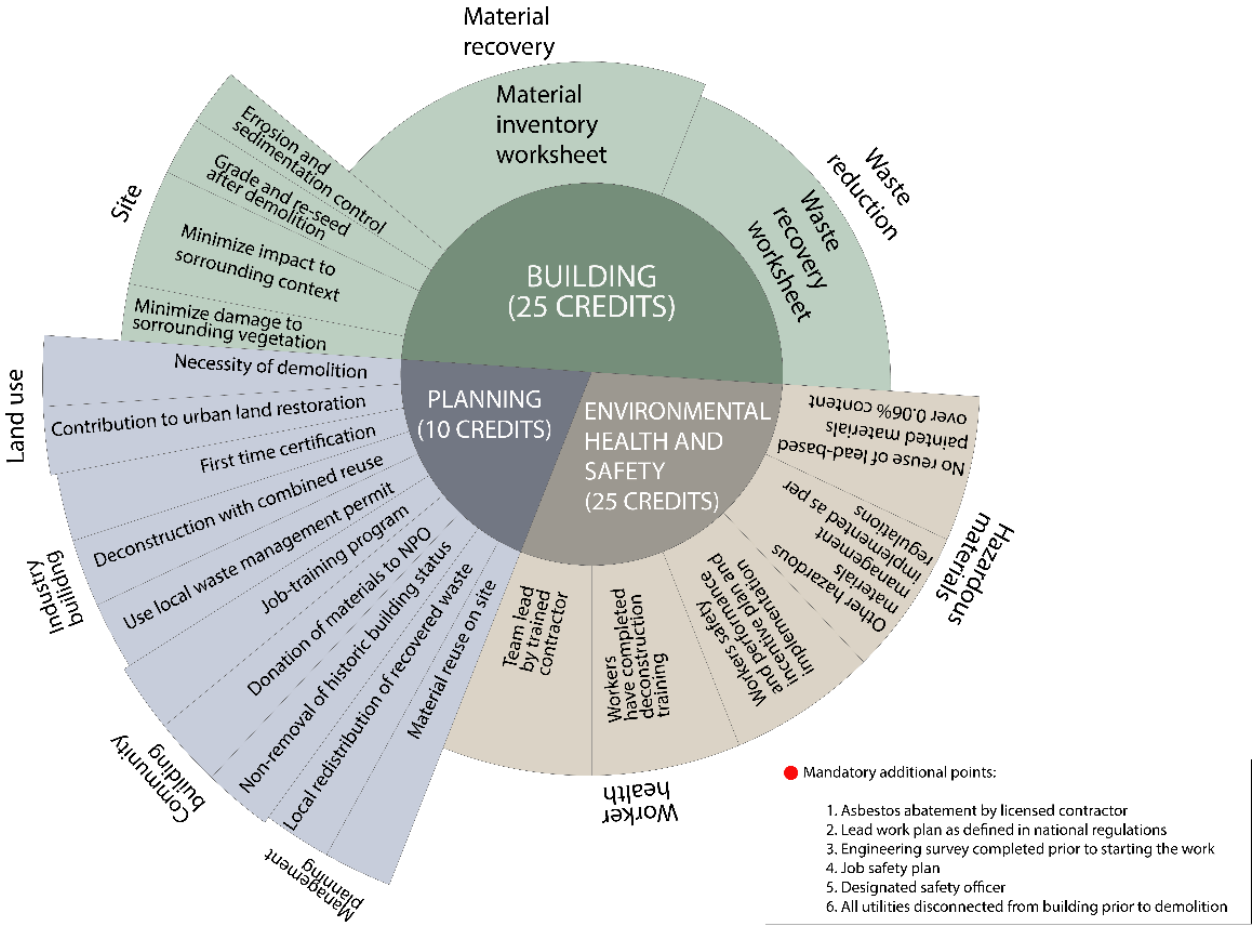

Figure 6-1. Demolition certification (adapted from Guy and Williams [267]*)*

The principal working methodology of this certification is shown in Figure 6-1. The major amount of credits can be achieved through the "building" category, which is divided into three subsets: material recovery (10 credits), waste reduction (10 credits) and site (5 credits divided into 4 different aspects). To achieve the credits for "material recovery", an inventory of all the material amounts from the demolition is required to be completed. This step represents a crucial point, as having this information on a database would be important in regulating the re-use and recycling afterwards. It would represent the most exact for of material flow quantification that can be done

in the construction sector. For this purpose, the authors also propose a format for this worksheet. However, in Luxembourg, there is already an existing official document that can be used for this purpose. The Excel sheet (seen in Figure 6-2) lists all the construction materials present in residential and commercial buildings and is required to be completed with descriptions and quantities.

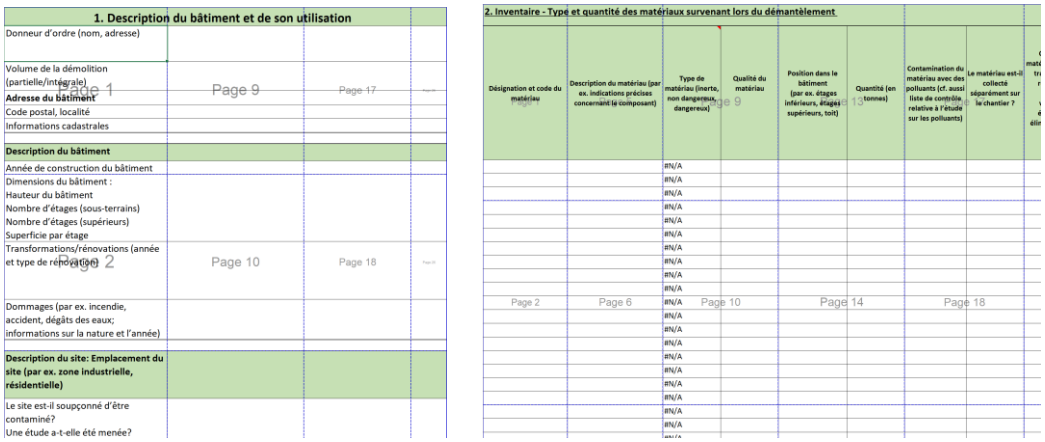

1. Description du bâtiment et de son utilisation	
Donneur d'ordre (nom, adresse)	
Volume de la démolition (partielle/intégrale)	
Adresse du bâtiment	
Code postal, localité	
Informations cadastrales	
Description du bâtiment	
Année de construction du bâtiment	
Dimensions du bâtiment : Hauteur du bâtiment Nombre d'étages (sous-terrains) Nombre d'étages (supérieurs) Superficie par étage	
Transformations/rénovations (année et type de rénovation)	
Dommages (par ex. incendie, accident, dégâts des eaux; informations sur la nature et l'année)	
Description du site: Emplacement du site (par ex. zone industrielle, résidentielle)	
Le site est-il soupçonné d'être contaminé? Une étude a-t-elle été menée?	

2. Inventaire - Type et quantité des matériaux survenant lors du démantèlement							
Désignation et code du matériau	Description du matériau (par ex. indications précises concernant la composant)	Type de matériau (inerte, non dangereux, dangereux)	Qualité du matériau	Position dans le bâtiment (par ex. étages inférieurs, étages supérieurs, toit)	Quantité (en tonnes)	Contamination du matériau avec des polluants (cf. aussi liste de contrôle relative à l'étude sur les polluants)	Le matériau est-il collecté séparément sur le chantier ?
		#N/A					
		#N/A					
		#N/A					
		#N/A					
		#N/A					
		#N/A					
		#N/A					
		#N/A					
		#N/A					
		#N/A					
		#N/A					
		#N/A					
		#N/A					
		#N/A					
		#N/A					
		#N/A					
		#N/A					
		#N/A					
		#N/A					

Figure 6-2. Extract from the worksheet of the construction waste inventory, Luxembourg (https://environnement.public.lu/fr/offall-ressourcen/types-de-dechets/dechets-construction-demolition-dcd/inventaire-dechets-construction.html)

On the "waste reduction" subset, the credits are achieved through filing another worksheet that contains information on the recovery of waste. More specifically, credits are awarded in a merit-based system, depending on the volume amount and the recovery ratio. The higher the recovery ratio, the more credits are awarded. In terms of volume, with smaller volumes, a higher recycling ratio is needed. There is also a base limit, which denotes the minimum possible re-use ratio. This limit can be set depending on the country's goals. Concerning Luxembourg specifically, the current legislation [268] demands a recovery of 70% of the material by mass. Therefore, the lower limit in material recovery, is represented by this specific amount. The building volume should be calculated as the volume of the envelope, therefore:

$$V_{building} = A_{gross} \cdot h_p^* \tag{6-1}$$

Where h_p^* is the height of the peak point of the building

The reason why the highest point is proposed and not the real volume of the building, is purely as a facilitating method to lower the operational costs of such procedure. In Luxembourg, five different height classes are proposed, based on the available volumes in the country. While more results are attained in workpackage 3 of this project, a clearer idea will be possible on the most efficient way of determining these classes. The credit allocation can be seen on Table 6-1.

Table 6-1. Proposed waste reduction sheet (the number in each box represent the credits)

Volume in m^3	>2700	P	8	10	10	10	10	10
	1100 - 2700	P	6	8	10	10	10	10
	700 - 1100	P	4	6	8	10	10	10
	270 - 700	P	2	4	6	8	10	10
	<270	P	1	2	4	6	8	10
		61-70 %	71-75 %	76-80 %	81-85 %	86-90 %	91-95 %	96-100 %
		Recovery rate in weight (%)						

The second category in terms of importance is “Environmental health and safety” which gives credits related to worker health, hazardous materials and job safety. Several of these sub-categories do not award credits, but are perquisite to achieving the certificate. Such categories are mostly related to safety of workers and hazardous materials. The “planning” category can give the project up to 10 credits and is related to land use, industry building, community building and planning of materials management.

The project approach to such certification will be based on case-studies of typical demolition projects in Luxembourg. These case studies will give a retro-active overview on the effectiveness of such methodology and will hint at possible country-related adaptions which can be specific for Luxembourg.

6.1.2. Results

6.1.2.1. Case study 1: Sports hall of the primary school in rue « Leon Kauffman » in Cents

The considered demolition case-study was proposed in light of workpackage 2 by the company Eneco, which partially worked in the process. The demolition project ran between 2014 and 2016 and constituted of the full dismantling of the structure.

Overview of the building

a. Situation

Cents is located on the eastern part of Luxembourg city on an area of approximately 4 km^2. It is a typical residential area with a population of 6316 (end of 2018). The primary school in itself is composed of a main building and the sporting facilities (playgrounds, gym and pool).

Figure 6-3. Situation of Cents (shown in red) and the plot of the building in 2013 and 2016

b. Age and usage

According to the building plans, the finalized design dates back to 1984. The final construction date is not known, but it can be expected that it was constructed immediately after, between 1985 and 1988. The complex is composed of three main volumes: Building A, Building B and the sports hall. The latter (depicted in green in Figure 6-4) is the demolished volume. In the original sketches, there appears to have been also a connecting structure between the sports hall and buildings A and B. These structure does not appear in recent records and it is likely that is was either never built (excluded from the project), or demolished in a previous effort.

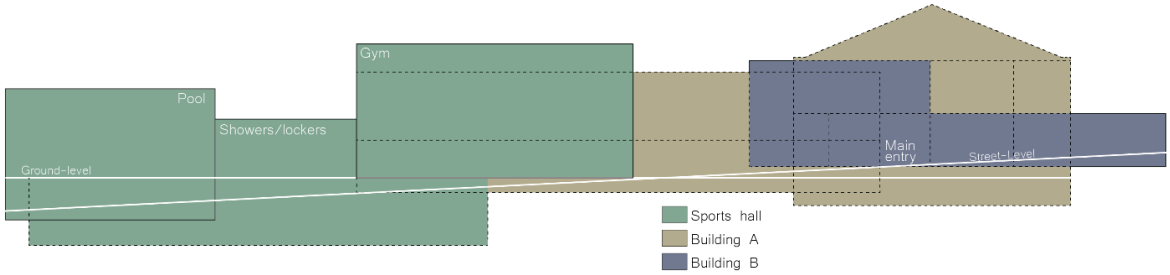

Figure 6-4. Volumetric composition of the structure, adapted from the original project (Source: Ville de Luxembourg - Direction de l'Architecte - Service Bâtiments)

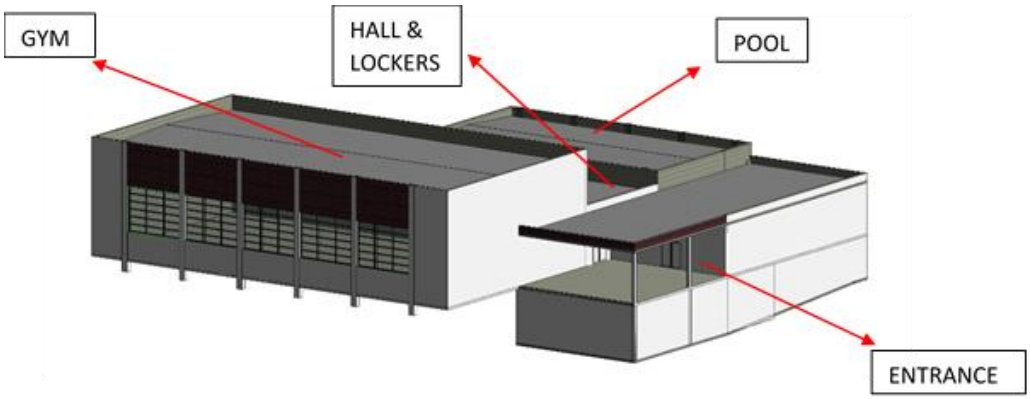

Figure 6-5. Functional composition of the building

The functional composition of the demolished building can be seen on Figure 6-5. It was made up of four different volumes: the gym, the pool, the hallway, the lockers and the entrance. The gym area is in one level only, with an elevation of 7.55 meters to the ceiling. The other volumes are at a consistent height of 4.00 meters, but have also an underground level which served as service area. The underground has different elevations of -4.50 meters (at the lockers) and -3.75 meters (at the pool area).

c. Structural system and material composition

The structural system of the building is based on columns and walls as bearing systems. The entire structure is precast and assembled on site, therefore, concrete is the major construction material. Few bricks can be seen on the façade as an architectural element. The pool basin is also reinforced concrete and that can be deduced by the structural support system made of rectangular columns in the basement.

The gross volume of the entire structure is 9854.635 m^3, which makes it a large structure based on the previously discussed classification. The volume of concrete according to a Revit model based on the original building plans is approximately 23672.065 m^3. Considering the density of concrete to be 2100 kg/m^3 (without taking into account the reinforcement), the total quantity of concrete in the building can be estimated to have been 49 557.33 tonnes. The considered volume is quite large for the Luxembourgish stock, therefore the demolition project can be considered a significant one in the country.

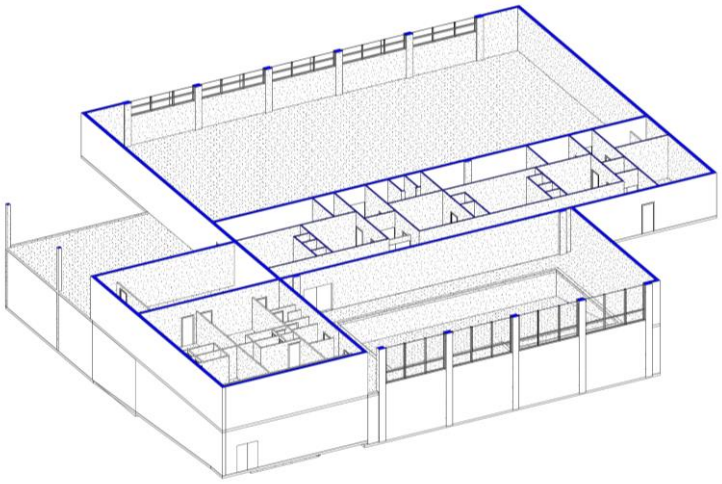

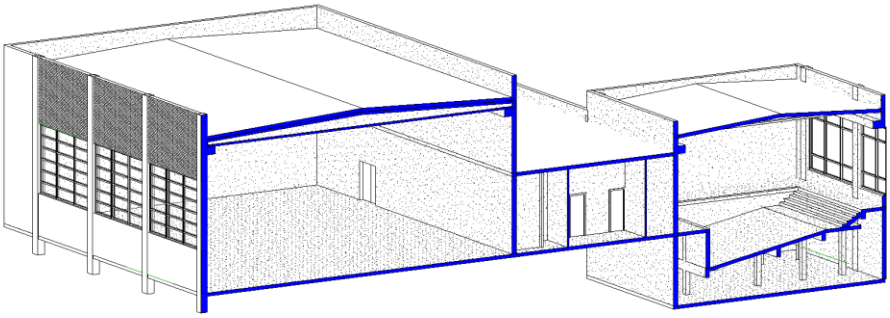

Figure 6-6. Section cuts of the structure

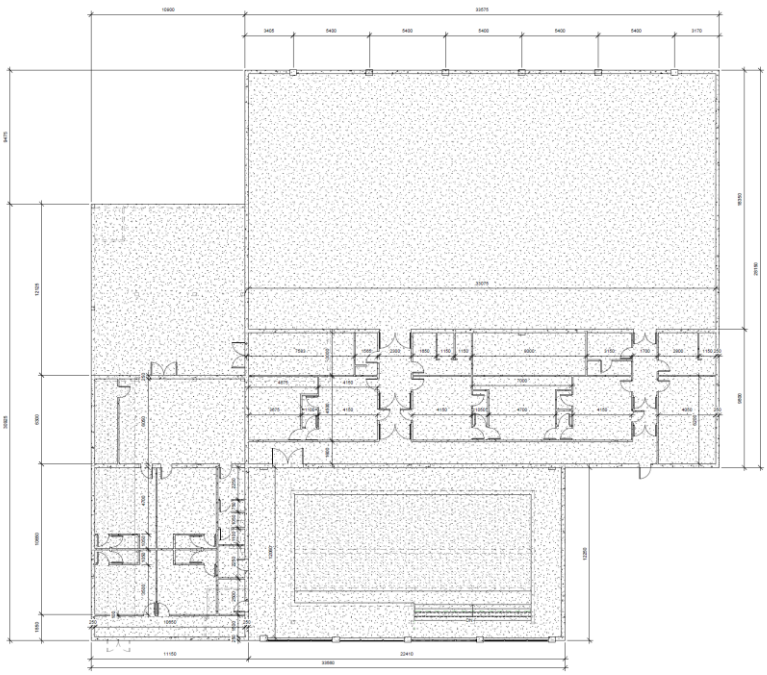

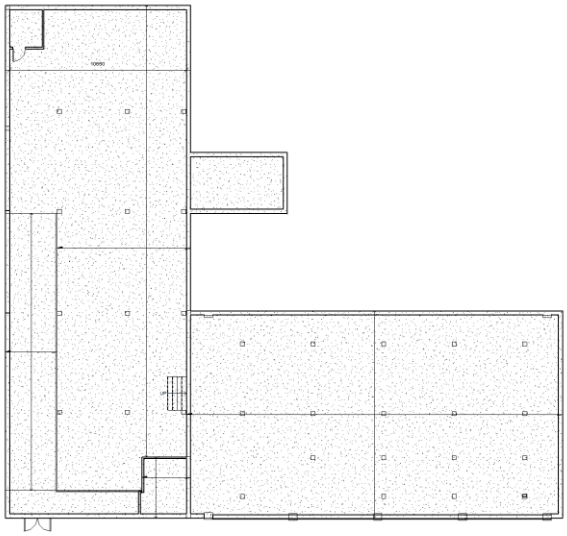

Figure 6-7. Plans of the ground level and the underground area

d. Demolition

The deconstruction of the building was partially done by the company ENECO. The main reason for the deconstruction was the presence of asbestos in the insulation of the structure.

First, all the installations such as gas pipes, water and electric lines were cut off, ensuring that no water, gas or electrical charge was present at the time of the dismantling. This ensures the safety of workers inside and is the core preparatory work. A standardized scaffolding system was set up for the workers to have access.

Figure 6-8. Deconstruction of the installations (courtesy of ENECO)

Afterwards the disassemble of the water, electrical and heating system was done. The materials were not separately sorted, but were sent to a waste site according to the Luxembourgish regulations. The further use of these materials is unknown. A similar procedure was followed for doors and windows. Following, the wall and floor covering was removed. The majority of walls were covered with painted chipboards. In the swimming hall, laminated sheets and wooden boards in the entrance hall. The floors were covered in laminated sheets. The outer walls had waterproofing and insulation with asbestos-cement plates which were removed consequently. Finally, the concrete structure was demolished by a demolition company. No information is present about the further handling of the resulting construction and demolition waste. Considering the current situation in Luxembourg, it is likely that this material is sent to a landfill to be crushed and reused for roadbase filling.

Figure 6-9. Demolition of the structure (courtesy of ENECO)

e. Certification

On Table 6-2, the described demolition is credited through the previously described methodology, taking into account the specifities of the project. The project as it was conducted would be awarded 26 credits and consequently the certification. However, there is an undeniable issue in the material recovery. As the recovery and further reuse of the waste is unrecorded. Volumes as well are unrecorded.

Table 6-2. Certification scores

Building	**Credits**
Site	

Minimize damage to surrounding vegetation or recover plants and protect heritage trees	1
Grade and re-seed site after demolition	1
Erosion and sedimentation control plan	1
Minimize impact on the surrounding context	2
Material recovery	
Use material inventory worksheet	0
Waste reduction	
Use waste recovery worksheet	0
Total credits for category	5
Planning	
Land use	
Necessity of demolition	1
Contribute to land restoration	1
Industry building	
First time certification	0
Deconstruction with combined reuse	0
Makes use of local regulatory waste management permit	1
Community building	
Job-training program	0
Donation of materials to non-profit organisations	0
Not removal from National Register of Historic Places	1
Material management plan	
Local redistribution of recovered materials	1
Material reuse on site	1
Total credits for category	6
Environmental health and safety	
Worker health	
Team led by certified demolition contractor	3
Workers have completed "green" demolition training	3
Workers safety and performance incentive plans and implementation	3
Hazardous materials	
Asbestos abatement by licensed contractor	P
Lead work plan as defined in national regulations	P

No reuse of lead-based painted materials over 0.06% content	3
Other hazardous materials management implemented as per regulations	3
Job safety	
Engineering survey completed prior to start of work	P
Job safety plan prepared and communicated to all workers	P
Designated safety officer for the project	P
All utilities disconnected from building prior to work	P
Total credits for category	15
Final score	26

Chapter 7 | Conclusion

7.1. Summary and discussion

The main aim of the research project is to investigate the circularity of concrete as a construction material and facilitate the transition towards circular economy in the construction sector. The main focus of the research is concrete recycling as one method of reusing construction waste in a sustainable way. Recycling of concrete can result in a saving of up to 8.71% in global warming potential, 18.42% in photochemical oxidation potential and 16.93% in abiotic depletion potential of fossil fuels and can be beneficial in saving landfill space, as well as offering an alternative source of resources for geographically limited areas. The inherent disciplinary nature of the topic creates two parallel but complementary approaches towards circularity, a technical approach and a global approach.

In this chapter, the main findings of the thesis are summarized. It is an initial aim of the research approach to not limit the investigation spectra into one specific area, but to treat the problem within its interdisciplinary nature with the goal of creating a valuable contribution for the scientific world, as well as the industry.

The mechanical properties of recycled concrete are studied using locally sourced recycled aggregates. The recycled aggregates show up to 13 times higher water absorption compared to natural aggregates and a 10% lower density in average. The compressive and tensile strength are also influenced, showing a decrease of up to 74% in comparison to the reference. When high quality recycle aggregates are used, the strength loss is less evident. By using aggregates from known sources, the total strength loss is limited to 25%, even for a full substitution. This shows the importance of the quality of the material and, more specifically, the necessity for applying a appropriate CDW treatment, but also shows the high variability of the quality of the material depending on the source. For example, the values of water absorption and bulk density of the

material have a significantly large spread from the existing literature as shown in Table 2-3 illustrate the necessity of having local data as a background for building up qualitative concrete mixtures. To tackle sustainability in the built environment we need not only to use sustainable materials, but also to build for resilience [269]. A building that lasts longer is inherently more sustainable, but, on the other hand, more importance needs to be given to the design of construction materials. This translates in deeper understanding of the material behavior and its parameters and the ability to predict the quality parameters of the construction materials. Creating models to simulate the structure of the mixture of concrete would give the immense flexibility of designing with smaller volumes, higher quality and increased resilience. Therefore, a significant focus of the present thesis is on the characterization of the underlying failure mechanisms of recycled concrete and on building a basis for complex modelling of the material.

One of the most dominant aspects of recycled aggregates, is the adhered mortar paste, which is responsible for the loss of mechanical quality of the concrete, more specifically due to a weaker interfacial bond. In this aspect, the interface is studied through a combination of experimental and numerical approaches. A large-scale experimental program is carried on through slanted shear tests to quantify the failure parameters of the interfacial contact area between recycled aggregates and new concrete matrix. It is shown that recycled aggregate concrete displays an internal friction coefficient between 0.69 and 0.88 and a cohesion value between 0.13 and 4.60 MPa, depending on the substitution rate. Partial substitution of recycled concrete show a slight increase in interfacial strength due to the non-hydrated cement particles remaining from the mother concrete. This benefit is, however, completely lost in full substitution. Scanning electron microscopy show an intrinsic microcrack network developing in the case of a full substitution, which counteracts the benefits of the hydrated cement. Therefore, it can be concluded that substitution rates of up to 50% in volume are advisable, both in technical terms as well as economical. Furthermore, a numerical model is constructed using the phase field method, to stimulate the fracture properties of recycled aggregate, based on the observed experimental results. The model allows an accurate prediction of the crack path, as well as crack initiation and propagation depending on an applied compressive load. Furthermore, the model allows for an automatic generation of aggregate geometry as well as for application of partial interfacial zone.

In terms of the global aspect, it is demonstrated that the end-of-life (EOL) phase is crucial in terms of the circular approach. The demolition phase as the first stage of the EOL needs to have a

better understanding and a better regulation in general. Categorically, it is necessary to create the right legislative approach in the regulation of deconstruction activities and more incentives need to be provided for the recording of the data. A certification process is proposed, which follows similar approaches as the most common sustainability certifications, such as BREEAM and LEED. It is shown in one case study that the collection of data regarding the volume of waste is the critical aspect of the certification process.

Finally, the thesis addresses the question of critical masses and whether the use of recycled aggregates is feasible in terms of CDW generation, especially for geographically limited areas. To assess the potential amount of CDW in the country of Luxembourg, an approach based on a combination of geospatial and image analysis is performed. This allows for a direct, digital, open-source modelling of the material flows in the country. Through this a database is built up containing volumetric information for mineral construction material for each building in the country. Furthermore, by using an image analysis from old topographic cartography spanning from 1927, it is possible to estimate the demolition trend of the buildings in the country. The total built in mineral material stock in Luxembourg is estimated to be 276.75 Mt and records a growth of up to 24.39% in the last 30 years. Based on stochastic predictions, the generated CDW weight can be up to 226.29 Mt by the year of 2100. It is estimated that the expected volumes of CDW give the opportunity and the feasibility to create a feasible economic activity in terms of concrete recycling if the production of recycled aggregates is well managed locally. This approach has significant potential to serve as a starting base for a material cadastre in the country and for a management system of not only CDW, but also the built-in environment in general. It has the potential to serve as a decision-making tool for a global sustainability management system, which can be customised and enriched with further information in the form of different layers. An example is show with the incorporation of LCA into the already existing model to create another layer into the database and allow for the estimation of the embedded carbon missions in the mineral construction stock. It is shown that the total embedded carbon equivalent is 34.38 Mt and an average of 5% is captured by the carbonation of concrete.

Finally, it can be stated that recycling of concrete is an attractive option, first and foremost in terms of the sustainable shift of our economy. It shows significant potential for high-end uses and also potential economic benefits if a correct management is applied. Therefore, it is imperative to take all the necessary steps and create a synergy between the research, the industry, private and

public stakeholders to ensure that our short-term sustainable goals are met and that we create a better, cleaner and safer world.

7.2. Outlook

The present thesis shows that recycled concrete can be a feasible option for utilization in the building industry. In outlook, a more complete characterization may be achieved by studying the durability of the material. Properties such as freeze-thaw resistance, acid penetration resistance, performance in contacts with salts and other saline and alkaline agents, as well as carbonation are still only partially studied for recycled aggregate concrete. Additionally, product-specific criteria may be investigated and a roadmap can be constructed with applications where recycled concrete is ready-for-market and applications where is not-recommended for use. This roadmap may guide the industry to a better application of the material.

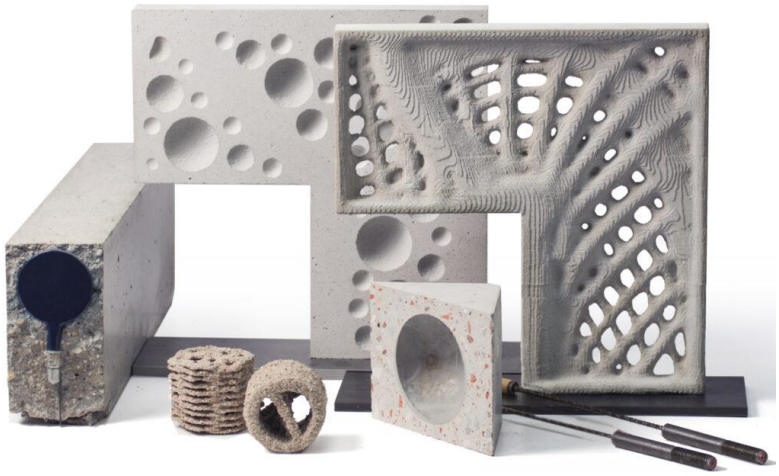

Figure 7-1. Gradient concrete and parametric design (courtesy of Werner Sobek)

Recycled concrete has the potential to play a key role in the upcoming trends of the construction industry. For example, it is promising to investigate the possibility of using recycled concrete in 3D printing applications, or in parametric approaches that aim to minimize the material volume used, such as the gradient concrete (Figure 7-1). The utilization of recycled concrete in applications as gradient concrete has the potential to yield a very sustainable concrete as it combines the optimization of concrete volume and a sustainable material such as recycled concrete. Likewise, an investigation on the use of recycled concrete in timber-concrete composite elements can result

in highly sustainable structures, which benefit from the use of timber as well as re-use of concrete. For all these applications, building up on the numerical models, similar to the phase-field model shown in this thesis is crucial. Intrinsic and complex models can allow for a better prediction of the failure mechanisms of recycled concrete and can help in adapting mixtures at a complexity that the current tools are incapable of performing. More realistic approaches, such as CT-scanning of specimen can allow for a better simulation of the lab conditions and the current model would greatly benefit both from a more complex reference model and also from a larger databank of lab-results. Ultimately, the model must be complex enough to be able to predict the end-quality of a concrete by a limited set of input.

Figure 7-2. 3D printing of concrete (Courtesy of Peri)

In the global aspect, more work needs to be done in the integration of data. At the moment, the state-of-the-art shows that the information regarding buildings is highly fragmented. Approaches such as shown on chapter 5 are limited and can be fed with real data from the construction industry to build a database containing the information needed for the management of the built environment. In this regard, one key player in the market is Madaster [270]. They offer an online database where building information such as materials, volumes, embodied carbon and much more can be stored and accessed in form of a material cadaster and accessed any time. It is designed to act as a facilitator of circular economy by offering life-time monitoring of the asset. Similar approaches are investigated by several other players in the construction market. Even though such ideas are regarded as success stories, there are two main drawbacks from these systems. First, the service is premium, and a fee is charged per each project to be featured in the database and,

secondly, the rising concern of data privacy and data ownership. In the ideal situation, the material cadaster should be public in the same way that a land cadaster dataset is public. This would be advantageous for public authorities to create the correct policies and to drive the circular economy further. Having private data on a selected few cases has clear limits in driving a system as a whole. In this thesis it is shown how the basis of such public, open-source system could look like. To create a functioning database, follow-up investigations need to be made. The data must be affined, including the addition of further materials and creating clear interfaces on how information can flow not only within the same system but also in interaction with other systems, similarly to what the industry foundation classes (IFC) do for BIM. Additionally, a functioning mechanism needs to be built to allow for the entry of new buildings in the system. The easiest way to achieve this is to feed the system data from digital models of buildings. This would entail that a clear standardization needs to be set in place to allow for the necessary resolution of digital models. A sample idea on how the system would work is previously presented in Section 5.3.

Lastly, it is clear that sustainability in the construction sector needs to be driven by a systematic approach and can never be complete just by addressing one material. It is imperative to use the tools available to reach the goals in the very near future and create a interdisciplinary integration of data that would allow for more control, more adaption and even more innovation.

Annex A

The Interreg SeRaMCo project

Overview of the SeRaMCo project

The SeRaMCo project (Secondary Raw Materials for Concrete precast products) is an Interregional effort aiming to increase the use of secondary raw materials in the precast industry. It is a three-year project, which started in 2017 and has a wide participation from regional universities (Uni Kaiserslaturen, Uni Liege, Uni Luxembourg, Uni Lorraine, TU Delft), several industrial companies (Prefer, Beton Betz, Tradecolwall, Contern), as well as public authorities from every country. The main goal of the project is to offer high quality substitution for primary raw materials in concrete and cement production. More specifically, a total (100%) substitution is aimed for concrete precast products (CPP).

The project's outcomes will be studied through different aspects, such as treatment process, concrete mixtures, cement formulations and several ideas for innovative concrete elements will be studied. One important outcome of the project is to produce several precast elements which will be installed in the city of Serraing (Belgium), Saarlouis (Germany) and the region of Moselle (France). These elements will be part of recreational parks and will be an excellent opportunity to showcase the importance of secondary raw materials in a broader public, aiming to increase awareness and also demonstrate their utility in the construction industry.

The benefit of the prefabrication industry from this project can be substantial, as it is still a highly controlled production and the introduction of recycled material can be done in a non-

invasive way for the efficiency of the production. Adding to that, the basis of the project is to go along the general European guidelines for sustainability and circular economy, therefore, working on prefabricated elements makes it easier to implement other aspects of sustainable production, such as modularity, selective demolition and reusability.

The collaboration with industrial partners is a very important aspect of the project, as it will assure the developed models are within all the standard requirement of the industry and have marketable characteristics, making them ready for a break-in into the construction industry.

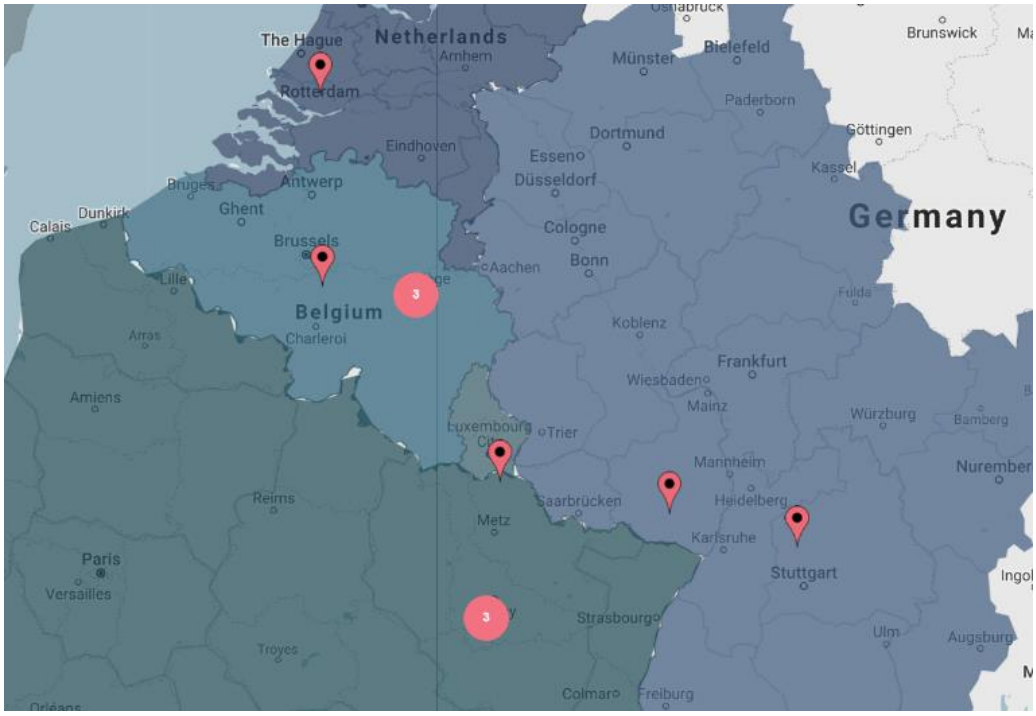

Figure A-0-1 SeRaMCo partners

Publication IV – SeRaMCo – Development of new concrete mixes from recycled aggregates from known resources (Waldmann, Bogoviku, Chewe Ngapeya)

Abstract

Within the project SeRaMCo a new approach combining numerical and experimental investigations has been proposed for designing and improving the formulation of recycled concrete. In a first approach, a set of numerical models using the phase field method was developed

and implemented for studying the earlier age behaviour, the micro cracking ignition and growing, the fracture behaviour and the overall load-deformation response of recycled concrete. The developed models enable to gain in-depth insights into the specific behaviour of recycled concrete, which has then been used for developing a high strength concrete (HSC) and an open structure concrete (OSC) using 100% of recycled aggregates. Different fractions of the initial recycled aggregate blend were combined for defining the required particle size distribution for the HSC and the OSC. The compression, splitting and flexural strength were then determined, as well as the E-modulus. The HSC and the OSC presented a compressive strength of 58.5 and 5.7 MPa respectively. The HSC also exhibits a higher E-Modulus, density, splitting and flexural strength than the OSC, thanks to better cement hydration and a uniform grain size distribution.

Keywords : Recycled Concrete, Phase Field Modelling, Open Structure Concrete, High Strength Concrete

Introduction

With recent advances in numerical simulation methods, new studies are now possible, allowing the development of computational models to predict the mechanical performance of concrete made of recycled aggregates [271]–[274]. In this study, a set of numerical models in the framework of the phase field method [142], [275], was developed to evaluate the fracture resistance, and also to get the in-depth insight the early-age behaviour of recycled concrete. The phase field model (PFM) makes use of a regularized description of discontinuities through an additional variable and strongly alleviates meshing problems for describing brittle cracking [276]. Furthermore, the PFM can effectively handle the phenomena of crack nucleation, interaction and arbitrary crack morphologies. The technique has proven to be very well suited to the simulation of microcracking in complex heterogeneous materials, such as cement-based materials [142], [277]–[279]. Recycled aggregates exhibit specific features like a high porosity and water absorption, a high Los Angeles coefficient and a low apparent density generated by the pieces of hardened cement paste bonded on the initial natural aggregates [280], [281]. These features induce a large shrinkage and a reduction of the mechanical properties of recycled concrete, which ultimately restrains its

application in constructions. Numerous investigations [55], [175], [282]–[287] show that the properties of recycled concrete are governed by factors like the amount of recycled aggregates, the water to binder ratio and the amount of hardened mortar paste on the recycled aggregates. Using experimental and numerical approaches, this research work is devoted to analysing the performance of recycled concrete.

Numerical approach

Phase field model has been proven to be a useful tool to study the fracture behaviours in heterogeneous materials. This method is able to model complex, multiple crack fronts, and branching in both 2D/3D without ad-hoc numerical treatments. During SeRaMCo project, a set of numerical models based on phase field method has been developed to evaluate the mechanical performance and durability of recycled concrete. These models allowed to gain a deep inside into the mechanical behaviour of recycled concrete and were used to better understand the load-deformation behaviour registered during the experimental tests performed on the developed mixes which will be presented in the section 12.2.2.

Early age behaviour of recycled concrete

The recycled concretes are known to be sensitive to early age cracking triggered by an increased shrinkage deformation in comparison to the one of conventional concrete. The increase in shrinkage behaviour is proportional to the amount of recycled aggregates used as a replacement for natural aggregates. Within the SeRaMCo project several computational chemo-thermo mechanical coupling phase-field models for complex fracture induced by early-age shrinkage and hydration heat in cement-based materials have been developed (and validated by experiment), to gain in depth insights into these phenomena [288]–[290].

The proposed model efficiently simulates the heat of hydration, thermal transfer, material strength’s development thanks to age effects, as well as the creeping phenomena of the early-age concrete. Thus, the risk of cracking is examined by means of the phase field method, see Figure 0-2. The obtained results show the critical shrinkage properties of recycled concrete. A high risk

of cracking is also captured. The major damage cause is noted due to the autogenous/drying shrinkage. The important effects of creeps at the early age, for instance, transient thermal creep and basic creep are also demonstrated.

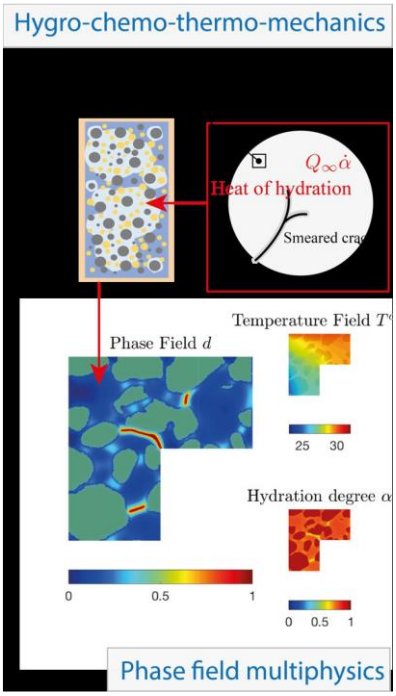

Figure 0-2. Simulation of the early-age behaviours of recycled concrete by using a phase field model. A high risk of cracking is noted [288], [290]

Modelling of fracture behaviour in recycled concrete by using a new strain split to model unilateral contact within the phase field method

The fracture behaviour of cement-based materials (brittle fracture) is known to be different in compression and traction. A new orthogonal split of strain tensor into compressive and tensile parts has been developed and implemented within the phase field model to describe such difference. The proposed model can efficiently mimic unilateral contact condition with which any existing cracks and any crack propagation have to comply. A comparison of the fracture responses predicted by the present model and experimental observation is provided in Figure 0-3, demonstrating its accuracy and efficiency.

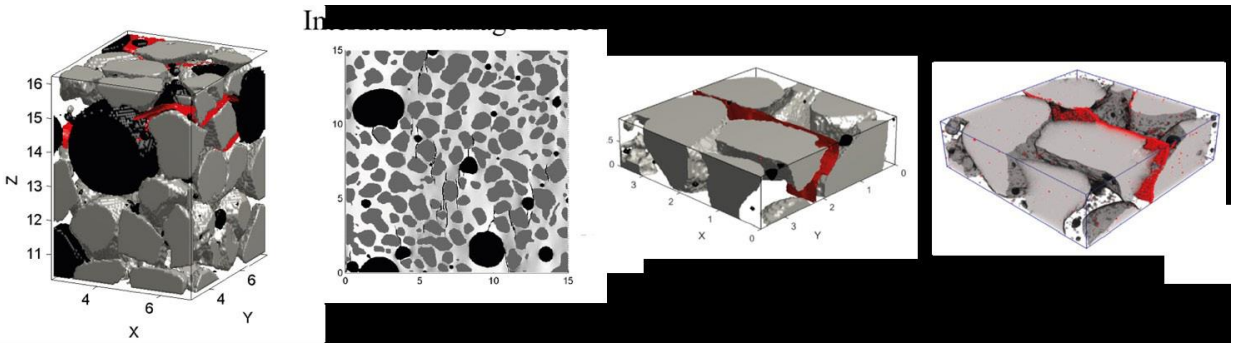

Figure 0-3. Modelling of fracture behaviour in cement-based materials [278]

The new formulation is also able to simulate the fracture behaviour of any arbitrary initial anisotropic behaviour. Hence, this proposed numerical model allows us to predict the complex cracking problem at different scales, ranging from microscopic to macroscopic scales. That will identify the important factors controlling the material performance, which need to be considered in the mix design, see Figure 0-4.

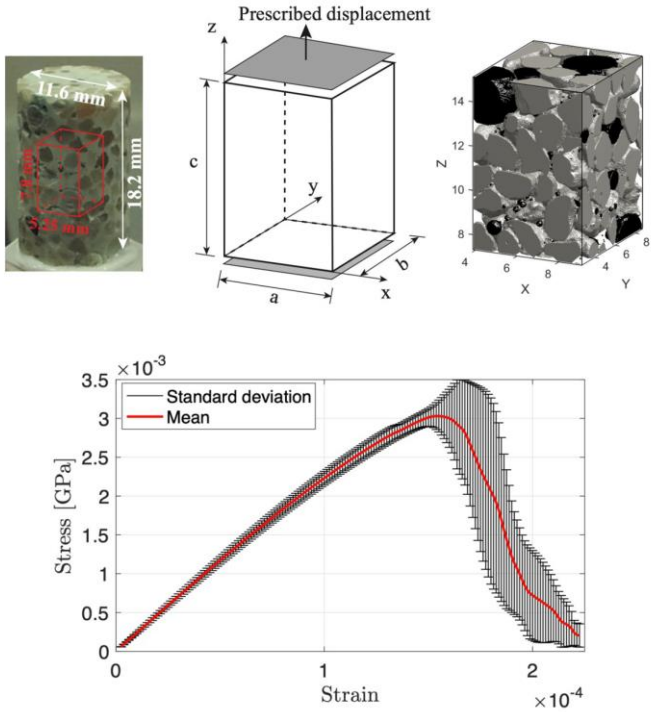

Figure 0-4. Numerical evaluation of the fracture performance of cement-based materials at microscopic scale for various grain size distribution of aggregates. The output can be used to estimate the concrete class with a given aggregate characterization

Modelling of interfacial crack propagation in strongly heterogeneous materials by using the phase field method

Mechanisms of the interfacial transition zone is often considered as one of the most important factors that governs the performance of recycled concrete [291], [292]. However, taking into account interfacial effects is not a trivial task in the numerical model, due to its complexity in geometry, length scale and especially its non-homogeneous materials in nature, in this study, a new interfacial cracking model in the phase field framework is proposed [292]. A dimensional-reduced model based on a rigorous asymptotic analysis is adapted to derive the null thickness imperfect interface models from an original configuration containing thin interphase. Then, the idea of mixing the bulk and interfacial energy within the phase field framework is used to describe the material degradation both on the interface and in the bulk. The new model is able to consider the complex interfaces with arbitrary geometry and properties, see Figure 0-5.

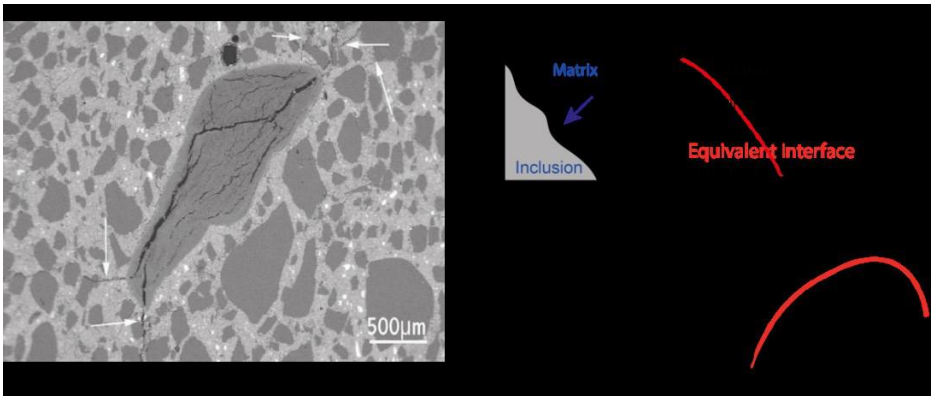

Figure 0-5. Modelling of interfacial crack propagation in strongly heterogeneous materials by using phase field method. The proposed model can be used to improve the mechanical strength by optimizing the interfacial transition zone. The red line of the loading curve shows the expected mechanical performance after performing the interfacial designing

We apply the present model to study the interfacial cracking in recycled concretes and to understand the effects of interfacial transition zone on the global behaviour of recycled concrete material. The new model predicts very well the complex cracking phenomena on interfaces such as initiation, delamination, coalescence, and deflection. This demonstrated the performance of the present computational framework. The developed numerical models constitute a promising tool to

optimize the mechanical performance of recycled concrete as well as of cement-based materials in general by enhancing the interface's characterization.

Experimental approach

Recycled concrete formulations

In the framework of the development of new recycled concretes, two mixes using 100% of recycled aggregates were composed. These used recycled aggregates are of known origin and come from a concrete precast element producer. Indeed, the recycled aggregate are produced on their site by crushing elements e.g., failing the self-control criteria of the producer or remaining on stock. The mixes developed out of these aggregates are the High-Strength Concrete (HSC) and the Open Structure Concrete (OSC) mixes. The recipes of the new mixes were chosen based on existent mixtures of a precast concrete producer for guaranteeing an easy transfer to an industrial application. Hence, for the new mixes, a similar rheology with the existent mixtures of the partnership was targeted to formulate mixes with the same production process using existing technical equipment. In the same light, materials with similar prices were chosen for maintaining the same economic competitiveness as the existent mixtures.

High strength concrete mix (HSC mix)

For the developed High Strength Concrete (HSC) mix, a blend of complementary fractions of recycled aggregates of known origin was chosen from the initial 0/63 fraction resulting out of the crushing process. The initial granulometry is represented in Figure 0-6. The raw aggregates have been sieved to different granulometric fractions. The refusals of sieves 1, 2, 4, 8 and 16 mm have been separated for reconstructing the particle size distribution of the aggregates used for the high strength concrete. Hence, for the coarse aggregates, the fraction 4/8 was obtained by mixing the refusals of sieve 4 mm with the refusals of sieve 8 mm in the proportion 1:1 in terms of weight. The 0.25/2 sand was obtained by removing the very fine particles from the raw fine aggregates. The final granulometry is ensuring a uniform distribution, with a maximum grain size of 8 mm

and a minimum grain size of 0.25 mm. These blends presented the best grain size distribution for reducing segregation and for having an optimized workability of fresh concrete. The coarse aggregates were used in saturated dry surface conditions.

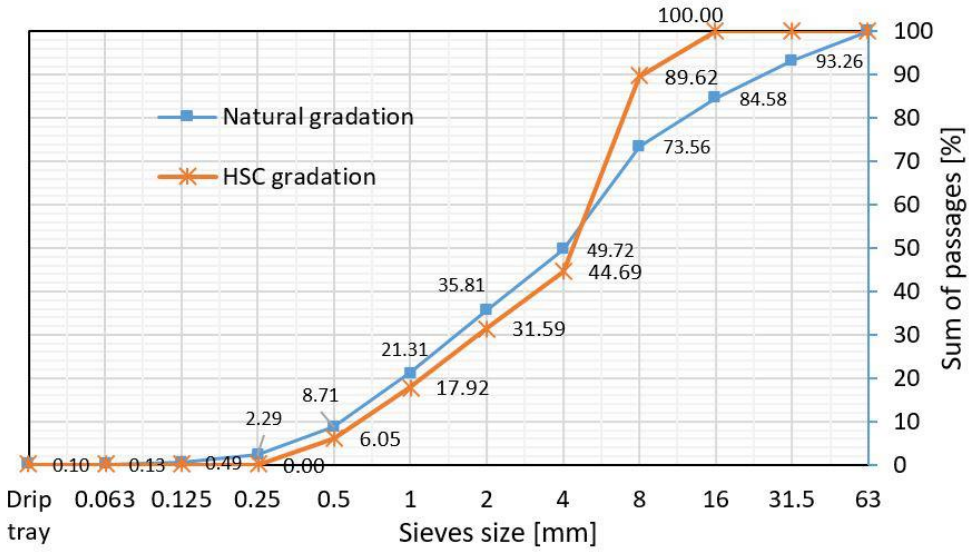

Figure 0-6. Granulometry of the initial and the reconstructed HSC aggregates

The used cement was a recycled cement including 10% of recycled fines provided by the project partner VICAT in France. In addition to the recycled cement, calcium carbonate (CaCO3) has been added in the proportions 1:3 with respect to the cement weight. The proportions of additives were mainly defined based on the existent recipe and on the expected concrete strength. The quantity of micro-silica and superplasticizer was respectively 2% and 3% in terms of weight of the binder. The binder to aggregate ratio was 1:3.6 and the water to binder ratio w/b 0.35. Table 0-1 shows the detailed recipe.

With regard to the mixing procedure, the aggregates and the total binder (cement + fillers) were first dry mixed for 30 seconds. Then, a half of the free water was added during 30 seconds and the whole was then mixed for 60 additional seconds. After the first 120 seconds of mixing, the remaining half of the free water as well as the superplasticizer were added during another 30 seconds. Following that, the whole was mixed for 60 seconds, then the edges were scraped, and the whole mixed again for 120 seconds, resulting in a total mixing time of 5 min 30 seconds.

Table 0-1. High strength (HSC) mix

Description		[kg/m³]
	Fraction 4/8 mm	1037.4
	Fraction 0.25/2 mm	558.6
Binder	Filler	131.9
	Cement R42.5	307.8
Additives	Superplasticizer	13.2
	Micro-silica	8.8
Water to binder ratio (w/b)		0.35

Open structure concret mix (OSC mix)

For the open structure concrete (OSC) mix, a coarse blend was chosen from the initial fraction 0/63 resulting from the crushing process. This coarse blend presents a maximum grain size of 16 mm and a minimum grain size of 4 mm. The fraction 4/16 was obtained by mixing the refusals of sieves 16, 4 and 8 mm in respective proportions of 20%, 60% and 20% in terms of weight. The fine particles with grain sizes less than 4 mm were purposely reduced for ensuring a high and connected porosity in the final concrete mixture. The same recycled cement was also used with an additional calcium carbonate filler in the proportion 1:3 in terms of weight. Moreover, 2% of micro-silica was also added. The binder to aggregate ratio was 1:2.9 and the water to binder ratio w/b 0.35. The detailed composition of the open structure concrete is presented in Table 0-2. The mix process was the same as for the HSC mix.

Table 0-2. Open structure mix

Table 2. Open structure concrete mix

Description		[kg/m³]
Aggregates	Fraction 4/16 mm	1417.3
	Fraction 0/2 mm	82.7
Binder	Filler	154.3
	R42.5	360.0
Additives	Micro-silica	10.3
Water to binder ratio (w/b)		0.35

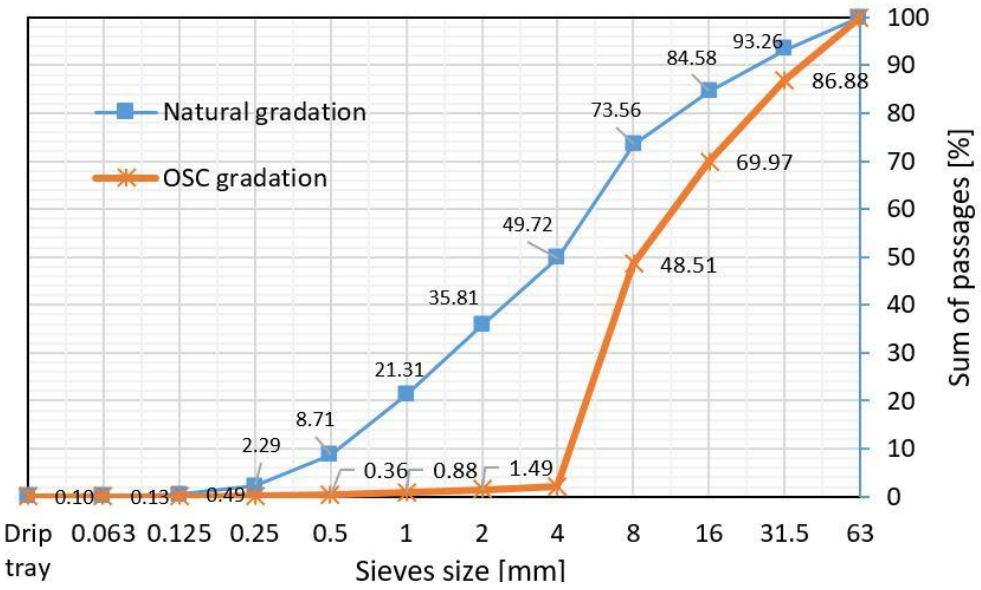

Figure 0-7. Granulometry of the initial and the reconstructed OSC aggregates

The used superplasticizer ACE 456 is based on polycarboxylate ether polymers. It acts as cement hydration accelerator by exposing more surfaces of the cement particles for reaction with water. The fast and complete hydration of the cement particles enables to reach higher strengths at an earlier age. Moreover, the most advantageous aspect of the used superplasticizer is the improvement of rheological aspects of fresh concrete, especially in concrete mixtures with a low water to binder ratio. The micro-silica used is a common pozzolan made of fines particles of silicon dioxide (SiO2) solved into water before adding into fresh concrete. The particles of micro-silica support a good hydration process by wide spreading the particles of cement. In addition, they reduce the porosity in the final mix by acting as fine aggregates in the blend. Indeed, the small grains of micro-silica fill the space between cement grains in a phenomenon that is referred to as particle packing. Moreover, micro-silica is very active in a chemical aspect. As the hydration of cement results, among other effects, in the release of calcium hydroxide, micro-silica reacts with it and creates an additional binding material called calcium silicate hydrate.

Experiemental test results

Experimental tests have been conducted for determining the mechanical performances of the developed recycled concrete. These experimental tests were conducted respecting the European norms: EN 12390-3: 2009 for the compressive strength, EN 12390-5: 2009 for the flexural

strength, EN 12390-6: 2009 for the tensile splitting strength and EN 12390-13: 2009 for the secant modulus of elasticity in compression.

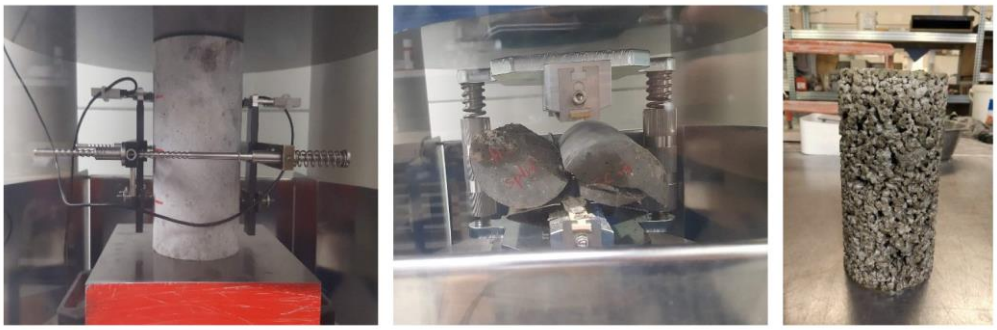

Figure 0-8. High strength and open structure concrete

The results of the experimental tests after 28 days of hardening are presented in Table 0-3. The compressive strength of the HSC was 58.5 MPa and the one of the OSC 5.7 MPa respectively. The low compressive strength of the OSC is due to the high porosity and the low density (1600 kg/m³), whereas the relative high compressive strength of the HSC is due to a better hydration and a more important density of roughly 2300 kg/m³. Concerning the tensile splitting strength, a mean value of 18.7 MPa at 28 days was found for the HSC.

Table 0-3. Mechanical properties of the developed recycled concrete

		High strength concrete (At 28 days)	**Open structure concrete** (At 28 days)
Compressive strength [MPa]	Mean value	58.5	5.7
	(Standard deviation)	(3.9)	(0.4)
E-Modulus [MPa]	Mean value	29 500	1500
	(Standard deviation)	(3000)	(160)
Splitting tests [MPa]	Mean value	18.7	-
	(Standard deviation)	(2.6)	-
Flexural strength [MPa]	Mean value	10.1	2.3
	(Standard deviation)	(0.7)	(0)

The shrinkage tests presented in Figure 0-9 are still in progress for assessing the fracture resistance and control the earlier-age behaviour of both the HSC and the OSC.

Figure 0-9. Shrinkage tests on High Strength Concrete (HSC) and Open Structure Concrete (OSC)

Future applications

As for an application, in common agreement with the partner Contern – Lëtzebuerger Beton, the developed self-compacting concrete will be used for manufacturing a set of products like platform edge for railway track, public bench, Maxiblocs and precast demountable timber concrete slab system (see Figure 0-10).

Figure 0-10. Application of self-compacting concrete (Product catalog og Contern - Letzebuerger Beton)

Conclusion

Within this research work a set of numerical models have been developed based on the phase field method to evaluate the mechanical performance and durability of recycled concrete. Different phase field models retraced the early age behaviour of recycled concrete, showing the cracking behaviour triggered by an increased shrinkage deformation of recycled concrete compared to conventional concrete and helped to gain in-depth insights into these phenomena. In addition, a new model is also developed to study the effects of interfacial transition zone on the global behaviour of recycled concrete. These models allowed to understand the load-deformation behaviour registered during the experimental tests. Following the numerical simulation, two mixes using 100% of recycled aggregates were developed and devoted for high strength and open structure concrete. Different fractions of the raw recycled aggregates were combined for constructing a uniform granulometry for the HSC and the OSC respectively. Compressive, splitting, flexural and E-modulus tests were conducted for characterizing the mechanical performance of the mixes. The HSC presented a satisfactory strength development at 28 days while the OSC exhibited a relative low strength.

Finally, the reduction of both the E-Modulus and the flexural strength of the OSC with respect to the HSC demonstrated the influence of the granulometry on the mechanical performance of recycled concrete.

Acknowedgements

This research is supported by the project SeRaMCo within the programme INTERREG – NEW. Furthermore, we acknowledge the support of Contern – Lëtzebuerger Beton during the whole project.

References

[1] K. E. Boulding, “The Economics of the Coming Spaceship Earth,” pp. 3–14, 1966.

[2] W. Stahel and G. Reday-Mulvey, “Jobs for tomorrow: the potential for substituting manpower for energy,” *Vantage Press*, 1976.

[3] W. Stahel, “The product life factor. An Inquiry into the Nature of Sustainable Societies: The Role of the Private Sector,” 1982.

[4] P. P. Marina, C. A. Daniela, M. Geissdoerfer, M. P. P. Pieroni, D. C. A. Pigosso, and K. Soufani, “Circular business models : A review,” *J. Clean. Prod.*, vol. 277, p. 123741, 2020, doi: 10.1016/j.jclepro.2020.123741.

[5] “Ellen MacArthur Foundation.” https://ellenmacarthurfoundation.org/.

[6] “Earth overshoot Day.” https://www.overshootday.org/.

[7] UNDP, “Human Development Index (HDI).” https://hdr.undp.org/en/content/human-development-index-hdi.

[8] GNHUSA, “Genuine Progress Indicator.” https://gnhusa.org/genuine-progress-indicator/.

[9] S. Stjepanovi, D. Tomi, and M. Škare, “Green GDP: An analyses for developing and developed countries,” 2019, doi: 10.15240/tul/001/2019-4-001.

[10] UK’s New Economic Foundation, “Happy Planet Index.” https://happyplanetindex.org/.

[11] B. van der Merwe, “GDP is flawed as a measurement, so why is it still in use?,” *Investment Monitor*, 2021.

[12] J. Hickel and G. Kallis, “Is Green Growth Possible?,” vol. 3467, 2020, doi: 10.1080/13563467.2019.1598964.

[13] M. Dittrich, S. Giljum, S. Lutter, and C. Polzin, *Green economies around the world? Implications of resource use for development and the environment*. 2012.

[14] T. Wiedmann, J. K. Steinberger, M. Lenzen, and L. T. Keyßer, “Scientists ’ warning on affl uence,” pp. 1–10, 2020, doi: 10.1038/s41467-020-16941-y.

[15] European Commission, “Communication from the commission to the European Parliament, the European Council, the Council, the European Economic and Social Committe and th Committee of the Regions - The European Green Deal,” 2019.

[16] J. D. Ward, P. C. Sutton, A. D. Werner, R. Costanza, S. H. Mohr, and C. T. Simmons, “Is Decoupling GDP Growth from Environmental Impact Possible ?,” pp. 1–14, 2016, doi: 10.1371/journal.pone.0164733.

[17] P. Söderholm, “The green economy transition : the challenges of technological change for sustainability,” 2020.

[18] M. Braungart and W. McDonough, *Cradle to cradle: remaking the way we make things*. North Point Press, 2002.

[19] W. Craft, L. Ding, D. Prasad, L. Partridge, and D. Else, “Development of a regenerative

design model for building retrofits," *Procedia Eng.*, vol. 180, pp. 658–668, 2017, doi: 10.1016/j.proeng.2017.04.225.

[20] J. F. V Vincent, O. A. Bogatyreva, N. R. Bogatyrev, A. Bowyer, and A. Pahl, "Biomimetics : its practice and theory," no. April, pp. 471–482, 2006, doi: 10.1098/rsif.2006.0127.

[21] M. Ramage and K. Shipp, *System Thinkers*. Springer, London, 2009.

[22] European Commission, "Directive 2008/98/EC of the European Parliament and of the Council of 19 November 2008 on waste and repealing certain Directives," 2008.

[23] Y. Kalmykova, M. Sadagopan, and L. Rosado, "Circular economy – From review of theories and practices to development of implementation tools," *Resour. Conserv. Recycl.*, vol. 135, no. February 2017, pp. 190–201, 2018, doi: 10.1016/j.resconrec.2017.10.034.

[24] P. Brunner and H. Rechberger, *Practical handbook of material flow analysis*. FL, USA: Lewis Publishers, 2004.

[25] C. Huang, J. Vause, H. Ma, and C. Yu, "Using material / substance flow analysis to support sustainable development assessment : A literature review and outlook," *"Resources, Conserv. Recycl.*, vol. 68, pp. 104–116, 2012, doi: 10.1016/j.resconrec.2012.08.012.

[26] C. Hendriks, R. Obernosterer, D. Müller, S. Kytzia, P. Baccini, and P. H. Brunner, "Material Flow Analysis: A tool to support environmental policy decision making. Case-studies on the city of Vienna and the Swiss lowlands," *Local Environ.*, vol. 5, no. 3, pp. 311–328, Aug. 2000, doi: 10.1080/13549830050134257.

[27] B. Goldstein, M. Birkved, and M. Quitzau, "Quantification of urban metabolism through coupling with the life cycle assessment framework : concept development and case study," 2013, doi: 10.1088/1748-9326/8/3/035024.

[28] D. B. Müller, "Stock dynamics for forecasting material flows — Case study for housing in The Netherlands," vol. 9, 2005, doi: 10.1016/j.eco.

[29] I. Sartori *et al.*, "Towards modelling of construction , renovation and demolition activities : Norway ' s dwelling stock , Towards modelling of construction , renovation and demolition activities : Norway ' s dwelling stock , 1900 ^ 2100," vol. 3218, no. February, pp. 412–425, 2016, doi: 10.1080/09613210802184312.

[30] P. E. Bradley, N. Kohler, P. E. Bradley, and N. Kohler, "Methodology for the survival analysis of urban building stocks Methodology for the survival analysis of urban building stocks," *Build. Res. Inf.*, no. December 2014, pp. 37–41, 2007, doi: 10.1080/09613210701266939.

[31] F. Kleemann, J. Lederer, H. Rechberger, and J. Fellner, "GIS-based Analysis of Vienna's Material Stock in Buildings," *J. Ind. Ecol.*, vol. 21, no. 2, pp. 368–380, 2017, doi: 10.1111/jiec.12446.

[32] M. A. Heinrich and W. Lang, "Capture and Control of Material Flows and Stocks in Urban Residential Buildings," 2019, doi: 10.1088/1755-1315/225/1/012001.

[33] A. Mastrucci, O. Baume, F. Stazi, and U. Leopold, "Estimating energy savings for the residential building stock of an entire city: A GIS-based statistical downscaling approach

applied to Rotterdam," *Energy Build.*, vol. 75, pp. 358–367, 2014, doi: 10.1016/j.enbuild.2014.02.032.

[34] H. Wu, J. Wang, H. Duan, L. Ouyang, W. Huang, and J. Zuo, "An innovative approach to managing demolition waste via GIS (geographic information system): A case study in Shenzhen city, China," *J. Clean. Prod.*, vol. 112, pp. 494–503, 2016, doi: 10.1016/j.jclepro.2015.08.096.

[35] A. Mastrucci, A. Marvuglia, E. Popovici, U. Leopold, and E. Benetto, "Geospatial characterization of building material stocks for the life cycle assessment of end-of-life scenarios at the urban scale," *Resour. Conserv. Recycl.*, vol. 123, pp. 54–66, 2017, doi: 10.1016/j.resconrec.2016.07.003.

[36] IPCC, "Climate change 2021 - The physical science basis," 2021.

[37] University of Luxembourg, Luxembourg Institute of Science and Technology, Institute for Organic Agriculture Luxembourg, and Office for Landscape Morphology, "Luxembourg 2050 - Prospects for a Regenerative City-Landscape," 2021.

[38] D. W. O'Neill, A. L. Fanning, W. F. Lamb, and J. K. Steinberger, "A good life for all within planetary boundaries," *Nat. Sustain.*, vol. 1, pp. 88–95, 2018.

[39] Ministere de l'Energie et de l'Amenagement du territoire, "Luxembourg in transition." .

[40] M. A. Curran, *Life Cycle Assessment Handbook : A Guide for Environmentally Sustainable Products*. John Wiley & Sons, Incorporated, 2012.

[41] H. P. de Heijungs, R.; Guinée, J.B.; Huppes, G.; Lankreijer, R.M.; Udo de Haes, H.A.; Wegener Sleeswijk, A.; Ansems, A.M.M.; Eggels, P.G.; Duin, R. van; Goede, "Environmental life cycle assessment of products: guide and backgrounds." 1992.

[42] M. Z. Hauschild and M. A. . Huijbregts, *Life cycle impact assessment*. Springer, 2015.

[43] ISO/TC 207/SC 5 Life cycle assessment, "ISO 14044:2006 - Environmental management - Life cycle assessment - Requirements and guidelines." 2006.

[44] Ellen MacArthur Foundation, "Growth within: a circular economy vision for a competitive europe." [Online]. Available: https://emf.thirdlight.com/link/8izw1qhml4ga-404tsz/@/preview/1?o.

[45] I. Hijazi, M. Ehlers, S. Zlatanova, T. Becker, and L. van Berlo, "Initial Investigations for Modeling Interior Utilities Within 3D Geo Context: Transforming IFC-Interior Utility to CityGML/UtilityNetworkADE," in *Advances in 3D Geo-Information Sciences*, 2010, pp. 95–113.

[46] H. Wang, Y. Pan, and X. Luo, "Integration of BIM and GIS in sustainable built environment: A review and bibliometric analysis," *Autom. Constr.*, vol. 103, no. September 2018, pp. 41–52, 2019, doi: 10.1016/j.autcon.2019.03.005.

[47] C. S. Poon, A. T. W. Yu, and L. H. Ng, "On-site sorting of construction and demolition waste in Hong Kong," *Resour. Conserv. Recycl.*, vol. 32, no. 2, pp. 157–172, 2001.

[48] S. Jalali, "Quantification of construction waste amount," 2007.

[49] K. M. Cochran and T. G. Townsend, "Estimating construction and demolition debris generation using a materials flow analysis approach.," *Waste Manag.*, vol. 30, no. 11, pp.

2247–2254, Nov. 2010, doi: 10.1016/j.wasman.2010.04.008.

[50] C. Llatas, “Methods for estimating construction and demolition (C&D) waste,” in *Handbook of Recycled Concrete and Demolition Waste*, pp. 25–52.

[51] L. B. Jayasinghe and D. Waldmann, “Development of a BIM-based web tool as Material and Component bank for a sustainable construction industry,” *sustainability*, 2020.

[52] A. Josa, A. Aguado, A. Heino, E. Byars, and A. Cardim, “Comparative analysis of available life cycle inventories of cement in the EU,” *Cem. Concr. Res.*, vol. 34, no. 8, pp. 1313–1320, 2004, doi: 10.1016/j.cemconres.2003.12.020.

[53] Bundesministerium des Innern für Bau und Heimat, “Ökobaudat - Informationsportal Nachhaltiges Bauen.” https://www.oekobaudat.de/.

[54] C. Knoeri, E. Sanyé-Mengual, and H. J. Althaus, “Comparative LCA of recycled and conventional concrete for structural applications,” *Int. J. Life Cycle Assess.*, vol. 18, no. 5, pp. 909–918, 2013, doi: 10.1007/s11367-012-0544-2.

[55] J. Wang, J. Zhang, D. Cao, H. Dang, and B. Ding, “Comparison of recycled aggregate treatment methods on the performance for recycled concrete,” *Constr. Build. Mater.*, vol. 234, p. 117366, 2020, doi: 10.1016/j.conbuildmat.2019.117366.

[56] F. Colangelo, T. G. Navarro, I. Farina, and A. Petrillo, “Comparative LCA of concrete with recycled aggregates: a circular economy mindset in Europe,” *Int. J. Life Cycle Assess.*, vol. 25, no. 9, pp. 1790–1804, 2020, doi: 10.1007/s11367-020-01798-6.

[57] W. Czernin, *Cement chemistry and physics for engineers*. London: Godwin.

[58] T. C. Hansen, *Recycling of Demolished Concrete and Masonry*. 1992.

[59] F. Pacheco-Torgal, V. W. Y. Tam, J. A. Labrincha, Y. Ding, and J. de Brito, *Handbook of recycled concrete and demolition waste*. Woodhead Publishing, 2013.

[60] M. Hiete, “Waste management plants and technology for recycling construction and demolition (C&D) waste: state-of-the-art and future challenges,” in *Handbook of Recycled Concrete and Demolition Waste*, Woodhead Publishing, 2013, pp. 53–75.

[61] U. Penzel and R. Kircher, “Technik der Aufbereitung.” Recyclingpraxis Baustoffe, Köln, 1997.

[62] C. Müller, “Latest developments in the standardization of concrete.”

[63] BSI, “EN 206:2013 - Concrete: Specification, performance, production and conformity.” BSI.

[64] BSI, “EN 12620 - Aggregates for concrete.” .

[65] BSI, “EN 1367-4: Tests for thermal and weathering properties of aggregates. Determination of drying shrinkage.” .

[66] BSI, “EN 1744-5 Tests for chemical properties of aggregates. Determination of acid soluble chloride salts.” .

[67] A. Katz, “Properties of concrete made with recycled aggregate from partially hydrated old concrete,” vol. 33, pp. 703–711, 2003, doi: 10.1016/S0008-8846(02)01033-5.

[68] V. Corinaldesi and G. Moriconi, “Behaviour of cementitious mortars containing different kinds of recycled aggregate,” *Constr. Build. Mater.*, vol. 23, no. 1, pp. 289–294, 2009, doi: 10.1016/j.conbuildmat.2007.12.006.

[69] L. Evangelista and J. De Brito, “Mechanical behaviour of concrete made with fine recycled concrete aggregates,” vol. 29, pp. 397–401, 2007, doi: 10.1016/j.cemconcomp.2006.12.004.

[70] A. Eduardo *et al.*, “Mechanical properties modeling of recycled aggregate concrete,” *Constr. Build. Mater.*, vol. 24, no. 4, pp. 421–430, 2010, doi: 10.1016/j.conbuildmat.2009.10.011.

[71] P. Kumar Mehta and P. J. M. Monteiro, *Concrete: Microstructure, properties and materials*, 3rd ed. McGraw-Hill, 2005.

[72] A. K. Padmini, K. Ramamurthy, and M. S. Mathews, “Influence of parent concrete on the properties of recycled aggregate concrete,” *Constr. Build. Mater.*, vol. 23, no. 2, pp. 829–836, 2009, doi: 10.1016/j.conbuildmat.2008.03.006.

[73] J. A. Bogas, J. De Brito, and D. Ramos, “Freeze e thaw resistance of concrete produced with fi ne recycled concrete aggregates,” *J. Clean. Prod.*, vol. 115, pp. 294–306, 2016, doi: 10.1016/j.jclepro.2015.12.065.

[74] A. Salesa *et al.*, “Physico - mechanical properties of multi - recycled concrete from precast concrete industry,” vol. 141, pp. 248–255, 2017, doi: 10.1016/j.jclepro.2016.09.058.

[75] A. Domingo-cabo, C. Lázaro, F. López-gayarre, M. A. Serrano-lópez, P. Serna, and J. O. Castaño-tabares, “Creep and shrinkage of recycled aggregate concrete,” *Constr. Build. Mater.*, vol. 23, no. 7, pp. 2545–2553, 2009, doi: 10.1016/j.conbuildmat.2009.02.018.

[76] J. Xiao, W. Li, Y. Fan, and X. Huang, “An overview of study on recycled aggregate concrete in China (1996 – 2011),” *Constr. Build. Mater.*, vol. 31, pp. 364–383, 2012, doi: 10.1016/j.conbuildmat.2011.12.074.

[77] M. Omrane, S. Kenai, E. Kadri, and A. Aït-mokhtar, “Performance and durability of self compacting concrete using recycled concrete aggregates and natural pozzolan,” *J. Clean. Prod.*, vol. 165, pp. 415–430, 2017, doi: 10.1016/j.jclepro.2017.07.139.

[78] C. S. Poon, Z. H. Shui, L. Lam, H. Fok, and S. C. Kou, “Influence of moisture states of natural and recycled aggregates on the slump and compressive strength of concrete,” vol. 34, pp. 31–36, 2004, doi: 10.1016/S0008-8846(03)00186-8.

[79] M. Etxeberria, A. R. Mari, and E. Vasquez, “Recycled aggregate concrete as structural material,” *Mater. Struct.*, pp. 529–541, 2007, doi: 10.1617/s11527-006-9161-5.

[80] S. Manzi, C. Mazzotti, and M. C. Bignozzi, “Cement & Concrete Composites Short and long-term behavior of structural concrete with recycled concrete aggregate,” *Cem. Concr. Compos.*, vol. 37, pp. 312–318, 2013, doi: 10.1016/j.cemconcomp.2013.01.003.

[81] X. H. Deng, Z. L. Lu, P. Li, and T. Xu, “An investigation of mechanical properties of recycled coarse aggrregate concrete,” *Gruyter Open*, vol. 62, no. 4, 2016.

[82] A. Abbas *et al.*, “Quantification of the residual mortar content in recycled concrete aggregates by image analysis,” *Mater. Charact.*, vol. 60, no. 7, pp. 716–728, 2009, doi: 10.1016/j.matchar.2009.01.010.

[83] A. Abbas, G. Fathifazl, O. B. Isgor, A. G. Razaqpur, B. Fournier, and S. Foo, “Durability of recycled aggregate concrete designed with equivalent mortar volume method,” *Cem. Concr. Compos.*, vol. 31, no. 8, pp. 555–563, 2009, doi: 10.1016/j.cemconcomp.2009.02.012.

[84] M. Sanchez de Juan and P. Alaejos Gutierrez, “Influence of attached mortar content on the properties of recycled concrete aggregate,” no. November, pp. 536–544, 2004.

[85] G. Troxell, H. Davis, and J. Kelly, “Composition and properties of concrete,” 1968.

[86] C. G. Lyman, “Growth and movement in Portland cement concrete,” *Oxford Univ. Press*, 1934.

[87] T. Nawa and T. Horita, “Autogeneous shrinkage of high-performance concrete,” *Proc. Int. Work. Microstruct. Durab. to Predict Serv. life Concr. Struct.*, 2004.

[88] T. C. Powers, “Mechanism of shrinkage and reversible creep of hardened cement paste,” *Proc. Int. Conf. Struct. Concr. London*, 1965.

[89] S. Mindess, J. . Young, and D. Darwing, *Concrete*. New York: Prentice Hall, 2003.

[90] R. V Silva, J. De Brito, and R. K. Dhir, “Prediction of the shrinkage behavior of recycled aggregate concrete : A review,” *Constr. Build. Mater.*, vol. 77, pp. 327–339, 2015, doi: 10.1016/j.conbuildmat.2014.12.102.

[91] Y. Cao, B. Liu, and Q. Xia, “Experimental research on the drying shrinkage property of the regeneration concrete,” *Eng. Constr.*, vol. 23, pp. 47–49, 2009.

[92] S. Kou, C. Poon, and H. Wan, “Properties of concrete prepared with low-grade recycled aggregates C & D Waste,” *Constr. Build. Mater.*, vol. 36, pp. 881–889, 2012, doi: 10.1016/j.conbuildmat.2012.06.060.

[93] J. Gómez-Soberón, “Porosity of recycled concrete with substitution of recycled concrete aggregate An experimental study,” vol. 32, pp. 1301–1311, 2002.

[94] K. Ouyang *et al.*, “An overview on the ef fi ciency of different pretreatment techniques for recycled concrete aggregate,” *J. Clean. Prod.*, vol. 263, p. 121264, 2020, doi: 10.1016/j.jclepro.2020.121264.

[95] O. Jensen and P. Lura, “Techniques and materials for internal water curing of concrete,” pp. 817–825, 2006, doi: 10.1617/s11527-006-9136-6.

[96] S. Yihune, K. Song, J. Song, B. Yeon, and H. Kim, “Internal curing effect of raw and carbonated recycled aggregate on the properties of high-strength slag-cement mortar,” *Constr. Build. Mater.*, vol. 165, pp. 64–71, 2018, doi: 10.1016/j.conbuildmat.2018.01.035.

[97] Y. Mao, J. Liu, and C. Shi, “Autogenous shrinkage and drying shrinkage of recycled aggregate concrete : A review,” *J. Clean. Prod.*, vol. 295, p. 126435, 2021, doi: 10.1016/j.jclepro.2021.126435.

[98] S. Yildirim, C. Meyer, and S. Herfellner, “Effects of internal curing on the strength , drying shrinkage and freeze – thaw resistance of concrete containing recycled concrete aggregates,” *Constr. Build. Mater.*, vol. 91, pp. 288–296, 2015, doi: 10.1016/j.conbuildmat.2015.05.045.

[99] Z. Li, J. Liu, J. Xiao, and P. Zhong, “Internal curing effect of saturated recycled fine

aggregates in early-age mortar," *Cem. Concr. Compos.*, vol. 108, no. October 2019, p. 103444, 2020, doi: 10.1016/j.cemconcomp.2019.103444.

[100] CEN, "Eurocode 2: Design of concrete structures," vol. 1, no. 2004. 2011.

[101] R. Wan-wendner, Z. B. Bazant, and M. . Hubler, "The B4 Model for Multi-decade Creep and Shrinkage Prediction," 2013, doi: 10.1061/9780784413111.051.

[102] Z. B. Bazant and S. Baweja, "Creep and Shrinkage Prediction Model for Analysis and Design of Concrete Structures : Model B3," vol. 83, pp. 38–39, 2001.

[103] H. Zhang, Y. Wang, D. E. Lehman, Y. Geng, and K. Kuder, "Time-dependent drying shrinkage model for concrete with coarse and fine recycled aggregate," *Cem. Concr. Compos.*, vol. 105, no. September 2019, p. 103426, 2020, doi: 10.1016/j.cemconcomp.2019.103426.

[104] H. Zhang, Y. Wang, D. E. Lehman, and Y. Geng, "Autogenous-shrinkage model for concrete with coarse and fine recycled aggregate," *Cem. Concr. Compos.*, vol. 111, no. September 2019, p. 103600, 2020, doi: 10.1016/j.cemconcomp.2020.103600.

[105] Y. Guo and X. Wang, "Experimental study on forecasting mathematical model of drying shrinkage of recycled aggregate concrete," vol. 2012, 2012, doi: 10.1155/2012/567812.

[106] G. Fathifazl, A. G. Razaqpur, O. B. Isgor, A. Abbas, B. Fournier, and S. Foo, "Creep and drying shrinkage characteristics of concrete produced with coarse recycled concrete aggregate," *Cem. Concr. Compos.*, vol. 33, no. 10, pp. 1026–1037, 2011, doi: 10.1016/j.cemconcomp.2011.08.004.

[107] Q. Wang, Y. Geng, Y. Wang, and H. Zhang, "Drying shrinkage model for recycled aggregate concrete accounting for the in fl uence of parent concrete," *Eng. Struct.*, vol. 202, no. May 2019, p. 109888, 2020, doi: 10.1016/j.engstruct.2019.109888.

[108] K. L. Scrivener and D. B. Technik, "The Interfacial Transition Zone (ITZ) Between Cement Paste and Aggregate," pp. 411–421, 2004.

[109] S. Diamond, "Percolation due to overlapping ITZs in laboratory mortars? A microstructural evaluation," *Cem. Concr. Res.*, vol. 33, no. 7, pp. 949–955, Jul. 2003, doi: 10.1016/S0008-8846(02)00996-1.

[110] S. Diamond and J. Huang, "The ITZ in concrete – a different view based on image analysis and SEM observations," *Cem. Concr. Compos.*, vol. 23, no. 2–3, pp. 179–188, Apr. 2001, doi: 10.1016/S0958-9465(00)00065-2.

[111] Y. Zhao, W. Zeng, and H. Zhang, "Properties of recycled aggregate concrete with different water control methods," *Constr. Build. Mater.*, vol. 152, pp. 539–546, 2017, doi: 10.1016/j.conbuildmat.2017.05.134.

[112] L. Struble, J. Skalny, and S. Mindess, "A review of the cement-aggregate bond," *Cem. Concr. Res.*, vol. 10, no. 2, pp. 277–286, Mar. 1980, doi: 10.1016/0008-8846(80)90084-8.

[113] R. Zimbelmann, "A Contribution to the Problem of Cement-Aggregate Bond," *Cem. Concr. Res.*, vol. 15, pp. 801–808, 1985.

[114] J. J. Zhang, "Rock strengths and rock failure criteria," in *Applied Pertoleum Geomechanics*, 2019, pp. 85–131.

[115] P. A. Bentur and M. G. Alexander, “A review of the work of the RILEM TC 159-ETC : Engineering of the interfacial transition zone in cementitious composites,” *Mater. Struct.*, vol. 33, no. March, pp. 82–87, 2000.

[116] M. Jebli, F. Jamin, E. Malachanne, E. Garcia-Diaz, and M. S. El Youssoufi, “Experimental characterization of mechanical properties of the cement-aggregate interface in concrete,” *Constr. Build. Mater.*, vol. 161, pp. 16–25, 2018, doi: 10.1016/j.conbuildmat.2017.11.100.

[117] S. Caliskan and B. L. Karihaloo, “Effect of surface roughness, type and size of model aggregates on the bond strength of aggregate/mortar interface,” *Interface Sci.*, vol. 12, no. 4, pp. 361–374, 2004, doi: 10.1023/B:INTS.0000042334.43266.62.

[118] F. Ceia, J. Raposo, M. Guerra, E. Júlio, and J. De Brito, “Shear strength of recycled aggregate concrete to natural aggregate concrete interfaces,” *Constr. Build. Mater.*, vol. 109, pp. 139–145, 2016, doi: 10.1016/j.conbuildmat.2016.02.002.

[119] T. Akçaoğlu, M. Tokyay, and T. Çelik, “Effect of coarse aggregate size and matrix quality on ITZ and failure behavior of concrete under uniaxial compression,” vol. 26, pp. 633–638, 2004, doi: 10.1016/S0958-9465(03)00092-1.

[120] Z. B. Bazant, “Fracture mechanics of concrete structures.” ACI Committee 446, 1992.

[121] S. Zhang, B. Schmidt, and S. Marx, “Experimental studies on the interface between concrete and cement-asphalt mortar,” in *Proceedings of the fib Symposium*, 2019, pp. 921–928.

[122] K. M. Alexander, D. J. Gilbert, and J. Wardlaw, “Aggregate-cement bond, cement paste strength and the strength of concrete,” *Cem. Concr. Assoc*, 1968.

[123] P. M. D. Santos and E. N. B. S. Júlio, “Review article A state-of-the-art review on shear-friction,” *Eng. Struct.*, vol. 45, pp. 435–448, 2012, doi: 10.1016/j.engstruct.2012.06.036.

[124] V. P. Nguyen, M. Stroeven, and L. J. Sluys, “Multiscale failure modeling of concrete: Micromechanical modeling, discontinuous homogenization and parallel computations,” *Comput. Methods Appl. Mech. Eng.*, vol. 201–204, pp. 139–156, Jan. 2012, doi: 10.1016/J.CMA.2011.09.014.

[125] P. Menetrey and K. J. William, “Triaxial failure criterion for concrete and its generalization,” *ACI Struct. J.*, vol. 92, no. 3, pp. 311–318, 1995.

[126] “Mohr-Coulomb plasticity.” https://abaqus-docs.mit.edu/2017/English/SIMACAEMATRefMap/simamat-c-mohrcoulomb.htm.

[127] J. Lubliner, J. Oliver, S. Oller, and E. Oñate, “A plastic-damage model for concrete,” vol. 25, no. 3, 1989, doi: 10.1016/0020-7683(89)90050-4.

[128] Y. J. Huang, Z. J. Yang, X. W. Chen, and G. H. Liu, “Monte Carlo simulations of meso-scale dynamic compressive behavior of concrete based on X-ray computed tomography images,” *Int. J. Impact Eng.*, vol. 97, pp. 102–115, Nov. 2016, doi: 10.1016/J.IJIMPENG.2016.06.009.

[129] H. Chen, B. Xu, Y. L. Mo, and T. Zhou, “Behavior of meso-scale heterogeneous concrete under uniaxial tensile and compressive loadings,” *Constr. Build. Mater.*, vol. 178, pp. 418–431, Jul. 2018, doi: 10.1016/J.CONBUILDMAT.2018.05.052.

[130] X. Du, L. Jin, and G. Ma, “Numerical simulation of dynamic tensile-failure of concrete at

meso-scale," *Int. J. Impact Eng.*, vol. 66, pp. 5–17, Apr. 2014, doi: 10.1016/J.IJIMPENG.2013.12.005.

[131] H. Chen, B. Xu, J. Wang, T. Zhou, X. Nie, and Y. L. Mo, "Parametric analysis on compressive strain rate effect of concrete using mesoscale modeling approach," *Constr. Build. Mater.*, vol. 246, p. 118375, Jun. 2020, doi: 10.1016/J.CONBUILDMAT.2020.118375.

[132] L. Jin, T. Wang, X. ang Jiang, and X. Du, "Size effect in shear failure of RC beams with stirrups: Simulation and formulation," *Eng. Struct.*, vol. 199, p. 109573, Nov. 2019, doi: 10.1016/J.ENGSTRUCT.2019.109573.

[133] A. Caballero, C. M. López, and I. Carol, "3D meso-structural analysis of concrete specimens under uniaxial tension," *Comput. Methods Appl. Mech. Eng.*, vol. 195, no. 52, pp. 7182–7195, Nov. 2006, doi: 10.1016/J.CMA.2005.05.052.

[134] C. M. López, A. E. Ignacio, C. Ae, and A. Aguado, "Meso-structural study of concrete fracture using interface elements. I: numerical model and tensile behavior," doi: 10.1617/s11527-007-9314-1.

[135] C. M. López, A. E. Ignacio, C. Ae, and A. Aguado, "Meso-structural study of concrete fracture using interface elements. II: compression, biaxial and Brazilian test," doi: 10.1617/s11527-007-9312-3.

[136] W. C. Zhu, J. G. Teng, and C. A. Tang, "Mesomechanical model for concrete. Part I: model development," *Mag. Concr. Res.*, vol. 56, no. 6, pp. 313–330, 2004, doi: 10.1680/macr.2004.56.6.313.

[137] A. Jayasuriya, M. P. Adams, and M. J. Bandelt, "Understanding variability in recycled aggregate concrete mechanical properties through numerical simulation and statistical evaluation," *Constr. Build. Mater.*, vol. 178, pp. 301–312, Jul. 2018, doi: 10.1016/J.CONBUILDMAT.2018.05.158.

[138] X. Tan, Z. Hu, W. Li, S. Zhou, and T. Li, "Micromechanical numerical modelling on compressive failure of recycled concrete using discrete element method (Dem)," *Materials (Basel).*, vol. 13, no. 19, pp. 1–17, 2020, doi: 10.3390/ma13194329.

[139] A. A. Griffith, "The phenomena of rupture and flow in solids," *Philos. Trans. R. Soc. London. Ser. A, Contain. Pap. a Math. or Phys. Character*, vol. 221, pp. 163–198, 1921.

[140] G. A. Francfort and J. J. Marigo, "Revisiting brittle fracture as an energy minimization problem," *J. Mech. Phys. Solids*, vol. 46, no. 8, pp. 1319–1342, Aug. 1998, doi: 10.1016/S0022-5096(98)00034-9.

[141] J. Y. Wu, V. P. Nguyen, C. T. Nguyen, D. Sutula, S. Sinaie, and S. P. A. Bordas, "Phase-field modeling of fracture," *Adv. Appl. Mech.*, vol. 53, pp. 1–183, Jan. 2020, doi: 10.1016/BS.AAMS.2019.08.001.

[142] C. Miehe, M. Hofacker, and F. Welschinger, "A phase field model for rate-independent crack propagation : Robust algorithmic implementation based on operator splits," *Comput. Methods Appl. Mech. Eng.*, vol. 199, no. 45–48, pp. 2765–2778, 2010, doi: 10.1016/j.cma.2010.04.011.

[143] T. T. Nguyen, D. Waldmann, and T. Q. Bui, "Phase field simulation of early-age fracture

in cement-based materials," *Int. J. Solids Struct.*, vol. 191–192, pp. 157–172, 2020, doi: 10.1016/j.ijsolstr.2019.12.003.

[144] X. Hu, H. Xu, X. Xi, P. Zhang, and S. Yang, "Meso-scale phase field modelling of reinforced concrete structures subjected to corrosion of multiple reinforcements," *Constr. Build. Mater.*, vol. 321, p. 126376, Feb. 2022, doi: 10.1016/J.CONBUILDMAT.2022.126376.

[145] Y. jie Huang, H. Zhang, B. bei Li, Z. jun Yang, J. ying Wu, and P. J. Withers, "Generation of high-fidelity random fields from micro CT images and phase field-based mesoscale fracture modelling of concrete," *Eng. Fract. Mech.*, vol. 249, p. 107762, May 2021, doi: 10.1016/J.ENGFRACMECH.2021.107762.

[146] M. Pise, D. Brands, G. Gebuhr, J. Schröder, and S. Anders, "Analysis of pullout behavior of single steel fibers embedded in concrete using phase-field modeling," *Proc. Appl. Math. Mech.*, 2018.

[147] "Schleibinger Testing Systems." http://www.schleibinger.com/cmsimple/en/?Shrinkage:Shrinkage-Cone.

[148] C. Jia, J. Yan, Q. Hu, C. Zou, and F. Chen, "Methods for Determination of Residual Mortar Content Adhered to Recycled Aggregate," vol. 579, pp. 568–571, 2014, doi: 10.4028/www.scientific.net/AMM.578-579.568.

[149] V. Corinaldesi, "Mechanical and elastic behaviour of concretes made of recycled-concrete coarse aggregates," *Constr. Build. Mater.*, vol. 24, no. 9, pp. 1616–1620, 2010, doi: 10.1016/j.conbuildmat.2010.02.031.

[150] S. C. Kou, C. S. Poon, and F. Agrela, "Comparisons of natural and recycled aggregate concretes prepared with the addition of different mineral admixtures," *Cem. Concr. Compos.*, vol. 33, no. 8, pp. 788–795, 2011, doi: 10.1016/j.cemconcomp.2011.05.009.

[151] I. Marie and H. Quiasrawi, "Closed-loop recycling of recycled concrete aggregates," *J. Clean. Prod.*, vol. 37, pp. 243–248, 2012, doi: 10.1016/j.jclepro.2012.07.020.

[152] S. Sadati, M. Arezoumandi, K. H. Khayat, and J. S. Volz, "Shear performance of reinforced concrete beams incorporating recycled concrete aggregate and high-volume fl y ash," *J. Clean. Prod.*, vol. 115, pp. 284–293, 2016, doi: 10.1016/j.jclepro.2015.12.017.

[153] A. M. Knaack and Y. C. Kurama, "Design of Concrete Mixtures with Recycled Concrete Aggregates," no. 110, 2013.

[154] V. Corinaldesi, V. Letelier, and G. Moriconi, "Behaviour of beam – column joints made of recycled-aggregate concrete under cyclic loading," *Constr. Build. Mater.*, vol. 25, no. 4, pp. 1877–1882, 2011, doi: 10.1016/j.conbuildmat.2010.11.072.

[155] J. Yang, Q. Du, and Y. Bao, "Concrete with recycled concrete aggregate and crushed clay bricks," *Constr. Build. Mater.*, vol. 25, no. 4, pp. 1935–1945, 2011, doi: 10.1016/j.conbuildmat.2010.11.063.

[156] CEN, "EN 12620:2013 - Aggregates for concrete." CEN, 2013.

[157] S. Mindess, J. F. Young, and D. Darwin, *Concrete*, 2nd ed. Prentice Hall, 2002.

[158] S. Mindess and C. D. M. Roy, "A review of the cement-aggregate bond," vol. I, no. c, pp.

277–286, 1980.

[159] M. Königsberger, B. Pichler, and C. Hellmich, “Micromechanics of ITZ – Aggregate Interaction in Concrete, Part I: Stress Concentration,” *J. Am. Ceram. Soc.*, vol. 97, pp. 535–542, 2014, doi: 10.1111/jace.12591.

[160] CEN, “EN 196-1 : Methods of testing cement - Part 1:Determination of strength.” 2005.

[161] P. M. D. Santos and E. N. B. S. Júlio, “A state-of-the-art review on roughness quantification methods for concrete surfaces,” *Constr. Build. Mater.*, vol. 38, pp. 912–923, 2013, doi: 10.1016/j.conbuildmat.2012.09.045.

[162] E. S. Gadelmawla, M. M. Koura, T. M. . Maksoud, I. M. Elewa, and H. H. Soliman, “Roughness parameters,” *J. Mater. Process. Technol.*, vol. 0136, no. April, pp. 1694–1701, 2002, doi: 10.1016/S0924-0136(02)00060-2.

[163] Union Europeenne des Producteurs de Granulats, “A sustainable industry for a sustainable europe annual review 2011-2012.” pp. 1–38, 2012.

[164] X. Hu, Q. Lu, Z. Xu, W. Zhang, and S. Cheng, “Compressive stress-strain relation of recycled aggregate concrete under cyclic loading,” *Constr. Build. Mater.*, vol. 193, pp. 72–83, Dec. 2018, doi: 10.1016/j.conbuildmat.2018.10.137.

[165] K. Paine and R. K. Dhir, “Recycled aggregates in concrete: a performance-related approach,” *Mag. Concr. Res.*, vol. 62, pp. 519–530, 2010.

[166] R. Zaharieva, F. Buyle-Bodin, and E. Wirquin, “Frost resistance of recycled aggregate concrete,” *Cem. Concr. Res. - CEM CONCR RES*, vol. 34, pp. 1927–1932, Oct. 2004, doi: 10.1016/j.cemconres.2004.02.025.

[167] S. Medjigbodo, A. Z. Bendimerad, E. Rozière, and A. Loukili, “How do recycled concrete aggregates modify the shrinkage and self-healing properties?,” *Cem. Concr. Compos.*, vol. 86, pp. 72–86, 2018, doi: https://doi.org/10.1016/j.cemconcomp.2017.11.003.

[168] M. Osmani, *Waste: A handbook for management*. Academic Press, Elsevier, 2011.

[169] S. W. Tabsh and A. S. Abdelfatah, “Influence of recycled concrete aggregates on strength properties of concrete,” *Constr. Build. Mater.*, vol. 23, no. 2, pp. 1163–1167, 2009, doi: https://doi.org/10.1016/j.conbuildmat.2008.06.007.

[170] D. Pedro, J. Brito, and L. Evangelista, “Performance of concrete made with aggregates recycled from precasting industry waste: influence of the crushing process,” *Mater. Struct.*, vol. 48, no. 12, pp. 3965–3978, 2015, doi: 10.1617/s11527-014-0456-7.

[171] T. Brown and A. H. Taylor, “Performance of concrete made with commercially produced coarse recycled concrete aggregate,” vol. 31, 2001.

[172] T. C. Hansen and H. Narud, “Strength of Recycled Concrete Made from Crushed Concrete Coarse Aggregate,” in *Concrete International*, 1983, pp. 79–83.

[173] S. Nagataki, A. Gokce, T. Saeki, and M. Hisada, “Assessment of recycling process induced damage sensitivity of recycled concrete aggregates,” *Cem. Concr. Res.*, vol. 34, no. 6, pp. 965–971, 2004, doi: 10.1016/j.cemconres.2003.11.008.

[174] L. Butler, J. S. West, and S. L. Tighe, “The effect of recycled concrete aggregate properties on the bond strength between RCA concrete and steel reinforcement,” *Cem. Concr. Res.*,

vol. 41, no. 10, pp. 1037–1049, 2011, doi: 10.1016/j.cemconres.2011.06.004.

[175] Z. H. Duan and C. S. Poon, "Properties of recycled aggregate concrete made with recycled aggregates with different amounts of old adhered mortars," *Mater. Des.*, vol. 58, pp. 19–29, 2014, doi: 10.1016/j.matdes.2014.01.044.

[176] K. McNeil and T. Kang, "Recycled Concrete Aggregates: A Review," *Int. J. Concr. Struct. Mater.*, vol. 7, Mar. 2013, doi: 10.1007/s40069-013-0032-5.

[177] I. B. Topcu, "Physical and mechanical properties of concretes produced with waste concrete," *Cem. Concr. Res.*, vol. 27, pp. 1817–1823, 1997.

[178] A. Khan et al, "Recycled concrete—a source for new aggregate," *Cem. Concr. aggregates*, pp. 17–27, 1984.

[179] M. Casuccio, M. C. Torrijos, G. Giaccio, and R. Zerbino, "Failure mechanism of recycled aggregate concrete," vol. 22, pp. 1500–1506, 2008, doi: 10.1016/j.conbuildmat.2007.03.032.

[180] V. W. Y. Tam, C. M. Tam, and Y. Wang, "Optimization on proportion for recycled aggregate in concrete using two-stage mixing approach," *Constr. Build. Mater.*, vol. 21, no. 10, pp. 1928–1939, 2007, doi: 10.1016/j.conbuildmat.2006.05.040.

[181] A. Ajdukiewicz and A. Kliszczewicz, "Influence of recycled aggregates on mechanical properties of HS/HPC," *Cem. Concr. Compos.*, vol. 24, pp. 269–279, Apr. 2002, doi: 10.1016/S0958-9465(01)00012-9.

[182] S. Yip and M. P. Short, "Multiscale materials modelling at the mesoscale," *Nat. Mater.*, vol. 12, no. 9, pp. 774–777, 2013, doi: 10.1038/nmat3746.

[183] L. Evangelista and J. de Brito, "Mechanical behaviour of concrete made with fine recycled concrete aggregates," *Cem. Concr. Compos.*, vol. 29, no. 5, pp. 397–401, 2007, doi: https://doi.org/10.1016/j.cemconcomp.2006.12.004.

[184] A. E. B. Cabral, V. Schalch, D. C. C. D. Molin, and J. L. D. Ribeiro, "Mechanical properties modeling of recycled aggregate concrete," *Constr. Build. Mater.*, vol. 24, no. 4, pp. 421–430, 2010, doi: 10.1016/j.conbuildmat.2009.10.011.

[185] J. Xiao, W. Li, Y. Fan, and X. Huang, "An overview of study on recycled aggregate concrete in China (1996–2011)," *Constr. Build. Mater.*, vol. 31, pp. 364–383, Jun. 2012, doi: 10.1016/j.conbuildmat.2011.12.074.

[186] G. Wardeh, E. Ghorbel, and H. Gomart, "Mix Design and Properties of Recycled Aggregate Concretes: Applicability of Eurocode 2," *Int. J. Concr. Struct. Mater.*, vol. 9, no. 1, pp. 1–20, 2015, doi: 10.1007/s40069-014-0087-y.

[187] C. S. Poon, Z. Shui, and L. Lam, "Effect of microstructure of ITZ on compressive strength of concrete prepared with recycled aggregates," *Constr. Build. Mater. - CONSTR BUILD MATER*, vol. 18, pp. 461–468, Jul. 2004, doi: 10.1016/j.conbuildmat.2004.03.005.

[188] W. Li, J. Xiao, Z. Sun, and S. Shah, "Failure processes of modeled recycled aggregate concrete under uniaxial compression," *Cem. Concr. Compos.*, vol. 34, pp. 1149–1158, Nov. 2012, doi: 10.1016/j.cemconcomp.2012.06.017.

[189] M. Guo, S. Y. Alam, A. Z. Bendimerad, F. Grondin, E. Rozière, and A. Loukili, "Fracture

process zone characteristics and identification of the micro-fracture phases in recycled concrete," *Eng. Fract. Mech.*, vol. 181, pp. 101–115, 2017, doi: https://doi.org/10.1016/j.engfracmech.2017.07.004.

[190] X. H. Deng, Z. L. Lu, P. Li, and T. Xu, "An investigation of mechanical properties of recycled coarse aggregate concrete," no. 2.

[191] V. Corinaldesi and G. Moriconi, "Behaviour of cementitious mortars containing different kinds of recycled aggregate," *Constr. Build. Mater.*, vol. 23, no. 1, pp. 289–294, 2009, doi: 10.1016/j.conbuildmat.2007.12.006.

[192] S. C. Wolski, J. E. Bolander, and E. N. Landis, "An In-Situ X-Ray Microtomography Study of Split Cylinder Fracture in Cement-Based Materials," *Exp. Mech.*, vol. 54, no. 7, pp. 1227–1235, 2014, doi: 10.1007/s11340-014-9875-1.

[193] Y. Huang, Z. Yang, W. Ren, G. Liu, and C. Zhang, "3D meso-scale fracture modelling and validation of concrete based on in-situ X-ray Computed Tomography images using damage plasticity model," *Int. J. Solids Struct.*, vol. 67–68, pp. 340–352, 2015, doi: https://doi.org/10.1016/j.ijsolstr.2015.05.002.

[194] Z. Yang and S. Dong, "A Roadmap for Discretely Energy-Stable Schemes for Dissipative Systems Based on a Generalized Auxiliary Variable with Guaranteed Positivity," *J. Comput. Phys.*, vol. 404, 2020.

[195] H. Yang, S. K. Sinha, Y. Feng, D. B. McCallen, and B. Jeremić, "Energy dissipation analysis of elastic–plastic materials," *Comput. Methods Appl. Mech. Eng.*, vol. 331, pp. 309–326, 2018, doi: https://doi.org/10.1016/j.cma.2017.11.009.

[196] C. Miehe, F. Welschinger, and M. Hofacker, "Thermodynamically consistent phase-field models of fracture: Variational principles and multi-field FE implementations," *Int. J. Numer. Methods Eng.*, vol. 83, no. 10, pp. 1273–1311, Sep. 2010, doi: https://doi.org/10.1002/nme.2861.

[197] G. ~A. Francfort and J.-J. Marigo, "Revisiting brittle fracture as an energy minimization problem," *J. Mech. Phys. Solids*, vol. 46, no. 8, pp. 1319–1342, Aug. 1998, doi: 10.1016/S0022-5096(98)00034-9.

[198] M. Ambati, T. Gerasimov, and L. De Lorenzis, "Phase-field modeling of ductile fracture," *Comput. Mech.*, Apr. 2015.

[199] H. Amor, J.-J. Marigo, and C. Maurini, "Regularized formulation of the variational brittle fracture with unilateral contact: Numerical experiments," *J. Mech. Phys. Solids*, vol. 57, pp. 1209–1229, Aug. 2009, doi: 10.1016/j.jmps.2009.04.011.

[200] M. Ambati, T. Gerasimov, and L. De Lorenzis, "A review on phase-field models of brittle fracture and a new fast hybrid formulation," *Comput. Mech.*, no. 2/2015, pp. 383–405, 2015.

[201] C. Methods, A. Mech, E. C. Bryant, and W. Sun, "A mixed-mode phase field fracture model in anisotropic rocks with consistent kinematics," *Comput. Methods Appl. Mech. Engrg.*, vol. 342, pp. 561–584, 2018, doi: 10.1016/j.cma.2018.08.008.

[202] C. Steinke and M. Kaliske, "A phase-field crack model based on directional stress decomposition," *Comput. Mech.*, vol. 63, May 2019, doi: 10.1007/s00466-018-1635-0.

[203] A. Johansson *et al.*, “MultiMesh Finite Element Methods : Solving PDEs on Multiple Intersecting Meshes,” vol. 343, no. 1, pp. 1005–1010, 2019, doi: 10.1016/j.cma.2018.09.009.

[204] N. Moës, T. Belytschko, N. Mo, and T. Belytschko, “Extended finite element method for cohesive crack growth,” pp. 0–21, 2017.

[205] B. Bourdin, G. Francfort, and J.-J. Marigo, “The Variational Approach to Fracture,” *J. Elast.*, vol. 91, pp. 5–148, Apr. 2008, doi: 10.1007/s10659-007-9107-3.

[206] K. M. Hamdia *et al.*, “Uncertainty quantification of the fracture properties of polymeric nanocomposites based on phase field modeling,” *Compos. Struct.*, vol. 133, no. C, pp. 1177–1190, 2015, doi: 10.1016/j.compstruct.2015.08.051.

[207] R. Dhir, K. Paine, and T. Dyer, “Recycling and reconstitution of construction and demolition waste,” 2004, pp. 123–132.

[208] UNEP 2019, “Sand and Sustainability: Finding new solutions for environmental governance of global sand resources,” Geneva, Switzerland, 2019.

[209] S. Book, “Not on my beach: The great German sand shortage,” *Handelsblatt Today*, 08-Mar-2018.

[210] European-Commission, “Construction and Demolition Waste (CDW).” https://ec.europa.eu/environment/waste/construction_demolition.htm.

[211] M. Menegaki and D. Damigos, “A review on current situation and challenges of construction and demolition waste management,” *Curr. Opin. Green Sustain. Chem.*, vol. 13, pp. 8–15, 2018, doi: 10.1016/j.cogsc.2018.02.010.

[212] Deloitte, “Document information Resource Efficient Use of Mixed Wastes,” no. October, 2017.

[213] USEPA, “Advancing sustainable materials management: 2014 Fact Sheet,” *United States Environ. Prot. Agency, Off. L. Emerg. Manag. Washington, DC 20460*, no. November, p. 22, 2016, [Online]. Available: https://www.epa.gov/sites/production/files/2016-11/documents/2014_smmfactsheet_508.pdf.

[214] Á. Salesa *et al.*, “Physico – mechanical properties of multi – recycled concrete from precast concrete industry,” *J. Clean. Prod.*, vol. 141, pp. 248–255, 2017, doi: 10.1016/j.jclepro.2016.09.058.

[215] S. Ulubeyli, A. Kazaz, and V. Arslan, “Construction and Demolition Waste Recycling Plants Revisited: Management Issues,” *Procedia Eng.*, vol. 172, pp. 1190–1197, 2017, doi: 10.1016/j.proeng.2017.02.139.

[216] The European Union Per Regulation, “EN 1990 - Eurocode - Basis of structural design,” 2002.

[217] I. 59/SC 14, “ISO 15686-8:2008: Buildings and constructed assests - Service-life planning - Refernce service life and service life estimation.” .

[218] J. O’Connor, “Survey on actual service lives for North American buildings,” *Woodframe Hous. Durab. Disaster Issues*, no. October, pp. 1–9, 2004.

[219] Z. Wu, A. T. W. Yu, L. Shen, and G. Liu, “Quantifying construction and demolition waste:

An analytical review," *Waste Manag.*, vol. 34, no. 9, pp. 1683–1692, 2014, doi: 10.1016/j.wasman.2014.05.010.

[220] P. E. Bradley and N. Kohler, "Methodology for the survival analysis of urban building stocks," *Build. Res. Inf.*, vol. 35, no. 5, pp. 529–542, 2007, doi: 10.1080/09613210701266939.

[221] F. Kleemann, J. Lederer, H. Rechberger, and J. Fellner, "GIS-based Analysis of Vienna ' s Material Stock in Buildings," *J. Ind. Ecol.*, vol. 00, no. 0, pp. 1–13, 2016, doi: 10.1111/jiec.12446.

[222] A. Gruen, M. Behnisch, N. Kohler, A. Gruen, M. Behnisch, and N. Kohler, "Perspectives in the reality-based generation , nD modelling , and operation of buildings and building stocks," *Buiilding Res. Inf.*, vol. 37 (5–6), pp. 503–519, 2009, doi: 10.1080/09613210903189509.

[223] A. Mastrucci, O. Baume, F. Stazi, and U. Leopold, "Estimating energy savings for the residential building stock of an entire city : A GIS-based statistical downscaling approach applied to Rotterdam," *Energy Build.*, vol. 75, pp. 358–367, 2014, doi: 10.1016/j.enbuild.2014.02.032.

[224] R. Ortlepp, K. Gruhler, and G. Schiller, "Material stocks in Germany's non-domestic buildings:a new quantifcation method," vol. 44, no. 8, pp. 840–862, 2016.

[225] N. Kohler and U. Hassler, "The building stock as a research object," *Build. Res. Inf.*, vol. 30:4, pp. 37–41, 2002, doi: 10.1080/09613210110102238.

[226] J. Li, Z. Ding, X. Mi, and J. Wang, "A model for estimating construction waste generation index for building project in China," *Resour. Conserv. Recycl.*, vol. 74, pp. 20–26, 2013, doi: 10.1016/j.resconrec.2013.02.015.

[227] Z. Wu, A. T. W. Yu, L. Shen, and G. Liu, "Quantifying construction and demolition waste: An analytical review," *Waste Manag.*, vol. 34, no. 9, pp. 1683–1692, 2014, doi: 10.1016/j.wasman.2014.05.010.

[228] A. Gruen, M. Behnisch, and N. Kohler, "Perspectives in the reality-based generation, nD modelling, and operation of buildings and building stocks," *Build. Res. Inf.*, vol. 37, no. 5–6, pp. 503–519, 2009, doi: 10.1080/09613210903189509.

[229] J. R. Jensen and E. J. Christensen, "Solid and hazardous waste disposal site selection using digital geographic information system techniques," *Sci. Total Environ.*, vol. 56, no. C, pp. 265–276, 1986, doi: 10.1016/0048-9697(86)90331-1.

[230] A. Gallardo, M. Carlos, M. Peris, and F. J. Colomer, "Methodology to design a municipal solid waste generation and composition map: A case study," *Waste Manag.*, vol. 34, no. 11, pp. 1920–1931, 2014, doi: 10.1016/j.wasman.2014.05.014.

[231] G. A. Blengini and E. Garbarino, "Resources and waste management in Turin (Italy): The role of recycled aggregates in the sustainable supply mix," *J. Clean. Prod.*, vol. 18, no. 10–11, pp. 1021–1030, 2010, doi: 10.1016/j.jclepro.2010.01.027.

[232] A. Mastrucci, A. Marvuglia, E. Popovici, U. Leopold, and E. Benetto, "Geospatial characterization of building material stocks for the life cycle assessment of end-of-life scenarios at the urban scale," *"Resources, Conserv. Recycl.*, vol. 123, pp. 54–66, 2017, doi:

10.1016/j.resconrec.2016.07.003.

[233] H. Wu, J. Wang, H. Duan, L. Ouyang, W. Huang, and J. Zuo, “An innovative approach to managing demolition waste via GIS (geographic information system): A case study in Shenzhen city, China,” *J. Clean. Prod.*, vol. 112, pp. 494–503, 2016, doi: 10.1016/j.jclepro.2015.08.096.

[234] “QGIS - A Free and Open Source Geographic Information System.” https://qgis.org/en/site/ (accessed Jun. 10, 2020).

[235] The Statistics Portal of Luxembourg, “Statec.lu.” .

[236] European Construction Sector Observatory, “European Construction Sector Observatory,” no. June, p. 27, 2017.

[237] The Statistics Portal of Luxembourg, “Statec.lu.” https://statistiques.public.lu/stat/TableViewer/tableView.aspx?ReportId=13443&IF_Language=eng&MainTheme=4&FldrName=4&RFPath=35 (accessed Apr. 05, 2020).

[238] P. Villoria Sáez and M. Osmani, “A diagnosis of construction and demolition waste generation and recovery practice in the European Union,” *J. Clean. Prod.*, vol. 241, 2019, doi: 10.1016/j.jclepro.2019.118400.

[239] European-Commission, “CDW: Material recovery & backfilling.” https://ec.europa.eu/environment/waste/studies/pdf/CDW Statistics 2011.pdf (accessed Apr. 05, 2020).

[240] Administration du cadastre et de la topographie, “La plate-forme de données luxembourgeoise.” https://data.public.lu/fr/organizations/administration-du-cadastre-et-de-la-topographie/.

[241] Administration du cadastre et de la topographie, “La plate-forme de données luxembourgeoise - LiDAR 2019.” https://data.public.lu/fr/datasets/lidar-2019-modele-numerique-de-la-surface-mns/.

[242] “Zonal Statistics Plugin.” https://docs.qgis.org/2.18/en/docs/user_manual/plugins/plugins_zonal_statistics.html.

[243] European Union, “TABULA WebTool.” http://webtool.building-typology.eu/#bm.

[244] STATEC, “Le portail des statistiques Grand-Duché de Luxembourg.” https://statistiques.public.lu/fr/acteurs/statec/index.html.

[245] T. Kameda *et al.*, “Asbestos: use, bans and disease burden in Europe,” *Bull. World Health Organ.*, vol. 92, no. 11, pp. 790–797, 2014, doi: 10.2471/blt.13.132118.

[246] S. Hardiman, “Insight into Construction in Luxembourg by the European Construction Sector Observatory,” 2018. https://www.construction21.org/articles/h/insight-into-construction-in-luxembourg-by-the-european-construction-sector-observatory.html.

[247] La Chambre de Commerce du Luxembourg, “Luxembourg economy: Open, dynamic, reliable,” 2017. https://www.luxinnovation.lu/wp-content/uploads/sites/3/2017/10/web_en_brochure_eco_lux_0917_cdc-1.pdf.

[248] The Statistics Portal of Luxembourg, “Indice des prix de la construction.” https://statistiques.public.lu/stat/ReportFolders/ReportFolder.aspx?IF_Language=fra&Mai

nTheme=4&FldrName=4&RFPath=36.

[249] G. Reding, D. Flies, M. Trauffler, and D. Sijaric, “Implementation of the EPBD in Luxembourg,” 2016. https://epbd-ca.eu/ca-outcomes/outcomes-2015-2018/book-2018/countries/luxembourg.

[250] S. Casali, “L’industrie sidérurgique luxembourgeoise depuis les années 60,” 2012. [Online]. Available: https://statistiques.public.lu/catalogue-publications/luxembourg/2013/PDF-02-13.pdf.

[251] S. Delvoie, S. P. De Wallonie, and Z. Zhao, “Market analysis of recycled sands and aggregates in NorthWest Europe : drivers and barriers Market analysis of recycled sands and aggregates in NorthWest Europe : drivers and barriers,” no. February, 2019, doi: 10.1088/1755-1315/225/1/012055.

[252] A. Coelho and J. De Brito, “Economic viability analysis of a construction and demolition waste recycling plant in Portugal e part I : location , materials , technology and economic analysis,” *J. Clean. Prod.*, vol. 39, pp. 338–352, 2013, doi: 10.1016/j.jclepro.2012.08.024.

[253] European Commission, “Construcion and demolitin waste,” 2018. https://ec.europa.eu/environment/waste/construction_demolition.htm.

[254] UEPG, “Annual review 2019-2020,” 2020. [Online]. Available: https://uepg.eu/mediatheque/media/UEPG-AR20192020_V13_(03082020)_spreads.pdf.

[255] UN Environmental Programme, “Buildings and Construction,” 2019. https://wedocs.unep.org/bitstream/handle/20.500.11822/35850/BC.pdf.

[256] R. Andersson, K. Fridh, and M. Ha, “Calculating CO 2 Uptake for Existing Concrete Structures during and after Service Life,” *Environ. Sci. Technol.*, 2013.

[257] F. Pacheco-Torgal, S. Miraldo, J. A. Labrincha, and J. de Brito, “An eco-efficient approach to concrete carbonation,” in *Eco-Efficient Concrete*, 2013, pp. 368–385.

[258] B. Lu, C. Shi, J. Zheng, and T. Ling, *Carbon dioxide sequestration on recycled aggregates*. Elsevier Ltd, 2018.

[259] R. Sacchi, “Should we neglect cement carbonation in life cycle inventory databases ?,” pp. 1532–1544, 2020.

[260] K. Yang, E. Seo, and S. Tae, “Carbonation and CO2 uptake of concrete,” *Environ. Impact Assess. Rev.*, vol. 46, pp. 43–52, 2014, doi: 10.1016/j.eiar.2014.01.004.

[261] E. Possan, E. . Felix, and W. . Thomaz, “CO2 uptake by carbonation of concrete during life cycle of building structures,” *J. Build. Pathol. Rehabil.*, vol. 1, no. 1, pp. 1–9, 2016, doi: 10.1007/s41024-016-0010-9.

[262] A. Souto-Martinez, J. H. Arehart, and W. V. S. Iii, “Cradle-to-gate CO2e emissions vs. in situ CO2 sequestration of structural concrete elements,” *Energy Build.*, vol. 167, pp. 301–311, 2018, doi: 10.1016/j.enbuild.2018.02.042.

[263] S. Jacobsen and P. Jahren, “Binding of CO2 by carbonation of Norwegian OPC concrete,” in *CANMET/ACI International Conference on Sustainability and Concrete Technology*, 2002.

[264] L. Bogoviku and D. Waldmann, “Modelling of mineral construction and demolition waste

dynamics through a combination of geospatial and image analysis," *J. Environ. Manage.*, vol. 282, no. January, 2021, doi: 10.1016/j.jenvman.2020.111879.

[265] A. Coelho and J. De Brito, "Resources , Conservation and Recycling Economic analysis of conventional versus selective demolition — A case study," vol. 55, pp. 382–392, 2011, doi: 10.1016/j.resconrec.2010.11.003.

[266] Recyma, "http://recyma.lu/fr/liste_prix/index.htm." .

[267] B. Guy and T. J. Williams, "'Green' Demolition Certification."

[268] European Commission, "Directive 2008/98/EC," *Off. J. Eur. Union*, pp. 3–30, 2008.

[269] R. Marsh, "Building lifespan: effect on the environmental impact of building components in a Danish perspective," *Archit. Eng. Des. Manag.*, vol. 13, no. 2, pp. 80–100, Mar. 2017, doi: 10.1080/17452007.2016.1205471.

[270] "Madaster." https://madaster.com/.

[271] J. Xiao, Y. Huang, J. Yang, and C. Zhang, "Mechanical properties of confined recycled aggregate concrete under axial compression," *Constr. Build. Mater.*, vol. 26, no. 1, pp. 591–603, 2012, doi: 10.1016/j.conbuildmat.2011.06.062.

[272] J. Xiao, W. Li, D. J. Corr, and S. P. Shah, "Cement and Concrete Research Effects of interfacial transition zones on the stress – strain behavior of modeled recycled aggregate concrete," *Cem. Concr. Res.*, vol. 52, pp. 82–99, 2013, doi: 10.1016/j.cemconres.2013.05.004.

[273] R. K. Choubey, S. Kumar, and M. C. Rao, "Modeling of fracture parameters for crack propagation in recycled aggregate concrete," *Constr. Build. Mater.*, vol. 106, pp. 168–178, 2016, doi: 10.1016/j.conbuildmat.2015.12.101.

[274] N. D. Stambaugh, T. L. Bergman, and W. V. S. Iii, "Numerical service-life modeling of chloride-induced corrosion in recycled-aggregate concrete," *Constr. Build. Mater.*, vol. 161, pp. 236–245, 2018, doi: 10.1016/j.conbuildmat.2017.11.084.

[275] G. A. Francfort and J. J. Marigo, "Revisiting brittle failure as an energy minimization problem."

[276] B. Bourdin, G. A. Francfort, and J. Marigo, "Numerical experiments in revisited brittle fracture," vol. 48, 2000.

[277] T. T. Nguyen, J. Yvonnet, Q. Zhu, M. Bornert, and C. Chateau, "A phase field method to simulate crack nucleation and propagation in strongly heterogeneous materials from direct imaging of their microstructure," *Eng. Fract. Mech.*, vol. 139, pp. 18–39, 2015, doi: 10.1016/j.engfracmech.2015.03.045.

[278] T. T. Nguyen, J. Yvonnet, Q. Zhu, M. Bornert, and C. Chateau, "A phase-field method for computational modeling of interfacial damage interacting with crack propagation in realistic microstructures obtained by microtomography," *Comput. Methods Appl. Mech. Engrg.*, vol. 312, pp. 567–595, 2016, doi: 10.1016/j.cma.2015.10.007.

[279] T. T. Nguyen, J. Yvonnet, M. Bornert, and C. Chateau, "Initiation and propagation of complex 3D networks of cracks in heterogeneous quasi-brittle materials: Direct comparison between in situ testing-microCT experiments and phase field simulations," *J. Mech. Phys.*

Solids, vol. 95, pp. 320–350, 2016.

[280] H. Ogawa and T. Nawa, "Improving the Quality of Recycled Fine Aggregate by Selective Removal of Brittle Defects," *J. Adv. Concr. Technol.*, vol. 10, no. 12, pp. 395–410, 2012.

[281] J. Kim, J. Sung, C. Jeon, S. Lee, and H. Kim, "A Study on the Properties of Recycled Aggregate Concrete and Its Production Facilities," 2019.

[282] B. B. Mukharjee and S. V Barai, "Influence of Nano-Silica on the properties of recycled aggregate concrete," *Constr. Build. Mater.*, vol. 55, pp. 29–37, 2014, doi: 10.1016/j.conbuildmat.2014.01.003.

[283] M. Behera, S. K. Bhattacharyya, A. K. Minocha, R. Deoliya, and S. Maiti, "Recycled aggregate from C & D waste & its use in concrete – A breakthrough towards sustainability in construction sector : A review," *Constr. Build. Mater.*, vol. 68, pp. 501–516, 2014, doi: 10.1016/j.conbuildmat.2014.07.003.

[284] C. Zhou and Z. Chen, "Mechanical properties of recycled concrete made with different types of coarse aggregate," *Constr. Build. Mater.*, vol. 134, pp. 497–506, 2017, doi: 10.1016/j.conbuildmat.2016.12.163.

[285] M. B. Leite and P. J. M. Monteiro, "Microstructural analysis of recycled concrete using X-ray microtomography," *Cem. Concr. Res.*, vol. 81, pp. 38–48, 2016, doi: 10.1016/j.cemconres.2015.11.010.

[286] M. Sánchez de Juan and P. Alaejos, "Study on the influence of attached mortar content on the properties of recycled concrete aggregate," *Constr. Build. Mater.*, vol. 23, no. 2, pp. 872–877, 2009, doi: 10.1016/j.conbuildmat.2008.04.012.

[287] W. Li, C. Long, V. W. Y. Tam, C. Poon, and W. Hui, "Effects of nano-particles on failure process and microstructural properties of recycled aggregate concrete," *Constr. Build. Mater.*, vol. 142, pp. 42–50, 2017, doi: 10.1016/j.conbuildmat.2017.03.051.

[288] T. Nguyen, D. Waldmann, and T. Quoc, "Computational chemo-thermo-mechanical coupling phase-field model for complex fracture induced by early-age shrinkage and hydration heat in cement-based materials," *Comput. Methods Appl. Mech. Eng.*, vol. 348, pp. 1–28, 2019, doi: 10.1016/j.cma.2019.01.012.

[289] T. Nguyen, D. Waldmann, and T. Quoc, "International Journal of Solids and Structures Phase field simulation of early-age fracture in cement-based materials," *Int. J. Solids Struct.*, vol. 191–192, pp. 157–172, 2020, doi: 10.1016/j.ijsolstr.2019.12.003.

[290] T. Nguyen, M. Weiler, and D. Waldmann, "Experimental and numerical analysis of early age behavior in non-reinforced concrete," *Constr. Build. Mater.*, vol. 210, pp. 499–513, 2019, doi: 10.1016/j.conbuildmat.2019.03.074.

[291] T. Nguyen, D. Waldmann, and T. Quoc, "Role of interfacial transition zone in phase field modeling of fracture in layered heterogeneous structures," *J. Comput. Phys.*, vol. 386, pp. 585–610, 2019, doi: 10.1016/j.jcp.2019.02.022.

[292] T. Nguyen, J. Yvonnet, D. Waldmann, and Q. He, "Phase field modeling of interfacial damage in heterogeneous media with stiff and soft interphases," *Eng. Fract. Mech.*, vol. 218, no. June, p. 106574, 2019, doi: 10.1016/j.engfracmech.2019.106574.